DEVELOPMENT OF TECHNIQUES TO CLASSIFY MARINE BENTHIC HABITATS USING HYPERSPECTRAL IMAGERY IN OLIGOTROPHIC, TEMPERATE WATERS

Matthew J. Harvey

This thesis is presented for the degree of Doctor of Philosophy

in the School of Environmental Science, Murdoch University

February 2009

Declaration

I declare that this thesis is my own account of my research and contains, as its main content, work which has not been previously submitted for a degree at any tertiary education institution.

……

Matthew J. Harvey

Abstract

There is an increasing need for more detailed knowledge about the spatial distribution and structure of shallow water benthic habitats for marine conservation and planning. This, linked with improvements in hyperspectral image sensors provides an increased opportunity to develop new techniques to better utilise these data in marine mapping projects. The oligotrophic, optically-shallow waters surrounding Rottnest Island, Western Australia, provide a unique opportunity to develop and apply these new mapping techniques. The three flight lines of HyMap hyperspectral data flown for the Rottnest Island Reserve (RIR) in April 2004 were corrected for atmospheric effects, sunglint and the influence of the water column using the Modular Inversion and Processing System. A digital bathymetry model was created for the RIR using existing soundings data and used to create a range of topographic variables (e.g. slope) and other spatially relevant environmental variables (e.g. exposure to waves) that could be used to improve the ecological description of the benthic habitats identified in the hyperspectral imagery. A hierarchical habitat classification scheme was developed for Rottnest Island based on the dominant habitat components, such as *Ecklonia radiata* or *Posidonia sinuosa*. A library of 296 spectral signatures at HyMap spectral resolution (~15 nm) was created from >6000 *in situ* measurements of the dominant habitat components and subjected to spectral separation analysis at all levels of the habitat classification scheme. A separation analysis technique was developed using a multivariate statistical optimisation approach that utilised a genetic algorithm in concert with a range of spectral metrics to determine the optimum set of image bands to achieve maximum separation at each classification level using the entire spectral library. These results

determined that many of the dominant habitat components could be separated spectrally as pure spectra, although there were almost always some overlapping samples from most classes at each split in the scheme. This led to the development of a classification algorithm that accounted for these overlaps. This algorithm was tested using mixture analysis, which attempted to identify 10 000 synthetically mixed signatures, with a known dominant component, on each run. The algorithm was applied directly to the water-corrected bottom reflectance data to classify the benthic habitats. At the broadest scale, bio-substrate regions were separated from bare substrates in the image with an overall accuracy of 95% and, at the finest scale, bare substrates, *Posidonia, Amphibolis*, *Ecklonia radiata*, *Sargassum* species, algal turf and coral were separated with an accuracy of 70%. The application of these habitat maps to a number of marine planning and management scenarios, such as marine conservation and the placement of boat moorings at dive sites was demonstrated.

Contents

Acknowledgments

I would firstly like to acknowledge my supervisors, Associate Professor Lynnath Beckley and Dr Halina Kobryn, without whom my PhD would never have been completed. Thank you for providing the guidance to enable me to integrate remote sensing and marine ecology for this thesis as well as ensuring financial assistance towards my research and attending conferences,. Thanks to Halina for introducing me to remote sensing and to Lynnath for providing an almost continuous stream of feedback on my work - it was instrumental in getting this thesis across the line

The PhD scholarship provided by Murdoch University and the research funds contributed by the Rottnest Island Authority and Department of Environment and Conservation are gratefully acknowledged. The Rottnest Island Authority also provided considerable in-kind support to facilitate my field work and I would particularly like to acknowledge Harriet Davie, Claire Wright, Emma Jackson and Melissa Robbins for their assistance with all things Rottnest over the last four years.

Thanks to everyone who helped with my field work especially Barb Muhling who persevered and helped me on almost every field trip. Thanks also to Warren Chisholm, Dave Holliday, Aaron McDonald, Thea Linke, Jessica Eastwell and Michelle Wildsmith for their contributions. Much appreciated, guys. I would also like to thank the Murdoch technicians, especially Gus Paccani, Michael Taylor, Phil Good and Steve Goynich, who made getting out in the field so much easier by keeping '*Squilla*' ship-shape and dive gear serviced and available (even at short notice). I am also grateful for the eternal patience and invaluable assistance of Heather Gordon and Frank Salleo in the School of Environmental Science who made negotiating the bureaucratic minefield that is any

university so much easier! Thanks also to Ross Lantzke for his support throughout my time at Murdoch and Karen Olkowski, from the graduate centre, for her assistance.

Thomas Hegge (EOMAP) is acknowledged for providing the corrected HyMap data that made my research possible as well as supporting and encouraging me during my PhD. Thanks to Peter Hausknecht (formerly of HyVista Corporation) for his involvement in the initial acquisition of the HyMap imagery and his continued interest and advice with respect to my research. Also, thanks to Nicole Pinnel for her advice and encouragement. Russ Babcock and Peter Fearns (CSIRO) are acknowledged for their support and interest in the early stages of my PhD and for inviting me to get some field time with them prior to starting my own research.

A big thanks to my close friends who always supported me and provided an escape from the all encompassing world that is a PhD - those distractions saved me more than once! Also, special thanks the Claire Smallwood for putting up with me in the office for so long and providing those essential distractions!

And last, but not least, I would like to thank my family for all their support throughout my PhD as, without them, I would not have been able to get through. I would especially like to thank my brother, Daniel, for his tireless efforts towards helping me realise some of my more obscure ideas about processing hyperspectral imagery by writing the reams of Java code to make it happen. I couldn't have done it without your help, thanks! A big thanks to my sister, Megs, and Grandad for their continuous encouragement. Finally, sincere thanks to my parents, Trevor and Brenda, for their constant support and making sure I had a place to live, even when things got tight. Without the support of my family and friends I could not have made it through. Thanks.

1 General introduction

1.1 Biodiversity conservation in Australia

The importance of biodiversity conservation was recognised on a global scale in 1992, when the United Nations Convention on Biological Diversity was formulated in Rio de Janeiro (United Nations 1993). Australia ratified the Convention in 1994 and, as such, is bound by its articles and obligations. These include the conservation of biodiversity through identifying and monitoring important components and understanding processes likely to have significant impacts on these components. The Convention also requires that, where possible, and when appropriate, signatory nations establish a system of protected areas and establish guidelines for the selection and management of these areas.

To meet its obligations to the Convention on Biological Diversity, Australia released the Oceans Policy in 1998 to provide a framework for integrated and ecosystem-based planning and management for Australia's vast marine territories (Commonwealth of Australia 1998). At the core of the policy is the development of regional marine plans for Australia's entire exclusive economic zone. The primary goals of the regional marine plans include ensuring the health of marine ecosystems, protecting marine biodiversity, promoting diverse and sustainable marine industries and ensuring the establishment of a National Representative System of Marine Protected Areas (NRSMPA) that spans both State and Commonwealth waters (Commonwealth of Australia 1998). In support of this policy is the Environmental Protection and Biodiversity Conservation Act (EPBC Act), enacted in 1999, which was designed to facilitate biodiversity conservation by providing the legislative framework for

identifying threatening processes, protection of critical habitats and the implementation of management plans for Commonwealth areas.

Each of the states and territories in Australia has legislation that provides for the protection of the marine biodiversity in the state waters, which extend seaward for three nautical miles from the low water mark. In Western Australia, marine conservation is enabled through marine protected areas (MPA) under three types of legislation, those being the Conservation and Land Management Act (1984), the Fish Resources Management Act (1994), and Special Acts of Parliament. The Conservation and Land Management Act (1984) provides for the establishment and management of MPAs which are vested in the Marine Parks and Reserves Authority (MPRA), a statutory body established in 1997. There are three types of protected areas vested in the MPRA, namely, Marine Nature Reserves, Marine Management Areas and Marine Parks. Western Australia has nine Marine Parks, with three in the Perth metropolitan area; Marmion Marine Park, Shoalwater Islands Marine Park and the Swan Estuary Marine Park. The Fish Resources Act (1994) includes legislation for the establishment of Fish Habitat Protection Areas, e.g. the Cottesloe Reef Fish Habitat Protection Area. They are designed for the conservation and protection of fish, fish breeding areas and the management of fish and activities relating to the appreciation or observation of fish. There is currently only one MPA established under a Special Act of Parliament, that being the Rottnest Island reserve which was established under the Rottnest Island Authority Act (1987).

Historically, marine protected areas (MPA) have often been selected based on the protection of a single species, e.g. for the protection of a threatened species, or for the

purposes of managing fisheries resources (Stevens 2002). There has been shift in recent times towards ecosystem-based approaches, which take a more holistic view to the design and management of MPAs. These approaches have resulted in the development of representative MPA systems, i.e. those that "reasonably reflect the biotic diversity of the marine ecosystems from which they derive" (ANZECC 1998). This approach has focused on the selection of MPAs that contain habitats that are both typical of, and unique to, a particular area. Therefore, in order to define representative areas, there is a basic need to measure and map the biodiversity of Australia's vast coastline (Margules *et al.* 2002, Stevens 2002).

A regional marine plan was completed for south-eastern Australia in 2004 and the process is underway to complete a plan for south-western Australia, with the bioregional profile being released in 2007 (Australian Government Department of the Environment Water Heritage and the Arts 2007). However, the most recent Australian State of the Environment report found that although progress is being made, as of 2006 there was still no nationally consistent system for measuring the condition, and monitoring the trends in Australia's coastal ecosystems (Beeton *et al.* 2006). This was further reinforced in the State of the Environment report for Western Australia, released in 2007, which found that for the majority of the West Australian coastline, no baseline habitat data exists (Environmental Protection Authority 2007).

As highlighted in these reports, the collection of baseline data and development of methods to be able to monitor coastal ecosystems is of paramount importance. This was further reinforced in the south-east regional marine plan where a key action was to gain a better understanding of the region's marine biodiversity and ecological processes

through better mapping of the benthic substrates, as surrogates for marine biodiversity (National Oceans Office 2004).

1.2 Surrogates for biodiversity

The general biodiversity of an area includes diversity at the genetic, species and ecosystem levels (Gray 1997, Vanderklift *et al.* 1998, Sarkar and Margules 2002). Ecosystem diversity can be further broken down into functional, community and habitat diversity. Functional diversity refers to the range of functions performed by organisms within a system, and species can be categorised into functional groups such as growth forms (e.g. canopy algae or turf algae) or feeding types (e.g. herbivores or omnivores) (Gray 2001). Habitat diversity is a commonly used measure for biodiversity as it is spatially more easily defined, with clearer boundaries than entities such as ecosystems, and can be assessed at a range of scales, from individual habitats, to the landscape level that comprises a mosaic of habitats. The importance of studying habitats for understanding of ecological systems has long being recognised, having been referred to as the 'templates' for ecology (Southwood 1977).

As it is impossible to quantify the actual biodiversity everywhere, using surrogates has become accepted as a practical solution to measuring or quantifying the biodiversity of an area (Faith and Walker 1996, Gray 1997, Ward *et al.* 1999, Faith *et al.* 2001, Banks and Skilleter 2002, Margules *et al.* 2002, Sarkar and Margules 2002, Stevens and Connolly 2004). These biodiversity surrogates aim to both serve as reliable indicators of general biodiversity and need to be readily measurable in the environment.

There are a range of surrogates that have been used to describe or attempt to define the biodiversity of an area, some of the most common being species richness, vegetation

class and environmental parameters (Sarkar and Margules 2002, Sarkar *et al.* 2006). When vegetation class and environmental parameters are used together, they can act to describe habitats. The term 'habitat' has been used to describe spatial structure and distribution of flora and faunal assemblages in the marine environment (O'Hara 2001). The term is now commonly used to describe a set of structural and environmental conditions, both biotic and abiotic, that affects all species at a particular site (O'Hara 2001, Kearney 2006, Olenin and Ducrotoy 2006). For example, Underwood *et al.* (1991) defined six habitat types for subtidal rocky reefs based on their dominant floral and faunal species. Another way the term 'habitat' has been applied is to describe the structural, biological and environmental components of an ecosystem that can be mapped. For example, Ward *et al.* (1999) used information gained from interpreting aerial photographs to describe different habitats on the basis of the presence or absence of ecosystem components (e.g. vegetation type, depth range). Marine habitat types have been linked to variations in the spatial distribution of many species and can act as surrogates for species richness and general biodiversity (Faith and Walker 1996). It is important to note here that the use of surrogates should not to be looked at as an absolute measure of general biodiversity for an area, but a means of comparing biodiversity between areas for marine conservation, planning and reporting applications.

Biophysical variables, such as depth, ocean primary production and seabed sediment properties, were used as surrogates to predict the relative biodiversity at a broad regional scale within the Commonwealth waters of south-western Australia (Harris *et al.* 2008). At a more local scale, examples of this in the marine environment include being able to quantify the differences in the fish and invertebrate communities between vegetated and bare sand regions (Orth *et al.* 1984, Ferrell and Bell 1991, Connolly

1994). In the shallow coastal environments of southern Australia, Jenkins and Wheatley (1998) found that areas of bare sand supported different fish populations compared to adjoining areas of seagrass and algae. This also applies to the invertebrate communities found in these different habitats (Orth *et al.* 1984, Edgar and Shaw 1993). Nanami (2005) determined that very specific species-habitat relationships existed for coral reef fishes at a family level in Amitori Bay, Japan. These clear relationships between habitat types and species distributions provide evidence that habitat types can be used as a surrogate for biodiversity with a reasonable level of confidence (Vanderklift *et al.* 1998, Ward *et al.* 1999, O'Hara 2001).

1.3 Mapping marine benthic habitats

Historically, the mapping of marine benthic habitats has been done using traditional field methods, which are both costly and labour intensive. These methods can include the use of transects carried out by SCUBA divers (Hochberg and Atkinson 2000), remotely operated vehicles (Parry *et al.* 2003) or towed video (Kendall *et al.* 2005, Stevens and Connolly 2005) (Figure 1-1). All these systems collect data only about the particular locations they cover and rely on some form of interpolation, based on some assumptions, to fill any gaps between these points, which can result in a misrepresentation of the benthic habitat types present (Hochberg and Atkinson 2000). An example of this form of habitat modelling is the probabilistic mapping of the spatial distribution of different seagrass species in Cockburn Sound, Western Australia (Holmes *et al.* 2007).

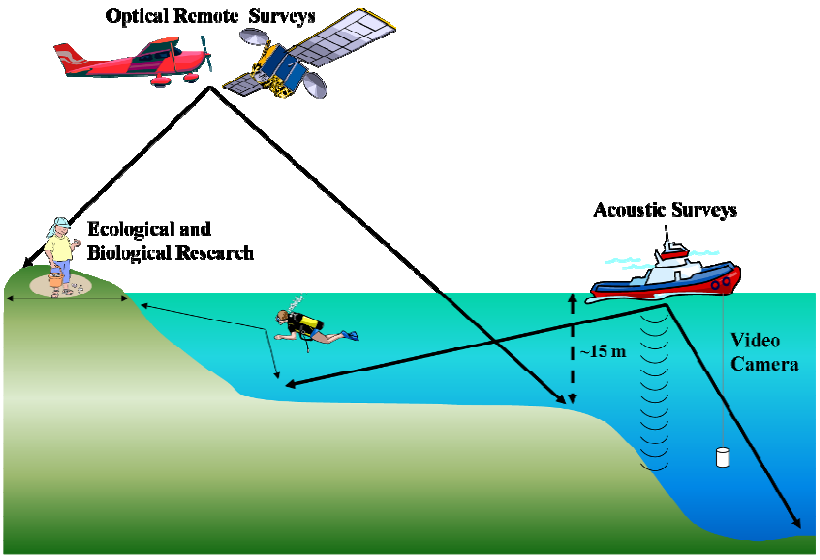

Figure 1-1: Conceptual diagram that illustrates how airborne and satellite remote sensing fits in with traditional ecological and biological research and acoustic surveys.

More recently, a range of remote sensing techniques, including optical (Armstrong 1993, Mumby *et al.* 1997, Dustan *et al.* 2001, Purkis *et al.* 2002, Louchard *et al.* 2003, Werdell and Roesler 2003, White *et al.* 2003, Naseer and Hatcher 2004) and acoustic (Sotheran *et al.* 1997, Kostylev *et al.* 2001, Brown *et al.* 2002, Freitas *et al.* 2003, White *et al.* 2003, Freitas *et al.* 2005, Jordan *et al.* 2005, Halley and Bruce 2007), have been used to map marine benthic habitats. Remote sensing is the science of obtaining information about an object or an area without any physical contact and can be either passive, which uses naturally available energy (e.g. aerial photography), or active, which provide their own energy source (e.g. acoustic techniques) (Lillesand *et al.* 2004). These sensors can be mounted on a range of different platforms including satellites, light aircraft and boats. They can collect data at a range of spatial, spectral and radiometric resolutions (Table 1-1). The spatial resolution refers to the size of each pixel or data point on the ground and can range from <1 m to >1 km. The spectral resolution refers to the wavelength intervals of the image data and has three broad categories, hyperspectral (greater than 20 narrow spectral bands each < 20 nanometres

wide), medium (3 – 20 broad spectral bands) and low (panchromatic or RGB analogue or digital images) (Table 1-1). The radiometric resolution refers to the sensitivity of the sensor to variations in the reflected light.

1.3.1 Acoustic remote sensing in the marine environment

Hydrographic surveys have long used acoustic data for ascertaining bathymetry and, more recently these, and other, acoustic techniques have been used successfully to map marine benthic, from deep water to shallow coastal waters. Three main types of acoustic sensors are used to map benthic habitats, namely, single beam echo sounders, multi-beam echo sounders and sidescan sonar (Table 1-1). A single beam acoustic ground discrimination system (AGDS) was used to map the benthic habitats of a small coastal section of Tasmania, Australia (Halley and Bruce 2007). White *et al*. (2003) used a AGDS to map coral reef classes in the Philippines using a hierarchical benthic habitat classification scheme that included mud, sand and a range of mixes of coral and algae.

The morphometric characteristics of some rocky reefs in Marmion Marine Park, Western Australia were mapped using multi-beam echo sounder bathymetric data (Lucieer 2007). Sidescan sonar data were used to map sea-bed assemblages in the English Channel, United Kingdom, by determining seven regional biotopes based on the acoustic data and relating these to species data collected using benthic grabs (Brown *et al.* 2002). Another application of sidescan sonar was habitat mapping of the Recherche Archipelago, Western Australia, which delineated the habitats into five broad categories including sand, seagrass and reefs (high and low profile) (Bickers 2003).

Table 1-1: Examples of remote sensing sensors applicable to marine benthic habitat mapping.

Data type	Sensor	Area mapped km^2hr^{-1}	Spatial resolution	Spectral resolution	Radiometric resolution
Aerial photography	Pan Stereo	> 10	Variable	Low	NA
	Colour stereo	> 10	Variable	Low	Variable
Airborne multi-spectral	SpecTerra DMSV Daedalus-1268 ADAR	> 10	0.5 – 3 m	Medium 350 – 2500 nm 3 – 20 bands	8 bit (256 levels)
Airborne hyperspectral	CASI HyMap	> 10	0.5 – 3 m	Medium 400 – 2500 nm > 20 bands	12 bit (4096 levels)
Satellite multi-spectral	Ikonos Quickbird	> 1000	1 – 4 m	Medium 400 – 1000 nm 3 – 4 bands	8 bit (256 levels)
	Landsat ETM Landsat TM SPOT XS IRS	> 1000	15 – 30 m	Medium 400 – 2500 nm 10 – 12.5 um 4 – 7 bands	8 bit (256 levels)
	SPOT VMI NOAA AVHRR	> 1000	1 km	Medium 400 – 2500 nm 10 – 12.5 um 4 bands	10 bit (1024 levels)
	SeaWifs	> 1000	1 km	Medium 400 – 885 nm 8 bands	10 bit (1024 levels)
Satellite hyperspectral	MODIS	> 1000	250, 500, 1000 m	High 400 – 2500 nm 10 – 12.5 um 36 bands	10 bit (1024 levels)
	Hyperion	> 1000	30 m	High 400 – 2500 nm 220 bands	10 bit (1024 levels)
	MERIS	> 1000	300 m	High 400 – 1000 nm 15 bands	10 bit (1024 levels)
Airborne laser altimeters	Variable	> 10	2 – 10 samples m^{-2}	NA	NA
Single beam echo sounder	QTC-View RoxAnn EcoPlus	1.5	0.1 – 100 m	NA	NA
Multi-beam echo sounder	Variable	5	0.1 – 100 m	NA	NA
Sidescan sonar	Variable	3.5	0.01 – 100 m	NA	NA
Video camera	Variable	0.2	0.01 – 1 m	NA	NA

Walker *et al.* (2008) used an approach which combined acoustic data, laser bathymetry and aerial photography to map coral reef habitats in Broward County, Florida. They used a classification scheme based on the NOAA scheme (Kendall *et al.* 2004), which did not include submerged vegetation, and were able to achieve an accuracy of 89.6% for the separation of unconsolidated sediments and coral reef / hard bottom. With further refinement of the coral reef category to linear reefs and colonised pavement the accuracy was only slightly reduced (88.1%).

The use of acoustics techniques has proved to be a reliable means of classifying benthic habitats, although the inability to discriminate between vegetation types is a major drawback. Likewise the vessels that acoustic sensors are mounted on are generally restricted to water deeper than 10 m, which means they are unable to map very shallow water or the land/water interface.

1.3.2 Passive optical remote sensing in the marine environment

Passive optical remote sensing records information about the radiant energy reflected from different objects on the earth's surface. When radiant energy (light) from the sun is incident on an object the light can be absorbed by, transmitted through or reflected by the object (Lillesand *et al.* 2004). The behaviour of the light reflected by an object is determined mostly by the roughness of that object. Those with a mirror-like surface are termed specular reflectors (the angle if incidence equals the angle of reflection), and those with rough surfaces act as diffuse reflectors, which means they reflect light uniformly in many different directions (Figure 1-2). In the natural environment, the surfaces of most objects are a combination of both, although in passive optical remote sensing, interest is predominantly in measuring the diffuse reflectance as it contains

information about the 'colour' of the object. It is the variations in the colour of object that allow for different objects to be distinguished in remotely-sensed data.

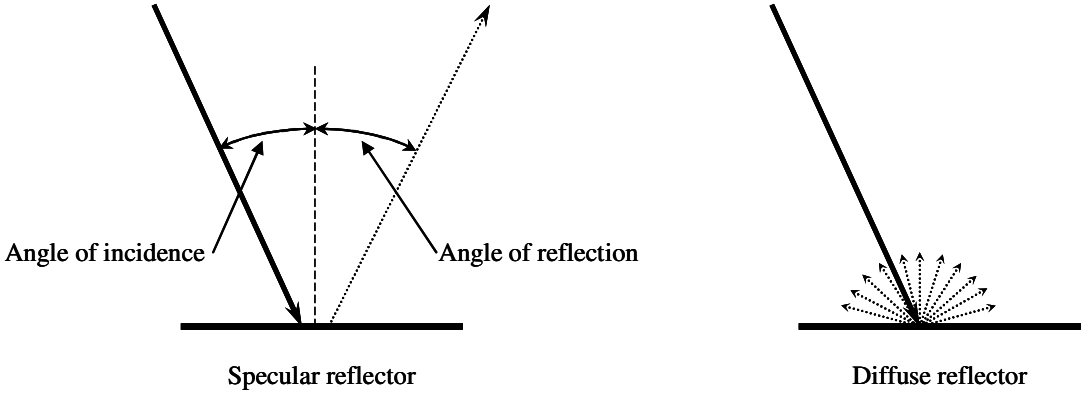

Figure 1-2: Conceptual diagram of the differences in the behaviour of reflected light between specular and diffuse reflectors (Adapted from Lillisand *et al.* 2004).

In the marine environment, reflected energy recorded by remote optical sensors consists of the combination of energy reflected by the atmosphere, the surface of the water, the water column itself and that transmitted through the water column and reflected by the seafloor (Figure 1-3). This adds an extra level of complexity when compared to optical remote sensing of the terrestrial environment.

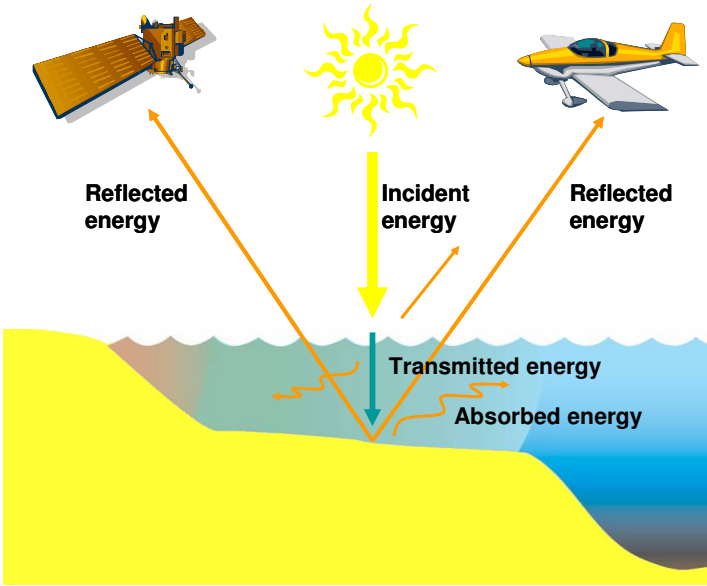

Figure 1-3: Conceptual diagram of remote sensing in the marine environment, highlighting the interaction of light with the water column.

Data from a range of passive optical sensors have been employed to map the spatial extent of shallow water marine benthic habitats at many locations around the world. Dekker *et al*. (2005) used a temporal series of Landsat 5TM and Landsat 7ETM satellite data to map the distribution of seagrass over time in Wallis Lake, a shallow coastal lake in NSW, Australia. They achieved accuracies up to 76% and were able to identify 11 vegetated substrate classes, three water types and bare sand. Mumby *et al*. (1998b) used CASI multi-spectral data to map coral reefs of the Turks and Caicos Islands, British West Indies, and were able to identify nine reef habitats, including algae, seagrass and coral. Their accuracy of 81% was significantly better that that achieved using Landsat or SPOT satellite imagery. Landsat data were also used to map the benthic habitats in Los Roques Archipelago National Park, Venezuela, and resulted in eight bottom types being identified, including sand, dense seagrass and reef communities, with an overall accuracy of 74% (Schweizer *et al.* 2005). The shallow water benthic habitats of Roatan Island, Honduras, were mapped using multi-spectral IKONOS data to identify six substrate classes including sand, coral, dense seagrass and a number of mixed classes, achieving an overall accuracy of 81% (Mishra *et al.* 2005b). One of the latest developments in remote sensing is airborne hyperspectral sensors, such as HyMap, which collect image data at higher spectral resolution (Kruse *et al.* 2000).

1.3.3 Hyperspectral remote sensing in marine environments

Hyperspectral sensors collect data at a high spectral resolution and often with a high spatial resolution. They record radiance values, as digital numbers, for every pixel in the image over numerous bands. For example HyMap records radiance data over 126 spectral bands that are ~15 nanometres (nm) in width. This provides the theoretical ability to map benthic habitat types by remote sensing to a much higher taxonomic

resolution than previously possible (Fyfe 2003). There are, however, several issues that need to be addressed before remote sensing, including hyperspectral, data can be used successfully in the marine environment. Firstly, the images have to be corrected for the confounding influence of the water column (Mumby *et al.* 1998a, Green *et al.* 2000). Secondly, the spectral separability of different habitat types, and the species that dominate them, needs to be determined and combined with the sensor's ability to detect these differences (Hochberg and Atkinson 2003, Hochberg *et al.* 2004).

To date, most habitat mapping using hyperspectral imagery has been restricted to shallow coral reef environments and freshwater systems, with reasonably clear water (Lesser and Mobley 2007). There has been limited work conducted in temperate waters, due to the generally poorer water clarity of most temperate marine environments. There has also been significant investigation into the spectral separability of the commonly found benthic substrates on coral reefs (Holden and LeDrew 1998, 1999, Hochberg and Atkinson 2000, 2003, Hochberg *et al.* 2003, Kutser *et al.* 2003, Hochberg *et al.* 2004, Karpouzli *et al.* 2004) and also in more temperate environments (Dekker *et al.* 2003, Fyfe 2003, Dekker *et al.* 2005). Such research is essential to understand the limits to which habitats can be identified using any spectral matching or unmixing classification algorithms on hyperspectral image data.

Lesser and Mobley (2007) implemented spectral matching and look-up table techniques to correct for the influence of the water column, estimate bathymetry and classify the benthic habitats for coral reefs near Lee Stocking Island, Bahamas. They used hyperspectral image data collected using the Ocean Portable Hyperspectral Imager for Low-Light Spectroscopy (Ocean PHILLS) sensor. They were able to map sand, corals

and mixed classes of seagrass/turfs/macrophytes and their work provides encouraging results for the potential of classifying of benthic habitats using hyperspectral imagery. Goodman and Ustin (2007) used AVIRS hyperspectral data in Kaneohe Bay, Hawaii and successfully corrected and classified the data to a maximum depth of 3 m using a physics-based semi-analytical and spectral unmixing approach to determine the relative contributions of sand, coral and algae to each pixel. Although their results were limited to shallow water, this work is indicative of the potential information that can be extracted from hyperspectral data when the influence of the water column is corrected for. Of particular relevance to this study is the work of Klonowski *et al*. (2007) who mapped the key benthic cover types of a section of temperate reef in Jurien Bay, Western Australia, using HyMap hyperspectral data. They were able to separate bare sediment, brown algae and seagrass using a physics-based, semi-analytical reflectance model that allowed for the extraction of bathymetry and the relative contributions of the three main benthic cover types. This work was the first application using hyperspectral imagery in temperate Western Australia and provided clear evidence that such data is an appropriate tool for broad-scale mapping of shallow water benthic habitats.

1.3.4 Classifying remotely sensed images

The classification of remotely sensed image data is the process of assigning categorical classes or a fractional value that represents the contribution from each of a number of possible classes (Goodman and Ustin 2007). There are two main types of classification methods for image data, namely, unsupervised and supervised (Lillesand *et al.* 2004). Unsupervised classification algorithms group image pixels into natural groups or clusters based on the similarity in their values while supervised classification techniques

use predefined values that describe different classes, to assign pixels to a categorical class.

Unsupervised classification techniques have the benefit of not requiring any *a priori* information about the region being mapped to produce a map that separates the pixels into discrete classes, which means that the natural groupings based on their spectral similarity are determined. However, these clusters or groups then need to be assigned to a class by the operator, which can result in subjective classifications. Call *et al.* (2003) applied the iterative self-organising data analysis (ISODATA) algorithm to classify the benthic substrate of a coral reef in Lee Stocking Island, Bahamans, using Landsat TM image data that had been corrected using the model developed by Lyzenga (Lyzenga 1978, 1981). The resulting clusters of pixels were assigned to a class based on field observations and achieved an overall accuracy of 74%. The ISODATA algorithm was also used to classify the coral reefs of Roatan Island, Honduras using Quickbird data that had been corrected for the influence of the water column (Mishra *et al.* 2006). The resulting clusters were assigned to benthic classes using the maximum likelihood approach and the final overall accuracy was calculated to be 81%. Joyce *et al*. (2004) also used the ISODATA algorithm as part of a project to integrate Landsat ETM+ derived and Reef Check coral reef classifications for the Capricorn Bunker Group on the Great Barrier Reef, Queensland.

Supervised classification techniques rely on the users having some prior knowledge about the classes to which pixels in the image data should be assigned and where these areas are located. In the case of benthic habitat mapping this implies knowledge of the likely benthic habitats that could occur in the image. The basic principle for supervised

classifications is that the values for each pixel are compared, using a classification algorithm, to the values that describe the training classes and the class with the best match is assigned to the pixel. One commonly applied technique is the maximum likelihood classification which calculates the mean vector and the covariance matrix for the values for each user-defined training class (benthic habitat type). From this the probability that a particular pixel belongs to a particular class is calculated and the class with the highest probability is assigned to the pixel. Purkis and Pasterkamp (2004) used this approach when classifying Landsat TM data to map the coral reefs of Marsa Shagra, located in the central Egyptian Red Sea, using *in situ* data to train the algorithm. Naseer and Hatcher (2004) also applied a maximum likelihood classification algorithm to Landsat ETM+ when creating an inventory of coral reefs in the Maldives, based on training data extracted directly from the image using ground validation locations to allocate classes to extracted signatures.

Spectral matching approaches, which match spectral signatures collected *in situ* to image pixel values, are another form of supervised classification (e.g. Lesser and Mobley 2007). These approaches generally use a spectral distance measure, such as spectral angle, to determine how similar a pixel's spectrum is to a reference spectral signature from a spectral library and the pixel is classified to the class with the best match (Lillesand *et al.* 2004). Another approach is linear spectral mixture analysis (e.g. Goodman and Ustin 2007) which is based on the assumption that a pixel's spectrum is a linear mixture of the spectral signatures of the substrate classes present in the pixel (Chang *et al.* 2002, Zhang *et al.* 2005, Small and Lu 2006). Both of these approaches require *a priori* knowledge about the habitat components that will be present in the

image being classified and a spectral library of these components, which are often transferable to different location locally and around the world.

All the methods mentioned have been applied successfully to a range of remotely sensed data to map marine benthic habitats, but never result in a perfect solution. The accuracies of the resulting maps can often be significantly improved with some form of contextual editing (Mumby *et al.* 1998a). The preferable method of contextual editing is one that is systematic and justified by ecological or local knowledge, for example, reclassifying pixels from seagrass to macroalgae at highly wave exposed sites where seagrass is not known to occur. There are many documented relationships between variables such as depth, benthic complexity and exposure to waves and the distribution of habitats in the marine environment (e.g. Garza-Perez *et al.* 2004) and as such, contextual editing can use these relationships to guide the reclassification of pixels. Lauer and Aswani (2008) utilised local indigenous knowledge to guide the supervised classification of marine benthic habitats of Roviana Lagoon, Solomon Islands.

1.4 Study rationale and aims

The overall aim of this project is to develop a toolkit to use hyperspectral image data to map the spatial distribution of shallow benthic habitats in a temperate marine environment, using a library of spectral signatures for the dominant habitat components. The general hypothesis for this project is that hyperspectral data can be used to create habitat maps for shallow temperate marine systems in Western Australia, based on the dominant sub-tidal marine benthos, at a scale that is both ecologically relevant and applicable to the management of these areas.

The project was carried out at Rottnest Island Reserve (RIR) as there was HyMap hyperspectral data available for the reserve that had been collected opportunistically in April 2006 by the HyVista Corporation. Added to this, there was a need for more comprehensive benthic habitat mapping to build on existing maps in order to assist with the management of the marine environments within the reserve. Furthermore, the unusually clear waters, a result of the pole-ward flowing Leeuwin Current provided an appropriate environment to develop these techniques.

The project was undertaken in four main steps. Firstly, a benthic habitat classification scheme was developed that was based on the known ecology of the region and could also be applied spatially at the scale at which the hyperspectral image data were captured. A hierarchically structured classification scheme was developed that attempted to capture the naturally occurring structure in the spatial arrangement of the benthic habitats. Secondly, a digital bathymetry model was developed for the RIR using existing echo-sounding data to form the basis for the creation of a range of abiotic environmental variables to assist with defining the benthic habitats, based on their documented influence on spatial distribution of different habitats. Thirdly, a library of spectral signatures for the dominant components of the benthic habitats defined in the classification scheme was created using signatures collected *in situ.* These data were then subjected to spectral separation analysis that determined the best method of separating the benthic habitats based on their spectral signatures and provided the basis for the development of a classification algorithm to apply to the image data. The final step was the application of the newly developed classification algorithm, in combination with the spectral library, to the hyperspectral image data to identify the habitats present in each pixel to create classified benthic habitat maps for Rottnest Island Reserve.

These habitat maps will be important to the planning and management of the Rottnest Island Reserve as they provide an inventory of both representative and unique habitat types. Such maps also provide a useful tool for the design of ecological sampling strategies. The innovative approaches taken in this study will also be of benefit to remote sensing practitioners with an understanding of marine ecology that use hyperspectral data to map marine habitats.

2 Study site description and habitat classification scheme

2.1 The nearshore marine environment of south-western Australia

The nearshore coastal environments of south-western Australia are located along a gently seaward sloping continental shelf which ranges in width from 43 to 93 km. It is influenced by both large scale climatic and oceanographic processes including winds, waves, ocean currents and tides (Lemm *et al.* 1999, Sanderson *et al.* 2000).

The region experiences a Mediterranean climate, with hot dry summers (December – February) and cool wet winters (June – August), and these weather patterns are predominantly driven by a subtropical belt of high pressure that moves southward over the region during the summer and northward during the winter (Gentilli 1972). The region receives the majority of its rainfall during the winter months as a consequence of the cold fronts that approach from the west and travel east across the continent (Hope *et al.* 2006). The prevailing wind conditions during the summer are typically offshore (easterly) in the morning and onshore (south-westerly) during the regularly occurring afternoon sea breeze. Although the sea breeze is infrequent during the winter, onshore winds occur associated with the regularly occurring cold fronts (Clarke and Eliot 1983, Masselink and Pattiaratchi 2001).

The southward flowing Leeuwin Current is the dominant oceanographic feature along the Western Australian coastline (Pearce 1991, Ridgway and Condie 2004). During winter, the Leeuwin current transports warm, low salinity, low nutrient water southward along the Western Australian coast (Cresswell and Peterson 1993, Cresswell 1996). This oceanographic feature leads to oligotrophic conditions with generally low concentrations of chlorophyll in the water column (Hanson *et al.* 2005). During

summer, the Leeuwin Current weakens and the shelf is influenced by the Capes Current, a wind-driven current that flows northward from Cape Leeuwin (Gersbach *et al.* 1999, Pearce and Pattiaratchi 1999). The mean monthly sea temperatures in coastal waters off Perth range from 15° to 23° C with an increase in temperature of up to 3° C in the offshore regions, such as Rottnest Island, affected by the Leeuwin Current (Godfrey *et al.* 1986, Pearce *et al.* 1999).

The wave climate of south-western Australia is dominated by persistent ocean swells that typically approach from a south to south-westerly direction in summer and a west to south-westerly direction in winter and have a mean deep water wave height of 2 – 3m (Lemm *et al.* 1999, Sanderson *et al.* 2000). The nearshore regions along much of the coast of south-western Australia are protected from the full impact of this offshore wave energy by a chain of islands, reefs, banks and sills that run parallel to the shore (Clarke and Eliot 1983, Hegge *et al.* 1996). These features act to attenuate up to 90 % of the offshore wave energy before it reaches the shoreline (Hegge *et al.* 1996).

As a result of this attenuation of the offshore wave energy, the locally generated nearshore wave energy can have substantial impact on the nearshore coastal environment. Prevailing winds are significant drivers of both locally generated incident wave energy and nearshore currents. The wave-field set up during a typical sea breeze, which blows almost parallel to the coast, can achieve significant wave heights up to 0.9m and increase nearshore currents from <0.5 ms^{-1} to 1.0 ms^{-1}, which has an impact on suspended sediment concentrations and longshore sand transport volumes (Pattiaratchi *et al.* 1997).

The tidal regime along the south-western coastline of Australia is mixed , but mainly diurnal and is described as micro-tidal, with an average range of only 0.7 m (Sanderson *et al.* 2000, Department of Defence 2009). In many cases fluctuations in the sea-level generated by other forces, such a barometric pressure or storm surges, are greater that that resulting from tidal forces, and thus play a greater role in shaping the nearshore environment than tides (Sanderson *et al.* 2000).

The nearshore marine environment of south-western Australia is considered to be a region of bio-geographical overlap, between the warm temperate biota of southern Australia and the tropical biota of northern-western Australia, a result of the influence of the Leeuwin Current which disperses tropical species southwards (Wells and Walker 1993). The interim marine and coastal regionalisation for Australia (IMCRA) defined Perth as the southern extent of the central west coast region and the northern extent of the Leeuwin-Naturalist region (Commonwealth of Australia 2006). The nearshore flora is dominated by seagrass and macroalgae assemblages, with both being amongst the most speciose in the world (Kirkman 1997, Kendrick *et al.* 2004, Carruthers *et al.* 2007). Macroalgal assemblages typically occur on nearshore reefs, comprised of either granite or limestone, and are found along the entire south-west coat of Australia (Wernberg *et al.* 2003b, Kendrick *et al.* 2004). The dominant features of these macroalgal assemblages are the canopy forming *Ecklonia radiata* and *Sargassum* species (Kendrick *et al.* 2004). Although there have been 18 species of seagrasses recorded in the region, mono-specific or mixed-species meadows of four species, *Posidonia sinuosa*, *Posidonia australis, Amphibolis griffithii* and *Amphibolis antarctica* are dominant (Department of Environmental Protection 1996). There are 528 neritic species of fish known to occur in the Perth region of the West Australian coast and of

those 78 are endemic to Western Australia (Fox and Beckley 2005). There are a large number of invertebrate taxa known to occur on reefs in the Perth region, with species of Mollusca being some of the most numerically dominant (Murphy *et al.* 2006). Species of Bryozoa, Cnidaria, Crustacea, Echinodermata, Porifera and Ascidiacea are also regularly recorded.

2.2 Rottnest Island

2.2.1 Introduction

This study was carried out in the waters surrounding Rottnest Island (32°00' S, 115°30' E) which lies approximately 18 km offshore from Fremantle, Western Australia (Figure 2-1). Rottnest Island is an iconic location in Western Australia, being a popular destination for Western Australians, Australians and international tourists alike, with more than 500 000 visitors a year (Rottnest Island Authority 2007). The island supports a range of recreational activities linked to the marine environment which include recreational fishing, SCUBA diving, snorkelling, surfing and boating (Rottnest Island Authority 2003). There are a large number of privately owned (864) and rental (35) boat moorings located in protected bays around the island. These moorings provide safe anchorage for some of the many private boats that visit the reserve annually. Vessels with no access to a fixed mooring anchor in the many bays around the island, which can result in damage to the benthos (Hastings *et al.* 1995, Rottnest Island Authority 2003, Milazzo *et al.* 2004).

Rottnest Island is managed by the Rottnest Island Authority as an A Class Reserve under the Land Administration Act 1997 (RIA). The marine regions of the reserve extend approximately 800 m from the shoreline, encompass an area of 3,828 ha and are

zoned as general use, recreational, demersal sanctuary or sanctuary zones (Figure 2-1). There are no special restrictions in the general use zone, while the recreational zone prohibits any net fishing and discharge of waste from boats and the sanctuary zone prohibits all extractive activities, placement of moorings and the discharge of waste from boats (Rottnest Island Authority 2003). One of the key aims of the management plan is to maintain and protect the natural environment and zoning is one of the management tools used to achieve this goal (Rottnest Island Authority 2003).

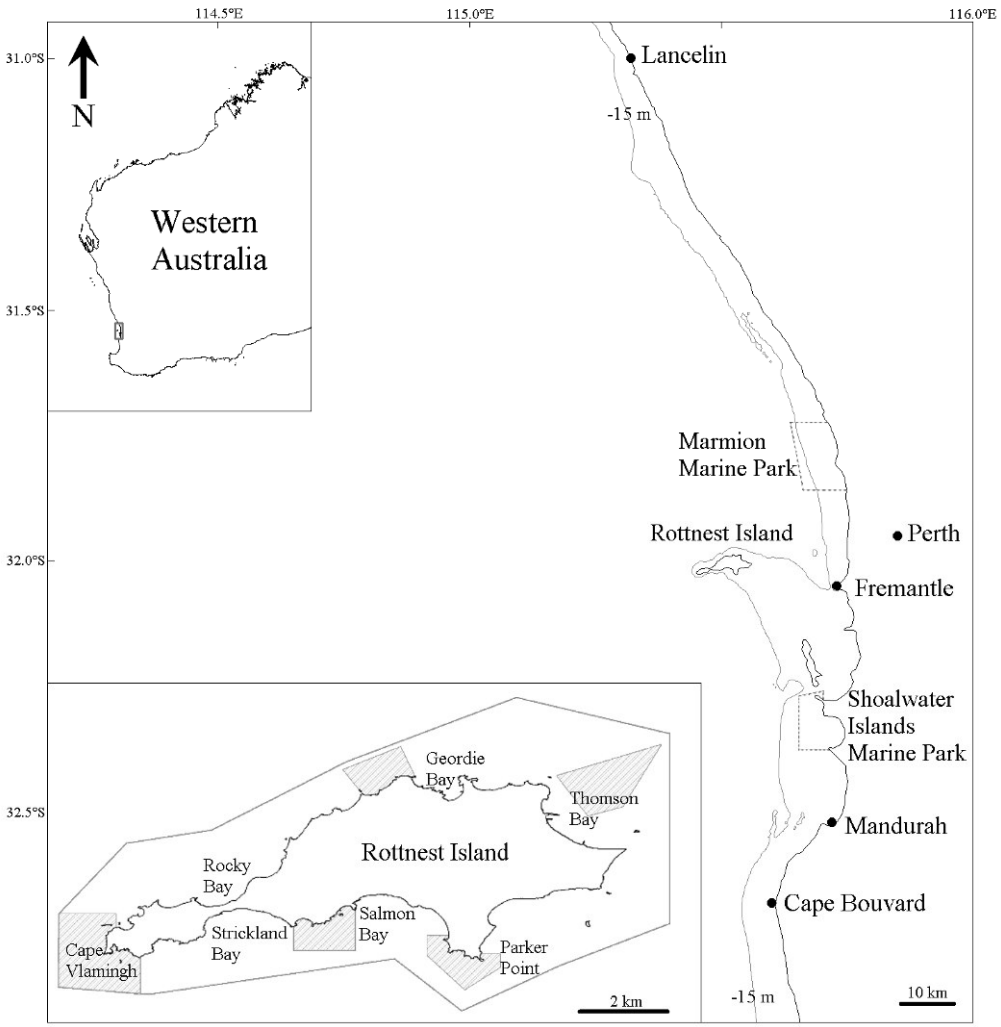

Figure 2-1: Map indicating the location of the Rottnest Island study site in south-western Australia and key locations at Rottnest Island, with reserve boundaries (grey line) and sanctuary zones (shaded) indicated.

2.2.2 The nearshore marine environments of Rottnest Island

Rottnest Island is orientated in a generally east-west direction and is 11 km long and 5 km across at its widest point. The island is part of a series of rocky ridges known collectively as the Rottnest Shelf, occurring at the eastern boundary of this feature, which forms part of the Perth Basin (Brooke *et al.* 2006). These ridges are both emergent and submarine and extend from Cape Bouvard to Lancelin (Searle and Semeniuk 1985) (Figure 2-1). The majority of the shelf consists of Tamala Limestone which comprises coastally derived carbonate sediment (Playford and Leech 1977, Brooke 2001). The waters surrounding the island vary in depth from exposed intertidal limestone platforms to subtidal regions >40 m deep. The intertidal platforms are a dominant feature of the coastline at Rottnest Island, making up a greater proportion of the coastline than sandy beaches and are typical of the coastline of central Western Australia, from Bunbury to Geraldton (Wells and Walker 1993). The sediments in the Perth region are dominated by cool-water and subordinate sub-tropical biogenic carbonate (James *et al.* 1999).

The majority of the marine habitats at Rottnest Island are exposed to moderate to high wave action during the typical winter storms, which generally approach from a south-westerly direction (Searle and Semeniuk 1985). The swell refracts around most of the island to impact the majority of the island's coast, with the exception of the bays located at the eastern end of the island (Wells and Walker 1993). The waters around Rottnest Island are typically oligotrophic due to the influence of the Leeuwin Current (Cresswell and Peterson 1993, Cresswell 1996). At times of peak flow, the warm Leeuwin Current waters bathe the western portion of the island and have had a significant impact on the diversity of flora and fauna found around the island (Morgan and Wells 1991). It has

also been found to influence the dispersal of tropical species as far east as the Great Australian Bight (Garrey *et al.* 1981). Sea temperatures at Rottnest Island generally range from 18 – 23ºC throughout the year (Hodgkin *et al.* 1959).

The intertidal platforms at Rottnest Island can vary in width from 1 – 100 m and in height from the mean low water mark to almost mean sea level (MSL). On the landward end of the platforms there is often a 1 – 2 m undercut rock face and at the seaward edge commonly ends abruptly with either a deep undercut ledge or a sloping ramp (Playford and Leech 1977). The zonation evident in the biota typically associated with these platforms tends to vary slightly depending on the width and slope of the platform (Hodgkin *et al.* 1959, Black *et al.* 1979, Scheibling 1994). The regions above the high water mark are dominated by periwinkles followed by limpets down to the MSL and then *Patelloida alticoststa* down onto the platform itself. The rock surfaces directly above the platform, which are regularly inundated by wave and tidal action, often support macroalgae during the winter, the dominant species being *Enteromorpha* sp., *Ulva* spp., *Chaetomorpha linum* and *Cladophora* spp.. The platforms themselves have four main zones starting at the landward edge of the platform, the *Patelloida* zone, the *Jania* zone, the brown algae zone and the *Lithothamnion* zone. The *Patelloida* zone includes large areas of the platform grazed bare by *P. alticoststa* and is typically in regions where the water drains at low tide. The *Jania* zone can also cover large areas of the platforms, predominantly where shallow water remains at low tide and, is dominated by the coralline algae, *Jania fastigiata* which forms a turf-like cover that acts to trap sediment on the platform and provides habitat for small crustaceans and polychaetes. The brown algae zone is covered by foliose brown algae, predominantly Fucoids such as *Sargassum* spp. and *Cystophora unifera*, and the red algae *Pterocladia capillacea*

and *Hypnea musciformis* that provide habitat for larger browsing gastropods. The L*ithothamnion* zone is covered by encrusting coralline algae, and is often better developed on platforms exposed to greater wave action. Large browsing molluscs, such as *Haliotis roei*, the anemone *Isanemonia australis* and the barnacle *Balanus nigrescens* are often associated with this region (Hodgkin *et al.* 1959).

The marine benthos of temperate south-western Australia comprises a high diversity of macroalgae and this is especially true for Rottnest Island where 222 species of Rhodophyta, 54 species of Chlorophyta and 71 species of Phaeophyta have been recorded in both the intertidal and subtidal regions (Huisman and Walker 1990, Wells and Walker 1993, Phillips *et al.* 1997). The subtidal limestone reefs of Rottnest Island can be separated into two broad categories based on their vertical relief; high relief (>1 m) or low relief (<1 m) (Harman *et al.* 2003, Toohey 2007). They are typically dominated by either canopy forming macroalgal species or lower growing foliose algal species, often referred to as algal turf. The canopy is generally a mix of *Ecklonia radiata* and *Sargassum* species, although *Scytothalia doryocarpa* and *Cystophora* sp. are often found forming part of the canopy (Wells and Walker 1993, Sanderson 1997, Wernberg *et al.* 2003b). At Rottnest Island, *E. radiata* has been found to occupy up to 20% of the shallow subtidal regions and occurs in depths to >30 m, while *Sargassum* species occur discontinuously in both the intertidal and the subtidal regions and display seasonal growth patterns, with peak abundance during spring and summer (Kendrick 1993, Wells and Walker 1993). Eight species of *Sargassum* have been recorded at Rottnest Island and these are almost always found growing as mixed assemblages. *Sargassum* beds occur on sand-inundated, subtidal rock platforms, as a border along intertidal reef platforms and in protected bays (Kendrick 1993). *Sargassum* is also

found growing in mixed stands with *E. radiata* and *Cystophora* species at more exposed sites (Kendrick 1993). Low growing foliose algae, filamentous turfing algae and coralline algae, both encrusting and articulated, also occur at Rottnest Island and occur primarily in the gaps between the *E. radiata* plants (Wells and Walker 1993, Kendrick *et al.* 1999, Phillips *et al.* 2006). The species diversity of canopy algae and the associated understorey algae is linked to factors such as topographic complexity and exposure to wave action, with greater diversity occurring in more exposed sites (Kendrick *et al.* 2004, England *et al.* 2006, Toohey 2007).

The invertebrate fauna of the subtidal rocky reefs in the Perth region includes large mobile, sessile, epifaunal and infaunal invertebrate species. O'Hara and Poore (2000) recorded 356 species of echinoderms and decapods in the Perth region and indicted that the high species richness was due to the region being an area of overlap between the tropical and southern faunas. There are 86 species of echinoderms recorded at Rottnest Island and approximately half of these are associated with subtidal rocky reefs (Marsh and Pawson 1993). In the Perth region the dominant species of herbivorous invertebrates include the sea urchins, *Heliocidaris erythrogramma*, *Phyllacanthus irregularis* and *Centrostephanus tenuipinus*, and the gastropods *Turbo torquatus*, *Australium squamifera* and *Haliotis scalaris* (Vanderklift and Kendrick 2004). Both *P. irregularis* and *C. tenuipinus* are most commonly found on the steep, complex rock face surfaces around the base of reef structures while *T. torquatus* and *A. squamifera* are mostly restricted on open flat reef surfaces. *H. erythrogramma,* on the other hand, can be found across both reef habitat types (Vanderklift and Kendrick 2004). A total of 189 species of marine crustaceans are known from Rottnest Island, with 13 of these endemic to the island (Jones and Morgan 1993). Of the molluscs found at Rottnest Island, 16%

are endemic to the Perth region, half have southern affinities and the rest are Indo-West Pacifc species (Morgan and Wells 1991). The underhangs of the rocky reefs are inhabited mostly by sessile fauna including sponges, hydroids, zoanthids, alcyonarians, corals, gorgonians, and ascidians (Hodgkin *et al.* 1959).

The subtidal limestone reefs at Rottnest provide an ideal habitat for the commercially important rock lobster *Panulirus cygnus* (Howard 1988, Babcock *et al.* 2007). Fish species that are often found in the reef undercuts or caves include *Shuetta woodwardi*, *Psammaperca waigiensis* and *Apogon victoriae* (Howard 1989). The reef margins often support herbivorous fishes such as *Parma occidentalis*, *Kyphosus sydneyanus* and *Odax cyanomelas* (Howard 1989). Other dermersal species found on these reefs include *Scorpis georgianus* and *K. cornelli* which are often associated with shallow limestone platforms around the island (Berry and Playford 1992). Several pelagic fish species, such as *Arripis georgianus*, *Pomatomus saltatrix*, *Pseudocaranx dentex* and *Sphyraena novaehollandiae*, are also often found around reefs (Hutchins 1979). A creel survey conducted over 12 months at Rottnest Island recorded 33 fish species from 25 families being caught by recreational anglers (Smallwood *et al.* 2006).

Nine species of seagrass have been recorded at Rottnest Island, the dominant species belonging to the genera *Posidonia* and *Amphibolis* (Huisman and Walker 1990, Wells and Walker 1993). *Posidonia sinuosa, P. australis, Amphibolis antarctica* and *A. griffithii* all form mono-specific meadows and are considered to be 'climax' species (Lavery and Vanderklift 2002). Although meadows are typically mono-specific, all nine species can be found in mixed meadows. Seagrasses at Rottnest Island are

restricted to sandy substrates and are generally found in the sheltered bays and areas protected by reefs (Wells and Walker 1993).

The invertebrate and fish assemblages in seagrass habitats at Rottnest Island are more species rich than adjacent bare sand habitats (Edgar and Shaw 1993). Further to this, Jernakoff and Nielsen (1998) determined that the epifaunal invertebrate assemblages were more diverse in *Amphibolis griffithii* meadows when compared to *Posidonia sinuosa* meadows, a feature attributed to the greater level of structure in *A. griffithii* meadows. Some of the most common species of epiphytic algae species found on *P. sinuosa* are *Ceramium monocanthum*, *Laurencia filiformis*, *Entromorpha* spp., *Giraudia* spp and *Metagoniolithon stelliferum.* Common epiphytic algae on *A. griffithii* are *Herposiphonia seccunda*, *M. stelliferum*, *Hypnea cervicornis*, *L. filiformis*, *Diacranema* spp. and *Haliptylon roseum* (Jernakoff and Nielsen 1998). Amphipods are the most common invertebrates associated with both seagrass species, being found in greater density in *P. sinuosa* meadows, while gastropod grazers, epifaunal bivalves and polychaetes all occur at lower densities among both seagrass species (Jernakoff and Nielsen 1998).

Species of fish which have been found to be associated with *Posidonia* meadows at Rottnest Island include *Spratelloides robusta*, *Siphonognathus radiatus*, *Halichoeres brownfeldii* and *Penicipelta vittiger* (Edgar and Shaw 1993). Seagrass meadows that are predominantly *P. sinuosa* are typically occupied by a greater number of species at higher densities than *A. griffithii* or *Posidonia coriacea* meadows (Hyndes *et al.* 2003). Species that were found almost predominantly in *P. sinuosa* meadows included *Apogon rueppellii*, *Acanthaluteres spilomelanurus* and *Cochleoceps viridis*, while *Odax*

acroptilus and *Pelsartia humeralis* occurred predominantly in *A. griffithii* meadows (Hyndes *et al.* 2003).

Twenty six species of corals have been recorded at Rottnest Island, with only *Pocillopora damicornis* occurring at a reef scale (Vernon and Marsh 1988, Wells and Walker 1993). The other species occur only as isolated colonies, and not at a scale detectable using remotely-sensed data. Other benthic fauna such as sponges and sea fans also exist at Rottnest, but are not detectable using remote sensing techniques as they often occur under ledges, in deeper water or occupy too small an area.

The Southern Metropolitan Coastal Waters Study (Department of Environmental Protection 1996) produced a map of the habitats of the Perth coastal waters between Mandurah, in the south, to just north of Rottnest Island. Imagery was obtained in February 1993 using a Geoscan multi-spectral scanner mounted in a light aircraft at a spatial resolution of approximately 5 m (Ong *et al.* 1998). Within the RIR the marine benthic habitats were classified into five classes; inshore coarse sand, offshore coarse sand, intertidal reef platforms, macroalgae (subtidal reefs) and seagrass meadows (Figure 2-2). These classes were all accounted for in the habitat classification scheme for the present study and provide a useful guide against which to validate the new hyperspectral imagery classifications produced from this study.

2.3 A benthic habitat classification scheme for south-western Australia with a focus on Rottnest Island

Three common and important features of most ecosystems are their diversity, complexity and heterogeneity (Steneck *et al.* 2002, Wu and David 2002). To be able to quantify and classify ecosystems, some form of order or structure needs to be rendered

within this complexity. Hierarchy theory, postulates that the spatial patterns within natural landscapes are a result of non-linear interactions between the biotic and abiotic components of the system. This leads to the assumption that most stable ecosystems are hierarchically structured (Cullinan *et al.* 1997, Wu and David 2002). Any hierarchical structure used to define the patterns and processes within any ecosystem will contain subjectively defined cut-offs between levels, which may result in some errors, but these should be outweighed by the information gained about patterns in the ecosystems (Cullinan *et al.* 1997).

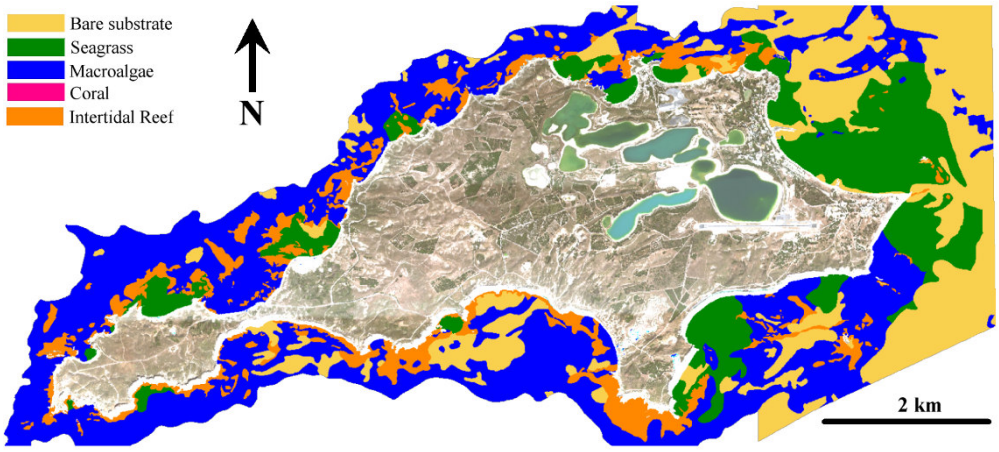

Figure 2-2: The benthic habitat map produced as part of the Southern Metropolitan Coastal Waters Study (Ong *et al.* 1998). Map has been clipped to areas < 15 m depth.

Hierarchy theory not only provides an appropriate framework to describe spatial patterns within ecosystems, but also allows description and examination of these patterns within remotely-sensed data (Hay *et al.* 2001). Wu (1999) examined the integration of hierarchical theory and patch dynamics as a means of both simplifying and gaining greater understanding of complex ecological systems and determined that the use of remote sensing and GIS techniques was indispensable in this process, especially when analysing the spatial dynamics of systems over large geographical

areas. Mumby and Harbourne (1999) also suggested that hierarchical habitat classifications were the most appropriate when classifying remotely sensed images.

A classification scheme was developed to describe the marine benthic habitats of Rottnest Island by accounting for the known dominant habitat components (Figure 2-3; Table 2-1). The scheme was organised into four levels in a nested hierarchical manner, with each successive level providing greater detail about the habitat. Level 1 separated the habitats into those that consist of bare substrate and those which contain living organisms, referred to as bio-substrate. Level 2 separated bio-substrate into mixed algae, seagrass and corals. These three categories all represent separate benthic habitat types found in Rottnest Island Reserve (Wells and Walker 1993, Department of Environmental Protection 1996, Rottnest Island Authority 2003). From a remote sensing perspective, this first distinction is highly desirable as in most shallow coastal environments regions of bare sand are clearly delineated in remotely sensed data. The reflectance signature of sand is under most circumstances significantly brighter than that of vegetated regions. This makes it relatively simple to separate these regions within the remotely sensed data.

Level 3 split the macroalgae into canopy forming algae and algal turf. Canopy forming algae found at Rottnest Island are all large brown algae (Phaeophyta), which made their grouping into the same category an obvious choice for a scheme designed to be applied to remotely sensed data as the spectral signatures, based on colour, will be similar. The mix of algal species which makes up the algal turf category can come from any of the three major algae groups, namely green (Chlorophyta), brown (Phaeophyta) and red

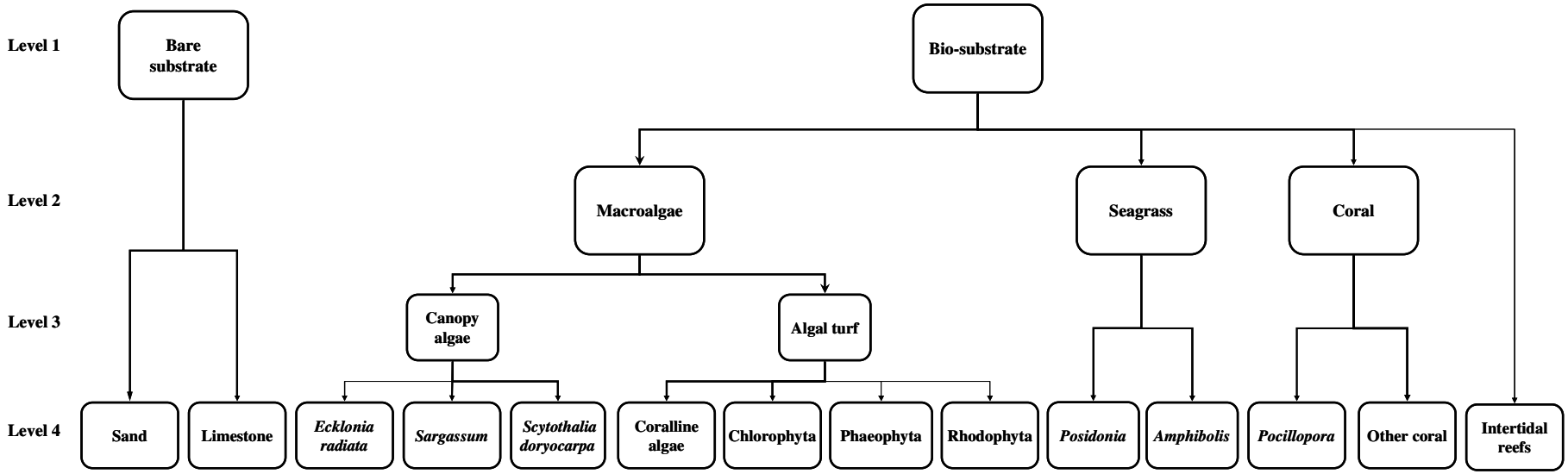

Figure 2-3: Hierarchical classification scheme developed for the marine benthic habitats of Rottnest Island.

Table 2-1: Description of the habitats defined by each level within the nested hierarchical classification scheme for Rottnest Island Reserve.

Habitat class	Description	Habitat class	Description
Level 1		*Level 4(continued)*	
Bare substrate	**Bare regions of sand or limestone, with no significant plant life**	***Ecklonia***	**Canopy algae habitats dominated by *Ecklonia radiata***
Bio-substrate	**Regions that contains living organisms**	***Sargassum***	**Canopy algae habitats dominated by *Sargassum* species**
Level 2		***S. doryocarpa***	**Canopy algae habitats dominated by *S. doryocarpa***
Macroalgae	**Macroalgae dominated habitats**	**Coralline algae**	**Algal turf habitats dominated coralline algae**
Seagrass	**Seagrass dominated habitats**	**Chlorophyta**	**Algal turf habitats dominated by foliose green algae**
Coral	**Coral dominated habitats**	**Phaeophyta**	**Algal turf habitats dominated by foliose brown algae**
Level 3		**Rhodophyta**	**Algal turf habitats dominated by foliose red algae**
Canopy algae	**Macroalgae habitats dominated by canopy forming species**	***Posidonia***	**Seagrass habitats dominated by *Posidonia* species**
Algal turf	**Macroalgae assemblages not dominated canopy forming species**	***Amphibolis***	**Seagrass habitats dominated by *Amphibolis* species**
Level 4		***Pocillopora***	***Pocillopora damicornis* coral colonies**
Sand	**Bare regions dominated by sand**	**Other coral**	**Other coral species forming colonies**
Limestone	**Bare limestone reefs or platforms**	**Intertidal reef**	**Intertidal reefs**

(Rhodophyta). The feature that most clearly separated the canopy and algal turf categories was the absence of large canopy-forming, brown algae.

Level 4 made the distinction between bare sand and bare limestone platforms. The 'canopy' category was split into habitats dominated by either *E. radiata*, *Sargassum* species or a mixture of these two, *S. doryocarpa* and *Cystophora* species. The algal turf category separated those habitats dominated by coralline, foliose green, foliose brown and foliose red algae. At Level 4 the 'seagrass' category of the classification scheme was split into those habitats dominated by either *Posidonia* or *Amphibolis* species. Of the corals, only *Pocillopora damicornis* occurs at Rottnest Island, at a spatial scale large enough to be potentially detected in remotely sensed data and thus only one species and a general grouping were listed at Level 4 of the classification scheme. Intertidal reef platforms were separated out as a separate class as they are often obscured by breaking waves in remotely sensed imagery in exposed coastlines (e.g. Anderfouet *et al.* 2004) or dominated by *Ulva*, a seasonal green macroalgae (Underwood and Kennelly 1990).

2.4 Discussion

The habitat classification scheme was designed using knowledge about the marine benthic ecology of south-western Australia, including specific work carried out at Rottnest Island. Although no high taxonomic resolution map of the marine benthic habitats of Rottnest Island exists, the typical habitats that occur there are well known (Kendrick 1993, Department of Environmental Protection 1996, Kendrick *et al.* 1999, Kendrick *et al.* 2004). In addition, general patterns and associations between the typical components of benthic habitats in temperate waters of the Australian coast are well described (Underwood and Kennelly 1990, Underwood *et al.* 1991, Melville and

Connell 2001). Organising this information within the framework of a nested, hierarchical classification system allowed the naturally occurring heterogeneity to be captured.

Wells and Walker (1993) indicated that the subtidal benthic habitats of Rottnest Island Reserve were typically dominated by either mixed algal assemblages, seagrass meadows or bare substrates. This was incorporated into the present scheme which separated the bare substrate and those containing living organisms, i.e. bio-substrate. This first split was an intuitive way to separate the benthic habitats for a number of reasons that link to both the ecology and remote sensing applications. By creating a split at this basic level, the scheme can easily be adapted to include other biota, such as sponges, making the scheme adaptable to other locations or allowing it to be extended to deeper waters using other mapping techniques.

Ecologically, bare and bio-substrates provide different habitats and support different communities (Orth *et al.* 1984, Ferrell and Bell 1991, Connolly 1994). The invertebrate and fish assemblages in seagrass habitats at Rottnest Island are more species rich and showed greater productivity than adjacent bare sand habitats (Edgar and Shaw 1995). Orth *et al.* (1984) cite numerous examples from around the world of significant differences in the fish assemblages associated with seagrass meadows and adjacent bare sand regions. For example, in a study from a southern Australian embayment, Jenkins and Wheatley (1998) found significant differences in the species richness of fish assemblages between vegetated regions and bare sand, citing that the main reason for this difference as the presence of structure in vegetated regions. This study further determined that the species richness of fish assemblages decreased from seagrass

habitats to algal habitats and finally to bare sand. Even with some closely related species of fish, such as whiting (Sillaginidae), the different species often preferentially utilise different habitats. Hyndes *et al.* (1996) found some whiting species, such as *Sillaginodes punctata*, mostly to occur in more protected nearshore habitats, while *Sillago bassensis* preferentially occupied more exposed sites.

The split at the second level of the scheme, where the bio-habitat regions were separated into mixed algae assemblages, seagrass and corals, was based on clear evidence of each of these being separate habitat types and, each supporting different communities (Edgar and Shaw 1993). This was essentially the basis of the classes at Level 2 of the scheme, with the addition of corals. Although corals are not a dominant feature in Rottnest Island Reserve, they do occur and were therefore included. In addition to this, having a category for corals at this level within the scheme allows it to be adaptable to other locations along the tropical coastline of Western Australia (e.g. Ningaloo Reef).

Seagrass habitats typically occur on sandy substrates in protected regions and are known to be important nursery areas for both fish and crustaceans and also support a diverse community of both fish and invertebrates (Edgar and Shaw 1995, Jernakoff and Nielsen 1998). Algal habitats can occur from protected to very exposed sites and support a diverse range of fish and invertebrates. In Western Australia, these rocky reefs dominated by algae provide habitats for commercially important species such as *Panulirus cygnus* (Howard 1988, Babcock *et al.* 2007). In terms of classifying the remotely sensed data, this class allocation was appropriate as seagrass habitats have significantly different spectral signatures to that of algae and also typically occur in less

topographically complex regions. Both habitat classes also occur at scales that are detectable in the remotely sensed imagery.

Madsen *et al*. (2001) split submerged macrophytes into two major categories, those that form canopies and those that are meadow formers and this was the basis for the Level 3 of the scheme which separated the mixed algae into canopy and algal turf. The canopy algae refer to those large brown algae, such as *E. radiata*, which form dense, true canopies with the bulk of their biomass above the substrate (Madsen *et al.* 2001, Wernberg *et al.* 2003a). These canopy algae can have significant effects on the structuring of their habitat due to their influence on variables such as available light and physical exposure (Kennelly 1989, Kendrick *et al.* 1999, Wernberg *et al.* 2003b, Toohey *et al.* 2004). Algal turf is diverse and widespread on temperate shallow reefs and shows a range of morphologies, often being shaped by the levels of physical and grazing pressure they are exposed to (Hay 1981). A functional group approach proposed by Steneck and Dethier (1994) was tested by Phillips *et al*. (1997) on a number of high-relief limestone reefs in Western Australia and, although it was able to detect some trends in the community structure, a species-based assessment was determined to be more appropriate. The key feature of this functional group approach applicable to the current work was the clear separation of the canopy forming algae from all another groups. The need to further study algal communities at species level, highlighted by Phillips *et al*. (1997), was also captured by the scheme with further splitting of the categories beyond Level 3.

The classification categories at Level 4 of the scheme separated classes into species or genera for the macrophytes or substrate types. The division of bare substrate into either

bare sand or bare limestone covered the typical substrates found in Rottnest Island Reserve. These two substrates provide different habitats and, as such, will support different communities. Bare limestone is most likely to occur in exposed intertidal platforms around Rottnest Island where the constant wave action and grazing by fish and invertebrates plays a role in controlling the growth of algae (Berry and Playford 1992). In the less exposed subtidal regions, most limestone is colonised by some form of turfing or encrusting coralline algae (Prince 1995). Edgar and Shaw (1995) found that bare sand substrates supported a community of both fish and invertebrates, that was less diverse than vegetated habitats. However, both the limestone and bare sand are carbonate based which would make them difficult to separate based on spectral data.

Canopy algae habitats were further divided into those regions dominated by *Ecklonia radiata*, *Sargassum* species and regions of mixed algae. These categories fit in with those used by Phillips *et al*. (2006) to describe the canopy algae, in a study on reef algal community structure along the south-western coast of Australia. This level of classification was as close as possible to a species level assessment when using remotely sensed data and was designed to take advantage of canopy-understorey algae relationships or assembly rules to further resolve these habitat descriptions (Irving *et al.* 2004).

Irving and Connell (2006) proposed an assembly rule for predicting understorey algae communities based on both the presence and composition of canopies. They proposed three main categories, namely, *E. radiata* canopies, *E. radiata*-Fucales canopies and the gaps between, each with associated understorey communities. Similarly Kendrick *et al*. (1999) showed that the density of the *E. radiata* canopy, in combination with wave

exposure, influenced the understorey algae assemblages present in Marmion Lagoon, Western Australia. *E. radiata* exerts this influence on the understorey algal communities by affecting the light and physical exposure the understorey algae community is exposed to (Kennelly 1987, 1989, Kendrick *et al.* 1999, Toohey *et al.* 2004, Wernberg *et al.* 2005). The relationship between the density of the *E. radiata* canopy and the abundance of encrusting coralline algae has been found to be one of co-existence (Melville and Connell 2001). Under dense canopies encrusting algae thrived, but when the canopy was removed, coralline algal abundance was reduced and the abundance of turfing filamentous algae increased (Melville and Connell 2001, Fowler-Walker and Connell 2002, Connell 2003). In contrast, Goldberg (2007) determined that the structure of the understorey algal community in fucalean dominated algal beds was not controlled by the presence of the canopy, but by other environmental effects such as propagule supply and recruitment success. *E. radiata* was found to have a negative influence on the species richness of the associated algal assemblages in south-western Australia, with *Sargassum* dominated canopies and gaps in the canopy having a greater species richness (Kendrick *et al.* 2004). These results point to the need to be able to separate these habitats using the remotely sensed data in order to be able to define ecologically relevant regions based on benthic habitats.

Although four further sub-classes of turf algal habitats were defined, turfing algae at Rottnest Island is typically made up of combinations from all three divisions (Chlorophyta, Rhodophyta and Phaeophyta), rather than occurring in large homogenous patches such as *E. radiata* (Wells and Walker 1993). These algal assemblages, which often form in the gaps between canopy forming algae are highly diverse and the species present vary greatly over small spatial scales (Underwood and Chapman 1998, Coleman

2002). Turfing algae is often positively impacted, in terms of growth and survival, by sedimentation, which often occurs in more exposed locations, and can act to exclude many canopy and encrusting coralline species (Hay 1981, Kennelly 1989, Coleman 2002).

Seagrass habitats were divided into meadows dominated by either *Posidonia* or *Amphibolis* species. Two species from each of these genera are commonly found in Rottnest Island Reserve, *Posidonia sinuosa*, *P. australis*, *Amphibolis griffithii* and *A. antarctica* (Wells and Walker 1993). *Posidonia* species have long strap-like leaves and *Amphibolis* species have a lignified, erect, central stem which supports short leaves arranged in terminal clusters (Jernakoff and Nielsen 1998, Lavery and Vanderklift 2002). Both of these seagrass genera support a variety of epiphytic algae, both small, filamentous and large, erect species, with *Amphibolis* species providing more suitable habitat for epiphytic growth (Jernakoff and Nielsen 1998, Lavery and Vanderklift 2002). In the case of *Amphibolis* species, the bulk of the epiphytic growth occurs on the stems, which are longer lived than the leaves (Borowitzka *et al.* 1990, Jernakoff and Nielsen 1998). In Perth coastal waters, the majority of the large erect epiphytic algae found on *P. sinuosa* and *A. griffithii* are Rhodophyta (Jernakoff and Nielsen 1998). Jernakoff and Nielsen (1998) determined that *P. sinuosa* and A. *griffithii* supported different communities of both fish and invertebrates. It has been suggested that the most probable reason for this was the difference in the structure of the two genera of seagrass, which means they provide different habitats for organisms to inhabit (Orth *et al.* 1984, Jernakoff and Nielsen 1998, Hyndes *et al.* 2003). The community of associated epiphytic algae and invertebrates is also known to vary significantly between seagrass species (Borowitzka *et al.* 1990, Trautman and Borowitzka 1999, Lavery and

Vanderklift 2002). Further to this, Jernakoff and Nielsen (1998) determined that the epifaunal invertebrate assemblages were more diverse in *Amphibolis griffithii* meadows than *Posidonia sinuosa* meadows, a feature again attributed to the greater level of structure in *A. griffithii* meadows.

The final class at Level 4 of the scheme was *Pocillopora* coral, this being the only hard coral present at a reef scale in Rottnest Island Reserve (Wells and Walker 1993). Hutchins (1999) indicated that small colonies of *Pocillopora damicornis* occurred all around the island with larger colonies only occurring at Parker Point and Little Salmon Bay. The *P. damicornis* colonies exist at the southern limit for reef-building coral in Western Australia and therefore provide a unique and important habitat type in Rottnest Island Reserve (Vernon and Marsh 1988).

The hierarchical classification scheme described for Rottnest Island provides an adaptable, structured framework for classifying marine benthic habitats using a remote sensing approach. The scheme defines each class by the dominant habitat component present, which makes it more suitable when attempting to classify mixed image pixels as their signature will be dominated by the signature of this component.

3 A digital bathymetry model for Rottnest Island Reserve

3.1 Introduction

Marine benthic habitats are not only described by their biotic variables, such as dominant vegetation, but also by a range of abiotic or environmental factors. For example, depth is directly linked to the availability of light on the seafloor and this influences the composition of the benthic communities that may occur there (Abal and Dennison 1996, Schwarz *et al.* 2000, Johansson and Snoeijs 2002, Toohey *et al.* 2004, Gattuso *et al.* 2006, Toohey 2007, Toohey *et al.* 2007). Other factors include exposure due to wind and waves, habitat complexity and distance from shore (Underwood *et al.* 1991, Ruuskanen *et al.* 1999, O'Hara 2001, Ekebom *et al.* 2003, Goldberg and Kendrick 2004, Taniguchi and Tokeshi 2004). The link between topographic complexity and the distribution of many marine organisms has also been investigated (McClanahan 1994, Jenkins and Wheatley 1998, Gaylord 2000, Garcia-Charton and Perez-Ruzafa 2001, Garpe and Ohman 2003, Johnson *et al.* 2003, Taniguchi and Tokeshi 2004, Zurita 2004, Frost *et al.* 2005, Gratwicke and Speight 2005). These factors can be collectively summarised using an ecological niche approach which assumes that species occur in a non-random arrangement in the natural environment, which is to some degree, controlled by abiotic variables (Hirzel *et al.* 2002).

Hutchinson (1957) first introduced the concept that an ecological niche could be quantified in multidimensional space and represented both the fundamental and realised niches. The fundamental niche, often the computed result of habitat suitability models, is the space in the environment where a species could occur and the realised niche is the space where it actually does occur (Figure 3-1). Modelling the ecological niche has been carried out using a variety of methods, all with the same core principle of using

spatially derived environmental variables to determine the regions with the greatest probability of that species occurring (Lehmann 1998, Hirzel *et al.* 2002, Wiley *et al.* 2003).

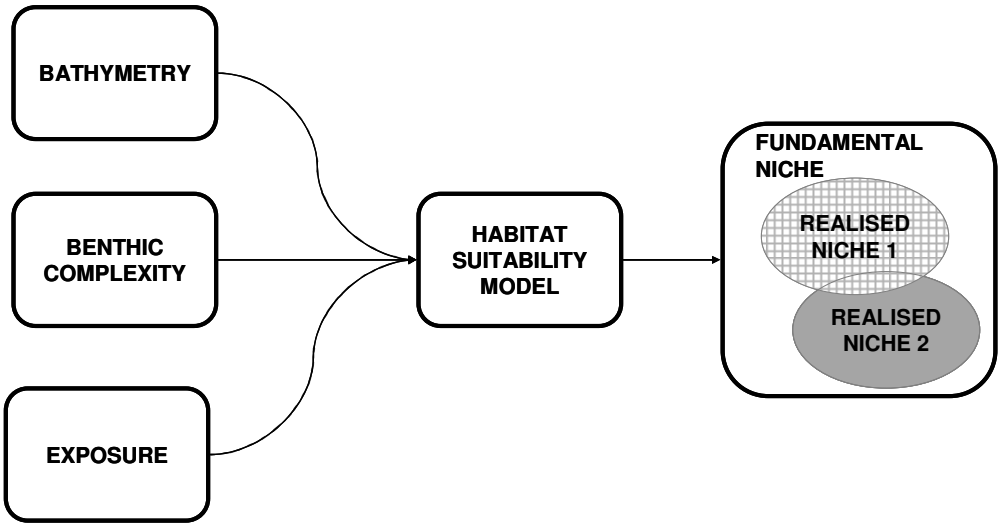

Figure 3-1: Conceptual diagram using environmental variables, such as bathymetry, benthic complexity and exposure, to define an ecological niche for a particular habitat. The example illustrates how the fundamental niche of two species may be the same, but the realised niche only partially overlaps.

The two dominant bio-substrate components, seagrass and macroalgae, that typically occur around Rottnest Island are ideal for models based on environmental variables. Seagrass habitats typically occur on sandy substrates in protected regions. In contrast, macroalgae habitats can occur from protected to very exposed sites and also support a diverse range of fish and invertebrates. This information can be used to complement classification of hyperspectral images to increase the accuracy of the final habitat maps.

Measures of benthic complexity require detailed knowledge of the bathymetry at the finest scale possible, whilst maintaining a reasonable level of accuracy. Bathymetry is also a basic requirement for many oceanographic applications, such as wave modelling and determining wave exposure (Moghimi *et al.* 2005). The standard methods for obtaining depth data are through depth soundings and hydrographic acoustic surveys.

The data points were traditionally plotted onto maps and contour lines drawn at regular intervals (Li *et al.* 2005). In more recent times, with the development of geographic information systems (GIS) and the advent of faster computers to run them, there has been an increased use of high resolution bathymetry data in a range of marine research. There are numerous advantages to expressing bathymetry as a spatially continuous data set, rather than the traditional points (soundings) or lines (contours). In GIS, such continuous data sets are referred to by a number of names, one of the most common being a digital bathymetric model (DBM). A DBM is most simply defined as a continuous surface that represents the bathymetry of the surface relative to a datum at every point of the image (Li *et al.* 2005).

DBM surfaces are generally interpolated into continuous surfaces from point data, such as soundings, using a range of algorithms. Interpolation algorithms can be broadly classified into two categories, exact and inexact interpolators (Burrough and McDonnell 1998). Exact algorithms preserve the data values in the original data set in the newly created DBM, while inexact algorithms use statistical methods to generate new values that best fit the data, which are not always equal to the original data (Li *et al.* 2005). In most situations when bathymetric soundings are being interpolated it is best practice to use exact interpolation algorithms as this will allow the continuous surface to be as accurate as possible (Burrough and McDonnell 1998). There are numerous exact interpolation algorithms that can be applied to point data, such as triangulated irregular networks (TIN), inverse weighted distance (IWD) interpolation, natural neighbour, various radial bias functions and kriging. Each of these interpolation algorithms has different properties and will result in interpolations of various accuracies depending on the spatial structure of the data (Kravchenko 2003).

Having detailed information for the bathymetry of a region, in the form of a continuous surface such as a DBM, provides the opportunity to examine the distributions of benthic habitats with respect to depth over the entire study area at a scale that matches the remotely-sensed imagery. Spatial data of this kind also provide the opportunity for deriving first order derivatives of the DBM, such as slope and aspect, and higher order derivatives such as different textural descriptors (Burrough and McDonnell 1998). These derivatives can also be used as inputs to the habitat classification scheme as the distributions of different coastal habitats types, often defined by the presence of dominant macroalgae or seagrasses, can be related to exposure and benthic complexity or texture (Goldberg and Kendrick 2004, Shears *et al.* 2004). The combination of classification inputs from remotely-sensed data, and those derived from the bathymetry, can enable a more accurate and comprehensive marine benthic habitat classification.

The aim of this chapter was to develop a digital bathymetric model for Rottnest Island using existing irregularly spaced bathymetry data and use it as a basis to calculate a range of abiotic variables that could be used to improve the ecological description of the benthic habitats of Rottnest Island.

3.2 Methods

The development of a DBM for Rottnest Island Reserve required a number of sequential steps, namely data acquisition and preparation, data validation, algorithm cross-validation and digital bathymetric model interpolation.

3.2.1 Datasets

Bathymetric soundings data were obtained in digital format, as text files containing longitude, latitude and depth values, from the Western Australian Department for Planning and Infrastructure (DPI). These data were collected between 1980 and 2004 using a single beam echo sounder and had horizontal and vertical accuracies of 1.0 and 0.1 m, respectively. These data covered the majority of the Rottnest Island Reserve and covered depths between 5 and 40 m. The vertical datum used in these data sets was Low Water Mark (LWM) Rottnest, while the horizontal datum varied between them (Table 3-1). There were some gaps in the data in the nearshore region adjacent to the

Table 3-1: Depth soundings data from DPI used to create the digital bathymetry model for Rottnest Island Reserve.

Data set name	Date	Description	Horizontal datum	Vertical datum	No. of points	Format
RO80	1980	Chart survey	66	LWM Rottnest (0.715m below AHD 1971)	147 780	Digital (xyz format)
RO82GEDE	1982	Geordie Bay	66		4 752	
RO82PAKR	1982	Parker Point	66		6 707	
RO82RCKY	1982	Rocky Bay	66		7 049	
RO82SPHT	1982	Spot heights	66		2 121	
RO83	1983	Stark, Marjorie & Rocky Bays	66		9 898	
RO87RK	1987	Rock investigation	66		5 886	
RO88CABY	1988	Catherine Bay	84		2 842	
RO981204	Dec. 1998	Ferry berth & sand bar	84		5 456	
Coastpoints_50 m	2004	HyMap coastline	UTM(2)		1 151	
Rottnest Sheet 1	Feb 1980	West End	UTM	AHD 1971	186	Hardcopy charts

Horizontal datum:
66 – refers to AMG66 based on AGD84
84 – refers to AMG84 based on AGD84
UTM – refers to UTM based on AGD66
UTM(2) – refers to UTM based on WGS84

Vertical datum:
LWM Rottnest refers to Low water mark Rottnest (0.715m below AHD1971)
AHD 1971 refers to Australian height datum 1971

coastline where hydrographic vessels were unable to operate. In regions that had been surveyed a number of times over a period of years the most recent data were used. Each

of the data files was reprojected to Universal Transverse Mercator (UTM) projection (Zone 50 South) based on the world geodetic system 1984 (WGS84) datum (UTM-50S) (Figure 3-2).

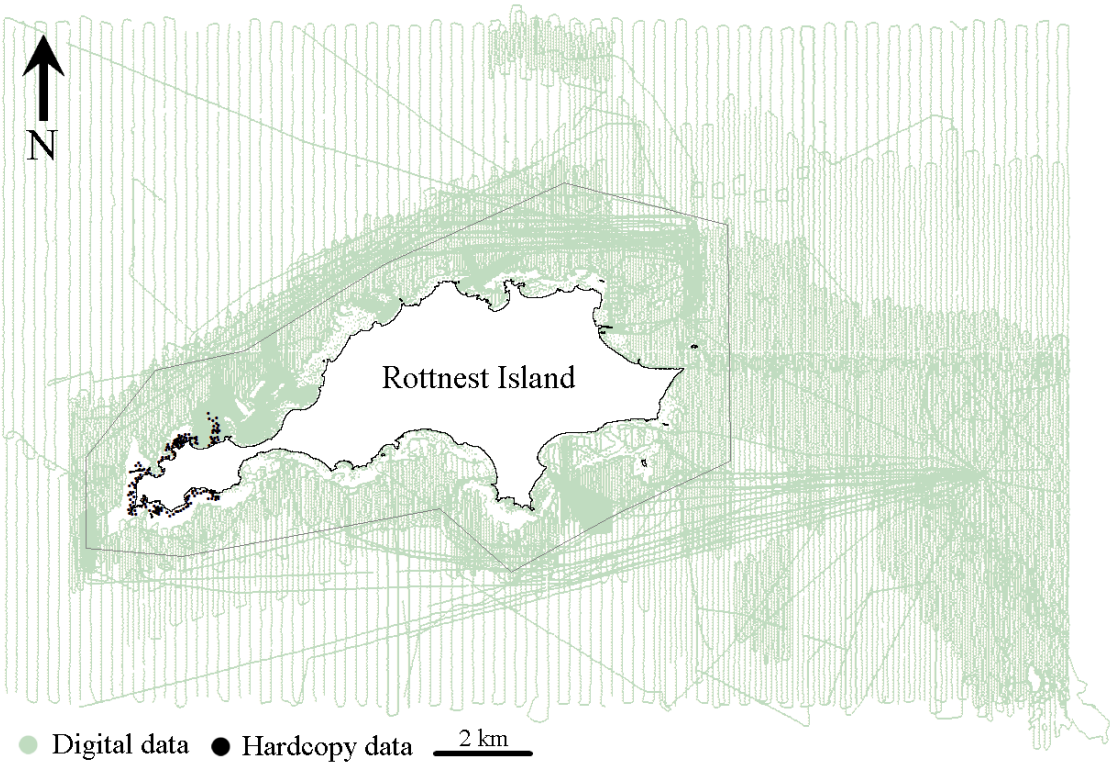

Figure 3-2: Bathymetric soundings data available in digital (grey dots) and hardcopy (black dots) format for Rottnest Island Reserve, sourced from the Western Australian Department for Planning and Infrastructure. Note that hardcopy soundings were only used close to the coast at the west end of Rottnest Island.

A number of hardcopy maps with sounding data for some of the shallow coastal areas around Rottnest Island for which no digital data were available, were also obtained from the DPI. Bathymetric sounding data from one of these analogue maps were digitised by hand to create digital data sets. This original map was projected using UTM projection based on the Australian geodetic datum 1966 (AGD66) and used the Australian height datum 1971 (AHD71) vertical datum (Table 3-1).

The hardcopy maps were first photographed, using a 3.2 megapixel digital camera, in sections using a support frame to reduce any distortions due to camera movement between map sections. The images were imported into the Environment for Visualising Images (ENVI 4.2) (RSI 2005) software and registered using ground control points (GCP) and then reprojected to the UTM-50S projection. The depth sounding points were then digitised, the values corrected to LWM Rottnest and exported as an ArcView shapefile (Figure 3-2).

3.2.2 Data assembly and tide correction

The complete set of depth soundings were combined to create a single point shapefile of the entire data set. All data points were corrected to account for the height of the tide during the period when the hyperspectral data were collected on April 26, 2004. The average height of the tide over the whole hour during which the survey was flown was calculated from tidal data, recorded at five minute intervals in Fremantle Harbour, supplied by the DPI. Using the relationship between LWM Rottnest, the tidal and the AHD datums, the data were corrected using the following equation (Figure 3-3):

$$D_{(CORR)} = D_{(LWMR)} + (T - 0.045)$$

where $D_{(CORR)}$ refers to the depth data corrected for the tidal level at time of image capture, $D_{(LWMR)}$ the depth of each pixel relative to the LWM Rottnest and T the tidal height at the time of image capture.

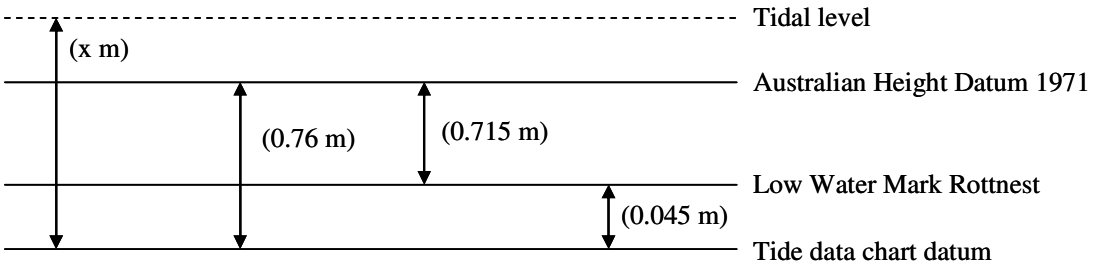

Figure 3-3: Relationship between various vertical datums and the tidal height data supplied by the West Australian Department for Planning and Infrastructure.

To ensure that the land/water interface was accurately depicted in the DBM with reference to tidal height at the time of image capture, the infrared bands of the geo-located HyMap image mosaic (see Chapter 5 for complete details) were classified using the unsupervised ISODATA routine in the ENVI software package to create a land/water mask (ITT Visual Information Solutions 2007). This is possible as the majority of infrared radiation is absorbed by water and reflected by land (Kirk 1994b). The ISODATA classification procedure is an iterative process that initially randomly allocates pixels to a given number of classes and then clusters the remaining pixels using minimum distance techniques. Then, during each iteration, the class means are recalculated and pixels reclassified with respect to the new means. This process continues until the number of pixels in each class changes by a number less than the predetermined threshold or the maximum number of iterations is reached (RSI 2004). Specifying the ISODATA routine to output only two classes resulted in a Boolean image in which land pixels were distinguished from water pixels. The result of the ISODATA routine was refined by hand-digitising and removing any pixels representing boats and masking inland lakes. The final classification image was converted to a polygon shapefile and then to a point shapefile with 50 m spacing using the "Poly to Points" extension for ArcView 3.2 (Huber 2002). Each point in the data, i.e. the coastline, was assigned a depth of 0 m.

3.2.3 Data validation

A number of steps were taken to isolate any errors, that may have been present in the original data or introduced during the data preparation, that would affect the accuracy of the final DBM. Each of these steps was carried out using ArcView 3.2 (ESRI 1999).

The complete data set was imported into ArcView and a polygon layer of uniformly sized hexagonal polygons was created (Jenness 2005b), resulting in 2 571 hexagons, each covering 0.1 km^2. Hexagon-shaped sampling units were chosen for this validation process as previous studies have established that they provide a statistically sound basis for spatial sampling purposes (Bassett and Edwards Jr. 2003). The minimum ($H_{\min}$) and maximum ($H_{\max}$) of the depth sounding points contained within each hexagon sampling unit were extracted to calculate the range (Hr) for each sampling unit. A value (A) was then calculated for each sampling unit using the following formula:

$$A = \left(H_{\max} - H_{\min}\right) - \left(\overline{Hr} + \left(3 \times Hr_{\sigma}\right)\right)$$

where ($\overline{Hr}$) refers to the mean sampling unit range values and (Hr_{σ}) refers to the standard deviation of the sampling unit range values. A value for $A > 0$ indicted that the range of values within that sampling unit was greater than the maximum range defined by the mean plus three standard deviations. This test was based on the assumption that the data were normally distributed and thus 99% of observations will fall within three standard deviations of the mean (Hayek and Buzas 1997). Depth sounding points contained within those sampling units with a value for $A > 0$ were further analysed to determine which point(s) may be erroneous.

The depth sounding data points that belonged to any sampling unit that was identified by the previous step ass potentially including erroneous points were tested individually, by calculating the probability of each point belonging to the data set, using a normal probability density function. The probability density function (PDF) for each point was calculated using the following formula (Jenness 2003):

$$PDF = \frac{1}{H_\sigma \sqrt{2\pi}} \exp\left(-\frac{1}{2}\left(\frac{H_i - \overline{H}}{H_\sigma} \right)^2 \right)$$

where $\overline{H}$ and H_σ refer to the mean and standard deviation of all sample points within each sampling unit, respectively and H_i refers to the individual data point being tested. All data points with a probability < 0.01 where checked manually in the context of the surrounding bathymetry and against navigational charts and any erroneous points were removed.

3.2.4 Interpolation algorithm cross-validation

Cross-validation was carried out for the complete data set using eight different exact interpolation algorithms to determine the most appropriate to use for the final DBM (Table 3-2) (Goovaerts 2000).

The inverse weighted distance (IWD^x) algorithm is a weighted average interpolator, where the weighting of surrounding points declines with distance based on the value of "x" (Franke 1982, Naoum and Tsanis 2004). Kriging is a geostatistical interpolator that attempts to express trends in the data based on surrounding points (Burrough and McDonnell 1998) and relies on the assumption that there is spatial autocorrelation in the

Table 3-2: The DBM interpolation algorithms tested using the cross-validation procedure in the Surfer 8 software package. 'x' indictes the power (2, 3 or 4) for the inverse weighted distance algorithm.

Interpolation algorithm	Acronym	References
Inverse weighted distance (Power 2, 3 or 4)	IWD^x	Franke (1982)
Kriging (standard)	Kriging	Cressie (1991)
Radial bias function (multiquadratic)	RBF(MQ)	Hardy (1990)
Radial bias functions (natural cubic spline)	RBF(NCS)	Franke (1982)
Triangulated irregular networks	TIN	Guibas and Stolfi (1985)
Natural neighbour	NN	Sibson (1981)

data. Kriging has proved to be a reliable and accurate method for interpolating irregularly spaced data (Burrough and McDonnell 1998, Bekkby *et al.* 2002). The third group of algorithms were radial bias functions, of which two variations were tested. Radial bias functions combine a diverse group of algorithms which all act as exact interpolators unless a smoothing factor is introduced (Amidor 2002). Triangulated irregular networks (TIN) create Delaunay triangles by joining all data points in such a way that no data points are contained within a triangle (Amidor 2002, Li *et al.* 2005). The DBM surface was generated from these triangular planar surfaces. Natural neighbour (NN) interpolation, which is a local interpolator, involves the generation of Thiessen polygons, which are essentially the dual of Delaunay triangles (Amidor 2002).

The cross-validation procedure was carried out by removing a single data point from the data set and then, using the interpolation algorithm being tested, estimating the interpolated value for that point using surrounding data. This procedure was carried out five times for each algorithm being tested due to computer and software limitations, each time using a randomly selected subset of 15 000 points. The outputs from this process were the actual value, the estimated value and the residual. For each run, the

root mean square (RMS) error was calculated using the following formula (Desmet 1997):

$$RMS = \sqrt{\frac{\sum_{i=1}^{n} \left| z_{i,act} - z_{i,est} \right|^2}{n-1}}$$

where z_{act} and z_{est} are the actual depth of the sample point and the depth estimated by the interpolation algorithm, respectively. The mean RMS error was then calculated across the five runs.

The total of 75 000 points, from the five runs, tested for each algorithm were pooled and analysed to determine the spread of the residual around zero, by calculating the mean absolute error (MAE) and the standard deviation of the MAE (MAE_σ) for the total data set. The MAE and the MAE_σ were calculated using the following formulae (Li 1988, Desmet 1997):

$$\mathrm{MAE} = \frac{\sum_{i=1}^{n} \left| z_{i,act} - z_{i,est} \right|}{n}$$

$$\mathrm{MAE}_\sigma = \sqrt{\frac{\sum_{i=1}^{n} \left(\left| z_{i,act} - z_{i,est} \right| - \mathrm{MAE} \right)^2}{n-1}}$$

For each of the eight algorithms, the data from first cross-validation run (15 000 points) were analysed using linear regression. The actual depth values were regressed against the estimated values and the R^2 and y-intercepts calculated. In an ideal situation, the R^2

value would equal one and the y-intercept would be zero. Using this information the algorithms were ranked by first using the R^2 value and then the y-intercept.

The residuals for all 75 000 cross-validation points were grouped as either being an exact estimate (residual = zero), an over-estimate (residual = +ve value) or an under-estimate (residual = -ve value). These results were calculated as a percentage of the total points tested and ranked using the percentage of points being an exact estimate and secondly, by the absolute difference between the percentages of over-estimated points and under estimated-points.

Digital bathymetric models were interpolated using the eight algorithms and the time taken to interpolate was recorded. These DBMs were interpolated using Surfer 8 software at 3.5m pixel resolution to match the resolution of the HyMap data. All the DBMs were ranked based on each of the cross-validation tests, namely, RMS, MAE, regression and estimate error, and the algorithm with the highest rank was used for the final DBM for Rottnest Island.

3.2.5 Digital bathymetric model interpolation and validation

The DBM chosen as the final surface to represent the bathymetry of Rottnest Island Reserve was validated using a series of depth data collected at Rottnest Island using a Garmin GPSMap 185 echo sounder, fitted with a differential GPS beacon, connected to a laptop computer. The data were logged in real-time in ArcView 3.2 using the DNR Garmin Extension, with information on the depth, location and estimated positional error of each point. The data were first corrected to the LWM Rottnest vertical height datum using tidal data, recorded at five minute intervals in Fremantle Harbour, supplied by the Western Australian Department for Planning and Infrastructure. The correction

was carried out using the mean tide height at hourly intervals, calculated for the time period when data were collected. The RMS, MAE and MAE_{σ} errors were calculated using all data collected and for data at depth ranges in 5 m intervals from 0m to 30 m. The tide correction and error calculation analysis were carried out using a DBM Error Analysis Extension for ArcView 3.2 developed for this study.

3.2.6 Topographic variables

Four topographic variables (depth, regular slope, directional slope and aspect) and four benthic complexity descriptors (mean direction of aspect, circular variance of aspect, circular standard deviation of aspect and up/down slope), were calculated at a spatial resolution to match that of the HyMap hyperspectral data (3.5 m x 3.5 m pixels). The Rottnest Island Reserve was divided into four quadrants for summary and analysis of the abiotic variables (Figure 3-4).

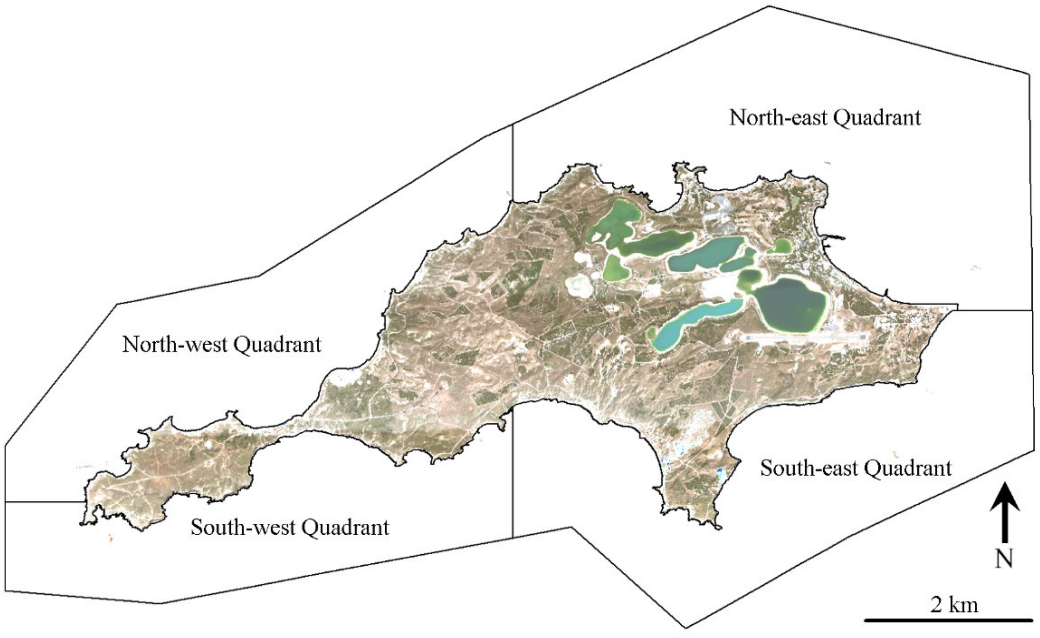

Figure 3-4: The four quadrants used to summarise the abiotic variables for the Rottnest Island Reserve.

The depth values were extracted directly from the DBM for Rottnest Island Reserve and were used as the input layer to calculate both the slope and aspect values. Regular slope and aspect values were calculated using the method described by Zevenbergen and Thorne (1987) using the following equations:

$$Slope = \left(Slope_{ROW}\right)^2 + \left(Slope_{COLUMN}\right)^2 \text{ and } Aspect = \frac{Slope_{ROW}}{Slope_{COLUMN}}$$

where:

$$Slope_{ROW} = \frac{z_3 - z_1}{2d} \text{ and } Slope_{COLUMN} = \frac{z_2 - z_4}{2d}$$

where z_i refers to the height values of each pixel and *d* refers to the grid interval (i.e. 3.5m for this study) (Figure 3-5). The Zevenbergen and Thorne method was used to calculate slope values as previous studies have indicated that it calculates results with greater accuracy than other methods (Zhilin *et al.* 2005). The DBMAT extension for ArcView 3.2 was used to calculate the slope and aspect values (Behrens 2005).

z_5	z_2	z_6
z_1	z_0	z_3
z_8	z_4	z_7

3 x 3 Grid Window

Figure 3-5: A conceptual 3x3 window from a grid data set used to describe how topographical variables were calculated from the data.

The regular slope and aspect were summarised using the "Grid tools" extension for ArcView 3.2 (Jenness 2006). Prior to analysis, the aspect data were reclassified to set

all regions with a slope < 5° to be flat. Due to the circular nature of aspect data, the descriptive statistics were calculated using modified formulas for mean direction ($\bar{\theta}$), circular standard deviation (v) and circular variance (V) based on a 3x3 kernel (Zar 1999, Jenness 2006):

$$\bar{\theta} = \tan^{-1}(S/C) \quad \text{where } S > 0 \text{ and } C > 0,$$
$$\bar{\theta} = \tan^{-1}(S/C) + \pi \quad \text{where } C < 0,$$
$$\bar{\theta} = \tan^{-1}(S/C) + 2\pi \quad \text{where } C < 0 \text{ and } S > 0,$$

$$v = \frac{180}{\pi}\sqrt{-2\ln\bar{R}}, \text{ and}$$

$$V = 1 - \bar{R}$$

where:

$$C = \sum_{i=1}^{n}\cos(\theta_i),\ S = \sum_{i=1}^{n}\sin(\theta_i),\ R^2 = C^2 + S^2,\ \bar{R} = \frac{R}{n}$$

where θ refers to the aspect direction in degrees, i the sample number and n the number of samples. The circular standard deviation is analogous to the standard deviation on a linear scale, and ranges from zero to infinity (Zar 1999). The circular variance is a dimensionless measure to define dispersion of the data and ranges from zero to one, where one represents maximum dispersion (Zar 1999).

The slope values were calculated in degrees for each pixel in all eight cardinal directions using the "Directional slope" extension for ArcView 3.2 (Jenness 2005a) (Figure 3-6). Directional slope values can range from -90° to 90°, indicating either a down-slope or an up-slope (Figure 3-6). All directional slope data sets where

reclassified to indicate whether they represented an up-slope or down-slope for each direction.

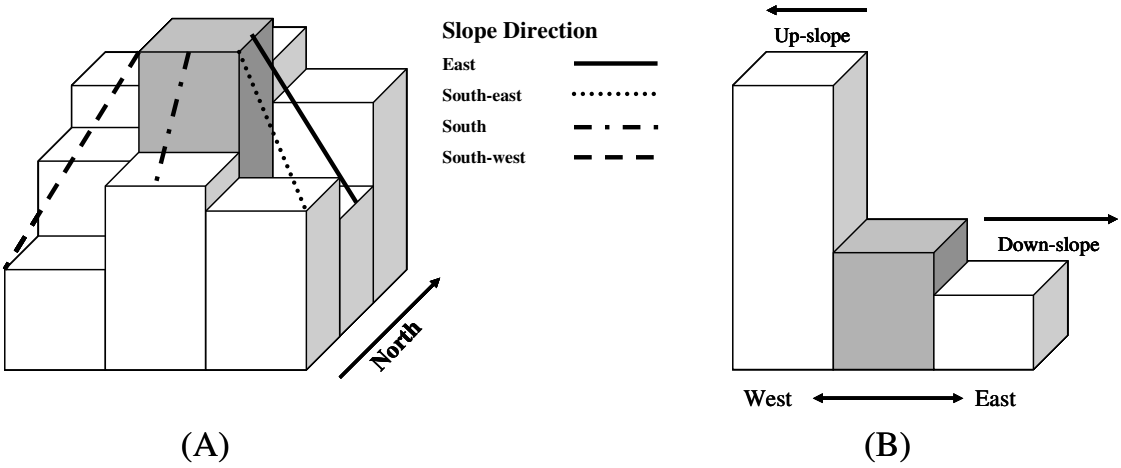

Figure 3-6: Conceptual diagram of the method used to calculate (A) the directional slope, for the target pixel (shaded), based on the digital bathymetric model for Rottnest Island Reserve and (B) the definition of up-slope and down-slope in relation to directional slope of a target pixel.

3.2.7 Abiotic variables affecting benthic habitats

Six additional abiotic variables were calculated at a spatial resolution to match that of the HyMap hyperspectral data (3.5 m x 3.5 m pixels). These variables were grouped into three categories; topographic relief classification, benthic complexity variables and location based variables. The benthic complexity variables were texture based and most used a kernel filter approach to determine local variability in topographic variables. The location based variable was the relative exposure index (REI) based on the effective fetch.

A topographic relief classification data layer, indicating the presence/absence of high or low relief reefs, was calculated using a circular kernel filter with a radius of five pixels (17.5m) which calculated the range of depth values within the kernel window (Figure 3-7). The data were reclassified using the definitions used by Toohey (2007), which

designated low relief reefs in Western Australia as having a vertical displacement of <1 m and high relief reefs as having a vertical displacement >1 m.

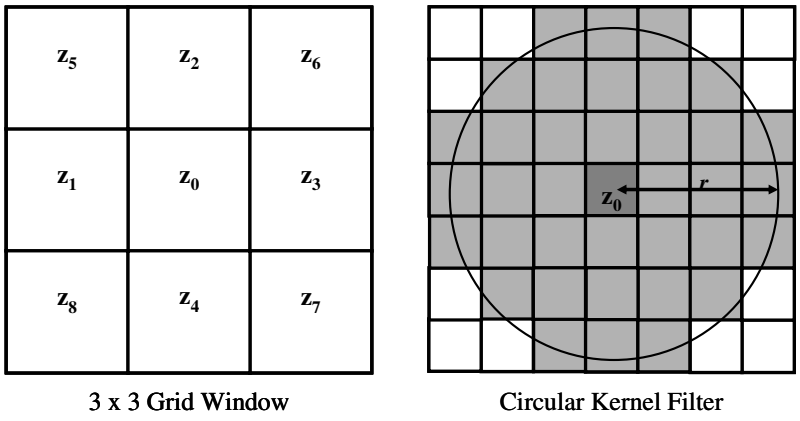

Figure 3-7: A conceptual 3x3 window from a grid data set used to describe how topographical variables were calculated from the data and a conceptual circular kernel filter with a radius (r) of 3 pixels.

Three of the benthic complexity variables were calculated using a five pixel (17.5 m) radius kernel filter to determine the local variability in the topographic variables (Figure 3-8). The Grid Tools extension for ArcView 3.2 was used to implement the radian kernel filter (Jenness 2006). The variability was quantified for each pixel in the digital bathymetric (DBM) as the natural log of the standard deviation of the depth and regular slope and the circular variance (*V*) of aspect values in the local region, defined by the five pixel radius of the filter (Figure 3-7). The absolute change in slope was calculated for all eight cardinal directions using the following equation (Li *et al.* 2005):

$$\left|\Delta Slope_i\right| = \left|\frac{Slope_i - Slope_0}{d}\right| \text{ for } i = 1,2,3,4$$

$$\left|\Delta Slope_i\right| = \left|\frac{Slope_i - Slope_0}{\sqrt{2}d}\right| \text{ for } i = 5,6,7,8$$

where $|\Delta\ Slope_i|$ refers to the absolute change in slope in the *i*th direction, $Slope_i$ is the slope of pixel *i*, $Slope_0$ is the slope of the target pixel and *d* is the grid interval (Figure

3-7). The mean change in slope was calculated for each pixel using all eight associated values. All benthic complexity layers were normalised by their maximum value to give each pixel a value between zero and one, where one refers to maximum complexity.

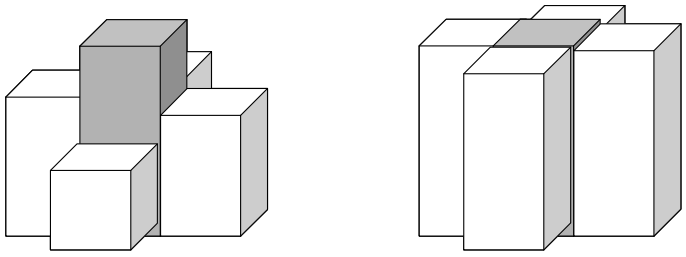

Figure 3-8: Conceptual diagram demonstrating the use of the standard deviation of the depth and slope vales associated with the target pixel (shaded). Note that for simplicity only four of the surrounding eight pixels are displayed here.

The wave exposure of coastal sites due to wind generated waves can be quantified using calculation of the effective fetch for each site (Burrows *et al.* 2008). Effective fetch is an index to quantify the exposure of a site based on the open water distance, as this will limit the length of water over which the wind can act to produce waves (Fonseca and Bell 1998, Lundqvist *et al.* 2006). Wind data for Rottnest Island, obtained from the Bureau of Meteorology at five minute intervals, were analysed for seven years (2000 – 2007) to calculate the mean direction ($\bar{\theta}$) and associated circular variance (V) for each month, and the monthly mean of the maximum wind speeds recorded for each time period. The percentage of time the wind blew in each of the eight cardinal directions and associated mean of the maximum wind speed for each month were also calculated.

Effective fetch takes the shape of the fetch into account by utilising the open water distance at six 7.5º intervals each side of the primary fetch direction (Figure 3-9). These distances are weighted by the cosine of the deviation angle from the primary fetch

direction. The effective fetch was calculated for each pixel in each of the eight cardinal directions using the following formula (Ruuskanen *et al.* 1999):

$$Effective\ Fetch = \frac{\sum_{i=1}^{n} d_i \times \cos(\theta_i)}{\sum_{i=1}^{n} \cos(\theta_i)}$$

where d_i refers to the distance from the nearest land along each radiating line and Θ_i refers to the deviation angle for each radiating line. They were calculated at a 30 m pixel resolution, due to practical limitations of the software, and then interpolated using an inverse weighted distance algorithm to 3.5 m pixels to match the HyMap data.

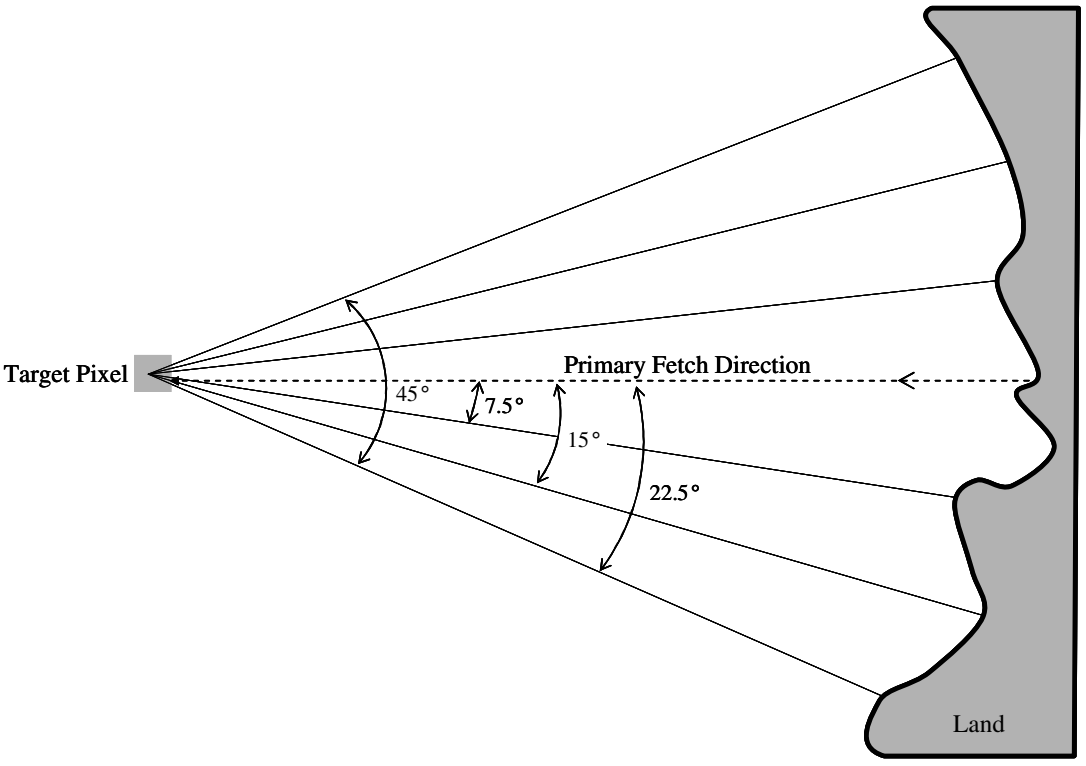

Figure 3-9: Conceptual diagram of the calculation of effective fetch for each pixel in the data, only showing the fetch lines out to 22.5°. Note that the effective fetch is actually calculated using six fetch lines out to 45°. Target pixels lie offshore from Rottnest Island.

The effective fetch data were used in conjunction with the wind analysis to calculate a relative exposure index (REI), using the method described by Keddy (1982). The REI was calculated using:

$$REI = \sum_{i=1}^{8} (V_i \times P_i \times F_i)$$

where i was the wind direction for the eight cardinal directions, V_i was the mean wind speed for each month from the ith direction, P_i was the percentage of time for the month the wind blew occurred from the ith direction and F_i refers to the effective fetch for the ith direction. The REI was calculated for each month and normalised against the maximum REI calculated across all 12 months. The REI results for all months were summed and normalised using the maximum possible value of 12 to give a yearly exposure index that ranged form zero to one.

3.3 Results

3.3.1 Data validation

The complete data set was validated using 2 571 hexagon sampling units that each covered 0.1 km^2 (Figure 3-10). Of these sampling units 32 were found to contain data points that were possibly erroneous, based on the first stage of the analysis which examined the gross relationships of all points within each sampling unit. These hexagon sampling units each contained between 18 and 382 individual depth sounding points making a total of 4 835 points to be tested further. A total of 84 data points were further analysed manually using aerial photographs and existing charts which resulted in only 20 data points being removed from the data set.

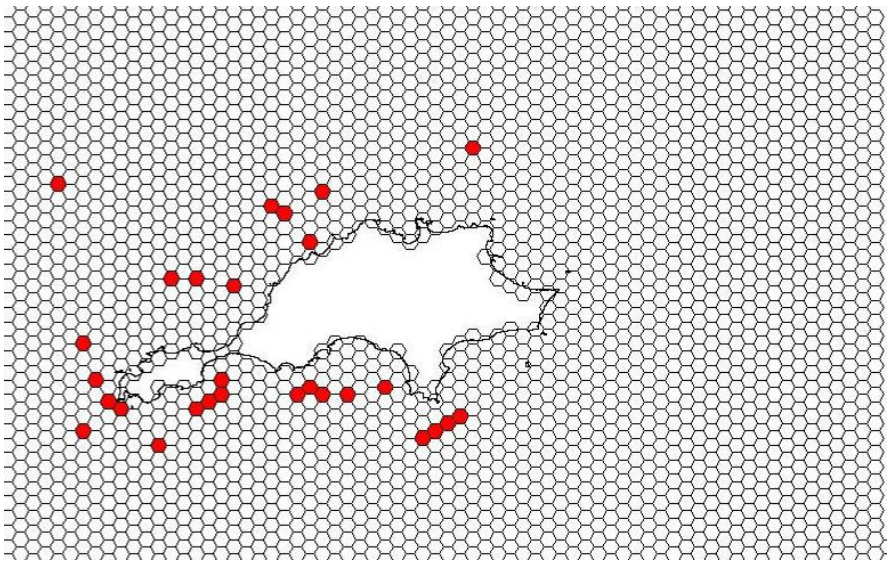

Figure 3-10: Hexagon sampling units used to validate the depth soundings data. Those highlighted are sampling units that were found to require further analysis to locate erroneous data.

The mean density of the depth sounding points in the Rottnest Island Reserve was 22 points per hectare. The density of the points was greatest in the north-west quadrant at 39 points per hectare and least in the south-west quadrant (9 points per hectare). The north-east and south-east quadrants had point densities of 22 and 16 points per hectare, respectively.

3.3.2 Interpolation algorithm cross-validation

The eight different interpolation algorithms were cross validated and the RMS error calculated for each using the complete data set (Table 3-3). The results indicated that the kriging algorithm using the linear variogram had the lowest RMS error of 4.86 $x10^{-3}$ m. The algorithm with the greatest RMS error was the radial bias function, using a natural cubic spline, which had an error of 8.63 x 10^{-3} m. Due to this large RMS error value, no further analysis was carried out using the RBF(NCS) algorithm. When all 75 000 validation points were aggregated and the MAE calculated, the radial bias function algorithm, using a multiquadic function, has the lowest error of 0.364 m. However, the kriging algorithm had the lowest variation within the estimated values with a standard

deviation of 0.470 m. With the exception of the RBF(NCS) algorithm, all were found to have RMS errors that fell within a 0.001 m range.

Table 3-3: Cross validation results for the Rottnest Island Reserve bathymetric data. Note that the sum of the number of points with estimates greater than actual and number of points less than actual does not always equal zero as the residual for some was equal to zero. (Est. refers to an estimated values, act. refers to actual values and Y^{Inter} refers to the y-intercept for the linear regression analysis.

Interpolation algorithm	RMS error (SD) (n = 5)	Mean Absolute Error (MAE)			MAE_σ	Time (hours)	R^2	Y^{Inter}
		All est.	Est.>act.	Est.<act.				
IWD^2	$5.72x10^{-3}$ ($1.43x10^{-4}$)	0.448 (n=75 000)	0.437 (n=40 491)	0.461 (n=34 503)	0.539	18.429	0.9955	0.130
IWD^3	$5.32x10^{-3}$ ($8.74x10^{-5}$)	0.398 (n=75 000)	0.394 (n=40 479)	0.403 (n=34 512)	0.515	19.880	0.9961	0.050
IWD^4	$5.21x10^{-3}$ ($5.82x10^{-5}$)	0.378 (n=75 000)	0.377 (n=40 231)	0.380 (n=34 760)	0.514	18.288	0.9962	0.074
Kriging	**$4.86x10^{-3}$** ($5.49x10^{-5}$)	0.366 (n=75 000)	0.365 (n=38 016)	0.367 (n=36 964)	**0.470**	18.570	**0.9968**	0.051
RBF(MQ)	$4.94x10^{-3}$ ($1.45x10^{-4}$)	**0.364** (n=75 000)	**0.367** (n=38 123)	**0.362** (n=36 858)	0.482	28.980	0.9965	0.056
RBF(NCS)	$8.63x10^{-3}$ ($2.08x10^{-3}$)	0.488 (n=75 000)	0.489 (n=37 383)	0.486 (n=37 617)	0.965	-	0.9921	0.061
TIN	$5.24x10^{-3}$ ($8.31x10^{-5}$)	0.378 (n=74 981)	0.455 (n=31 415)	0.472 (n=29 760)	0.518	**0.003**	0.9966	0.058
NN	$5.15x10^{-3}$ ($1.73x10^{-5}$)	0.376 (n=74 974)	0.378 (n=37 953)	0.400 (n=34 528)	0.507	1.098	0.9967	**0.045**

The results of the linear regression of the actual depth values against the estimated depth values calculated during the first cross-validation run for each algorithm indicated that the kriging algorithm performed the best (Table 3-3). As with the previous RMS error and MAE analysis, the RBF(NCS) demonstrated the worst performance. Each of the algorithms was ranked using the R^2 value first, then the y-intercept. A higher ranking was given to those algorithms with an R^2 value closer to one and a y-intercept closer to zero.

The time taken to interpolate a DBM from the complete data set varied significantly between algorithms. The two fastest interpolation times were found to be the TIN algorithm, taking only 0.003 hours, and the NN algorithm which took 1.098 hours

(Table 3-3). The slowest was the RBF(MQ) which took 28.980 hours to generate a DBM.

The depth values estimated by each algorithm were analysed with respect to how they varied to the actual measured value. With the exception of the RBF(NCS), all algorithms showed some bias towards over-estimating values (Figure 3-11). However, the three IWD^x algorithms, independent of their power function, showed the greatest bias towards over estimating values. The TIN algorithm had the greatest number of values estimated correctly (18.67%), followed by the NN algorithm (3.33%).

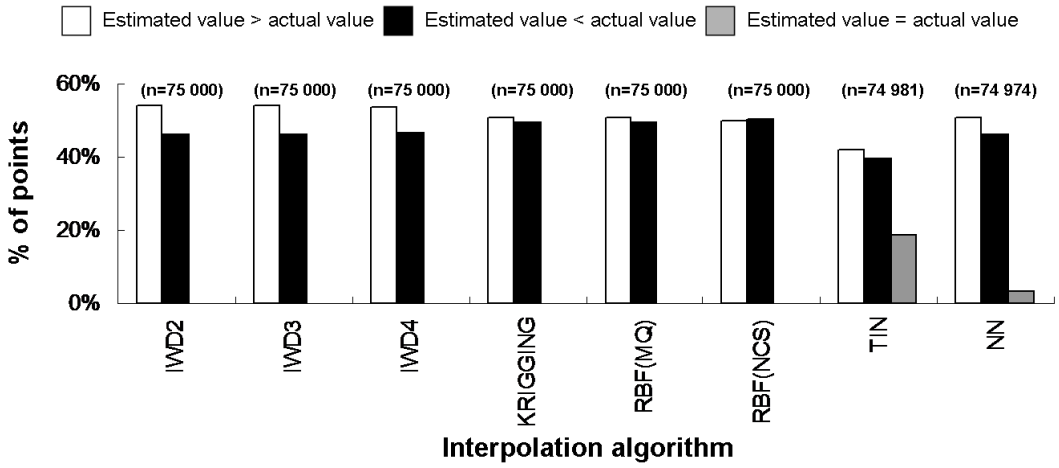

Figure 3-11: Summary of how estimated depth values for each algorithm related to the actual measured depth values for the 75 000 test points randomly selected from the complete Rottnest Island Reserve data set.

When all four analyses of the cross-validation data were combined to provide an overall ranking for the performance of each different interpolation algorithm, the kriging performed best overall, followed by the NN and the RBF(MQ) (Table 3-4).

Table 3-4: The final ranking of the eight interpolation algorithms based on the four analyses carried out using the cross-validation data for Rottnest Island Reserve.

Interpolation algorithm	Ranks				
	RMS error	MAE	Regression	Estimate error	Overall
Kriging	1	2	1	3	1
NN	3	3	2	2	2
RBF(MQ)	2	1	4	4	3
TIN	5	5	3	1	4
IWD^4	4	4	5	5	5
IWD^3	6	6	6	6	6
IWD^2	7	7	7	7	7
RBF(NCS)	8	8	8	8	8

3.3.3 Digital bathymetric model interpolation and validation

Seven DBMs were interpolated using all the algorithms which were cross-validated, with the exception of the RBF(NCS). The DBM interpolated using the kriging algorithm was taken to be the final surface to be used in further analysis within this project, as this algorithm obtained the highest ranking during the cross-validation process (Figure3-12; Figure 3-13).

A total of 503 depth soundings were collected for DBM validation over two days. These data were corrected to the LWM Rottnest datum and corrected for tide at time of capture. The RMS error for the entire RIR was calculated to be 0.871 m and the MAE was 0.656 m with a standard deviation of 0.811 (Table 3-5). These errors were significantly greater than those found as part of the cross-validation process. The errors calculated using the depth ranges showed a trend of increasing error as the depth increased. The shallowest water (0 – 5 m) had the smallest MAE error (0.440 m), which increased to 1.371 m in the deeper water (10 – 15 m) (Table 3-5). This increase in error is most probably related to the lack of validation data points collected for this

depth range. Overall, despite there being some errors in the final DBM, it was deemed to be suitable for further analysis for the purposed of benthic habitat mapping.

Table 3-5: Summary of the validation statistics for the digital bathymetric model for Rottnest Island Reserve.

DBM Region	% of Area of RIR (hectares)	No. of validation points	% of validation points	RMS	MAE	MAE_{σ}
0 – 5 m	30.6 %	259	51.5 %	0.569	0.440	0.359
5 – 10 m	25.7 %	221	43.9 %	1.043	0.827	0.633
10 -15 m	23.6 %	25	5.0 %	1.573	1.371	1.195

3.3.4 Topographic variables

The depth of the water column within the study area ranged from 0 m at the shore to -31 m (Table 3-6). The mean depth of the Rottnest Island Reserve (RIR) was -9.48 m, with most pixels (91.09%) shallower than -18 m.

The south-west quadrant of the reserve had both the greatest maximum (-30.93 m) and mean (-13.68 m) depths (Table 3-6). The north-west quadrant had the shallowest mean

Table 3-6: Summary statistics for the topographic variables of depth, slope and aspect for the whole Rottnest Island Reserve (RIR) and each individual quadrant.

DBM Region	Depth (m)			Slope (degrees)			Aspect (degrees)		
	Min	Max	Mean (SD)	Min	Max	Mean (SD)	Mean	Circular SD	Circular variance
RIR	0	-30.93	-9.48 (6.68)	0	49.09	2.10 (2.20)	167.09	122.83	0.90
NW	0	-27.08	-8.36 (5.91)	0	49.09	2.83 (2.70)	330.79	104.42	0.81
NE	0	-22.60	-8.71 (5.28)	0	40.72	1.44 (1.67)	9.20	88.64	0.70
SE	0	-27.55	-8.40 (5.75)	0	45.34	1.99 (2.13)	164.56	76.30	0.59
SW	0	-30.93	-13.68 (8.90)	0	37.66	2.54 (2.07)	168.46	71.45	0.54

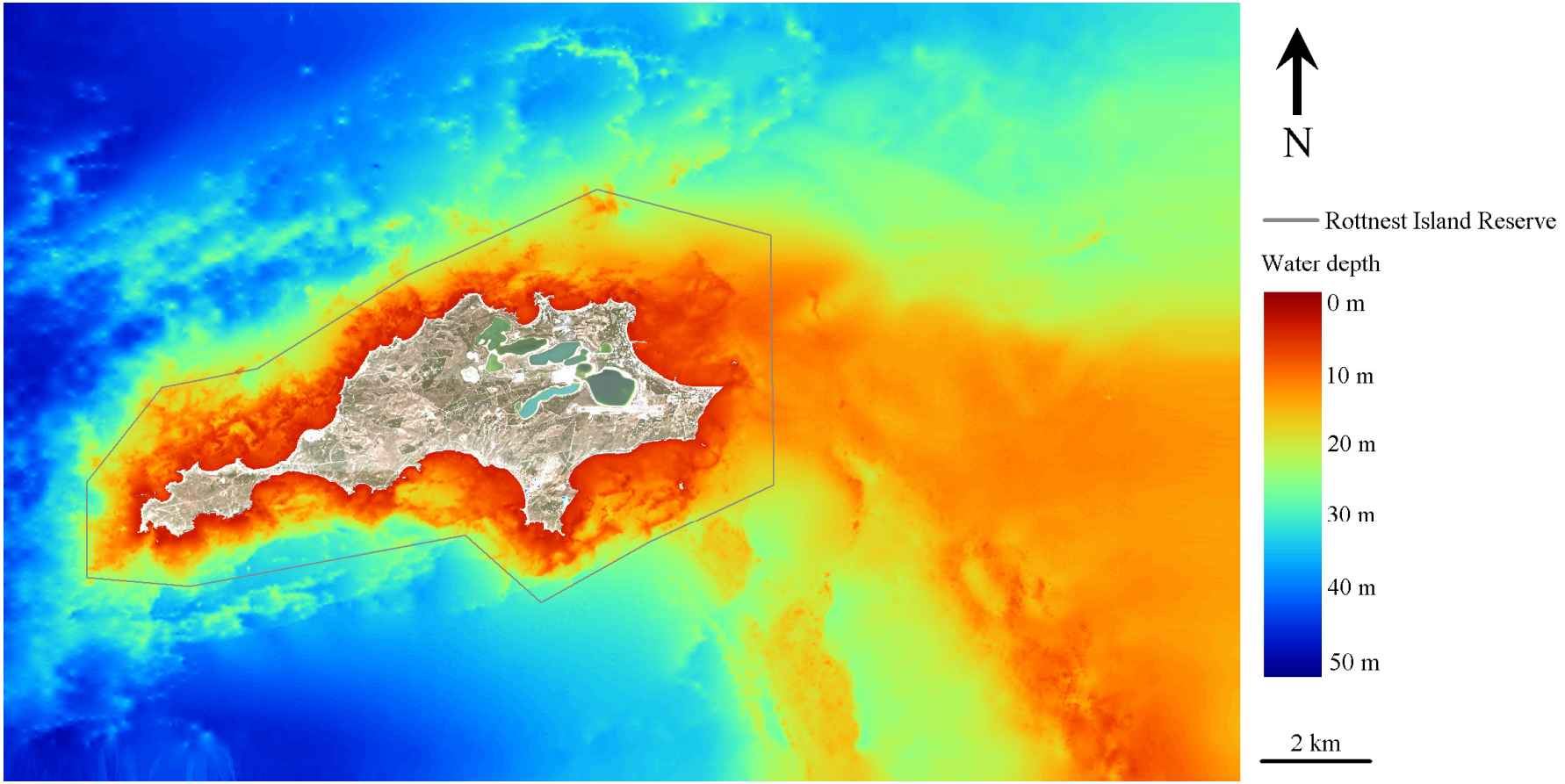

Figure3-12: Digital bathymetric model of the seafloor surrounding Rottnest Island interpolated using the kriging algorithm from DPI sounding data (1980 – 1998).

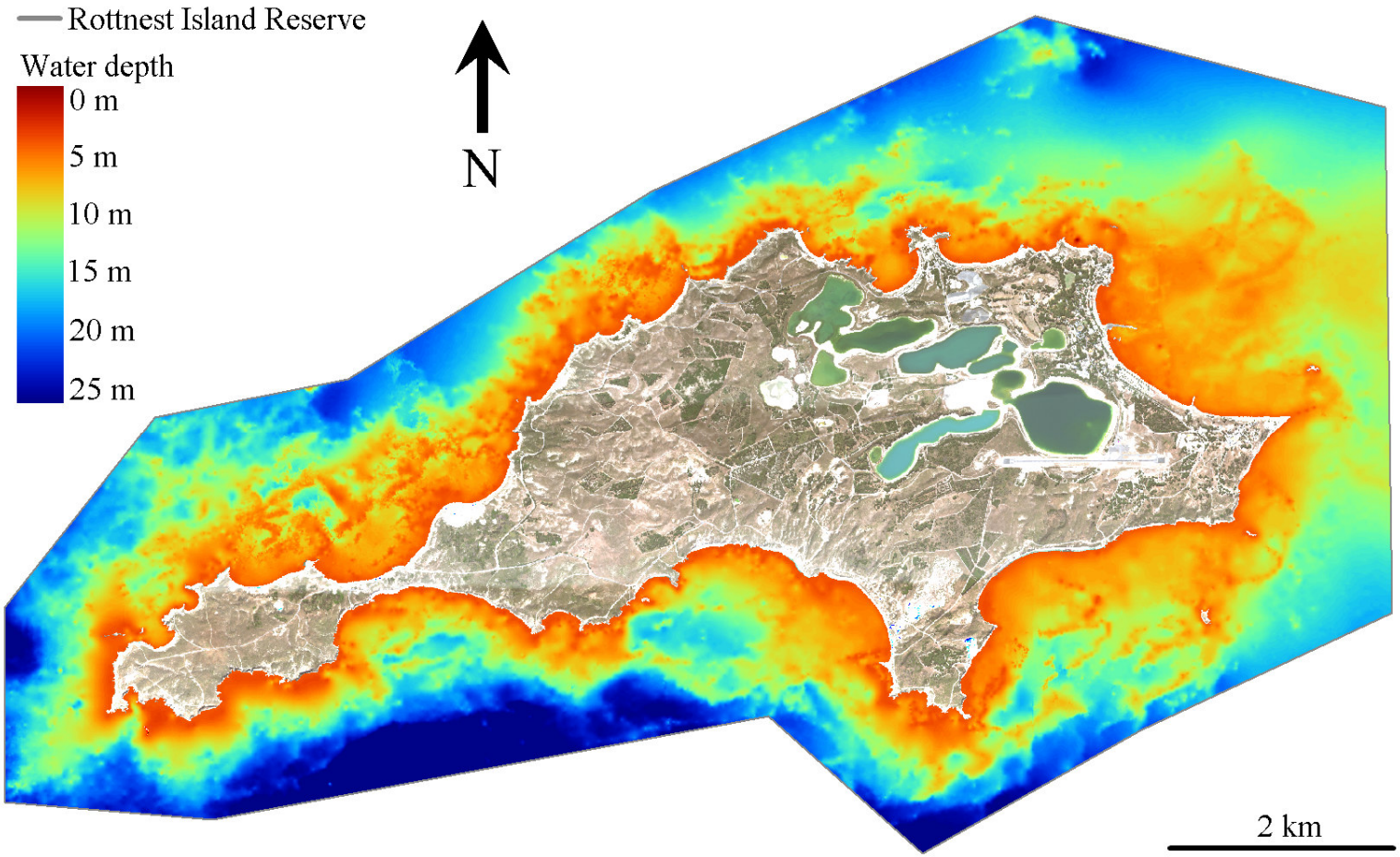

Figure 3-13: Digital bathymetric model of the seafloor of Rottnest Island Reserve interpolated using the kriging algorithm from DPI sounding data (1980 – 1998).

depth (-8.36 m) and the south-west quadrant had the greatest variability in depth with a standard deviation of -8.90 m. The majority of pixels in all quadrants occurred at depths shallower than -15 m (Figure 3-14). The south-west quadrant showed an unusual distribution with a relatively even distribution across all depths to -15 m (Figure 3-14).

The regular slope values for the RIR ranged from 0° to 49.09°, with a mean value of 2.10°. The majority of the pixels (91.5%) within the data set had slope values < 5° (Figure 3-15). The quadrants with the greatest slope values were the north-west (49.09°) and the south-east (45.34°) (Table 3-6). The north-east quadrant had both the lowest mean and standard deviation of the slope (1.44° & 1.67°), indicating it had the flattest and least variable topography. The north-west quadrant had the greatest variability in topography with a standard deviation value of 2.70°.

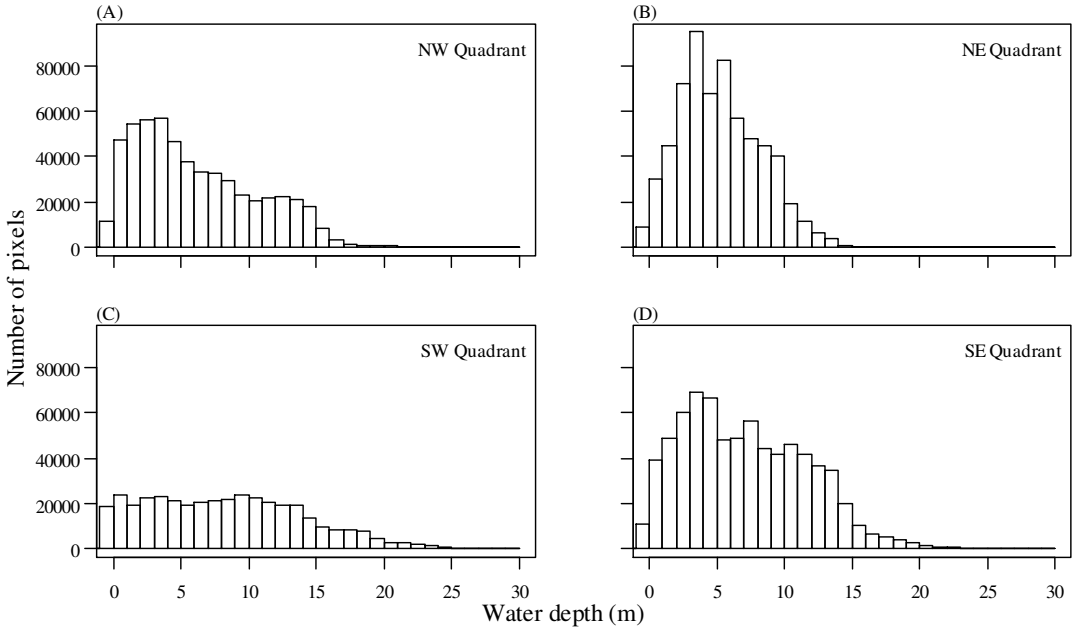

Figure 3-14: Histograms of the depth distribution of pixels within the Rottnest Island Reserve analysed by quadrant. Pixels with values less than zero meters water depth indicate exposed reefs and intertidal platforms.

The mean aspect of the seafloor of the RIR was towards the south (167°), with the majority of the sloped surfaces of the seafloor facing either towards the north or south most likely due to the east-west orientation of the island (Figure 3-16). The north-west quadrant of the RIR had a mean aspect of 331° and the majority of the sloped surfaces faced in a north-westerly direction (Figure 3-17). The north-east quadrant had a mean aspect of 9°, with the majority of sloped surfaces facing towards the north. The majority of sloped surfaces in both the south-east and south-west quadrants faced towards the south, with mean aspects of 164° and 168°, respectively (Figure 3-17).

The up-slope and down-slope analysis identified that the majority of slopes in both a south and south-westerly direction were down-slopes on the southern side of the island, making them exposed to the prevailing south-westerly swells (Figure 3-18). In contrast

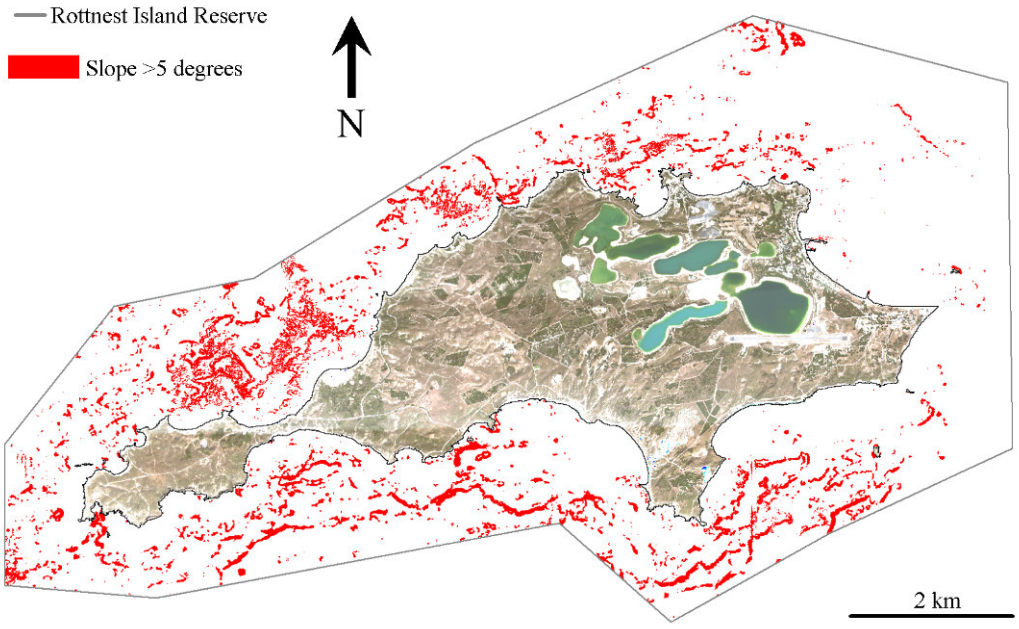

Figure 3-15: The areas within the Rottnest Island Reserve that had slopes >5°.

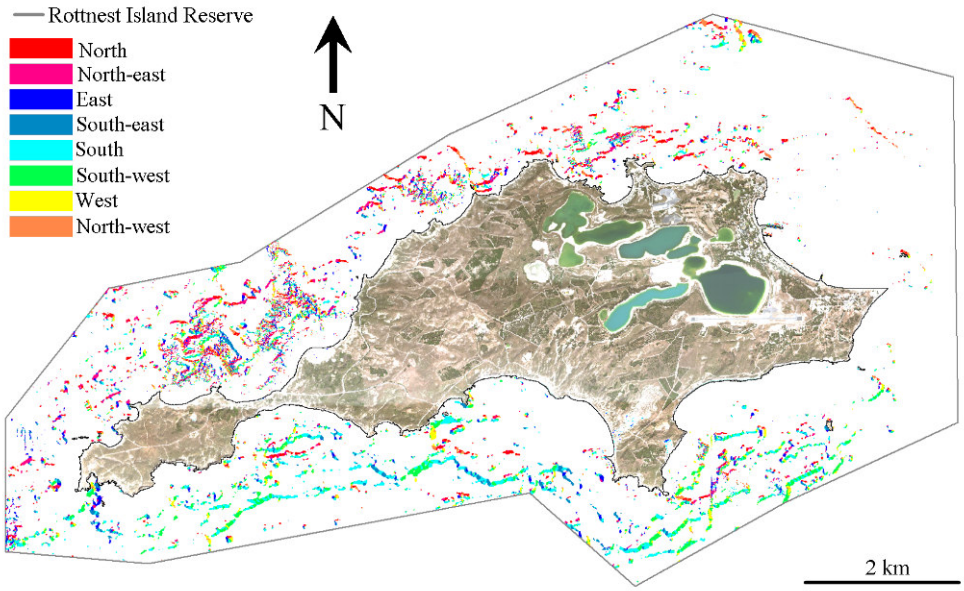

Figure 3-16: The aspect of the seafloor around Rottnest Island where the slope was >5°.

to this, slopes in these directions on the northern side of the island were mostly up-slopes. However, the slopes in north and north-westerly directions, on the northern side of the island, were predominantly down-slopes, thus making them exposed to the prevailing swell as it is diffracted around the island, to approach from an approximately north-westerly direction. There were very few up or down-slopes identified in the north-east quadrant.

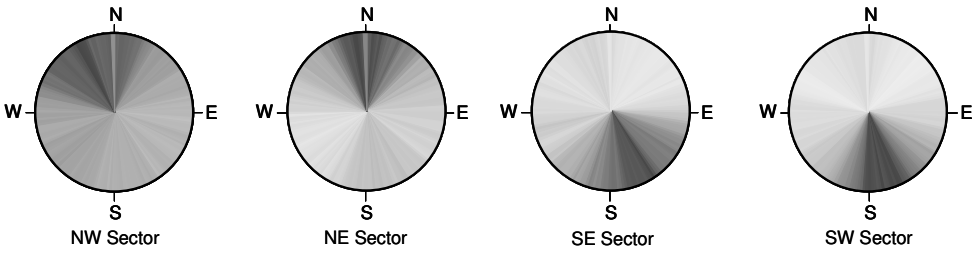

Figure 3-17: Distribution of the aspect values for all pixels with a slope >5°, analysed for each quadrant of the Rottnest Island Reserve. The darker the segment, the more pixels in the quadrant with that aspect.

3.3.5 Abiotic variables affecting the benthic habitats

3.3.5.1 Reef type

The delineation of the substrate into high (>1 m relief) and low (<1 m relief) relief reefs using the DBM identified 196 hectares of high relief reef and 140 hectares of low relief reef in the Rottnest Island Reserve (Figure 3-19). The north-west had the highest proportion of reefs, the majority being high relief (Figure 3-20). There was a notable lack of high relief reefs in the north-east quadrant, compared to the other three quadrants.

3.3.5.2 Benthic complexity

The benthic complexity based on the local variability of the depth showed an array of complex structures around most of the island with the exception of the north-east region which had a markedly less complex environment (Figure 3-21). The RIR had complexity values that ranged from 0.33 to 1.0 and a mean complexity of 0.74. The benthic complexity layer based on local variability of the regular slope had a mean complexity of 0.73 and highlighted more clearly than the depth, the lack of complexity in the north-east of the reserve (Figure 3-21). The benthic complexity calculated using the circular variance of the aspect values within the analysis window had a mean benthic complexity of 0.16 and only clearly highlighted the structures to the north-west of the island (Figure 3-21). The complexity layer representing mean change in slope indicated a mean complexity for the RIR of 0.62 and again indicated the lack of complexity in the north-east quadrant (Figure 3-21).

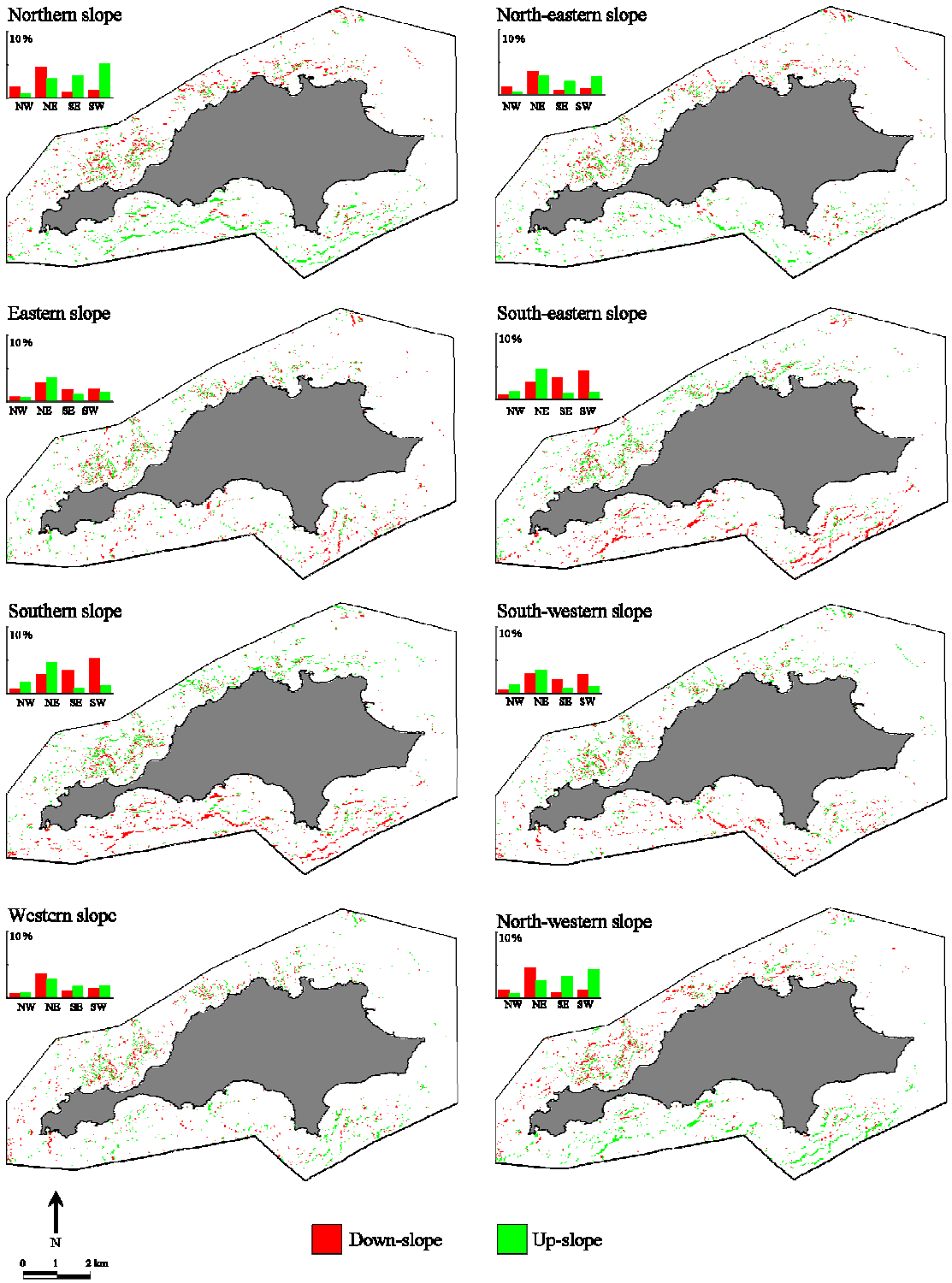

Figure 3-18: Maps indicating the regions of Rottnest Island Reserve that have either an up-slope or down-slope in each cardinal direction. Column charts indicate the distribution within each of the four analysis quadrants of Rottnest Island Reserve with red bars representing down-slopes and green bars representing up-slopes.

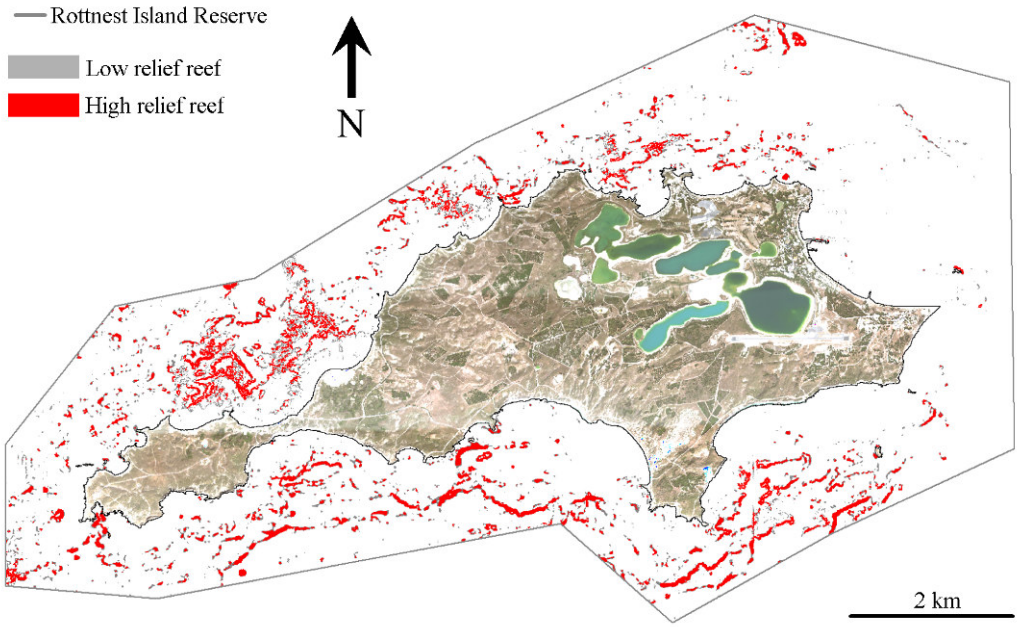

Figure 3-19: Map indicating the areas of Rottnest Island Reserve that have high or low relief reef. High relief is defined as having vertical relief >1 m and slope < 5 degrees.

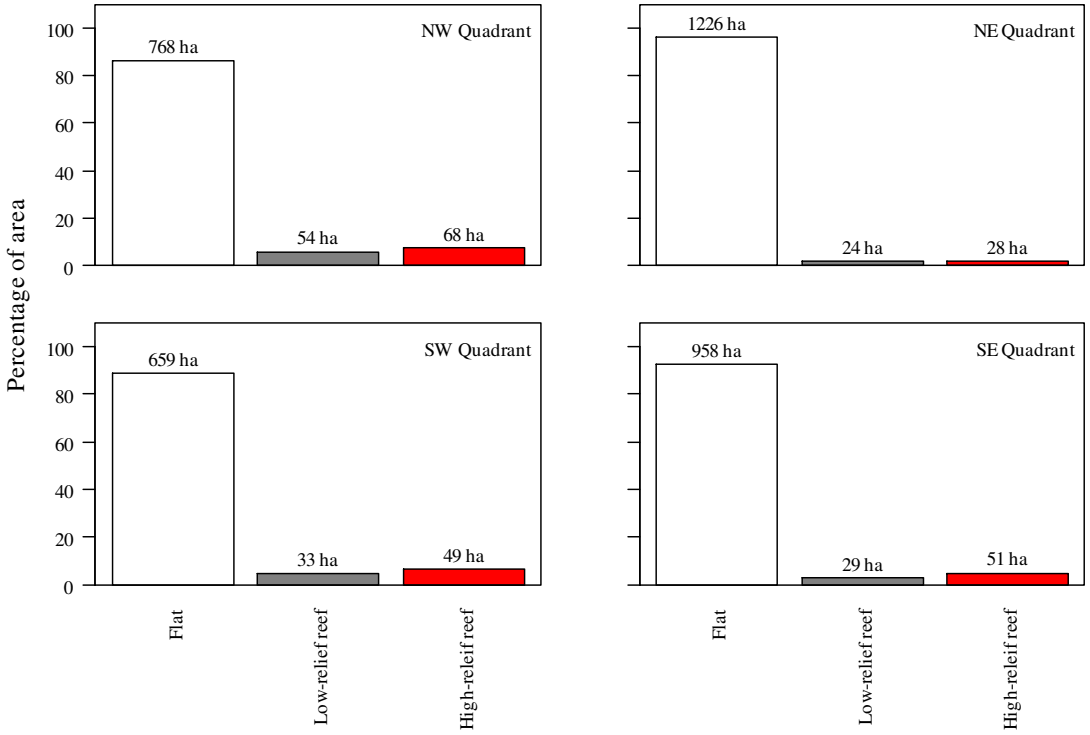

Figure 3-20: The percentage of the area of each quadrant within Rottnest Island Reserve that was identified as low or high relief reef or flat.

3.3.5.3 Exposure

The percentage of time the wind blew from each direction went through a seasonal cycle. Winds blowing from the south dominate from October to March, with the winds becoming much more variable during the intervening months (Figure 3-22). The monthly mean of the maximum wind speeds was the greatest in December (11.64 ms^{-1}) and the lowest was in April (9.25 ms^{-1}) (Table 3-7). However, the highest monthly mean wind speed was seen in July for north-west winds (14.43 ms^{-1}). On average the strongest winds occur from the northwest (12.33 ms^{-1}) and the lightest from the northeast (8.55 ms^{-1}).

The REI values calculated on a monthly basis indicted a seasonal trend that showed the southern side of the island being exposed during the summer months (December – February), a lessening of exposure through autumn, then a shift to greater exposure on the north-western side of the island during winter followed by the south-western side being exposed during spring (Figure 3-23). The yearly relative exposure index (REI) calculated for the RIR showed that the maximum exposure was experienced on the south-western facing coast of the island (Figure 3-24). The southern side of the RIR was more exposed than the northern side, while the most protected regions were found in sheltered bays on the north side of the island.

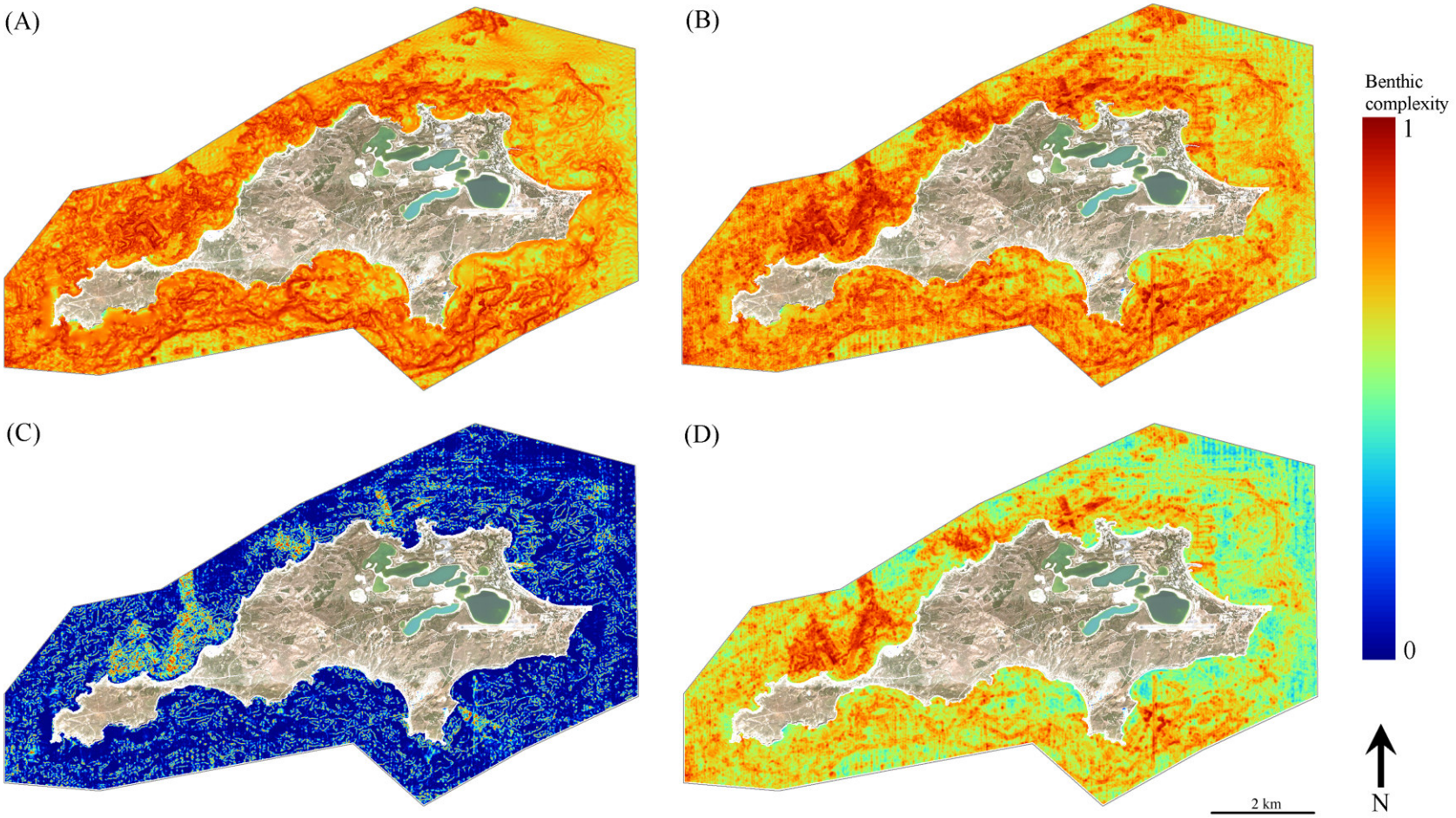

Figure 3-21: The benthic complexity layers for Rottnest Island Reserve based on the natural logarithm of the standard deviation of the bathymetry (A) and the slope (B), the circular variance of the aspect (C) and the mean change in slope in all cardinal directions for each pixel (D). All values were calculated using a five pixel radius (17.5 m) circular kernel filter and were normalised so values ranges from zero to one for minimum to maximum complexity.

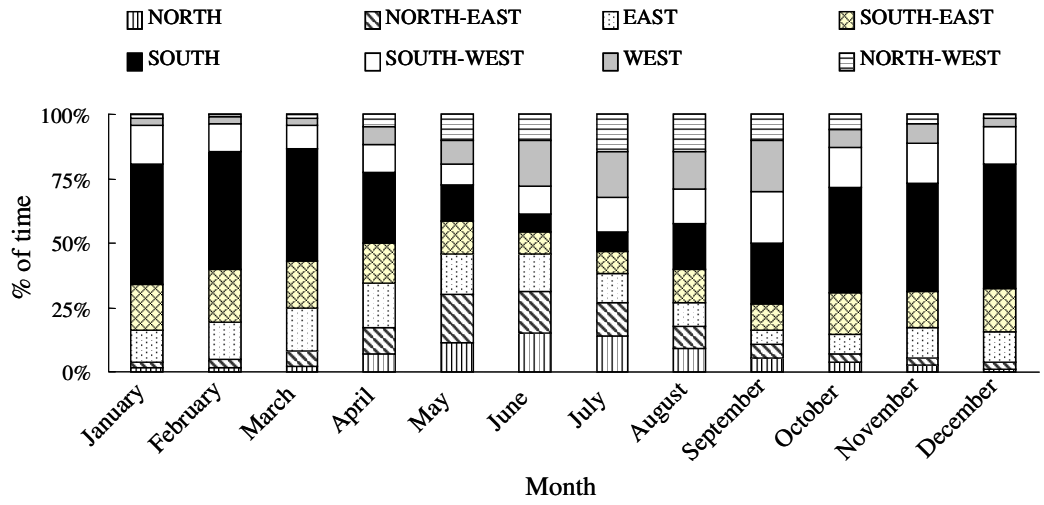

Figure 3-22: Percentage of time wind blew in each cardinal direction (N, NE, E, SE, S, SW, W, NW) over the years 2000-2006. Note calm conditions are too infrequent to represent on graph

Table 3-7: The summary of the mean maximum wind speed (ms^{-1}) for each month in each of the eight cardinal directions for Rottnest Island Reserve for the years 2000 – 2007.

Month	North	North-east	East	South-east	South	South-west	West	North-west	Mean
January	8.75	9.42	10.69	10.67	12.35	11.22	8.38	8.35	11.38
February	8.01	8.64	10.67	10.63	11.87	10.63	7.46	7.67	10.98
March	8.43	9.13	9.92	10.54	11.67	9.94	8.45	7.95	10.64
April	9.33	8.74	9.29	8.76	9.60	9.20	9.74	9.09	9.25
May	11.19	8.83	7.14	8.31	9.38	11.70	10.68	13.51	9.72
June	12.30	8.79	6.80	8.52	10.46	12.40	13.08	13.32	10.74
July	11.51	8.62	7.33	8.48	10.91	13.40	13.44	14.43	11.37
August	10.29	6.88	6.10	8.78	10.96	13.42	12.62	13.21	10.72
September	10.12	7.30	6.36	7.31	9.35	11.19	11.47	11.20	9.89
October	10.32	8.45	9.54	9.69	11.31	10.58	10.90	10.59	10.60
November	11.13	9.24	10.33	10.52	12.10	11.54	11.08	10.70	11.35
December	10.45	9.28	11.05	10.99	12.58	11.08	8.90	9.13	11.64
Mean	10.87	8.55	8.91	9.65	11.44	11.42	11.65	12.33	10.69

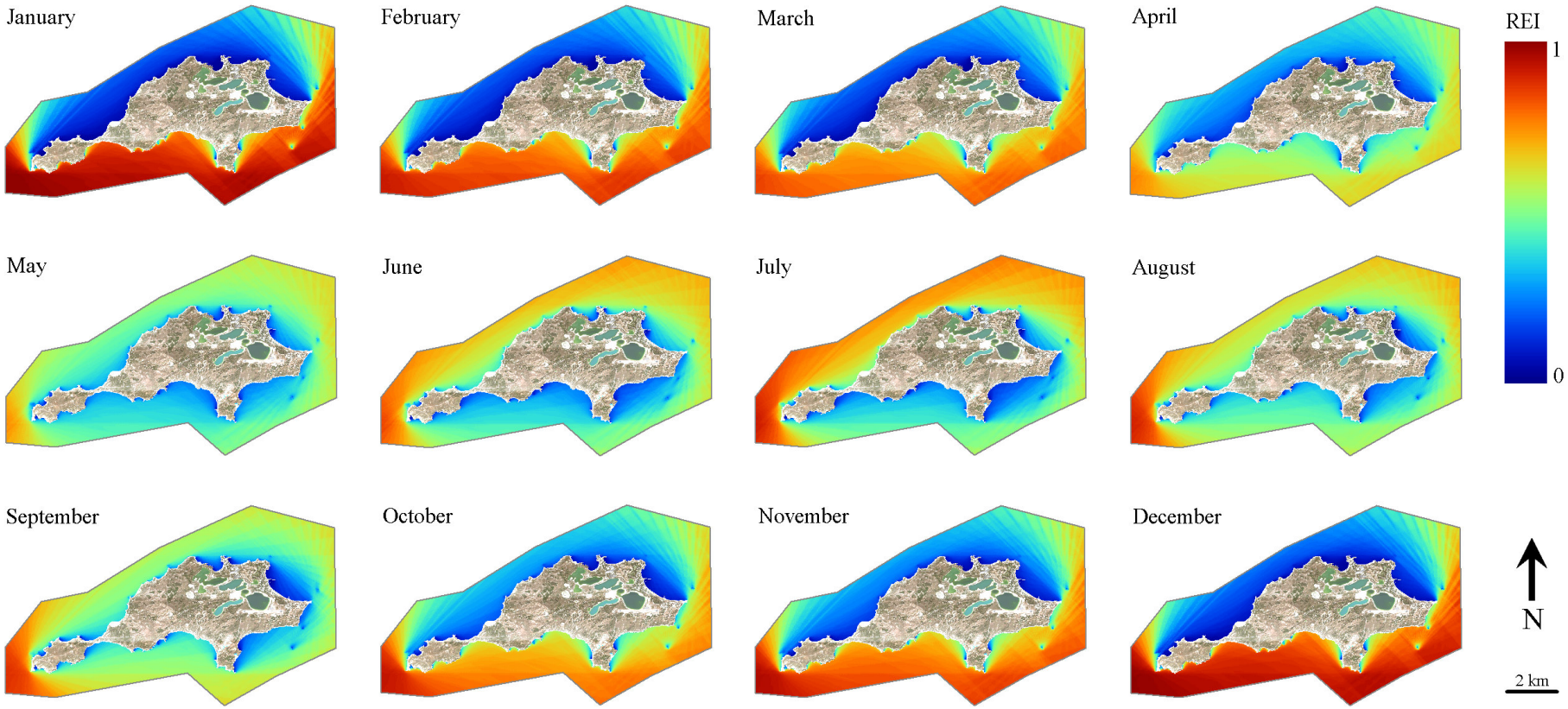

Figure 3-23: The relative exposure index (REI) for areas within Rottnest Island Reserve, to waves generated by prevailing winds. REI values calculated based on the mean maximum wind speeds and percentage of time winds blew in each of eight cardinal directions calculated for each month over 2000 – 2007. The REI values range from zero to one for minimum to maximum exposure.

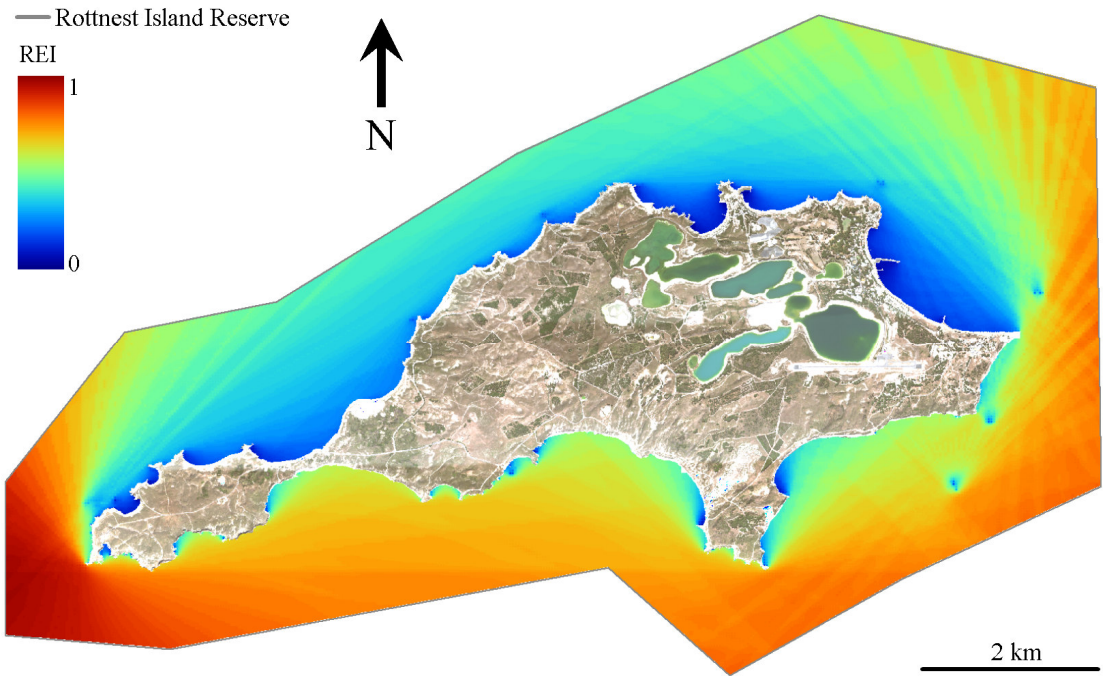

Figure 3-24: The relative exposure index (REI) for areas within Rottnest Island Reserve, to waves generated by prevailing winds. REI values calculated based on the mean of the maximum wind speeds and percentage of time winds blew in each of eight cardinal directions calculated for 2000 – 2006. The REI values range from zero to one for minimum to maximum exposure.

3.4 Discussion

The bathymetric data used to create the Rottnest Island DBM consisted of nine digital data sets, data from one hardcopy map sheet supplied by the Western Australian Department for Planning and Infrastructure and the coastline data set extracted directly from the HyMap image. These data covered the majority of the Rottnest Island Reserve, but left significant areas in the shallow regions immediately adjacent to the shoreline such as the very shallow reefs in Thomson Bay, with no data. This created the possibility for significant error in the depth estimates generated by the interpolation algorithm. All of the bathymetric sounding data were corrected to account for the tidal height at the time the HyMap image was flown, thus allowing for as accurate as possible correction for the influence of the water column on the image on a pixel by pixel basis.

By rigorously validating the data set prior to DBM interpolation, to remove any erroneous data, and cross-validating the interpolation method used, the most accurate DBM for the Rottnest Island Reserve was created. It is often the case in the marine environment that bathymetric data does not exist in a single data set, collected at the same time, using a standardised method. This means that it is often necessary to utilise any data available to generate the best DBM surface possible. This chapter demonstrates a method of utilising all the available data for a region to create a DBM.

The cross-validation results indicated that the RMS errors for all interpolation algorithms were < 0.01 m. This compares favourably with results of Desmet (1997) in a study on errors in DEM interpolation. The results of the MAE for the different algorithms ranged from 0.36 – 0.48 m which is significantly greater than the range of RMS errors. This was not the case with the data tested by Desmet (1997), who found the RMS error and MAE to be within the same ranges. However, the data tested by Desmet (1997) was very flat undulating terrestrial farm land and not a highly complex environment such as the subtidal areas of Rottnest Island Reserve. These results may also be due to the assumptions made when using RMS errors, those being that the errors are random, have a mean of zero and are normally distributed around the actual value (Li 1988, Desmet 1997).

By using the combination of RMS error and MAE with standard deviation as proposed by Li (1988), and incorporating a regression and estimate error analysis, it was possible to determine that the kriging algorithm provided the most reliable and accurate interpolation of the bathymetric surface for the Rottnest Island Reserve. This concurs with Bekkby *et al*. (2002) who, for various reasons, including it being an exact

interpolator and providing a grid of estimate variance, concluded that kriging was the most appropriate algorithm to develop a DBM for a coastal region in Norway. There has been no definitive method published for assessing a scattered point data set to determine which spatial interpolation algorithm is most appropriate to create a DBM. This was the reason for developing a means for ranking the different algorithms that used a number of different accuracy assessment indices in combination. Each of the different indices addressed the accuracy of the data estimates from a slightly different perspective, with each contributing to the overall accuracy of the final product.

Further validation of the final DBM product using new depth data collected in the field provides the user with a measure of accuracy of the actual bathymetry found at the study site. Unlike the cross-validation process, this approach uses data that is collected independently of the data set used to create the DBM. This is especially important when creating a DBM from data that has been collected over a long time period, at different densities and using various methods, such as was the case with the Rottnest data. However, the use of independent data for bathymetric DBM validation does require careful consideration to ensure that both the effect of tides and the inherent inaccuracy of GPS systems and depth sounders are taken into account. The spatial resolution of the DBM needs also to be considered as a depth sounding collected in the field records the value for a point, while a grid cell represents the average depth over a region. This study attempted to account for these factors in a relatively simple and uncomplicated manner that can be easily applied.

The availability of an accurate DBM to represent the bathymetry of a study region is often an essential component of many marine studies, including benthic habitat

mapping, modelling faunal distributions and oceanographic modelling. Here a method to develop an accurate DBM using the available sounding data has been described and is able to provide users with some guidance regarding the overall accuracy and the spatial distribution of any errors in the final DBM.

The analysis of the bathymetric features of slope and aspect in Rottnest Island Reserve has highlighted the low level of complexity in the north-east quadrant and the high frequency of sloped surfaces in the north-west quadrant. This variation in the sloped surfaces has most probably developed over time as a result of the exposure of the island to ocean swells which predominantly approach from the south-west. The north-eastern side of the island is the most protected and, as a result, has the greatest areas of shallow flat sandy substrate, much of it populated with seagrass meadows (Wells and Walker 1993). In contrast, the majority of the benthic habitats in those regions highlighted by the sloped surfaces are most likely to be rocky reefs dominated by macroalgae.

The abiotic variables generated for this study have previously been found to influence the distribution of various subtidal macrophytes. Water depth has long been accepted as being an important factor that influences the distribution of subtidal macrophytes, with many having optimal depth ranges leading to zonation of assemblages (Womersley and Edmonds 1952). Water depth can influence the levels of exposure, light and sedimentation a habitat is exposed to (Goldberg and Kendrick 2004, Kendrick *et al.* 2004). Goldberg and Kendrick (2004) found that the macroalgae assemblages differed with depth in the Recherche Archipelago, Western Australia. This finding is consistent with those of O'Hara (2001) in Victoria, Australia and Schiel (1988) in New Zealand. The slope of the substrate is one of the most important features of subtidal temperate

systems with regard to influencing the distributions of organisms (Connell 2007). Those rocky substrates surfaces that are horizontal or gently sloping are typically dominated by algae and, as the slope gets steeper, sessile invertebrates become more dominant.

Benthic, substrate or habitat complexity has been linked to the composition and species richness of algal assemblages associated with *E. radiata* in south-western Australia (Toohey 2007, Toohey *et al.* 2007). This makes it an ideal abiotic variable to use for applications such as habitat suitability modelling. Added to this, habitat complexity has been linked to the distribution, abundance and species richness of fish assemblages in both tropical and temperate reef systems where regions of higher benthic complexity will typically have greater biodiversity (McClanahan 1994, McCormick 1994, Angel and Ojeda 2001, Garcia-Charton and Perez-Ruzafa 2001, Friedlander *et al.* 2003, Gratwicke and Speight 2005). The exposure of habitats to wave action also has a significant effect on the occurrence and maintenance of viable populations of many subtidal macrophytes. Kendrick *et al*. (1999), Wernberg *et al*. (2003b) and Goldberg and Kendrick (2004) all found that wave exposure influenced the distribution and diversity of macroalgae assemblages in southwestern Australia. Although it should be noted that REI, the measure of exposure used in this study, is limited to exposure caused by wind-generated waves and not swell. This can be problematic in regions like Strickland and Salmon Bays on Rottnest's south coast where the REI predicted a lower exposure during winter than summer. However they are both known to experience high levels of exposure due to the south-westerly swells during winter storms. Friedlander *et al*. (2003) identified that wave exposure, in combination with habitat complexity,

played a significant role in determining the fish assemblage structure in the Hawaiian archipelago.

By using abiotic variables linked to habitats at different levels of the habitat classification scheme, improved benthic classifications using hyperspectral image data can be obtained. This is a similar approach to that taken by Garza-Perez *et al*. (2004), who linked a habitat modelling approach with remotely sensed data to map coral reefs in the Mexican Caribbean. They used a generalised additive model (GAM) to utilise geomorphic features as part of their classification (Lehmann *et al.* 2002). Lehman (1998) used a GAM to model macrophyte distribution in Lake Geneva, Switzerland, with environmental variables including bathymetry, effective fetch and substrate type as inputs for the model. Fonseca *et al*. (2002) modelled the presence/absence of seagrass in Beaufort, North Carolina, using a combination of environmental variables similar to those generated in this study.

In the context of the marine benthic habitat mapping study at Rottnest Island, the DBM provided information for a number of aspects of the project. These included validation of the correction for the influence of the water column on the image reflectance data carried out using the MIP software, modelling the wave climate of Rottnest Island and providing the base layer for analysis of other topographical features of the seafloor, such as slope and aspect. The outputs of all these applications were used as inputs into the final hierarchical classification scheme developed for classifying temperate habitat types using hyperspectral data.

The independence of this classification method can be further enhanced by using the final DBM product to test the accuracy of a number of algorithms used to extract water

depth directly from hyperspectral data without any external inputs, such as MIP which was used in this project. This will aid in the development of a toolkit for the mapping of shallow marine benthic habitats based solely on hyperspectral imagery and an associated spectral reflectance library, without the need for extensive field campaigns. This could increase the cost effectiveness and applicability of this data type in marine planning scenarios.

Overall, the approach taken in this study has provided a comprehensive means of linking the benthic habitats of Rottnest Island Reserve described by the nested hierarchical classification scheme with environmental abiotic variables as part of hyperspectral imagery classification. This integration provides the means to both validate, and further separate, habitats identified in the hyperspectral data based on their optical properties. The use of the abiotic variables to predict habitat suitability and provide the basis for decision rules allows for the optical hyperspectral data to be pushed further with regard to mapping benthic habitats at a higher resolution than is possible with spectral library based techniques.

4 Development of a spectral library for the dominant habitat components of Rottnest Island Reserve

4.1 Introduction

The difficulty of measuring and mapping information on the distribution of marine biodiversity at spatial scales relevant to marine planning has resulted in the use of biodiversity surrogates (Vanderklift *et al.* 1998, Ward *et al.* 1999). In terms of shallow coastal systems, benthic habitat types have been found to be a reasonably reliable surrogate for marine biodiversity (Ward *et al.* 1999). Moreover, readily available and relatively robust methods for interpretation of remotely sensed data have become a cost effective way to classify marine benthic habitat at the scales required for marine planning (Mumby *et al.* 1999).

In the past, most interpretation of remotely sensed data was carried out using image-based classification techniques, in combination with ground validation and/or expert knowledge of an area, to allocate each pixel to a particular habitat class (Sotheran *et al.* 1997, Ong *et al.* 1998, Purkis *et al.* 2002, Kutser *et al.* 2003). While these methods often provided suitable results for marine planning, their use was generally limited to either specific sensors or data sets (Kutser *et al.* 2003). As such, it was impossible to apply a standardised image processing protocol to multiple data sets collected at different resolutions and times.

These problems have been overcome by developing physics-based approaches, which enable images from a variety of sources to be processed using standardised protocols (Kutser *et al.* 2003, Heege and Fischer 2004). They use a series of physics-based optimisation algorithms to correct remotely sensed data collected over water by removing the influence of the overlying water column, and sun-glint. They also allow

for the classification of image data using techniques that have been developed for spectroscopy, which require spectral signature data on potential benthic habitat components (Kutser *et al.* 2003). Spectral signature data are often collected *in situ* using field spectrometers and collated to form spectral libraries. Spectral libraries have been applied in a number of research fields (e.g., geology, terrestrial vegetation, fresh water systems and marine benthic habitats) and used to identify target cover classes within hyperspectral image pixels (Drake *et al.* 1999, Holden and LeDrew 2000, Okin *et al.* 2001, Shepherd and Walsh 2002, Kutser *et al.* 2003).

The spectral characteristics of benthic habitat components can be split into two broad categories, the bare substrate where reflectance signature is influenced by the chemical composition of the substrate (Palacios-Orueta and Ustin 1998) and bio-substrate which consists of living organisms such as plants. The spectral reflectance characteristics of bio-substrate habitat components result from a combination of the surface properties of the leaves or fronds, the internal structure of the plant, and the presence and concentrations of various pigments, the most influential, in the visible region (400 – 700 nm), being chlorophyll (Richardson *et al.* 2002, Thorhaug *et al.* 2007). Chlorophyll absorbs light in both the blue and red regions of the visible spectrum, with the absorbance maxima being in the red region, just before the 'red edge' (Sims and Gamon 2002).

Although considerable research has been undertaken on the spectral characteristics of various marine habitat components, few studies have used the collected spectra to classify benthic habitats for these environments from image data. Several studies have focused on analysing the spectral characteristics of coral reefs, as the clear, shallow

waters where they are found provide ideal conditions for optical remote sensing (Holden and LeDrew 1998, Hochberg and Atkinson 2000, Hochberg *et al.* 2003). Such analyses enable different corals and algae to be separated based on their spectral characteristics. This is a prerequisite for image classification, as it allows for the identification of those habitat components that can be theoretically distinguished in an image acquired under ideal conditions (Karpouzli *et al.* 2004).

At the scale of the pixels in most hyperspectral remotely-sensed data (1 – 5 m), marine benthic environments are often made up of a complex mixture of habitat components. This inherent variability provides some unique challenges to remote sensing practitioners when attempting to classify each pixel into a habitat component or mix of components. Thus, it is necessary to conduct some form of separability analysis on the *in situ* spectral signatures available in the spectral library. These analyses determine the dissimilarity between spectra and thus identify benthic habitats that theoretically can be identified in an image.

Methods such as principal components analysis (PCA) and cluster analysis have been used as a measure of similarity between spectral signatures (Holden and LeDrew 1998, Fyfe 2003). Both of these statistical methods are based on some form of Euclidean distance, which has a number of features that make it less desirable to use in hyperspectral data analysis (Clarke and Warwick 2001, McCune and Grace 2002). The first of these is that it is not invariant to scalar multiplication and thus will have difficulty distinguishing habitat components when spectral signatures were obtained at different levels of illumination (Keshava 2004, Robila 2005). Moreover, the values obtained using the Euclidean distance do not occur within a set interval, making it

difficult to integrate the algorithm into any automated or semi-automated classification system which uses thresholds of the distance measure to separate classes (Robila 2005). Finally, Euclidean distance is monotonic in nature, which means that as the number of spectral bands used in a separation analysis increases, the Euclidean distance will also increase (Keshava 2004). Thus, when attempting to maximise the separation between substrate classes, and simultaneously trying to reduce the dimensionality of the data, the best result will be to use all the spectral bands available. Other distance measures such as the spectral angle, which do not share these features, may be a more appropriate method of distinguishing between spectra and result in better solutions (Keshava 2004).

The aim of this study was firstly to use and extend existing techniques for the collection and analysis of *in situ* spectral reflectance data. A comprehensive library of the spectral signatures of the spectrally dominant habitat components was collected to match the nested hierarchical classification scheme developed for Rottnest Island (Chapter 3). This library was subjected to spectral separability analysis to ascertain the best method to classify the hyperspectral image data to identify the different habitats using the spectral library. This required testing of a number of non-Euclidean spectral distance measures to determine the best methods and band combinations to separate the different habitat components present at Rottnest Island using spectral signatures at HyMap (~15 nm) resolution. A classification algorithm was developed that could use the results from the spectral separability analysis, in combination with the spectral library, to classify hyperspectral image data by identifying the dominant habitat component in a mixed pixel. This classification algorithm was further tested against synthetic spectral signatures, designed to mimic the spectral signatures expected from the image data, to assess its ability to accurately classify mixed pixels.

4.2 Methods

4.2.1 Collection of *in situ* spectra

The spectral signatures for 13 different habitat components were collected from various substrates in Rottnest Island Reserve, and nearby Marmion and Shoalwater Marine Parks (Figure 2-1). The additional sampling areas were chosen to provide a representative sample of spectral signatures for Perth coastal waters.

The collection of reflectance spectra was carried out using a single channel Ocean Optics USB2000 spectrometer, attached to a laptop computer. The spectrometer was fitted with a 30 m long, 500 µm diameter fibre-optic cable equipped with a 100 mm long stainless steel probe and used the same settings for all data collection (Table 4-1).

Table 4-1: Typical settings used when collecting spectral signatures underwater with an Ocean Optics USB2000 spectrometer.

Variable	Setting
Integration Time	70 msec
Spectra Averaged	1
Boxcar Smoothing	10
Correct for electrical dark current	ON
Fibre-optic length	30 m
Fibre-optic diameter	500 µm
Fibre-optic field of view	22°
Distance of probe from target	~10 cm
Area of habitat component sampled	~40 cm^2

The spectral data were recorded as a text file, when triggered by the diver using a control cable attached to the fibre optic (Figure 4-1). Spectral data, as individual spectra, were recorded as both the upwelling radiance (E_u) from the target habitat component and the downwelling irradiance (E_d), from a calibrated white Teflon reflectance panel, i.e. spectral pairs. The E_u and E_d spectra were measured using digital

numbers (DN) that ranged between 0 and 4000. A Teflon panel (115 x 200 mm) was used as it reflects almost 100 percent of light in the visible portion of the spectrum (Dekker *et al.* 2003). Ten pairs of spectra were collected for each target. A dark current measurement was taken before and after each dive by recording 10 replicate spectra with all light blocked from the spectrometer. The dark current refers to the digital numbers recorded by the spectrometer when no light is present.

Figure 4-1: The underwater spectrometer setup for collecting spectral reflectance signatures of habitat components in shallow water. Note the remote trigger held in the diver's left hand and the Teflon reflectance panel in the foreground. Note that this image was not taken at Rottnest Island.

4.2.2 Data Processing

The *in situ* spectral data of the dominant habitat components were used to calculate a range of spectral statistics based on reflectance data (Table 4-2). The spectral statistics were based on the absolute spectral reflectance (ASR) for each habitat component and

included the mean, median, standard deviation, minimum, maximum and first and second derivatives (Table 4-2). A spectral library was developed to provide a framework for the assessment of the spectral separability of the various habitat components at each level of the hierarchical classification scheme (see Chapter 2).

Table 4-2: Summary of the spectral statistics calculated from the absolute spectral reflectance spectra recorded in Perth coastal waters. Statistics were calculated using the full resolution spectra and then re-sampled to HyMap resolution. ASR refers to absolute spectral reflectance and DN refers to the digital number.

Statistic	Definition
ASR_{mean}	The mean DN at each wavelength for 10 ASR spectra per target
ASR_{median}	The median DN at each wavelength for 10 ASR spectra per target
ASR_{sd}	The standard deviation of the DN at each wavelength for 10 ASR spectra
ASR_{+2sd}	$(ASR_{mean}) + (2*(ASR_{sd}))$
ASR_{-2sd}	$(ASR_{mean}) - (2*(ASR_{sd}))$
ASR_{min}	The minimum DN at each wavelength for 10 ASR spectra
ASR_{max}	The maximum DN at each wavelength for 10 ASR spectra
$ASR_{1st(x)}$	The 1st derivative spectra of the ASR_{mean} using an "x" point window
$ASR_{2nd(x)}$	The 2nd derivative spectra of the ASR_{mean} using an "x" point window

4.2.2.1 Calculation of spectral statistics

The Teflon panel, used to measure downwelling irradiance was calibrated against a Spectralon diffuse reflectance standard, which is known to reflect 99% of light in the 400 – 1500 nm range. A series of reflected radiance spectral signatures were recorded in full sunlight and cloudless conditions over both the Teflon and the Spectralon whilst the probe was held at constant angle and distance from the panels on a mounting frame. The reflectance of the Teflon (R_{Teflon}) was then calculated with the Spectralon as the reference, using the following equation:

$$R_{teflon} = \frac{teflon_{\lambda}}{spectralon_{\lambda}}$$

where $spectralon_{\lambda}$ and $teflon_{\lambda}$ refer to the radiance digital number at each recorded wavelength for the Spectralon and Teflon diffuse reflectance targets. This reflectance value was then used to correct all *in situ* measurements during the calculation of the target reflectance values. Although the calibration was carried out using dry panels, it was assumed that the differences in reflectance of wet panels would negligible.

The E_d and E_u spectra were filtered to remove spectra that differed significantly from the other replicates. This process was required as conditions under which *in situ* spectra were collected, i.e. sudden wave surges, often resulted in a spectrum being collected from an incorrect target. In order for this filtering process to be carried out in a manner that was both systematic, and based on the shape of the spectra rather than changes in illumination, a method was devised based on the spectral angle metric.

The spectral number (SN) is defined as the spectral angle (SA) between a test spectrum and a flat line spectrum, which has the same value across all wavelengths. The SN was calculated using the following equation (Robila 2005):

$$SN = \cos^{-1}\left[\frac{\sum(A_i * B_i)}{\left(\sqrt{\sum(A_i * B_i)}\right)\left(\sqrt{(B_i * B_i)}\right)}\right]$$

where *A* refers to the spectrum being tested (E_u or E_d), *B* refers to the flat line reference spectrum and *i* refers to wavelength. The SN was calculated for wavelengths of 450 to 700 nm. For each spectrum being tested, the mean and standard deviation of the SN

were calculated and any spectra with a SN outside the range of the mean ± 1.5 standard deviations were excluded from further analysis.

Each individual pair of spectra (E_u, E_d) was then converted to absolute spectral reflectance (*ASR*) values using the following formula (adapted from Murphy *et al.* 2005):

$$ASR(\%) = \frac{[E_u(dn) - Dark(dn)] \times T_{CAL}}{E_d(dn) - Dark(dn)}$$

where *Dark (dn)* refers to the dark current spectrum and T_{CAL} refers to the calibration spectrum used to correct the reflectance of the Teflon panel to 100% reflectance.

The spectral reflectance signatures were processed at a resolution of 1 nm and re-sampled to match the spectral response of the 2004 HyMap sensor, which had a spectral resolution of ~15 nm. This was carried out by assuming that the spectral response could be modelled as a Gaussian function and using the full width at half maximum (FWHM) values of the sensor (Table 4-3). The FWHM values were used to define the spectral width of the imaging spectrometer in terms of the actual wavelengths at which it would record data around the defined central wavelength. The data were re-sampled by convoluting the data using a calculated Gaussian response function (Lucey *et al.* 2001):

$$(S_{HyMap})_{\lambda_0} = G(S_{Library})_{\lambda_1}$$

where S_{HyMap} was the HyMap resolution library signature, $S_{Library}$ was the full resolution signature and *G* was the matrix used to covert between the two. *G* was defined as:

$$G_{\lambda_0,\lambda_1} = \exp^{-\left[\frac{\lambda_0-\lambda_1}{\Delta\lambda}\right]^2}$$

where λ_0 was the wavelength of the HyMap band, λ_1 was the wavelength of the library band and $\Delta\lambda$ is the FWHM of the HyMap band at wavlength λ_0.

Table 4-3: The full width half maximum (FWHM) values of the first 17 bands of the 2004 HyMap sensor.

Band No.	Central wavelength (nm)	FWHM
1	454.7	13.6
2	469.3	16.5
3	485.2	15.6
4	500.1	15.6
5	515.0	15.4
6	530.7	16.4
7	546.3	15.9
8	561.4	15.2
9	576.3	15.3
10	591.5	15.5
11	607.0	16.1
12	622.5	15.3
13	637.6	15.4
14	652.6	15.1
15	667.6	15.3
16	682.8	15.5
17	698.2	15.9

The ASR spectra were cropped to retain only those values for wavelengths of 400 - 750 nm because this is the visible part of the spectrum that can be used in mapping subtidal habitats due to strong absorption by water in the infrared region (i.e. >750 nm). The mean (ASR_{mean}), median (ASR_{median}), standard deviation (ASR_{sd}), minimum (ASR_{min}) and maximum (ASR_{max}) were calculated for each target typically using 10 ASR spectra (Figure 4-2). By calculating the mean and median of the spectral data pairs remaining after filtering, it is assumed that any natural variability in the data was captured and any

spikes or dips due to isolated fluctuations in the underwater light field were smoothed out (Becker *et al.* 2005). For each ASR_{mean} and ASR_{median} spectrum the first and second derivatives were calculated using a third order Savitzky-Golay least squares approximation, with a 15 point window (Savitzky and Golay 1964).

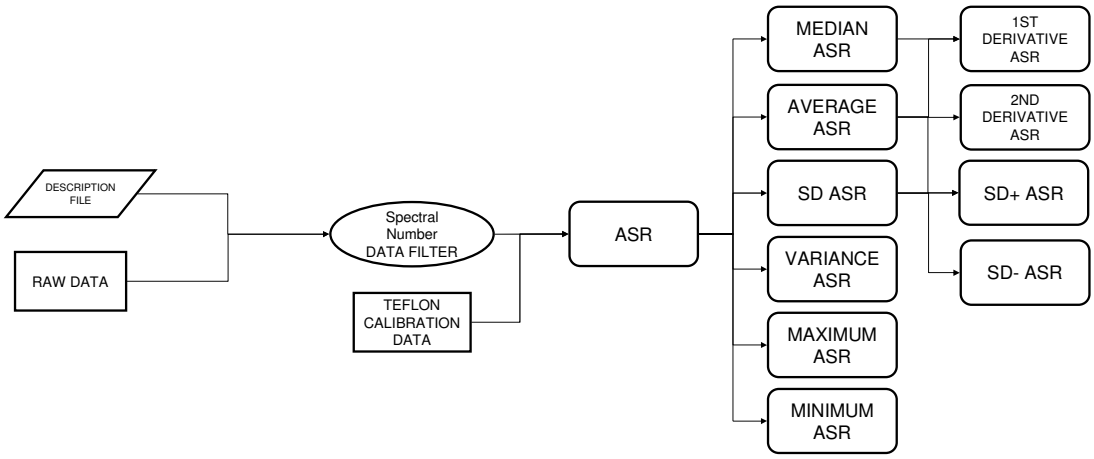

Figure 4-2: The analysis steps to generate the spectral statistics used to develop the spectral library. The spectral number filter removes any spectra with a significantly different spectral shape to others in each sample. ASR refers to absolute spectral reflectance. Note that the spectral signatures were re-sampled to HyMap resolution after ASR was calculated.

4.2.2.2 Creation of the spectral library using spectral statistics

A spectral library was created which contained the spectral signatures for the dominant habitat components and the associated spectral statistics (Table 4-2). The habitat components were combined at a number of levels as defined by the nested hierarchical classification scheme developed for Rottnest Island (see Chapter 2).

Each spectral signature was available at 1 nm and at the HyMap 2004 sensor resolutions of ~15 nm. Providing the spectral data for the habitat components at these different levels allowed for greater flexibility and accuracy for possible future applications. At each level within the classification scheme the spectral summary data available included the number of spectral samples at that level, the mean, median, standard deviation,

variance and 1st and 2nd derivatives of the spectral signatures for all samples from that level.

4.2.3 Spectral separability analysis of library

4.2.3.1 Spectral distance metrics

A number of different spectral distance metrics have been used successfully in hyperspectral analysis as a method of matching reference spectra to those of an unknown target (Du *et al.* 2003, Keshava 2004, Robila 2005). Those used in this study were the spectral angle (*SA*), the spectral correlation angle (*SCA*), the spectral gradient angle (*SGA*), the spectral information divergence (*SID*) and two measures that combined *SID* and *SA*, the *SID* multiplied by either the sine (*SID(SIN)*) or tangent (*SID(TAN)*) of the *SA* (Du *et al.* 2003, Du *et al.* 2004, Robila and Gershman 2005).

The spectral angle is one of the most commonly implemented metrics in hyperspectral remote sensing and discriminates between spectra by calculating the angle between two spectra using the following formula (Robila 2005):

$$SA(a,b) = \cos^{-1}\left[\frac{\sum(a_i * b_i)}{\left(\sqrt{\sum(a_i * a_i)}\right)\left(\sqrt{(b_i * b_i)}\right)}\right]$$

where a and b refer to individual spectra from the library being tested. The spectral angle is invariant to scalar multiplication and, as such, calculates the distance between spectra based solely on their shape (Robila 2005) (Figure 4-3). This feature makes it particularly appropriate to an application in the marine environment where the highly variable underwater light field can create changes in illumination that will result in

changes in the reflectance values, although the spectral shape of the signature has not changed.

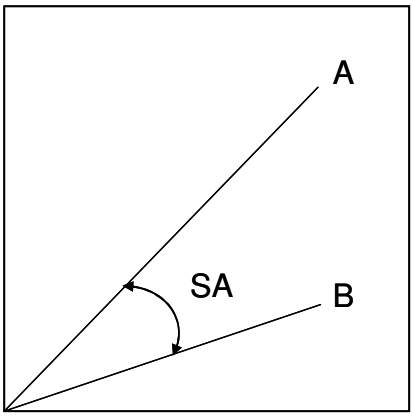

Figure 4-3: Conceptual diagram demonstration of the invariance to scalar multiplication of the spectral angle distance metric (*SA*). The *SA* between spectrum A and B will not change with the length of the vectors.

The spectral correlation angle (*SCA*), which is based on the spectral correlation coefficient (*SCC*), is ≥0, and is invariant to scalar multiplication (Robila 2005). The *SCA* between two vectors, *a* and *b*, is defined as (de Carvalho and Meneses 2000, Robila 2005):

$$SCA(a,b) = \arccos\left(\frac{SCC(a,b)+1}{2}\right)$$

where

$$SCC(a,b) = \left(\frac{\left\langle a-\bar{a}, b-\bar{b}\right\rangle}{\left\|a-\bar{a}\right\|_2 \left\|b-\bar{b}\right\|_2}\right)$$

and where $\bar{a}$ and $\bar{b}$ are the expected values for the two vectors.

The spectral gradient angle (*SGA*) is based on the *SA* and is also invariant to illumination conditions, but unlike the *SA*, takes into consideration the changes in slope

within the spectral vector (Robila and Gershman 2005). The *SGA* is defined as (Robila and Gershman 2005):

$$SGA(a,b) = SA\left(SG_a, SG_b\right),$$

where the spectral gradient (*SG*) of an n-dimension spectrum is defined as

$$SG(a) = \left(a_2 - a_1, a_3 - a_2, ..., a_n - a_{n-1}\right).$$

The spectral information divergence is a discrimination measure that evaluates the similarity between two spectra based on discrepancies between the probability distributions derived from each individual spectral signature, calculated using the spectral information measure (*SIM*) (Chang 2000). The *SIM* is a stochastic measure which considers the band to band variability within a spectrum based on the uncertainty resulting from randomness (Du *et al.* 2004). In basic terms, the *SIM* is a measure of spectral variability of an individual spectral signature based on the inter-band correlation. For a given spectral signature, $s = \left(s_1, s_2, ..., s_L\right)^T$, where each component s_j represents the reflectance value at band data B_j which is collected at specific wavelengths ω_j. Given that $\left\{\omega_j\right\}_{j=1}^{L}$ is a set of *L* wavelengths, each of which corresponds to a spectral band in the data (e.g., HyMap image bands), *s* can be modelled as a random variable by defining its probability space $\left(\Omega, \Sigma, \mathrm{P}\right)$, where $\Omega = \left\{\omega_1, \omega_2, ..., \omega_L\right\}$ is the sample space, Σ is the power set of Ω (i.e. the set of all subsets of Ω) and *P* is the probability measure, defined as $P\left(\left\{\omega_j\right\}\right) = p_j$, where

$$p_j = \frac{s_j}{\sum_{l=1}^{L} s_l}.$$

Thus, the probability vector of *s* is defined as $p = (p_1, p_2, ..., p_L)^T$ and represents the probability mass function of *P* and the desired probability distribution of the spectral vector *r*. Using information theory this enables the definition of the self-information (*I*) provided by a particular band, such as *j*, to be

$$I_j(r) = -\log p_j.$$

The entropy of the spectral vector *s*, represents the uncertainty resulting from the spectral vector *s* and is calculated using the formula:

$$H(s) = \sum_{j=1}^{L} I_j(s)\, p_j = -\sum_{j=1}^{L} p_j \log p_j$$

Now let $p = (p_1, p_2, ..., p_L)^T$ and $q = (q_1, q_2, ..., q_L)^T$ represent the probability density mass functions of two spectral signatures $s = (s_1, s_2, ..., s_L)^T$ and $s' = (s'_1, s'_2, ..., s'_L)^T$. From this the discrepancy in the self-information of spectral band B_j in *s* relative to the self-information for band B_j in s' can be defined as

$$D_j(s \| s') = I_j(s) - I_j(s') = \log(p_j / q_j).$$

Averaging $D_j(s \| s')$ across all image bands $\{B_l\}_{l=1}^{L}$ results in

$$D(s \| s') = \sum_{j=1}^{L} D_j(s \| s')\, p_j = \sum_{j=1}^{L} p_j \log(p_j / q_j)$$

where $D(s \| s')$ is the relative entropy of s' relative to s and is also know as the Kullback-Leiberler information measure or cross entropy. Thus, the relative entropy of s relative to s' can be defined as

$$D(s' \| s) = \sum_{j=1}^{L} D_j(s' \| s) q_j = \sum_{j=1}^{L} p_j \log(q_j / p_j).$$

The *SID* calculated by combining the two relative entropies defined as (Du *et al.* 2004)

$$SID(s, s') = D(s \| s') + D(s' \| s).$$

A number of metrics which combine the *SID* and the *SA* have been found to result in greater accuracy in matching spectra, than either measure used individually (Du *et al.* 2004). Taking either the sine or tangent of the *SA* and multiplying it by the *SID* results in the projection of one signature being calculated orthogonal to the other, rather than along the same plane, thus increasing the spectral discrimination between different signatures, while increasing the similarity between similar signatures (Du *et al.* 2004). *SID(TAN)* and *SID(SIN)* are defined as

$$SID(TAN)(s, s') = SID(s, s') \times \tan(SA(s, s'))$$
$$SID(SIN)(s, s') = SID(s, s') \times \sin(SA(s, s'))$$

4.2.3.2 Genetic algorithms

The genetic algorithm is an optimisation algorithm, based on evolutionary theory, that is able to efficiently solve problems for which there may be many solutions (Holland 1992). The initial step of the genetic algorithm analysis is to generate a random population as an array which consists of a predefined number of individuals (e.g. spectral signatures) and variables (e.g. wavelengths). The individuals used by the

genetic algorithm are a subset of the original wavelengths for each signature being used in the analysis (Jarvis and Goodacre 2005). The aim of the genetic algorithm is to optimise, by maximising or minimising, a fitness function that defines the relative fitness of each solution obtained to others obtained previously. The fitness function used depends on the aim of the optimisation being carried out.

The typical steps taken by a genetic algorithm to find an optimal solution for a multivariate problem, based on a fitness function, are analogous to the evolutionary process proposed by Darwin (Jarvis and Goodacre 2005).

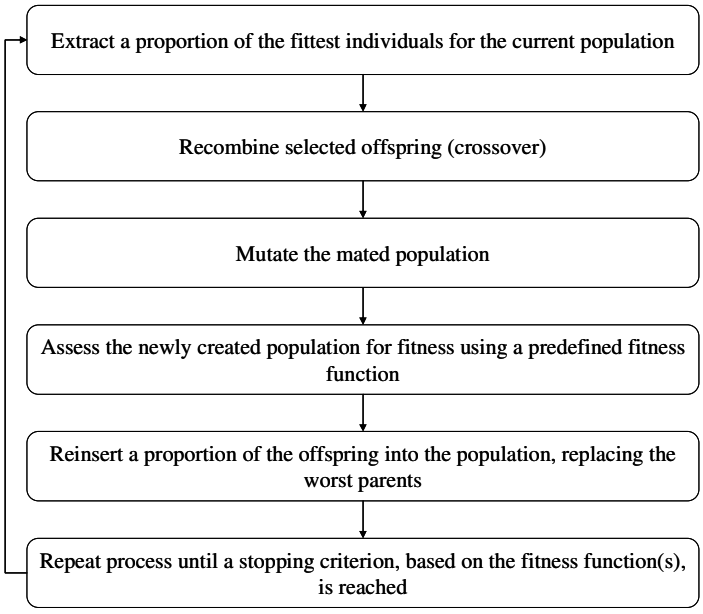

Figure 4-4: The steps taken by the genetic algorithm to find the optimal solution to a problem.

4.2.3.3 The 'R' statistic and the ANOSIM test

The '*R*' statistic is implemented in the Primer software (Clarke and Warwick 2001) as part of the analysis of similarity (ANOSIM), a statistical permutation test used to calculate the significance of separations observed between *a-priori* classes based on ecological data. The *'R'* statistic is calculated based on the rank similarities within a

similarity matrix, rather than actual distances, between all samples in the data set (Clarke and Warwick 2001). It is calculated using the following formula:

$$R = \frac{\left(\overline{r_B} - \overline{r_W}\right)}{\frac{1}{2}M}$$

where $\bar{r}_B$ refers to the mean of all rank similarities between classes, $\bar{r}_W$ refers to the mean rank similarities within classes, $M = n(n-1)/2$ and n is the total number of samples in the data set. The values of *'R'* can range from -1 to 1, however they will normally range between 0 to 1. *'R'* will only equal one if all replicates within classes are more similar to each other than any replicates from other classes. *'R'* will equal zero if the differences between classes and within classes are the same.

The ANOSIM first calculates the *'R'* statistic based on the rank similarity matrix and then runs a permutation test to calculate the significance of the *'R'* statistic calculated between all *a priori* classes defined for the data set, referred to as the global *'R'*. The permutation test randomly reallocates the labels to all the samples and recalculates the global *'R'* for each permutation. This is carried out a large number of times (T), as carrying it out for all possible permutations of a large data set would be computationally excessive. The significance of the global *'R'* can then be calculated using the following formula (Clarke and Warwick 2001):

$$p = (t+1)/(T+1)$$

where p refers to the significance value and t the number of the global *'R'* values calculated during the permutation test that are larger that the actual global *'R'* value.

4.2.3.4 Selection of best image bands to separate classes

The spectral separation analysis was carried out using a test developed to combine the different spectral metrics, a genetic algorithm, the *'R'* statistic and the ANOSIM test to determine which image bands in combination with a particular spectral metric provided the best separation between classes of the hierarchical habitat classification scheme at each level.

The test was carried out using the following steps for each group of classes tested:

1. The range and the minimum number of image bands to be used in the analysis were defined. The range was either bands 1 – 17 or bands 1 – 9 in the HyMap image and the minimum number of image bands was set at 2, as many of the spectral metrics require at least two values to be able to be calculated;
2. The fitness function that determined the stop point of the GA was defined. In this case it was attempting to maximise the *'R'* statistic;
3. The genetic algorithm was started with the multivariate array which represented the total population, consisting of individuals (rows, i.e. habitat components) and the variable that defined these individuals (columns, i.e. reflectance values at HyMap wavelengths);
4. The initial population was evaluated against the fitness function (the 'R' statistic);
5. A sub-set of individuals from the initial population was selected (individual habitat components, described by varying variables (reflectance values at HyMap wavelengths));

6. The new subset of individuals from the population were recombined (genetic crossover) to create offspring (more individuals);
7. The new individuals were mutated. This step was included to avoid the genetic algorithm finding local minima of the fitness function, by not always selecting only the fittest individuals for a population, but taking a semi-random selection that was weighted towards the fitter individuals;
8. Reinserted best individuals, replacing the worst individuals from the previous population;
9. Ended the genetic algorithm when the fitness function had been maximised;
10. Determined the statistical significance, p-value, of the optimal result using the ANOSIM permutation test.

The two different band ranges (1-17 and 1-9) were used due to the nature of the image data, which often did not always have a consistent number of image bands with useable data across an entire image. The results from the top five band / spectral metric combinations were visualised using a non-metric multidimensional scaling plot (nMDS) based on the rank order similarity matrices generated using the optimal image bands in combination with a particular spectral metric.

The tests were carried out at each level of the hierarchical classification scheme (Chapter 2) using library reflectance spectra at the HyMap sensor resolution (~15 nm). The separability analysis was carried out using the median ASR signatures. The genetic algorithm optimisation was run five times with each iteration starting with a random

population of 150 individuals, and being followed over 100 generations. Each ANOSIM test was run using 10 000 permutations.

4.2.4 Development of the classification algorithm

A classification algorithm was developed to identify the dominant habitat component of a pixel's spectrum, based on the spectral signatures in the library. The algorithm needed to take into account the variability within the spectral signatures of individual habitat components (e.g. *Ecklonia radiata*) and the effect of the predominately mixed signatures found in image pixels resulting from heterogeneity in nature.

For each target spectrum (i.e. image pixel) the dominant habitat component was identified by calculating the relative spectral discriminatory probability (RSDPB) between its spectral signature (*t*), and all the relevant spectral reference signatures ($S = \{s_1, s_2, ..., s_n\}$) from the spectral library using the spectral metric (*d*) defined by the optimal solution for each split in the habitat classification scheme, using the following formula (Du *et al.* 2004):

$$RSDPB_S^d(t, s_i) = d(t, s_i) \Big/ \sum_{j=1}^{n} d(t, s_i)$$

The mean RSDPB was calculated for each habitat component group and the pixel was allocated to the group with the minimum mean RSDPB.

4.2.5 Testing the classification algorithm using mixture analysis

The accuracy of the classification algorithm was tested by creating randomly mixed synthetic spectral signatures based on the linear mixture model (Chang *et al.* 2002) of up to six habitat components and attempting to identify the dominant habitat

component. The synthetic signatures were created to test the classification at each level of the habitat classification scheme (see Chapter 2). For each test, 10 000 synthetic signatures were randomly created and identified using the algorithm. The signature had to have one dominant habitat component (> 50% contribution) from one of the habitat classes being identified, and have contributions from other habitat components from any other classes in the library that were likely to occur in the same pixel. For example when testing at Level 2 (seagrass/macroalgae/coral) the dominant component might be *E. radiata*, with a contribution of 60%, and the other contributing components, *Sargassum* (10%), *Posidonia sinuosa* (15%), Chlorophyta (10%) and Rhodophyta (5%). For each of the 10 000 synthetic signatures the classification algorithm assigned an appropriate habitat class to each signature for the level being tested and the results were summarised into an error matrix and the overall, producer's and user's accuracies were calculated (Figure 4-5). The accuracies were calculated as (Congalton and Green 1999):

$$\text{overall accuracy} = \frac{\sum_{i=1}^{k} n_{ii}}{n},$$

$$\text{producer's accuracy}_j = \frac{n_{jj}}{n_{+j}} \text{ and}$$

$$\text{user's accuracy}_i = \frac{n_{ii}}{n_{i+}},$$

where

$$n_{i+} = \sum_{j=1}^{k} n_{ij} \text{ and } n_{+j} = \sum_{i=1}^{k} n_{ij} .$$

The overall accuracy is the percentage of ground validation points correctly classified in the mapped image and does not take chance agreement into account. The producer's accuracy, calculated using column values of the error matrix, indicates the probability of a reference pixel being classified correctly and is more specifically an error of omission (Congalton 1991). The user's accuracy, or an error of commission, is calculated using the row values of an error matrix and indicates the probability of a classified pixel actually representing that class in the field (Story and Congalton 1986).

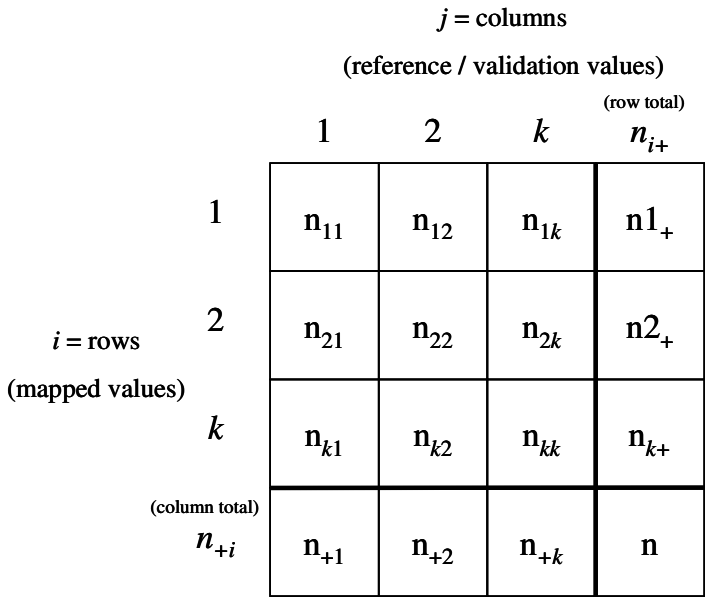

Figure 4-5: Mathematical representation of an error matrix adapted from Congalton and Green (1999).

The *kappa* and *tau* coefficients were also calculated for each error matrix. The *kappa* coefficient ($\hat{K}$) was calculated using the following formula

$$\hat{K} = \frac{\sum_{i=1}^{k} n_{ii} - \sum_{i=1}^{k} n_{i+} n_{+i}}{n^2 - \sum_{i=1}^{k} n_{i+} n_{+i}},$$

and the *tau* coefficient (*T*) was calculated using the following formula (Ma and Redmond 1995):

$$T = \frac{P_o - P_r}{1 - P_r}$$

where

$$P_r = \frac{1}{N^2} \sum_{i=1}^{M} n_i \times x_i$$

and P_o refers to the overall accuracy, *N* refers to the number of samples, *M* the number of habitat classes, n_i the number of samples mapped as habitat class *i* and x_i the number of correctly classified samples for habitat class *i*. The *kappa* coefficient is a measure of the agreement between the overall accuracy of the error matrix and the chance agreement that may occur in that same error matrix (Congalton and Green 1999). The *kappa* values generally range between 0 and 1, where >0.8 represents strong agreement, 0.4 – 0.8 a moderate agreement and <0.4 a poor agreement (Congalton 2001). The *tau* coefficient is an adjustment of the overall accuracy by the number of classes and the *a priori* probabilities used for the classification (Ma and Redmond 1995).

4.3 Results

4.3.1 Calibration of the Teflon reflectance panel

The reflectance values of the Teflon panel (R_{Teflon}) calculated using 10 replicate spectral data pairs ranged from 89.45% at 450 nm to 82.66% at 700 nm (Figure 4-6).

4.3.2 The spectral library

The spectral signatures of 13 different habitat components at Level 4 of the habitat classification scheme developed in Chapter 3 were documented in the library and

constituted 24 individual species or genera (Table 4-4; Figure 4-7). The spectral characteristics of two classes of bare substrate were sampled in the field, namely, sand (n = 76) and limestone (n = 8) (Table 4-4). Eleven major habitat components were sampled for the bio-substrate class, with a total of 224 samples (Table 4-4). These habitat components all occur in different combinations to form the various classes used to define habitats at Rottnest Island Reserve.

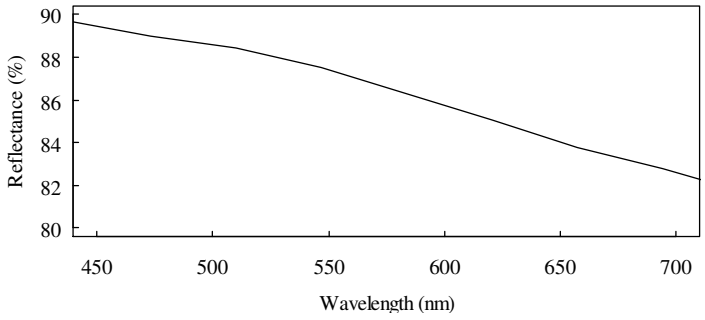

Figure 4-6: The reflectance of the Teflon calibration panel calculated from the Spectralon reflectance standard.

Table 4-4: Summary of the 296 spectral reflectance signatures contained in the spectral library created for Rottnest Island Reserve. (Numbers in brackets indicated the number of samples).

Level 1	Level 2	Level 3	Level 4
Bare substrate (84)			
			Sand (76)
			Limestone (8)
Bio-substrate (212)			
	Mixed algae (148)		
		Canopy algae (64)	
			Ecklonia radiata (26)
			Sargassum spp. (30)
			Scytothalia doryocarpa (8)
		Algal turf (84)	
			Red foliose (10)
			Coralline (18)
			Green foliose (38)
			Brown foliose (18)
	Seagrass (64)		
			Posidonia (28)
			Amphibolis (28)
			Halophila (8)
	Coral (12)		
			Pocillopora (12)

Figure 4-7: Some of the dominant habitat components contained in the spectral library for the benthic substrates of Rottnest Island Reserve, including *Amphibolis* (A), *Posidonia* (B), mixed seagrass (C), *Sargassum* (D), *Ecklonia radiata* (E), algal turf (F), *Pocillopora damicornis* (G) and bare substrate (H).

4.3.2.1 Bare substrate

The mean reflectance of sand increased gradually with increasing wavelength (Figure 4-8). The standard deviation of the mean reflectance at each HyMap band reflected the consistent variation between samples across all wavelengths. The mean reflectance for limestone showed a very similar signature to that of sand, but with a lower reflectance at all wavelengths (Figure 4-8).

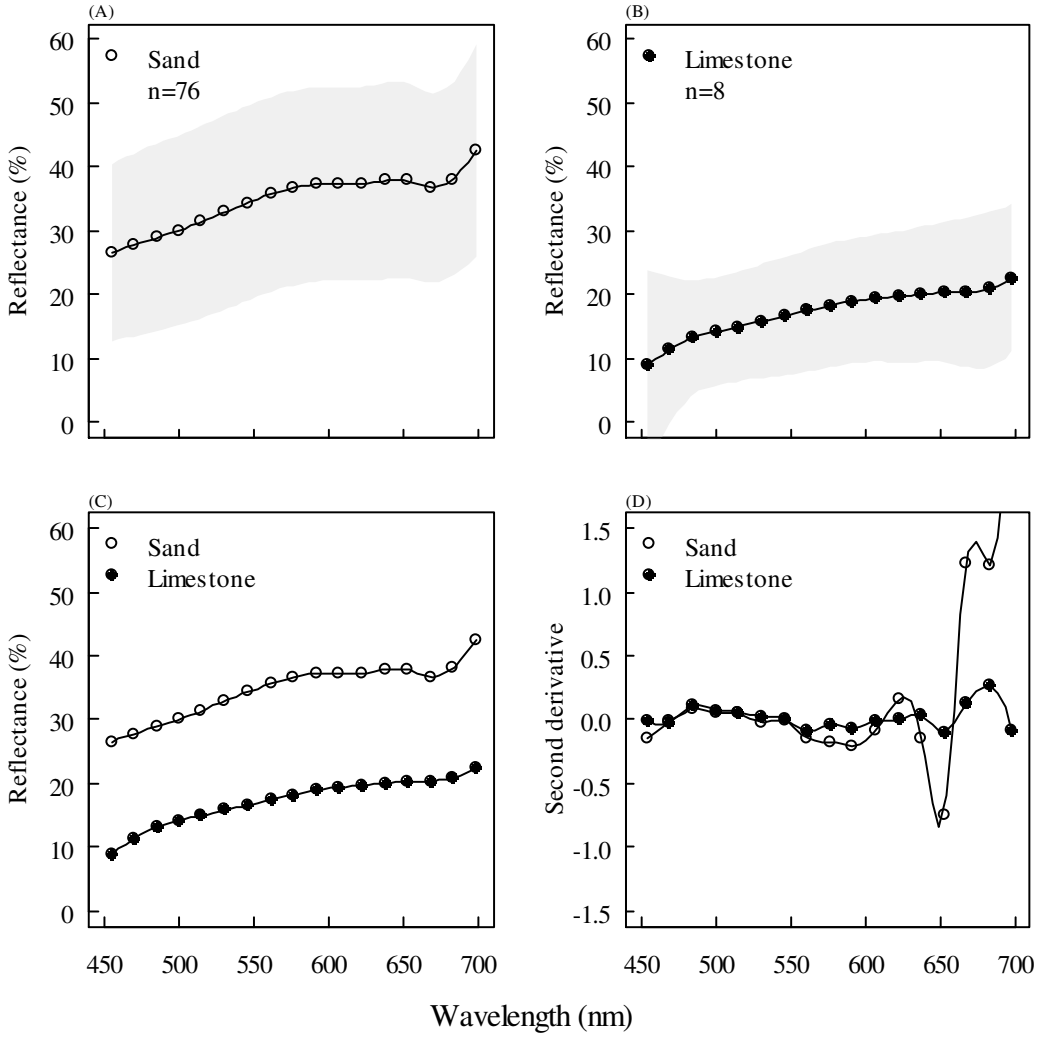

Figure 4-8: The mean reflectance signature for sand (A), limestone (B), the comparison of the two (C) and their second derivatives (D), based on the median signature for each individual sample. The shaded areas represent ±1 standard deviation from the mean. Symbols represent the central positions of the HyMap image bands.

The second derivative for sand and limestone highlighted some differences that may provide a diagnostic tool to separate these classes based on their spectral characteristics, although most of these features occurred at wavelengths >600 nm.

4.3.2.2 Bio-substrate

4.3.2.2.1 Canopy algae

The major components of the canopy algae class were *Ecklonia radiata*, *Sargassum* spp. and *Scytothalia doryocarpa*. The mean reflectance of *E. radiata* showed low reflectance values that rose towards a small peaks at both ~590 and ~650 nm and then decreased until the reflectance minimum at ~670 nm whereafter reflectance values increased rapidly (Figure 4-9). These features are characteristic on some algae species. This reflectance minimum between 670 – 680 nm was a characteristic of all the signatures in the bio-substrate class, known as the 'red edge' (Sims and Gamon 2002). The variability in reflectance was greatest around the ~590 nm peak and the ~670 nm inflection and beyond.

The mean reflectance for *Sargassum* spp. showed the same general trends as *E. radiata* with a peak at ~590 nm and an inflection at ~670 nm (Figure 4-9). However, *Sargassum* spp. showed less variation in reflectance across all wavelengths < 670 nm. *S. doryocarpa* showed the same trends as the other components in the macroalgae class, although it exhibited a lower reflectance at the inflection point. The second derivatives of all three components showed a significant difference between *Sargassum* and both *E. radiata* and *S. doryocarpa*.

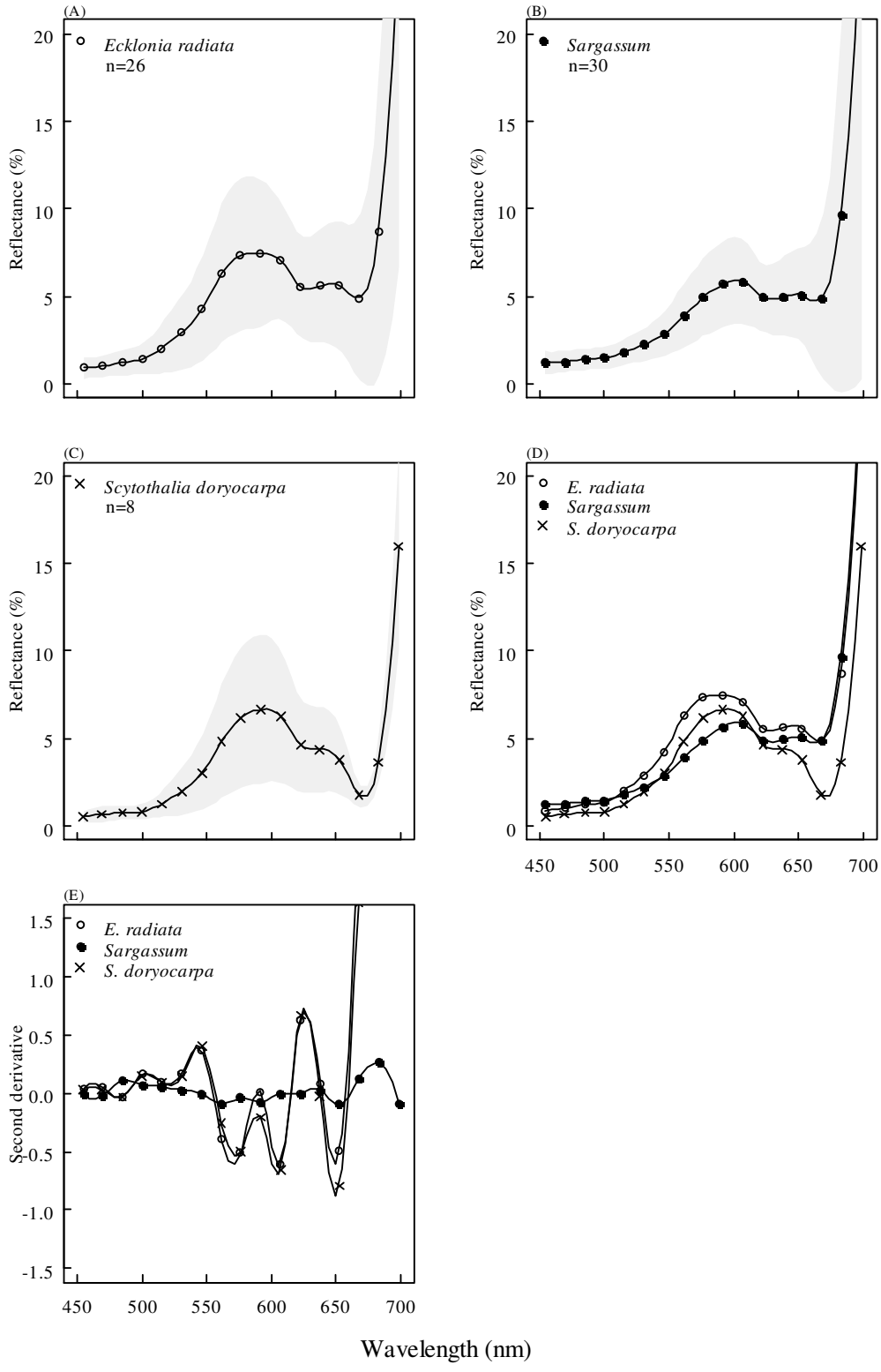

Figure 4-9: The mean reflectance signatures for *E. radiata* (A), *Sargassum* spp. (B), *S. doryocarpa* (C), the comparison between the three (D) and their second derivatives (E), based on the median signature for each individual sample. The shaded areas represent ±1 standard deviation from the mean. Symbols represent the central positions of the HyMap image bands.

4.3.2.2.2 Algal turf

The major components of the algal turf class were red foliose, coralline, green foliose and brown foliose algae. The mean reflectance signatures for red foliose and coralline algae showed relatively constant reflectance until ~ 590 nm, remaining higher until ~650 nm dropping thereafter until the reflectance minimum at ~670nm (Figure 4-10).

The variation in reflectance was greater across all wavelengths for the red foliose algae, with coralline algae the showing maximum variation at ~600 nm. The reflectance signature for green foliose algae showed an almost linear increase in reflectance up to ~590 nm and then decreased until the inflection point at ~670 nm. The brown foliose algae showed similar spectral shape to both the red foliose and coralline algae, although reflectance values were greater at all wavelengths and the 'red edge' inflection occurs at a lower wavelength. The signatures of both the red foliose and coralline algae appeared to be very similar, in comparison to the brown foliose algae

4.3.2.2.3 Seagrass

The seagrass class had three major components, *Posidonia*, *Amphibolis* and *Halophila* species. The reflectance signatures for both *Posidonia sinuosa* and *P. australis* showed very similar patterns, with a peak in reflectance at ~590 nm and the typical inflection point at ~670 nm (Figure 4-11). The main difference between the two species was the greater variability in reflectance values found for *P. australis* in comparison to *P. sinuosa*.

The second major components of the seagrass class were *Amphibolis* species, which have a spectral reflectance signature with a similar shape to *Posidonia*, but with much

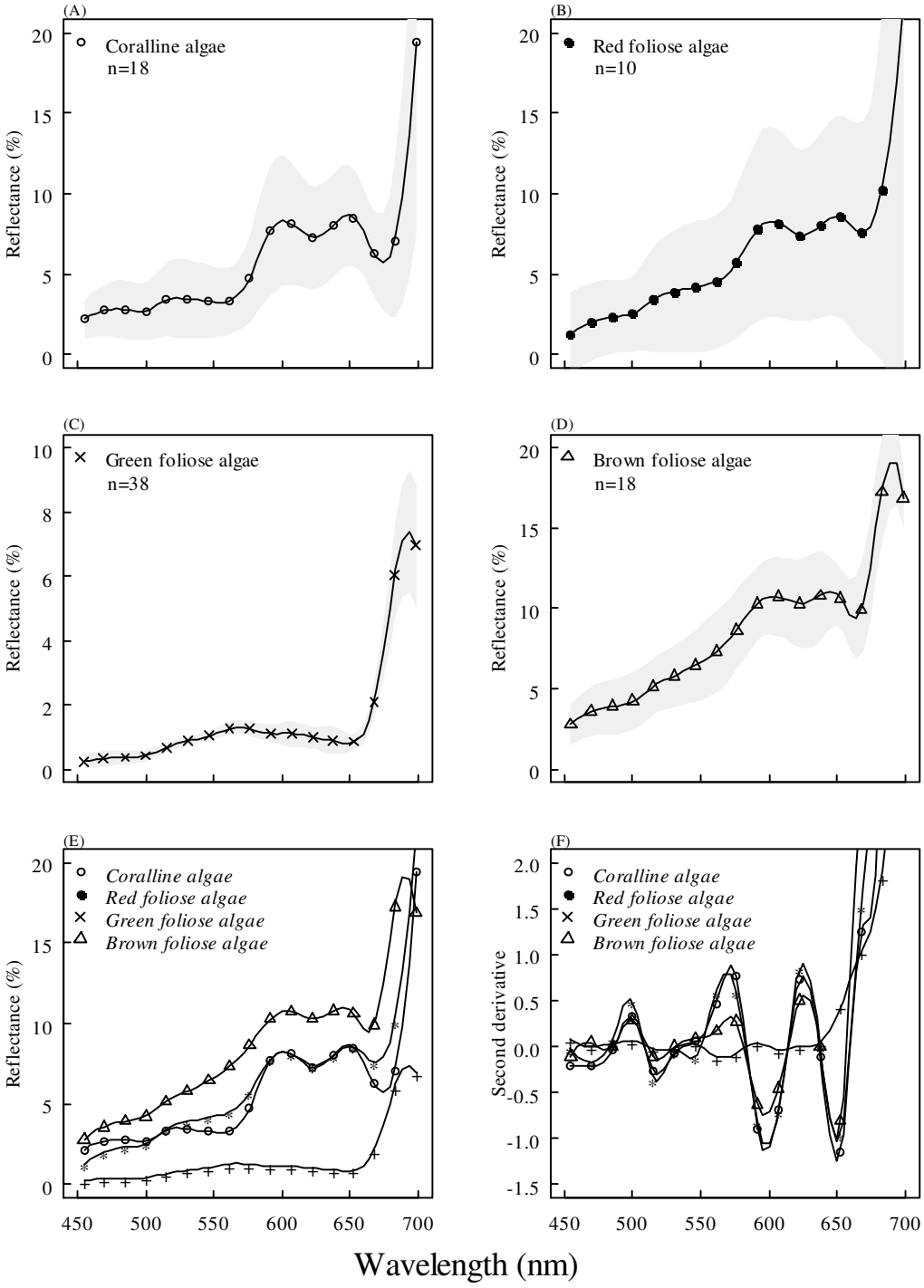

Figure 4-10: The mean reflectance signatures for coralline (A), foliose red (B), foliose green (C), foliose brown (D) algae, the comparison between all four groups (E) and their second derivatives (F), based on the median signature for each individual sample. The shaded areas represent ±1 standard deviation from the mean. Symbols represent the central positions of the HyMap image bands.

greater variability at all wavelengths (Figure 4-11). The reflectance peaked at ~590 nm, with that also being the point of greatest variability in reflectance values within the class. *A. griffithii* exhibited a greater variability in reflectance values compared to *A. antarctica* at all wavelengths < 500 nm.

The spectral reflectance signature for *Halophila ovalis* showed a similar shape to the signatures for both the *Posidonia* and *Amphibolis* genera (Figure 4-11). The most obvious difference between them was the significantly higher reflectance values. All four species of seagrass from the genera *Posidonia* and *Amphibolis* had very similar spectral reflectance signatures, with the only discriminating factor being the higher reflectance values of *A. griffithii*. This difference appeared to be more pronounced when the second derivatives were calculated, with different peaks occurring at ~ 550, 570 and 610 nm.

4.3.2.2.4 Coral

The coral class had only one component at Rottnest Island, *Pocillopora damicornis*, which exhibited the same characteristic feature of all chlorophyll containing organisms, the 'red edge' at ~660 nm (Figure 4-12). There was a peak in reflectance at ~620 nm and low reflectance at all wavelengths below 550 nm.

4.3.3 Spectral separability analysis

4.3.3.1 Level 1 – Bare substrate/Bio-substrate

The spectral separation between the signatures from the bare substrate class and those from the bio-substrate class was found to be good, with a maximum significant *'R'* value of 0.935 being achieved using the spectral correlation angle (*SCA*), calculated

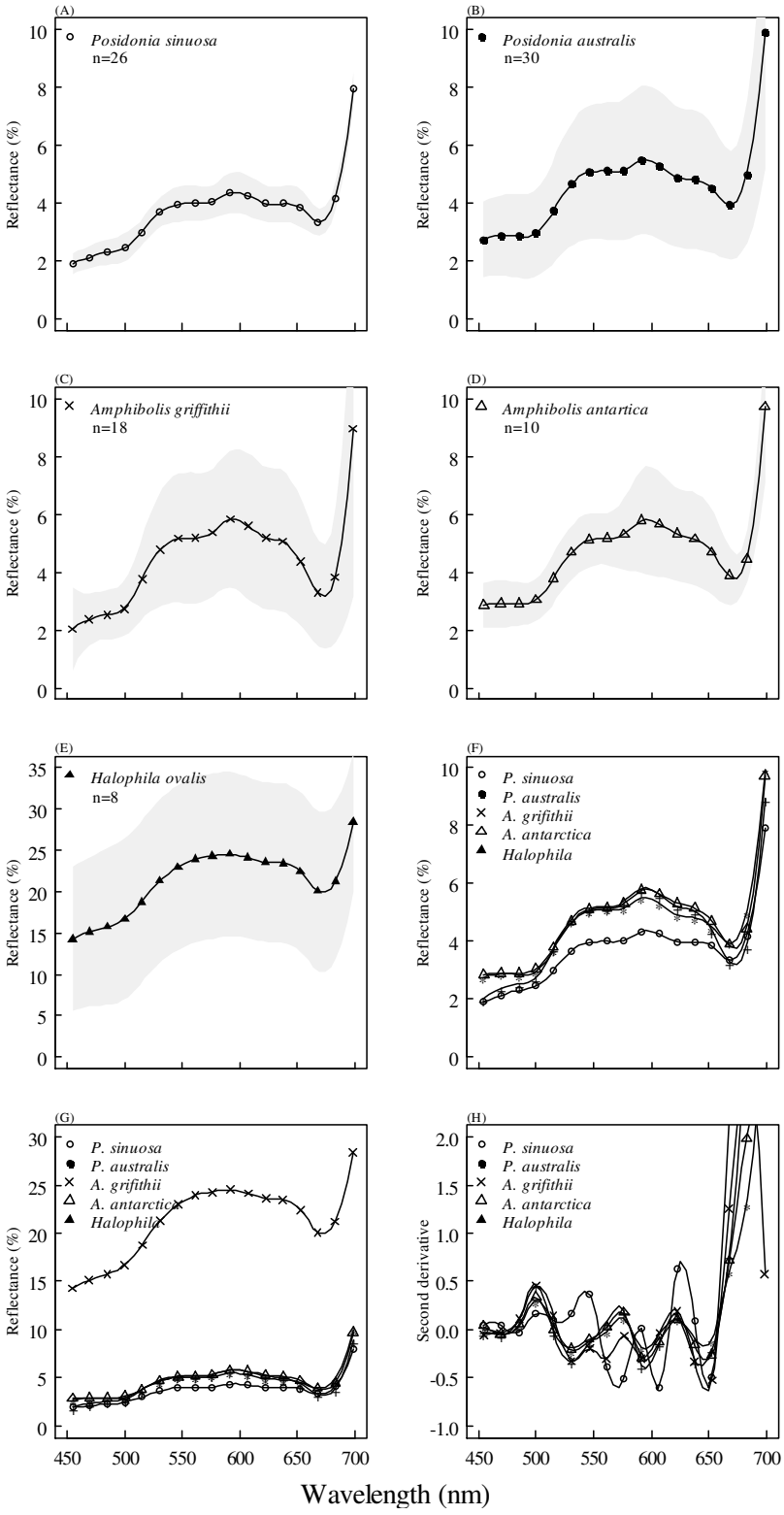

Figure 4-11: The mean reflectance signatures for *P. sinuosa* (A), *P. australis* (B), *A. griffithii* (C), *A. antarctica* (D), *H. ovalis* (E), the comparison between *Posidonia* and *Amphibolis* species (F), the comparison of all species (G) and their second derivatives (H), based on the median signature for each individual sample. The shaded areas represent ±1 standard deviation from the mean. Symbols represent the central positions of the HyMap image bands.

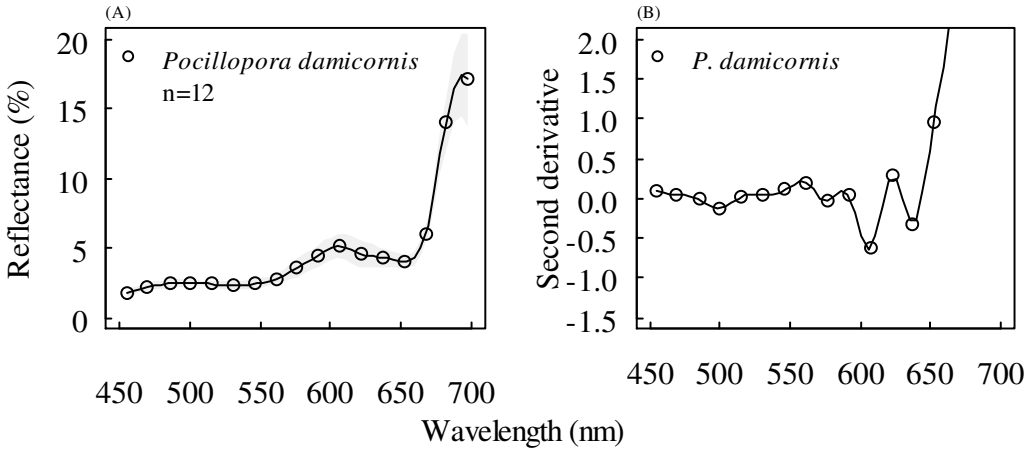

Figure 4-12: The mean reflectance signature for *Pocillopora damicornis* (A) and its second derivative (B), based on the median signature for each individual sample. The shaded areas represent ±1 standard deviation from the mean. Symbols represent the central positions of the HyMap image bands.

from HyMap bands 4, 15 and 17 (500.1 nm, 667.6 nm and 698.2 nm, respectively) (Table 4-5). When the input to the optimisation analysis was restricted to the first nine HyMap bands an *'R'* value of 0.806 was achieved using the *SCA* metric calculated using bands 1, 2, 3 and 9 (454.7 nm, 469.3 nm, 485.2 nm and 576.3 nm, respectively).

Table 4-5: Results of the spectral separation analysis carried out using a genetic algorithm to determine the optimum band combination to separate between bare substrate and bio-substrate dominated habitats for each spectral metric. Each test was carried out five times using 74 spectral signatures from the library. Best results in bold.

Spectral metric	Bands tested	Optimal bands	'R' statistic	p-value	Occurrences
SA	1 - 17	4, 17	0.683745	<0.001	4 / 5
	1 – 9	4, 9	0.465046	<0.001	5 / 5
SCA	**1 - 17**	**4, 15, 17**	**0.935240**	**<0.001**	**5 / 5**
	1 – 9	**1, 2, 3, 9**	**0.805661**	**<0.001**	**5 / 5**
SGA	1 - 17	1, 3	0.654422	<0.001	3 / 5
	1 – 9	1, 3	0.654422	<0.001	5 / 5
SID	1 - 17	4, 17	0.497661	<0.001	1 / 5
	1 – 9	4, 5	0.376518	<0.001	5 / 5
SID(TAN)	1 - 17	16, 17	0.651613	<0.001	2 / 5
	1 – 9	4, 9	0.385004	<0.001	5 / 5
SID(SIN)	1 - 17	4, 10, 11	0.528787	<0.001	2 / 2
	1 – 9	4, 9	0.383069	<0.001	5 / 5

The nMDS plots of the complete data set, with no spectral separation optimisation, and the top two optimisation results clearly demonstrated the effect of the optimisation with tighter within class sample groupings and improved *'R'* values (i.e. closer to the ideal value of one) (Figure 4-13).

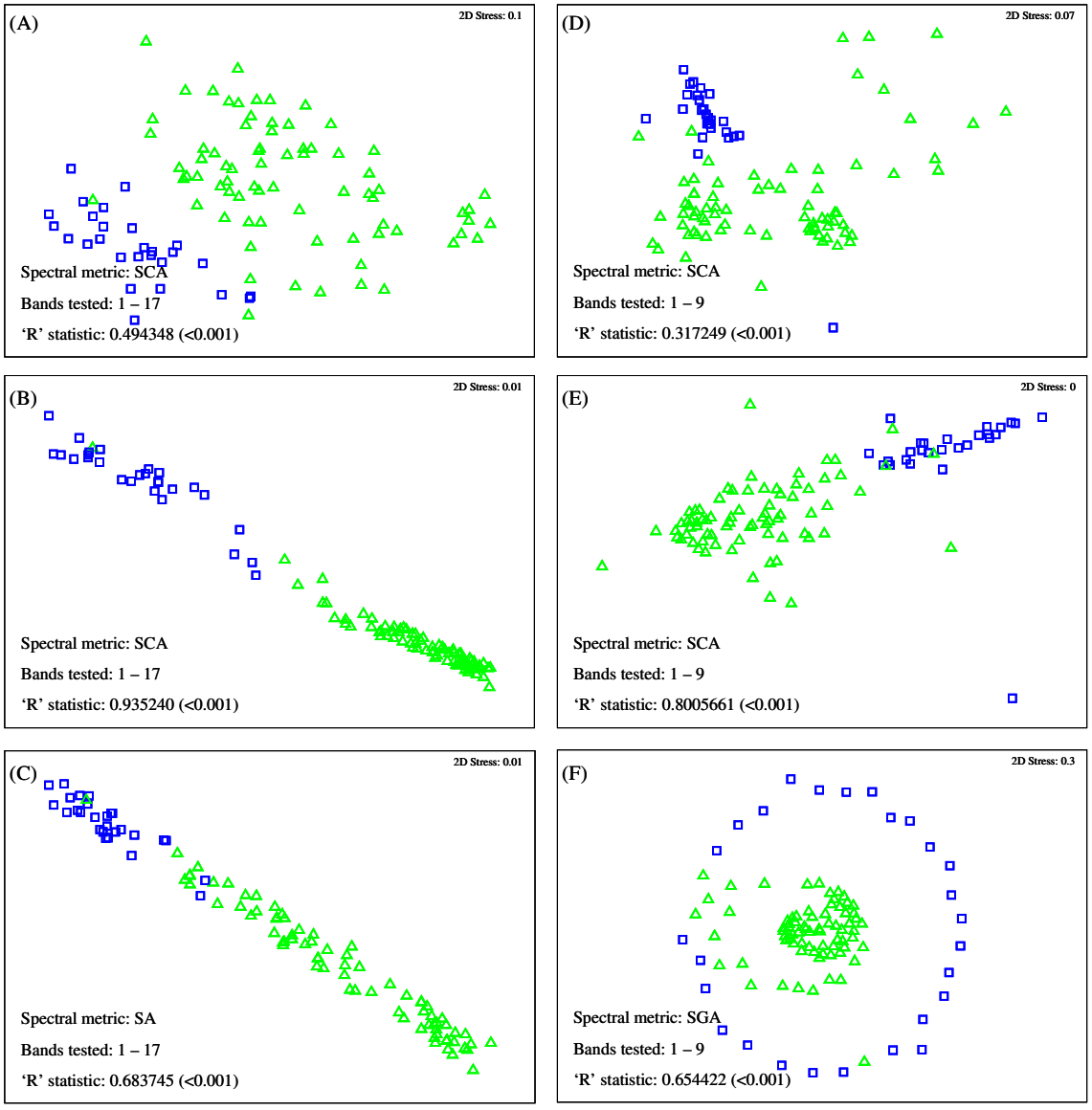

Figure 4-13: Results of the spectral separation analysis carried out using a genetic algorithm to determine the optimum band combination to separate between bare substrate (□) and bio-substrate (Δ) dominated habitats. nMDS plots were constructed for the optimal spectral metric, spectral correlation angle (*SCA*), using bands 1 – 17 (A) and the two best band/metric combinations, the *SCA* (B) and the spectral angle (*SA*) (C). nMDS plots were constructed for the optimal spectral metric, spectral correlation angle (*SCA*), using bands 1 – 9 (D) and the two best band/metric combinations, the *SCA* (E) and the spectral gradient angle (*SGA*) (F). All analyses were carried out using 101 spectral signatures from the library.

The bio-habitat samples that overlapped with the bare substrate samples were mostly *Halophila ovalis* signatures, which always included a significant sand component due to the typical growth habit of this seagrass species (Figure 4-7). It should also be noted that the nMDS plot for the spectral gradient angle data, based on the first nine bands, had a high stress value, indicating that the two-dimensional representation of the data was poor and that the separation indicated by the *'R'* value of 0.654, exists in multidimensional space.

4.3.3.2 Level 2 – Macroalgae/Seagrass/ Coral

The greatest overall separation was achieved, at Level 2, between macroalgae, seagrass and coral using spectral correlation angle and HyMap image bands 4, 6, and 9 (500.1 nm, 530.7 nm and 576.3 nm, respectively), with an *'R'* value of 0.844 (Table 4-6). The nMDS plots showed a clear delineation of coral and only a slight overlap of macroalgae and seagrass samples in the optimised solutions, with a significant improvement in separation compared to the raw data (Figure 4-14). Closer examination of these overlapping samples revealed that most of them were green foliose algae (Chlorophyta) and unidentified turf algae. There was no significant effect from restricting the analysis to the first nine image bands, as the optimal bands generally occurred within this restricted range. The spectral gradient angle was found to provide the lowest level of separation with an optimal *'R'* value of only 0.152 (Table 4-6). All of the optimal solutions, with the exception of the SGA, were obtained in all five optimisation runs, indicating that the genetic algorithm was converging on a global, rather than a local, maximum.

Table 4-6: Results of the spectral separation analysis carried out using a genetic algorithm to determine the optimum band combination to separate between macroalgae, seagrass and coral dominated habitats for each spectral metric. Each test was carried out five times using 74 spectral signatures for the library. Best results in bold.

Spectral metric	Bands tested	Optimal bands	'R' statistic	p-value	Occurrences
SA	1 - 17	4, 6, 10, 11	0.684107	<0.001	5 / 5
	1 – 9	7, 9	0.647195	<0.001	5 / 5
SCA	**1 - 17**	**4, 6, 9**	**0.844120**	**<0.001**	**5 / 5**
	1 – 9	**4, 6, 9**	**0.844120**	**<0.001**	**5 / 5**
SGA	1 - 17	1, 2	0.152039	0.001	4 / 5
	1 – 9	1, 2	0.152039	<0.001	5 / 5
SID	1 - 17	4, 6, 10, 11	0.603431	<0.001	5 / 5
	1 – 9	7, 9	0.620409	<0.001	5 / 5
SID(TAN)	1 - 17	4, 6, 10, 11	0.634592	<0.001	5 / 5
	1 – 9	7, 9	0.629725	<0.001	5 / 5
SID(SIN)	1 - 17	4, 6, 10, 11	0.633844	<0.001	5 / 5
	1 – 9	7, 9	0.629528	<0.001	5 / 5

4.3.3.3 Level 3 – Canopy/Algal turf

The spectral angle (*SA*) provided the greatest degree of separation between canopy and turf algae, at Level 3 of the classification scheme, with an *'R'* value of 0.792 using HyMap bands 6, 7 and 8 (530.7 nm, 546.3 nm and 561.4 nm, respectively) (Table 4-7).

These bands were determined to be the best band combination in 7 out of 12 separation analysis results and achieved an *'R'* value of 0.786 using *SID(TAN)* when analysis was carried out using bands 1 – 17 (Figure 4-14). With the exception of the *SGA* metric, all the metrics resulted in *'R'* values greater than 0.71 at a significance <0.001. It should be noted that for the optimisation analyses carried out using HyMap bands 1 – 17, none of the optimal results were achieved in all five replicate analyses, and in the case of the *SCA*, the optimal result was never achieved, as demonstrated by the improved result achieved by the analysis carried out on the first nine bands (Table 4-7). A significant improvement was achieved using the optimisation analysis, illustrated by the tighter

grouping of the sample points and improved *'R'* value between the analysis of all HyMap bands and the optimal solution, 0.532 and 0.792, respectively (Figure 4-15).

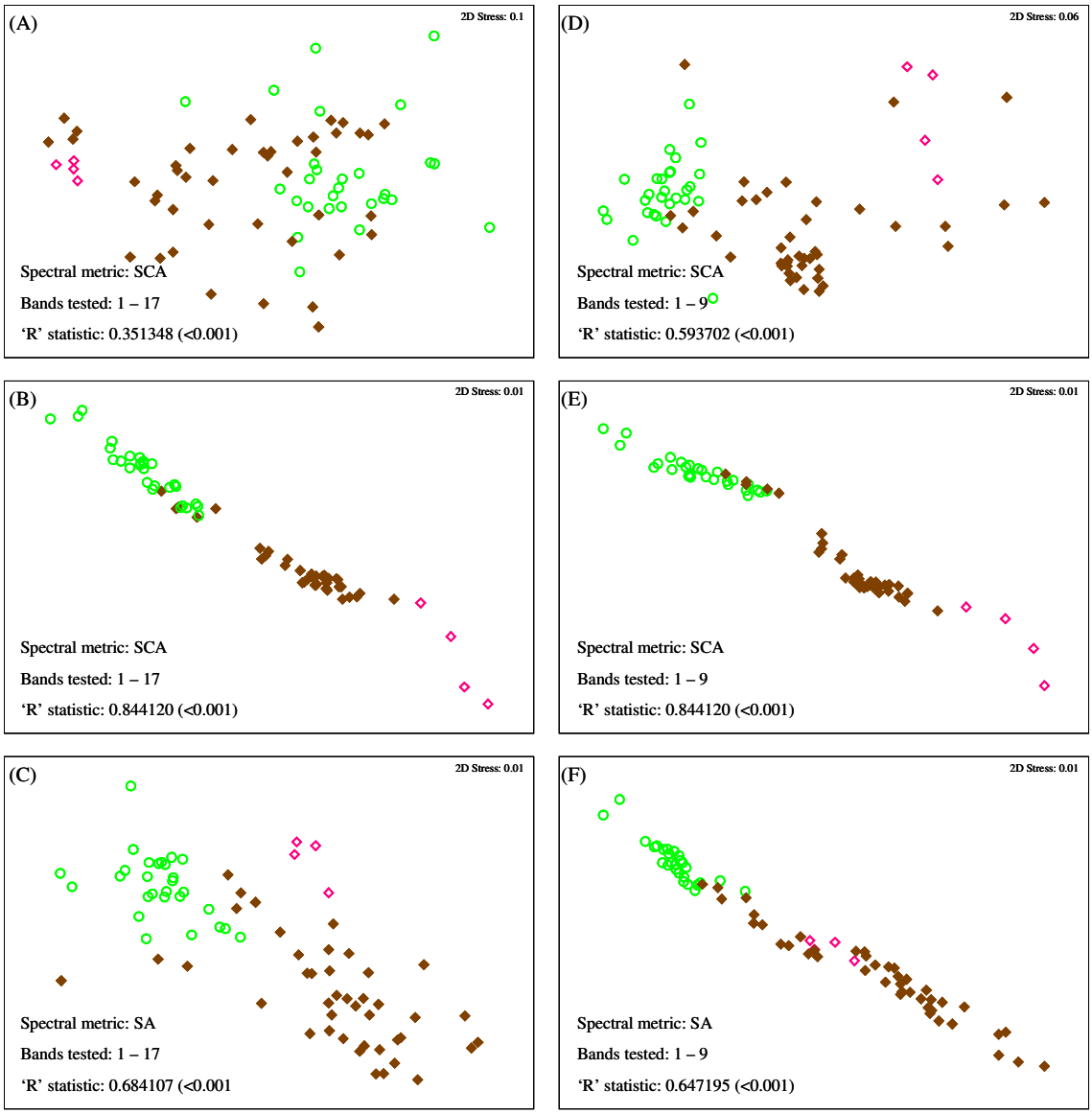

Figure 4-14: Results of the spectral separation analysis carried out using a genetic algorithm to determine the optimum band combination to separate between macroalgae (♦), seagrass (○) and coral (◊) dominated habitats. nMDS plots were constructed for the optimal spectral metric, spectral correlation angle (*SCA*), using bands 1 – 17 (A) and the two best band/metric combinations, the *SCA* (B) and the spectral angle (*SA*) (C). nMDS plots were constructed for the optimal spectral metric, spectral correlation angle (*SCA*), using bands 1 – 9 (D) and the two best band/metric combinations, the *SCA* (E) and the spectral angle (*SA*) (F). All analyses were carried out using 74 spectral signatures for the library.

Table 4-7: Results of the spectral separation analysis carried out using a genetic algorithm to determine the optimum band combination to separate between canopy and turf algae dominated habitats for each spectral metric. Each test was carried out five times using 74 spectral signatures for the library. Best results in bold.

Spectral metric	Bands tested	Optimal bands	'R' statistic	p-value	Occurrences
SA	1 - 17	6, 8	0.785458	<0.001	2 / 5
	1 – 9	**6, 7, 8**	**0.792431**	**<0.001**	**5 / 5**
SCA	1 - 17	1, 6, 8	0.712286	<0.001	2 / 5
	1 – 9	4,5,9	0.733485	<0.001	3 / 5
SGA	1 - 17	6, 14	0.138973	<0.001	4 / 5
	1 – 9	1, 2	0.074004	<0.05	5 / 5
SID	1 - 17	6, 7, 8	0.782868	<0.001	1 / 5
	1 – 9	6, 7, 8	0.782868	<0.001	5 / 5
SID(TAN)	**1 - 17**	**6, 7, 8**	**0.786376**	**<0.001**	**2 / 5**
	1 – 9	6, 7, 8	0.786376	<0.001	5 / 5
SID(SIN)	1 - 17	6, 7, 8	0.786343	<0.001	2 / 5
	1 – 9	6, 7, 8	0.786343	<0.001	5 / 5

4.3.3.4 Level 4 – *Posidonia/Amphibolis*

No spectral metric was able to achieve an *'R'* value greater than 0.5 between *Posidonia* and *Amphibolis* species of seagrass. The *SID* achieved the greatest separation with an *'R'* value of 0.475 , when analysed using HyMap bands 1 – 17 and determined that the best band combination was 13 and 15 (637.6 nm and 667.6 nm, respectively) (Table 4-8). However the *SA, SID(TAN)* and *SID(SIN)* metrics also achieved comparable results using the same band combination. All results for the analysis carried out using only the first nine HyMap bands were <0.2 and all but one, that for *SCA* using bands 1 and 6, were statistically insignificant (Table 4-8). Although the results indicated that separation of these habitat components would be difficult based solely on their spectral signatures, there was still an improvement on the separation resulting from the optimisation analysis (Figure 4-16).

Table 4-8: Results of the spectral separation analysis carried out using a genetic algorithm to determine the optimum band combination to separate between *Posidonia* and *Amphibolis* dominated habitats for each spectral metric. Each test was carried out five times using 24 spectral signatures for the library. Best results in bold.

Spectral metric	Bands tested	Optimal bands	'R' statistic	p-value	Occurrences
SA	1 - 17	13, 15	0.472842	<0.001	5 / 5
	1 – 9	1, 2	0.111520	<0.05	4 / 5
SCA	1 - 17	1, 13, 15	0.444030	<0.001	5 / 5
	1 – 9	**1, 6**	**0.194910**	**<0.05**	**5 / 5**
SGA	1 - 17	6, 9, 17	0.065987	0.059	1/ 5
	1 – 9	7, 8, 9	0.053263	0.110	5 / 5
SID	**1 - 17**	**13, 15**	**0.474525**	**<0.001**	**5 / 5**
	1 – 9	1, 2	0.111625	0.030	5 / 5
SID(TAN)	1 - 17	13, 15	0.473684	<0.001	5 / 5
	1 – 9	1, 2	0.111836	0.031	5 / 5
SID(SIN)	1 - 17	13, 15	0.473684	<0.001	5 / 5
	1 – 9	1, 2	0.111836	0.029	5 / 5

4.3.3.5 Level 4 – *Ecklonia/Sargassum/Scytothalia doryocarpa*

The separability of the three main canopy algae, *Ecklonia radiata*, *Sargassum* and *Scytothalia doryocarpa*, was greater than was achieved for seagrass (Table 4-9). The greatest separation was achieved using the *SCA* metric with bands 3 and 5 (530.7 nm and 546.3 nm, respectively; $R = 0.611$), and all other metrics, with the exception of the *SGA*, had *'R'* values around 0.48. As has been observed previously, the best result was achieved using the restricted band set as an input, which may indicate that the genetic algorithm was becoming stuck on local maxima and not achieving the global maximum when using the complete band set. The improvement in the separation achieved using the optimisation algorithm was clearly demonstrated by the tighter groupings of samples within each group observed in the nMDS plots of the optimised results, compared to the plot of original data, which only achieved an *'R'* value of 0.048 (Figure 4-17).

Table 4-9: Results of the spectral separation analysis carried out using a genetic algorithm to determine the optimum band combination to separate between *Ecklonia, Sargassum* and *S. doryocarpa* dominated habitats for each spectral metric. Each test was carried out five times using 23 spectral signatures for the library. Best results in bold.

Spectral metric	Bands tested	Optimal bands	*'R'* statistic	*p*-value	Occurrences
SA	1 - 17	6, 7	0.484790	<0.001	1 / 5
	1 – 9	6, 7	0.484790	<0.001	4 / 5
SCA	1 - 17	9, 10, 11	0.408331	<0.001	2 / 5
	1 – 9	**3, 5**	**0.611263**	**<0.001**	**5 / 5**
SGA	1 - 17	6, 7, 8, 9, 15	0.137024	<0.05	3/ 5
	1 – 9	6, 7	0.123596	0.079	5 / 5
SID	1 - 17	5, 6, 8	0.445053	<0.001	4 / 5
	1 – 9	6, 7	0.488627	<0.001	5 / 5
SID(TAN)	**1 - 17**	**6, 7**	**0.487942**	**<0.001**	**1 / 5**
	1 – 9	6, 7	0.487942	<0.001	5 / 5
SID(SIN)	1 - 17	6, 7	0.487942	<0.001	1 / 5
	1 – 9	6, 7	0.487942	<0.001	5 / 5

4.3.3.6 Level 4 – Algal turf

Some level of separation was achieved between the four main habitat components that made up the algal turf class, namely coralline, foliose green, foliose brown and foliose red algae. The greatest separation was achieved using the *SCA*, followed by the *SA*, with *'R'* values of 0.870 and 0.672, respectively (Table 4-10). In both cases the nMDS plots indicate that the only samples that were difficult to separate were foliose red and coralline algae (Figure 4-18).

4.3.4 Testing the classification algorithm using mixture analysis

The accuracy of the classification algorithm was tested for levels 2, 3 and 4 in just the bio-substrate class in the classification algorithm. The overall accuracy of the algorithm at Level 2, between seagrass, coral and macroalgae habitats, was 87% and the *kappa* and *tau* coefficients were 0.87 and 0.82, respectively (Table 4-11). Both seagrass and

coral had user's accuracies of almost 100%. Macroalgae had a lower user's accuracy of 74%, with there being some confusion with both coral and seagrass habitats.

Table 4-10: Results of the spectral separation analysis carried out using a genetic algorithm to determine the optimum band combination to separate between coralline, foliose green, foliose brown and foliose red algae dominated habitats for each spectral metric. Each test was carried out five times using 14 spectral signatures for the library. Best results in bold.

Spectral metric	Bands tested	Optimal bands	'R' statistic	p-value	Occurrences
SA	1 - 17	8, 9, 10	0.671831	<0.001	1 / 5
	1 – 9	5, 7	0.607042	<0.05	5 / 5
SCA	**1 - 17**	**3, 7, 9**	**0.870423**	**<0.001**	**4 / 5**
	1 – 9	**3, 7, 9**	**0.870423**	**<0.001**	**5 / 5**
SGA	1 - 17	1, 6	0.304225	<0.05	3 / 5
	1 – 9	1, 6	0.304225	<0.05	5 / 5
SID	1 - 17	8, 10	0.629577	<0.05	1 / 5
	1 – 9	5, 7	0.600000	<0.05	5 / 5
SID(TAN)	1 - 17	8, 9, 10	0.653521	<0.001	2 / 5
	1 – 9	5, 7	0.601408	<0.05	5 / 5
SID(SIN)	1 - 17	8, 9, 10	0.652113	<0.001	2 / 5
	1 – 9	5, 6, 7	0.601408	<0.001	3 / 5

Table 4-11: Error matrix for the classification on seagrass, coral and macroalgae mixed signatures.

	Reference class			
Mapped class	Seagrass	Coral	Macroalgae	User's accuracy
Seagrass	2 897	0	71	98 %
Coral	0	2 532	15	99 %
Macroalgae	479	699	3 307	74 %
Producer's accuracy	86 %	78 %	97 %	

At Level 3 of the classification scheme the only split is that of the macroalgae habitat class into either the canopy or algal turf class. The overall accuracy of this split was 81% and the tau coefficient was 0.67. The highest producer's accuracy was 92% for algal turf, while the user's accuracy was greater for canopy algae (90%) (Table 4-12).

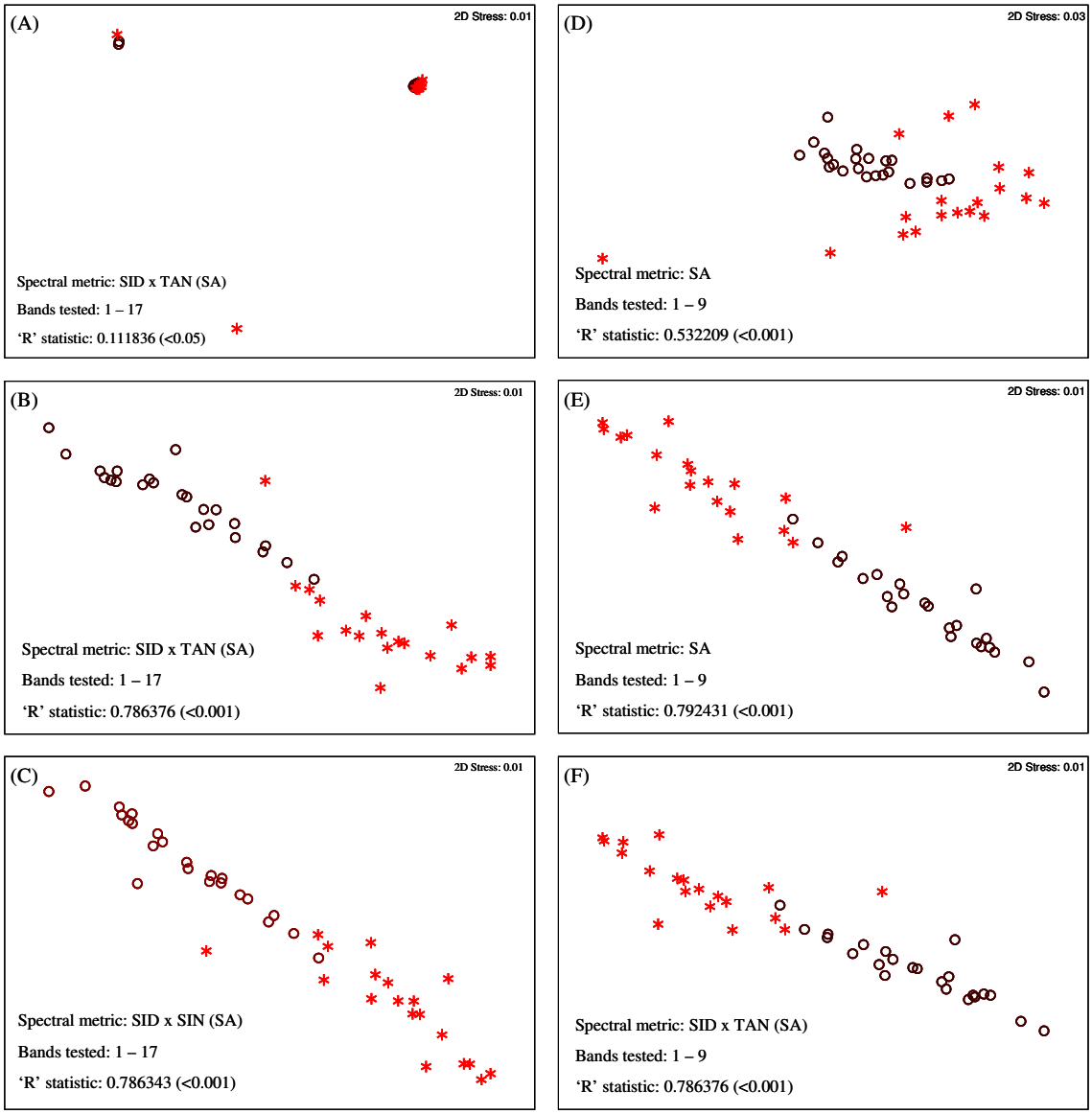

Figure 4-15: Results of the spectral separation analysis carried out using a genetic algorithm to determine the optimum band combination to separate between canopy (○) and turf (*) algae dominated habitats. nMDS plots were constructed for the optimal spectral metric, spectral information divergence – tangent spectral angle (*SID x TAN(SA)*), using bands 1 – 17 (A) and the two best band/metric combinations, the *SID x TAN(SA)* (B) and the *SID x SIN(SA)* (C). nMDS plots were constructed for the optimal spectral metric, spectral angle (*SA*), using bands 1 – 9 (D) and the two best band/metric combinations, the *SA* (E) and *SID x TAN(SA)* (F). All analyses were carried out using 74 spectral signatures for the library.

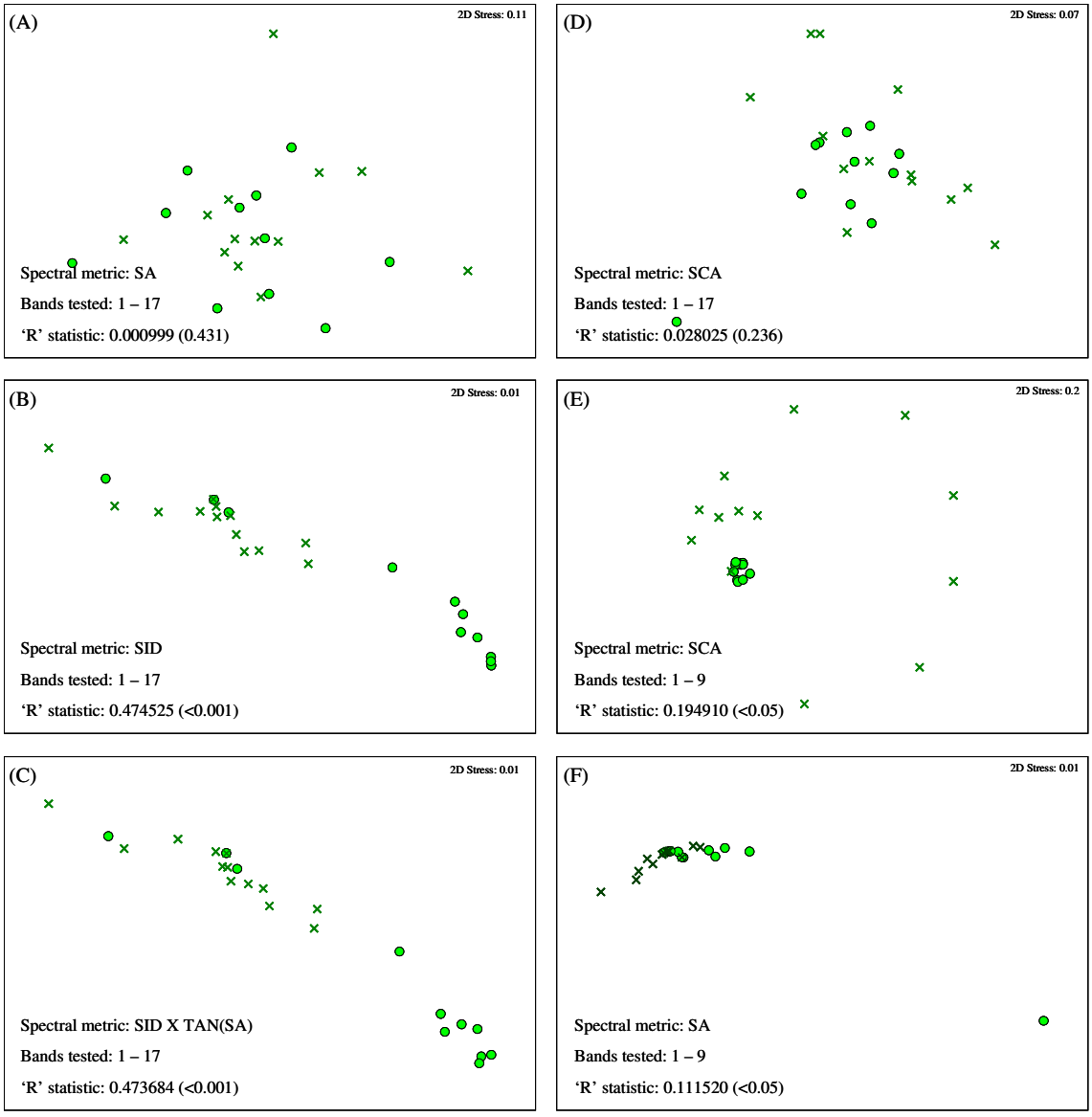

Figure 4-16: Results of the spectral separation analysis carried out using a genetic algorithm to determine the optimum band combination to separate between *Posidonia* (x) and *Amphibolis* (●) seagrass dominated habitats. nMDS plots were constructed for the optimal spectral metric, spectral information divergence (*SID*), using bands 1 – 17 (A) and the two best band/metric combinations, the *SID* (B) and the *SID x TAN(SA)* (C). nMDS plots were constructed for the optimal spectral metric, spectral correlation angle (*SCA*), using bands 1 – 9 (D) and the two best band/metric combinations, the *SCA* (E) and *SA* (F). All analyses were carried out using 24 spectral signatures for the library.

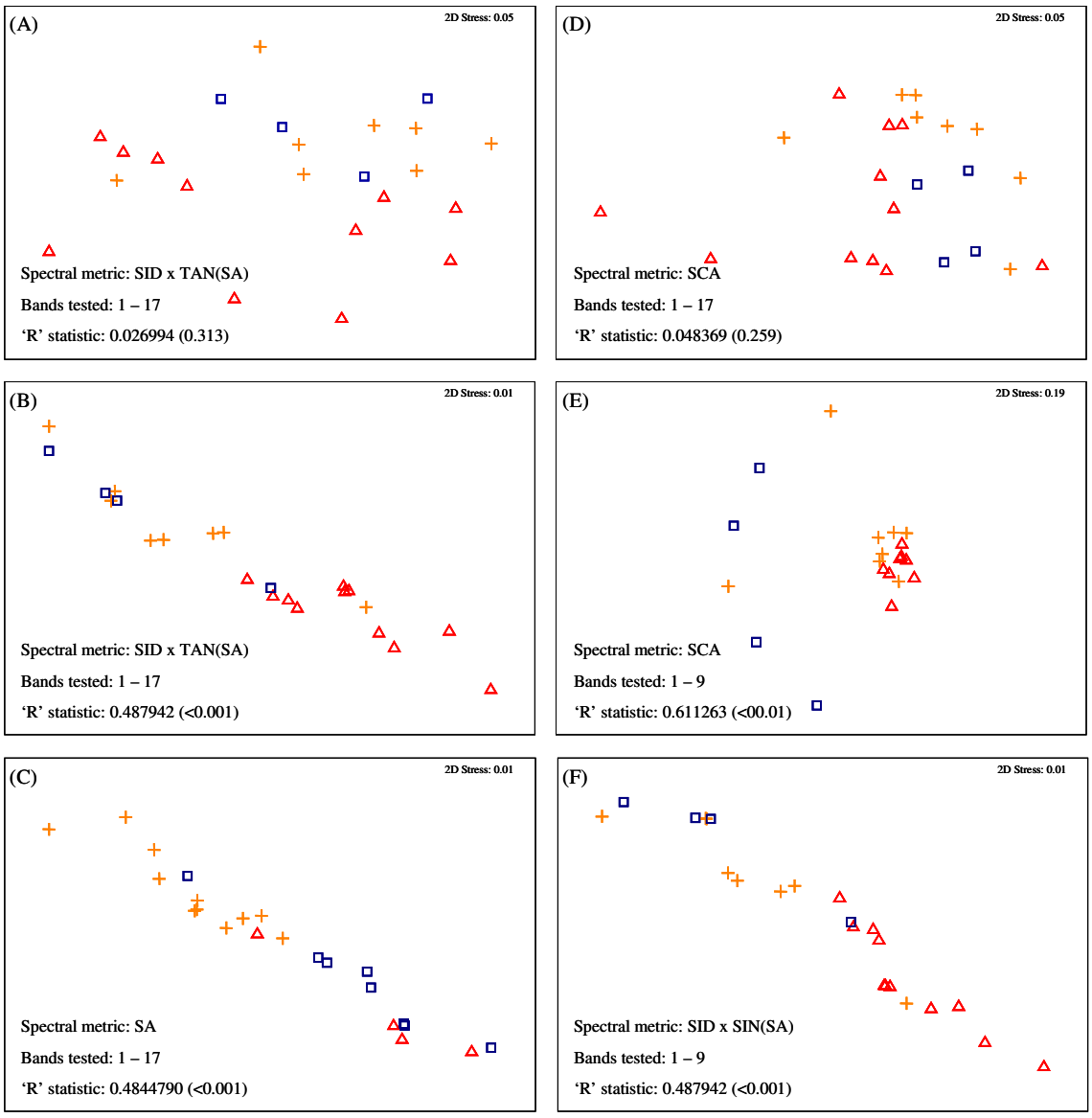

Figure 4-17: Results of the spectral separation analysis carried out using a genetic algorithm to determine the optimum band combination to separate between *Ecklonia radiata* (+) and *Sargassum* spp. (Δ) and *S. doryocarpa* (□) dominated habitats. nMDS plots were constructed for the optimal spectral metric, spectral information divergence – tangent spectral angle (*SID x TAN(SA)*), using bands 1 – 17 (A) and the two best band/metric combinations, the *SID x TAN(SA)* (B) and the *SA* (C). nMDS plots were constructed for the optimal spectral metric, spectral correlation angle (*SCA*), using bands 1 – 9 (D) and the two best band/metric combinations, the *SCA* (E) and *SID(SIN)(SA)* (F). All analyses were carried out using 23 spectral signatures for the library.

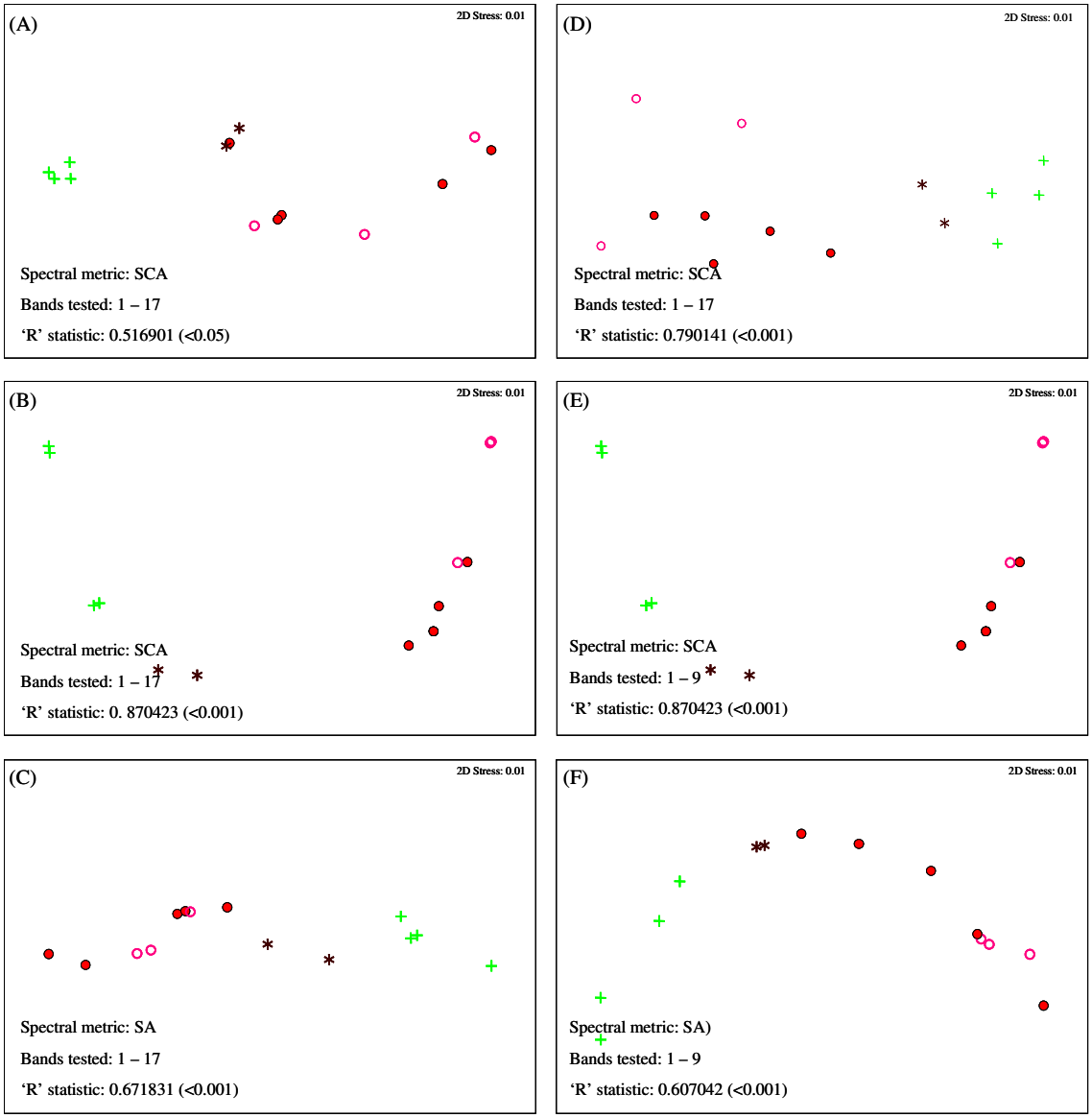

Figure 4-18: Results of the spectral separation analysis carried out using a genetic algorithm to determine the optimum band combination to separate between coralline (○), foliose green (+), foliose brown (*) and foliose red (●) algae dominated habitats. nMDS plots were constructed for the optimal spectral metric, spectral correlation angle (*SCA*), using bands 1 – 17 (A) and the two best band/metric combinations, the *SCA* (B) and the *SA* (C). nMDS plots were constructed for the optimal spectral metric, *SCA*, using bands 1 – 9 (D) and the two best band/metric combinations, the *SCA* (E) and *SA* (F). All analyses were carried out using 14 spectral signatures for the library.

There appeared to be a significant level of confusion with 31 % of canopy algae signatures being misclassified as algae turf.

Table 4-12: Error matrix for the classification on canopy algae and algal turf mixed signatures

	Reference class		
Mapped class	Canopy algae	Algal turf	User's accuracy
Canopy algae	3 427	395	90 %
Algal turf	1 555	4 623	75 %
Producer's accuracy	69 %	92 %	

The overall accuracy of the algorithm in being able to determine if a seagrass signature was dominated by either *Posidonia* or *Amphibolis* species was 68%, with a *tau* coefficient of 0.5, indicating that overall chance agreement contributed almost 20% of the overall accuracy. The producer's accuracy was greater for *Posidonia* (82%) than *Amphibolis* (54%) (Table 4-13). This indicates that if a signature was identified as being dominated by *Posidonia* then there was high probability that it was correct. However, if it was identified at being dominated by *Amphibolis,* then there was an almost equal probability that it was actually *Posidonia*.

Table 4-13: Error matrix for the classification on *Posidonia* and *Amphibolis* mixed signatures.

	Reference class		
Mapped class	*Posidonia*	*Amphibolis*	User's accuracy
Posidonia	4 025	2 319	63 %
Amphibolis	894	2 762	76 %
Producer's accuracy	82 %	54 %	

The overall accuracy of canopy algae signatures being classified as either *E. radiata*, *Sargassum* or *S. doryocarpa* was 59%. The highest producer's accuracy was for *Sargassum* (91%) and the highest user's accuracy was *S. doryocarpa* (82%) (Table 4-14). The *tau* coefficient was 0.46 which indicates that at this level the classification

has an almost equal chance of misclassifying a pixel as it does of determining the correct classification.

Table 4-14: Error matrix for the classification on *E. radiata*, *Sargassum* spp. and *Scytothalia doryocarpa* mixed signatures.

	Reference class			
Mapped class	*E. radiata*	*Sargassum*	*S. doryocarpa*	User's accuracy
E. radiata	1 030	265	1 042	44 %
Sargassum	1 905	3 086	521	56 %
S. doryocarpa	352	32	1 767	82 %
Producer's accuracy	31 %	91 %	53 %	

The division of the algal turf class into its components, coralline algae, red, green and brown foliose algae, had the lowest overall accuracy (32%) and a *tau* coefficient of 0.19. However if the two classes, coralline and red foliose were combined (both belonging to Rhodophyta) then the overall accuracy was 63%, an almost two-fold increase. The producer's accuracy for coralline algae was the greatest (73%), while the brown foliose algae had the lowest at 7% (Table 4-15). The results indicated that identifying these components was not feasible using the spectral data in the visible region.

Table 4-15: Error matrix for the classification on algal turf mixed signatures

	Reference Class				
Mapped class	Coralline	Red	Green	Brown	User's accuracy
Coralline	1 850	519	106	989	53 %
Red	84	407	1 532	867	14 %
Green	563	1 566	732	446	22 %
Brown	28	37	99	175	52 %
Producer's accuracy	73 %	16 %	30 %	7 %	

Based on the results of the spectral separation analysis and the testing of the classification algorithm using synthetic signatures, a subset of the complete habitat classification scheme described in Chapter 2 was used to classify the hyperspectral images (Figure 4-19). The limestone class was not included due to the very low number of spectral signatures in the library. This also applied to *Scythothalia doryopcarpa* together with the observation that this species very rarely dominated pixel sized areas at Rottnest Island. The four subclasses of the algal turf habitat type were not used due to the low accuracies achieved in testing the classification algorithm at that level. *Halophila* seagrass was not used as it very rarely occurs at a spatial scale that will be detected in an image pixel; it often occurs on the margins of seagrass meadows of other genera and has a spectral signature highly influenced by bare substrate.

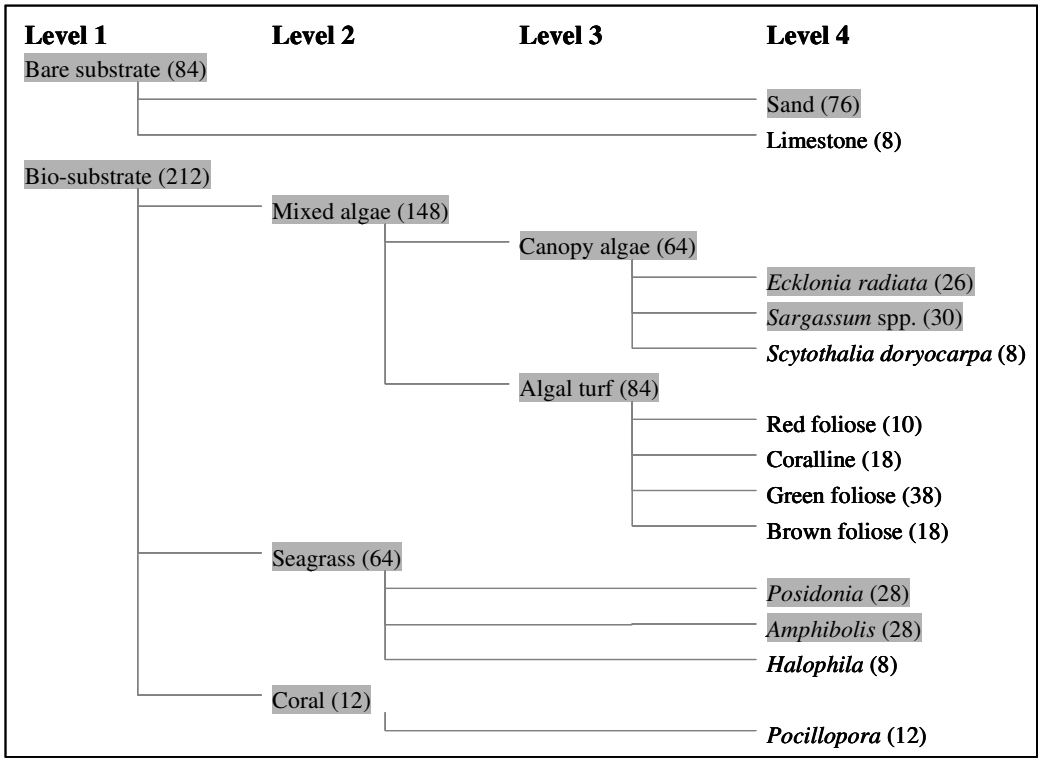

Figure 4-19: Summary of the levels within the original habitat classification scheme which were used to classify the hyperspectral imagery in the following chapter. The habitats types highlighted in grey were used as part of the classification process and the remainder were grouped under the next level up in the hierarchy.

4.4 Discussion

4.4.1 Spectral library

The development of a spectral library of the dominant marine benthic macroalgae, seagrass, coral and bare substrate types formed the basis for using remotely-sensed hyperspectral data to classify marine benthic habitats at Rottnest Island. The development of the library required the underwater collection of spectral reflectance data for the dominant benthic plant and coral species and bare substrate types, i.e. habitat components, and the processing of that data to create a spectral library. The spectral library was used to determine the spectral separability of the various habitat components and also to identify which algorithms and classification techniques were best suited to obtaining the optimal classification results based solely on the spectral data (Hochberg and Atkinson 2000). The results presented here allowed the library to be used as the core input for hyperspectral image processing to facilitate identification of benthic habitat components based on whichever was dominant within each pixel in the image.

The collection of the *in situ* data for the spectral library for the dominant components of the benthic substrates of Rottnest Island Reserve was carried out using similar techniques to those of Hochberg and Atkinson (2003). This method was chosen as it provided a cost-effective and reliable method for the collection of reflectance data. However, it does have a number of shortcomings that needed to be accounted for when processing the data and could be avoided using a more sophisticated, and expensive, spectrometer setup. These shortcomings include the changes in the downwelling light field between the capture of the upwelling radiance from the target and the capture of the downwelling irradiance from the Teflon reflectance panel. Although every attempt

was made to minimise the time delay between the capture of these two readings, there was always the inherent variation in the underwater light field, which could often change faster than the measurement pairs could be captured. One possible solution to this problem is to use a dual channel spectrometer which would capture the upwelling and downwelling measurements at the same time, thus completely removing any effect of the temporal variation in the underwater light field. This study has made an effort to remove any effects of the variable light field by using the average downwelling irradiance across the ten replicates taken for each sample. This approach was taken as visual inspection of the data indicated that the effect of the variable underwater light field was significantly greater on measurements taken over the highly reflective Teflon panel and than those taken over most benthic substrates.

The spectral signatures collected in this study appear to have features comparable to spectral signature data collected elsewhere, even those which used different collection methods, such as Fyfe (2003), who measured the spectral reflectance out of the water. The reflectance signature for bare sand collected for this study did exhibit less spectral shape than signatures collected at the Great Barrier Reef and Hawaii (Hochberg *et al.* 2003, Kutser *et al.* 2003). The reflectance signatures for sand in this study have much less defined spectral features, maximum at ~650 nm and minimum at ~670 – 680 nm, than those recorded in the other studies. The signatures did match carbonate sand signatures collected by Louchard *et al*. (2002), in the Bahamas, and also other sediments that had some level of pigments, including chlorophyll, in the sediment. This may explain the slight absorption feature at ~650 nm, and an increase in reflectance into the near-infrared.

The signatures for both the seagrass and macroalgae collected in this study compare favourably with those collected elsewhere (Fyfe 2003, Hochberg *et al.* 2003, Kutser *et al.* 2003). The signatures for all the bio-substrate habitat components all exhibited the characteristic feature of all chlorophyll containing organisms, the 'red edge' which has been documented in seagrass and marine algae reflectance signature recorded elsewhere in the world (Hochberg *et al.* 2003, Kutser *et al.* 2003, Thorhaug *et al.* 2007). The 'red edge' is a feature of the reflectance signature of all chlorophyll containing organisms and is where the reflectance of light in the red region exhibits strong absorbance followed by a rapid increase in the reflectance of light in the near-infrared, with the reflectance minimum often occurring around 680 nm. It is caused by the red part of the spectrum (~680 nm) being strongly absorbed by the chlorophyll in leaf and the near-infrared wavelength being mostly reflected as a result of scattering within the leaf itself (Slaton *et al.* 2001, Sims and Gamon 2002, Thorhaug *et al.* 2007). The position of the 'red edge' has been found to correlate with the chlorophyll content of the leaves, and in the case of seagrass, has been found to shift in relation to senescence and in response to changes in salinity of the water column (Thorhaug *et al.* 2006, 2007). The differences observed between the seagrass and macroalgae signatures were most likely due to the variations in chlorophyll content and other accessory pigments, in combination with the structural characteristics of their leaf (frond) morphology and structure (Thorhaug *et al.* 2007). As noted by these authors, more work needs to be conducted to fully understand the effects on the spectral reflectance of the varying combination of pigments, morphological and structural characteristics of marine plants.

As noted by Kutser *et al*. (2003), many of the obvious spectral features in the these plant spectral signatures were found at wavelengths >550 nm, which can present

problems when using this information in image classification as the light at these longer wavelengths (i.e. the red portion of the spectrum) is absorbed strongly by water, resulting in limited, and often unreliable, image data at these wavelengths. The combination of these obvious differences in spectral signatures often occurring at the red end of the visible spectrum and the commonly limited image data available is a primary reason for conducting spectral separability analysis to make the best use of the available data in order to classify image data.

4.4.2 Spectral separability analysis

The nature of hyperspectral data results in large numbers of continuous bands leading to significant data redundancy due to high levels of correlation between bands (Landgrebe 2003). This means that techniques that reduce the dimensionality of the data are often carried out as part of data analysis for classification (Robila 2005). Many of these techniques focus on reducing the number of bands prior to classification, a process which can often increase the accuracy of the classifications, and reduce the likelihood of false positives resulting from the algorithms over-fitting the data. This means determining which wavelengths or image bands best discriminate between the spectral signatures of different classes, while at the same time maximising the spectral similarity within classes. By minimising the number of bands processed not only is classification accuracy increased but processing time can be reduced for these very large data sets.

Hochberg and Atkinson (2000) collected *in situ* spectral reflectance signatures of three corals, five algal species, and three sand types on coral reefs in Kaneohe Bay, Oahu, Hawaii, to determine their spectral separability. They used the fourth derivatives, in combination with linear discriminant function analysis to separate three main classes,

coral, algae and sand, in their hyperspectral data. This information was used to demonstrate that it was possible to map the spatial extent of these benthic covers, with a reasonable level of accuracy, based on *in-situ* spectral information. In a similar study, Hochberg and Atkinson (2003) analysed the separability of coral, algae and bare sand using linear discriminant function analysis and achieved classification accuracies of up to 98% when identifying *in situ* reflectance signatures, using a linear discriminant function algorithm trained on a subset of the *in situ* data.

Karpouzli *et al*. (2004) conducted a study in the western Caribbean, using *in situ* spectral signatures of coral, algae, seagrass and sediments, and determined that they could be separated with the greatest accuracy using hyperspectral data, which allowed for derivatives to be calculated because of the large number of data points. Minghelli-Roman *et al*. (2002) used a different approach to discriminate between the reflectance spectra of a 14 different coral genera in the Red Sea. They used the absolute reflectance, the slope and wavelength ratios in combination with the Tukey-Kramer test to determine the separability of the different genera. They indicated that these overcame the problems of varying light levels by focussing on the shape of the spectra rather than the intensity. However, neither Karpouzli (2004) or Minghelli-Roman (2002) applied their results directly to the classification of image data.

Studies were carried out by Holden and LeDrew (1998, 2000) to determine the spectral separability of *in situ* spectra collected from coral reefs in Fiji and Indonesia. Both studies used principal component and derivative analyses as the means for determining how separable the different benthic components were. The Fijian study also used a cluster analysis to group the spectra using no *a priori* information about the grouping of

the data. This approach provided information about how the spectra grouped based solely on their spectral characteristics. The Fijian study determined that healthy and bleached corals had distinct spectral signatures and the Indonesian study indicated that healthy corals, bleached corals, macroalgae, rubble and sand could be differentiated with reasonable accuracies, based on their spectral signatures. Neither study demonstrated a means of applying their results to image classification.

Fyfe (2003) studied the spectral separability of a number of common seagrass species found in estuaries along the south-eastern coast Australia using a multivariate approach with the Bray-Curtis coefficient as a measure of similarity between spectral signatures of the various seagrass species. The similarity matrices generated were analysed using a combination of non-metric multidimensional scaling, ANOSIM and SIMPER within the Primer software, to determine their separability along with the statistical significance of those bands (wavelengths) in the spectral data which made the greatest contributions to these separations. This approach shares many similarities with that taken in this study, but rather than use similarity measures that have been specifically developed for spectral analysis, such as the spectral angle, Fyfe used the Bray-Curtis coefficient, which is generally applied to ecological assemblage data (Clarke *et al.* 2006).

Although all the approaches to spectral separability analysis discussed above have resulted in gaining a greater understanding of the spectral separability of the habitat components being studied, many have failed to provide a direct means to apply their results to image data. The analysis carried out in this study attempted to take many aspects of work previously undertaken and integrate them with more appropriate spectral metrics, as measures of similarity between spectral signatures. They then

provide a framework for classifying hyperspectral images based on spectral signatures of the dominant habitat components contained in a spectral library.

The results of this study demonstrate that the spectral signatures of the habitat components that typically dominate the marine benthic habitats of Rottnest Island can be differentiated based on their spectral signatures. Use of an optimisation approach, based on a genetic algorithm, enabled the simultaneous determination of both the best spectral metric and image band combination to identify pixels dominated by the particular habitat component at a pre-defined classification level. Added to this, the approach taken was hierarchical, allowing the analysis to follow the structure of the habitat classification scheme and take advantage of this known ecological structural within marine benthic habitats.

This study has found that, although the spectral angle and the spectral correlation angle metrics performed best overall, there is justification for using all the metrics tested in the analysis of the spectral data for benthic habitat mapping in appropriate situations. The spectral gradient angle was the worst performer, only providing reasonable separation for one analysis, a result which agrees with the findings of Robilla and Gersham (2005). Although Du *et al.* (2004) determined that the two metrics that combined the spectral angle and the spectral information divergence provided increased performance over either metric on its own, this was not so for the Rottnest data set, where the performances of all four metrics were often similar.

Although the inclusion of both first and second order derivatives in spectral separation analysis has been shown to improve the separability of different classes based on their spectra (Karpouzli *et al.* 2004), they were not included in the analysis carried out for

this study. The reason for this was that there was no means available to use derivatives when classifying the image, often due to the limited image bands that contained reliable data. In future work, the inclusion of the derivatives in the classification process, for pixels in the image with sufficient data, could provide increased accuracy in the classification results and the ability to classify habitats to a higher level in the classification scheme.

The multivariate approach used in this study while, in essence, similar to the analyses carried out by Fyfe (2003), took a slightly different approach to answer the same question, namely, which is the best method to separate benthic habitats based on their spectral signatures. By taking a multivariate approach that was able to use all relevant spectral signatures from the library in each analysis, the natural spectral variability within each habitat component was accounted for. This, in combination with testing six spectral metrics to measure the discrepancy between pairs of spectra, allowed for the greatest level of flexibility in classifying data. This is an important feature when applying this approach to image data which does not always have reliable reflectance data for all image bands, largely as a result of varying depth and sea conditions.

The classification algorithm developed, in response to the results of the spectral separability analysis, provided the ability to utilise the entire spectral library to classify the hyperspectral imagery in a hierarchical manner, as defined by the habitat classification scheme. The accuracy of the classification algorithm when identifying the dominant habitat component in a mixed signature indicated that it provided a reliable tool for identifying the benthic habitats at Rottnest Island. The results of the accuracy assessment also provided the user with guidance when interpreting image classification

results generated by the algorithm. For example, the results indicated that there was often confusion when a macroalgae dominated signature was further classified as algal turf, with a significant proportion of those actually being canopy algae, whereas when classified as canopy algae, only a small proportion were actually algal turf. This means that in the image classification results there was likely to be an over estimation of the algal turf habitats and potential users of the habitat maps can be made aware of the possible confusion.

The overall result of the creation of the spectral library and the subsequent spectral separation analysis is a robust classification algorithm that can be used directly, in conjunction with the spectral library, to identify marine benthic habitats in hyperspectral imagery.

5 HyMap image classification for the benthic habitats of Rottnest Island

5.1 Introduction

In the past, the mapping of marine benthic habitats has been done using traditional field methods, which are both costly and labour intensive. These methods can include the use of transects carried out by SCUBA divers, remotely operated vehicles (Parry *et al.* 2003) or towed video (Kendall *et al.* 2005). There has also been an increasing interest and research into the use of remotely sensed data to map marine benthic habitats. One of the more recent developments is the availability of airborne hyperspectral data which can theoretically allow for benthic habitats to be mapped to a higher taxonomic level than previously possible (Fyfe 2003). One of the key requirements to be able to utilise the full potential of these data is to be able to correct the image for the confounding influence of the overlying water column, and thereby reveal the true spectral reflectance characteristics of the benthic habitats represented by each pixel (Mumby *et al.* 1998a, Green *et al.* 2000, Lesser and Mobley 2007).

Reflectance data collected from the marine environment include light that has interacted with the atmosphere, the water, both on its passage from the surface to the seafloor, and again on the return journey to the sensor (See Figure 1-3). These interactions result in variable changes to the radiance recorded for each pixel depending on factors including the depth (i.e. the thickness of the layer of water), the quality of the water, the sea-state and the bottom type that is reflecting the light back to the surface (Holden and LeDrew 2002).

Light which strikes the surface of the water column can be reflected by the surface, attenuated by or transmitted through the water column and, in the case of shallow

waters, reflected by the seafloor (Kirk 1994b, Holden and LeDrew 2002). The surface of the ocean often acts as specular reflector and results in what is often referred to as sunglint (Goodman *et al.* 2008). The attenuation of light by the water column is dependent on absorption and scattering. The degree to which light is attenuated is directly linked to the main constituents of the water column, these being pure water, salt, suspended matter, yellow substance (or Gelbstoff) and chlorophyll (Jerlov 1976, Haltrin 1999).

The attenuating effect of pure water on light is through absorption and can be considered invariant between different water bodies (Pope and Fry 1997). The salt content of oceanic water has a negligible influence on the attenuation of light (Jerlov 1976), but the concentration of suspended matter has a significant influence, most significantly through the process of scattering (Babin *et al.* 2003). The process of light being scattered by suspended particles is not wavelength selective, and it affects light across the entire spectrum resulting in significant influence on the structure of the underwater light field (Jerlov 1976). Added to this, the concentration of yellow substance, also referred to as Gelbstoff or Gilvin, has a significant influence on the level of light absorption, with the level of absorption increasing with decreasing wavelength (Jerlov 1976, Kirk 1976, Bricaud *et al.* 1981). Yellow substance refers to the combination of dissolved and colloidal organic compounds present everywhere in the ocean, with higher concentrations occurring in regions of higher productivity. The chlorophyll concentration is an indicator of the amount of phytoplankton present in the water column and can affect both the scattering and absorption of light (Haltrin 1999).

The absorption and scattering of light due to the factors mentioned above are considered inherent optical properties of water and are described by the absorption and angular scattering coefficients (Haltrin 1999). In many cases it is not possible to determine these individually and the relationship can be simplified through the use of an apparent optical property of water, the diffuse attenuation coefficient (K_d) (Mishra *et al.* 2005a). The K_d is dependent on both the composition of the water and the structure of the ambient light field, although the former has a greater effect than the structure of the light field (Kirk 1994b, Mishra *et al.* 2005a). The K_d can be derived both from remotely sensed imagery and *in situ* measurements, making it an useful measure to validate remotely sensed products (Kirk 1994a, Mishra *et al.* 2005a).

These variable interactions of light have been investigated since the 1970s, to understand their effects, and also to correct imagery to minimise or remove these effects, with the ultimate aim of getting images that represent the true spectral characteristics of the seafloor cover (Goodman and Ustin 2007). There have been a number of methods developed to correct for these variable effects on the reflectance signatures of the seafloor. One on the earliest and most basic methods was developed by Lyzenga (1978, 1981) and uses the concept of band ratios to create a depth invariant bottom index. The advantage of this approach is that for multi-spectral data (limited number of image bands) it can be easily implemented using many standard image processing software packages.

Mumby *et al*. (1998a) used the Lyzenga method to correct CASI multi-spectral data, flown over the Turks and Caicos Islands, and achieved classification accuracies up to 81% for nine coral reef habitats. Benfield *et al*. (2007) used the Lyzenga method on

both Landsat ETM+ and Quickbird data from Pacific Panama, prior to successful habitat classification of a coral reef environment. Tassan (1996) demonstrated that, although the Lyzenga method had been validated in environments with clear water of uniform water quality, it could also be modified to achieve results in more turbid waters with non-uniform water quality. However, for application to hyperspectral data the implementation becomes much more cumbersome, with the number of possible band ratios increasing with each additional image band. A major disadvantage of this approach, which is especially relevant to hyperspectral data, is that the image data after the correction has been applied cannot be used in conjunction with a spectral library to identify the various bottom types.

The development of high resolution hyperspectral sensors, such as HyMap, with numerous image bands in the visible spectral range, has led to research on developing methods to utilise these improved data to more accurately correct for the effects of the water column on the reflectance at the benthic surface. These techniques were primarily aimed at closing the radiative transfer loop, which describes the effect of water on radiant energy passing through it, and allow for the inversion of the remotely sensed data to obtain, not only a corrected bottom reflectance signature, but also the water depth and the concentration of the major water constituents responsible for variation in light attenuation. This approach provides a solution for generating results aimed at habitat mapping, as it generates information on the depth, which is often essential in defining accurate and ecologically relevant habitat classes, and the bottom reflectance corrected for the influence of the overlying water column.

Lee *et al*. (1998, 1999) developed a semi-analytical approach to deriving the depth and water properties by inverting the radiative transfer equation using an optimisation approach. This approach was applied by Goodman and Ustin (2007) to AVIRIS hyperspectral data in Kaneohe Bay, Hawaii and they successfully corrected and classified the data to a maximum depth of 3 m. They were able to extract depth values up to 20 m, but results indicated the un-mixing of the relative contributions of different bottom types (coral, sand and algae) were not reliable enough without further model calibration to classify the data from >3 m depth. The marine benthic habitats of Jurien Bay, Western Australia, were mapped using HyMap hyperspectral data that was corrected to the influence of the water using an approach based on the Lee *et al*. (1998, 1999) method, and successfully identified three main cover types, bare substrate, brown algae and seagrass (Klonowski *et al.* 2007).

The Modular Inversion and Processing system (MIP) has been developed to provide complete data correction (atmospheric, sun-glitter and water corrections), and results in data on the depth and bottom reflectance for each pixel (Heege *et al.* 2004). This system has been designed as a physics based process chain which links a series of modules together to recover the information directly from the data. MIP has been tested extensively over a number of different water body types, including inland lakes, coral reefs and temperate marine environments. MIP was used to successfully map the water constituents, bathymetry and benthic coverage in Lake Constance (Heege and Fischer 2004) and is being applied to hyperspectral data at Ningaloo Reef in tropical Western Australia (Kobryn *et al*. unpublished data).

Although it has been long accepted that even basic water correction, such as the Lyzenga method, can increase the final habitat classification accuracy, in order to use a classification approach based on a spectral library, the more complex approaches that can provide corrected bottom reflectance signatures are needed (Mumby *et al.* 1998a, Goodman and Ustin 2007). MIP is one of the few methods available that has achieved this aim. Most previous work using hyperspectral data to classify marine benthic habitats has been restricted to shallow coral reef environments and freshwater systems, with reasonably clear water. There has been very little work conducted in temperate waters, due to the often poor water clarity of most temperate marine environments. This study will be one of the first application of hyperspectral data collected over optically-deep temperate marine waters (due to the oligotrophic Leeuwin Current).

The aim of this study is to generate habitat maps of the Rottnest Island Reserve (<15 m deep) that represent the dominant components at each level of the habitat classification scheme using a spectral library to classify the HyMap hyperspectral image data.

5.2 Methods

5.2.1 HyMap data collection and water correction

Three flight lines of HyMap hyperspectral data were collected on the 26th April 2004 by the HyVista Corporation (Figure 5-1) using a twin engine light aircraft, fitted with a HyMap sensor and flying at an altitude of 1600 m to record data at a ground resolution of 3.5 m. The data were collected at 125 spectral bands ranging from 450 – 2480 nm, with an average spectral sampling interval of 15 nm. HyVista applied a geometric correction to enable the data to be geo-located within a GIS framework.

The atmospheric, sun-glint and water correction of the hyperspectral HyMap data was carried out by EOMAP, a remote sensing company based in Germany which provides standardised mapping products from remote sensing data, using the Modular Inversion and Processing System (MIP). MIP uses a physics based process, with no external inputs, to extract from the data information on the water constituents, bathymetry,

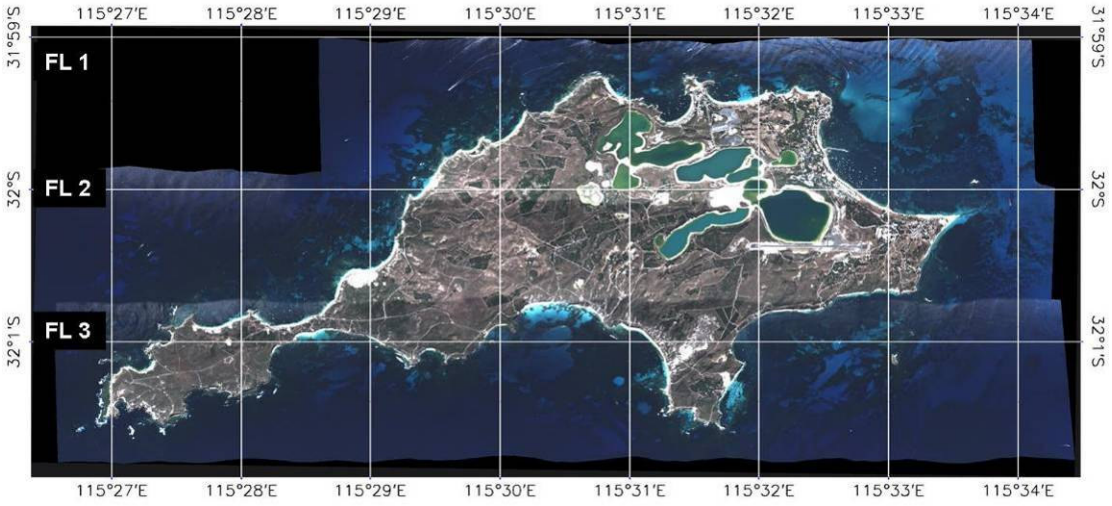

Figure 5-1: Three flight lines of uncorrected HyMap reflectance data for Rottnest Island, Western Australia, collected on 26th April 2004.

bottom cover type and bottom reflectance. The architecture of the program combines a set of general and transferable computational methods in a chain, which connects the bio-physical parameters of the water column with the measured sensor radiances. MIP converts the subsurface reflectance to bottom reflectance using equations of Albert and Mobley (2003). The depth is determined iteratively in combination with un-mixing of the bottom reflectance, with the final depth, bottom reflectance and coverage being retrieved when the residual error is at a minimum (Heege and Fischer 2004). The Rottnest hyperspectral data were corrected using generic bottom cover types for bare sediment, light and dark submerged aquatic vegetation. The signatures used as inputs were extracted directly from the image. The outputs of the MIP processing were the

bottom reflectance values corrected for the water column, percent cover of bare sediment per pixel and submerged aquatic vegetation (light and dark), and other summary layers (Table 5-1).

Table 5-1: The main data outputs from the MIP processing of the HyMap image data. (* indicates the data were used in the classification of the Rottnest Island image for benthic habitat mapping)

MIP output	Description
Bottom reflectance*	A multi-band raster image with reflectance data that have been corrected for the influence of the water column
Depth	The depth calculated for each pixel
Bare sediment cover*	The percent cover of bare sediment for each pixel
Light vegetation cover	The percent cover of light vegetation for each pixel
Dark vegetation cover	The percent cover of dark vegetation for each pixel
First band*	The band number index of the first useable bottom reflectance image band resulting from the correction process for each pixel
Last band*	The band number index of the last useable bottom reflectance image band resulting from the correction process for each pixel

5.2.2 Image classification for benthic habitat maps

The bottom reflectance values, bare sediment cover, the first band and last band data were used as inputs into the image classification process. The first and last bands were used to guide the classification algorithm to the most appropriate image band / spectral metric to use for each pixel. Each flight-line was processed individually, prior to being geo-located, mosaiced and assessed for classification accuracy. The image classification was carried out hierarchically using the results of the spectral separability analysis

(Chapter 4) in conjunction with the abiotic variables to guide the classification algorithm and follow the hierarchical classification scheme. All image classification processing was carried out using a plug-in[1] developed for the BEAM-VISAT software which is an open-source extensible framework for remote sensing image analysis (Brockmann Consult 2008). The plug-in linked the spectral library (Chapter 4) to BEAM to enable the implementation of the classification algorithm, as described previously, by extracting the spectral signature for each pixel and identifying the dominant habitat component present. The images were geo-located using geometric lookup tables provided by HyVista Corporation and mosaiced using the ENVI 4.2 software package (RSI 2005).

The data were first classified to Level 1 of the classification scheme to identify pixels dominated by bare substrate or bio-substrate, by using a threshold on the bare sediment cover data for each pixel using MIP output (Figure 5-2). A histogram of the bare sediment cover data was created for regions <15 m depth using the digital bathymetry model for Rottnest Island Reserve (Chapter 3). The data were classified using major breaks in the histogram as thresholds, and the accuracy of each classification was assessed using ground validation data to determine the best result. The classification was used to mask out those pixels classified as bare substrate from further analysis.

[1] Plug-in was developed by D. Harvey to implement the algorithms developed as part of this thesis within the BEAM-VISAT framework.

The pixel-by-pixel spectral algorithm approach described in Chapter 4 was used to hierarchically determine the classification, defined as the dominant habitat component, of each pixel classified as bio-substrate for levels 2, 3 and 4 of the habitat classification scheme. Each pixel was assigned a habitat class at each level of the classification scheme using the classification algorithm in combination with the complete spectral library.

The classification at Level 2 was first classified using the spectral library and then the results were subjected to a second stage classification using decision rules based on abiotic variables to identify the intertidal reefs and re-assign misclassified pixels from all other classes (seagrass, macroalgae and coral) (Figure 5-2). Classifications for both Level 3 and 4 where based solely on the spectral classification algorithm.

The decision rules for Level 2 were based on the digital bathymetry model (DBM) and the annual relative exposure index (REI) for the Rottnest Island Reserve (Chapter 3). Decision rules were applied separately to each of the four quadrants of the reserve using different rules for each sector. Intertidal reefs were defined as regions where the depth in the DBM was above mean sea level (MSL) for all level two classes, except coral. Coral was excluded as the *Pocillopora damicornis* coral that occurs at Parker Point is found in very shallow water and may occur above MSL in the digital bathymetry model. The threshold for the REI was determined by examining the range of REI values where seagrass occurred in the validation data (see Section 5.2.3 for details) within each quadrant, where validation data existed.

The classification process generated class maps for each level and also maps that represent the probability that a pixel belongs to each class, which is often a more

realistic view as at a pixel scale benthic habitats are rarely homogenous. As this process was hierarchical, the reference signatures used to refine the classification at each successive level were restricted to only those signatures that occured below the previously identified class in the habitat classification scheme.

5.2.3 Validation of image classification

5.2.3.1 Bathyscope validation data

Validation of the classified images was conducted from a boat, using a bathyscope, to record the benthic habitat type at numerous locations within the bounds of the study area. Data were collected at as many locations as possible around Rottnest Island, given the prevailing conditions and navigational hazards such as exposed reefs. A Garmin GPSMap 185 Sounder, fitted with a differential GPS receiver, and a laptop computer were used to monitor the boat's location and log ground validation data. The boat's position was monitored via a real time link between the GPS and ArcView 3.2 using the DNR Garmin extension (Minnesota Department of Natural Resources 2007) and enabled validation points to be recorded with the greatest accuracy possible. For each validation point latitude, longitude, benthic habitat type, time, depth and estimated positional accuracy were stored in an ESRI shapefile format.

Ground validation data were analysed using a method that incorporated the inherent positional uncertainty in both the hyperspectral imagery and the ground validation data. For each validation data point, a polygon, with a radius defined by its estimated positional error (EPE), was used to extract information about the classification of the pixels surrounding the point to assign a mapped class to the each point. If a pixel with

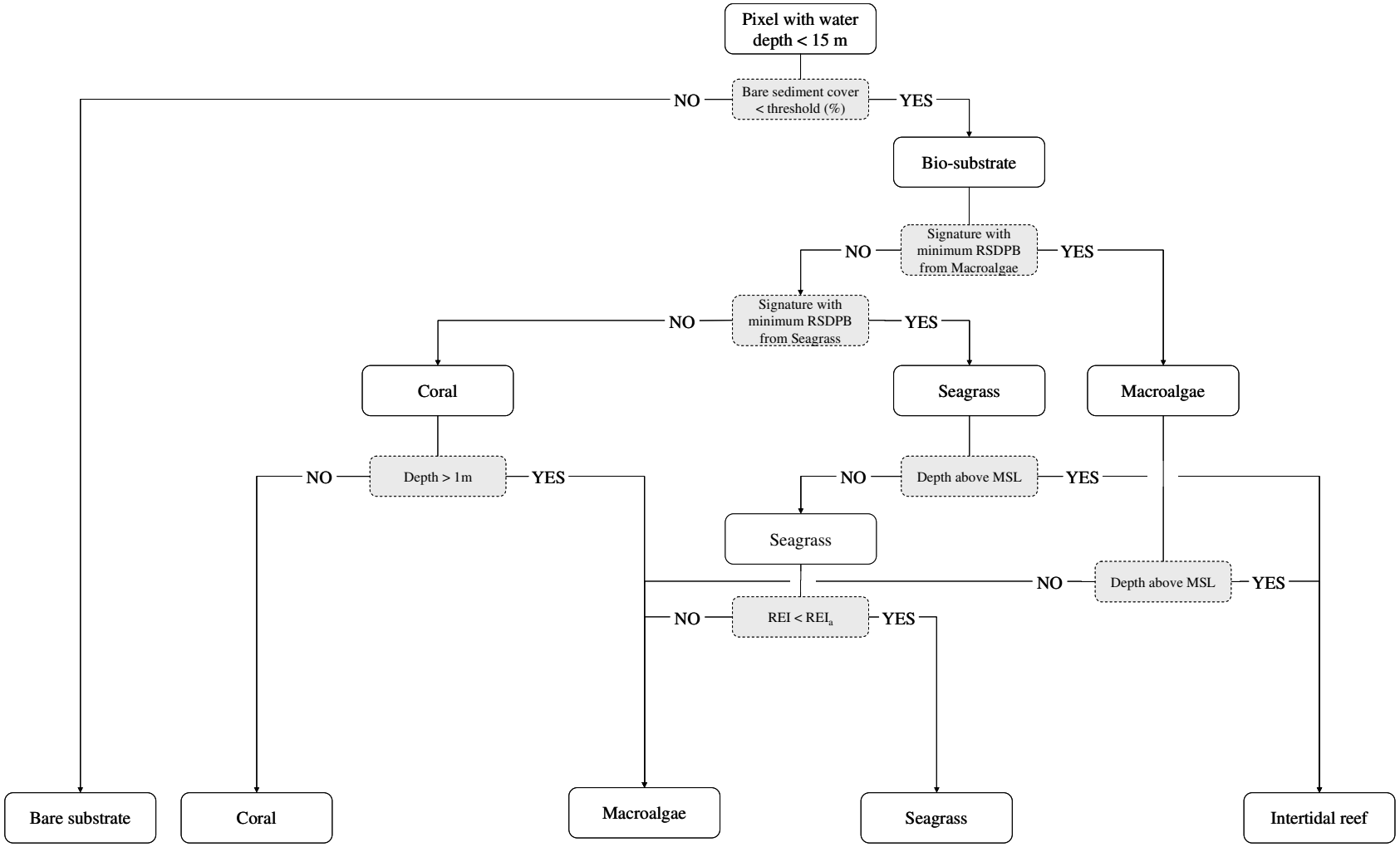

Figure 5-2: Decision tree used to classify the HyMap image data to Level 2 of the classification scheme. RSDPB = relative spectral discriminatory probability, REI = relative exposure index and MSL = mean sea level.

the correct classification was located within the polygon the validation point was identified as a correct classification (i.e. reference class = mapped class), and if not, then the most commonly occurring pixel classification within the polygon was allocated to the mapped class for inclusion in the error matrix (Figure 5-3).

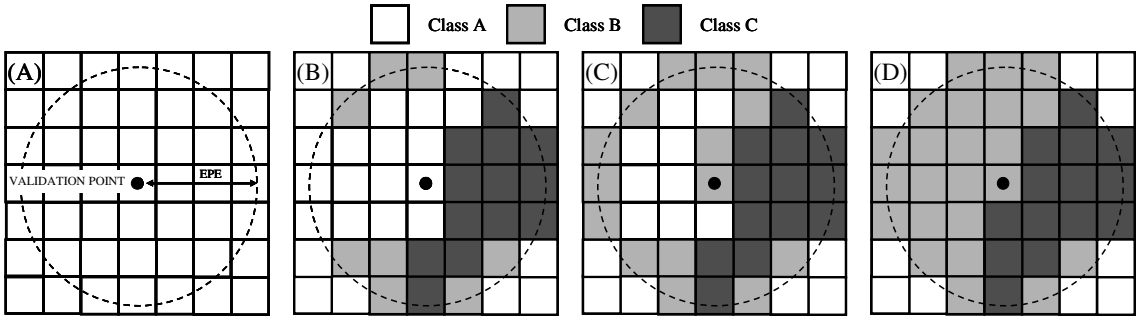

Figure 5-3: Conceptual diagram of a validation point in relation to its estimated positional error (EPE) and the pixels of the classified image being assessed, with the dashed circle indicating the region of pixels being processed (A). For a validation point which is defined as Class A in the validation data, (B) and (C) are examples of a correctly classified region and (D) represents a region validated as Class A, but incorrectly classified as Class B.

These data were summarised into an error matrix and the overall, producer's and user's accuracies were calculated. The *kappa* and *tau* coefficients were also calculated for each error matrix (See Chapter 4 for details). The processing for the accuracy assessment was carried out using custom software developed around the StarSpan pixel extraction tool to extract data from raster images (Rueda *et al.* 2005). The software uses polygon shapefiles, which represent the estimated positional error for each validation point, and the raster grids of the classified images to generate error matrices and calculate the accuracy measures described above.

5.2.3.2 High resolution validation data

Additional high spatial and thematic resolution validation data were collected as part of another study using a digital underwater drop camera system (Wildsmith *et al.* 2008). As these data were collected as part of a larger project there were insufficient data

collected within the RIR for quantitative accuracy assessment of these habitat classifications, however, they can be used to explore localised trends in the classified data to better understand how the classification algorithm performs. An example was presented for two transects carried out in Geordie Bay.

The system consisted of a digital video camera suspended in the water column via an electric winch to control the height above the substrate, an integrated depth sounder, to determine the field of view for the images captured, and a DGPS to obtain geo-location data. The system was controlled by a computer onboard the boat that enabled the operator to capture images as the boat travelled along a transect. The system collected quantitative data about the composition of the benthic substrates in a systematic fashion that mirrored the scale of an image pixel (i.e. 2.5 – 5 m).

The percentage contribution of each benthic substrate type was determined using a point intercept method using points overlaid on each image as a spacing of 0.2 m. The substrate under each point was identified and the percentage contribution for each type was calculated for each image (for a full description of the image capture and analysis system see Wildsmith *et al.* (2008)).

5.3 Results

5.3.1 Data collection pre-processing

The three flight lines of HyMap data processed using the MIP System are given in Figure 5-4. In areas where the water is deepest, the correction is not as effective (highlighted as bright red pixels in the top of flight line two).

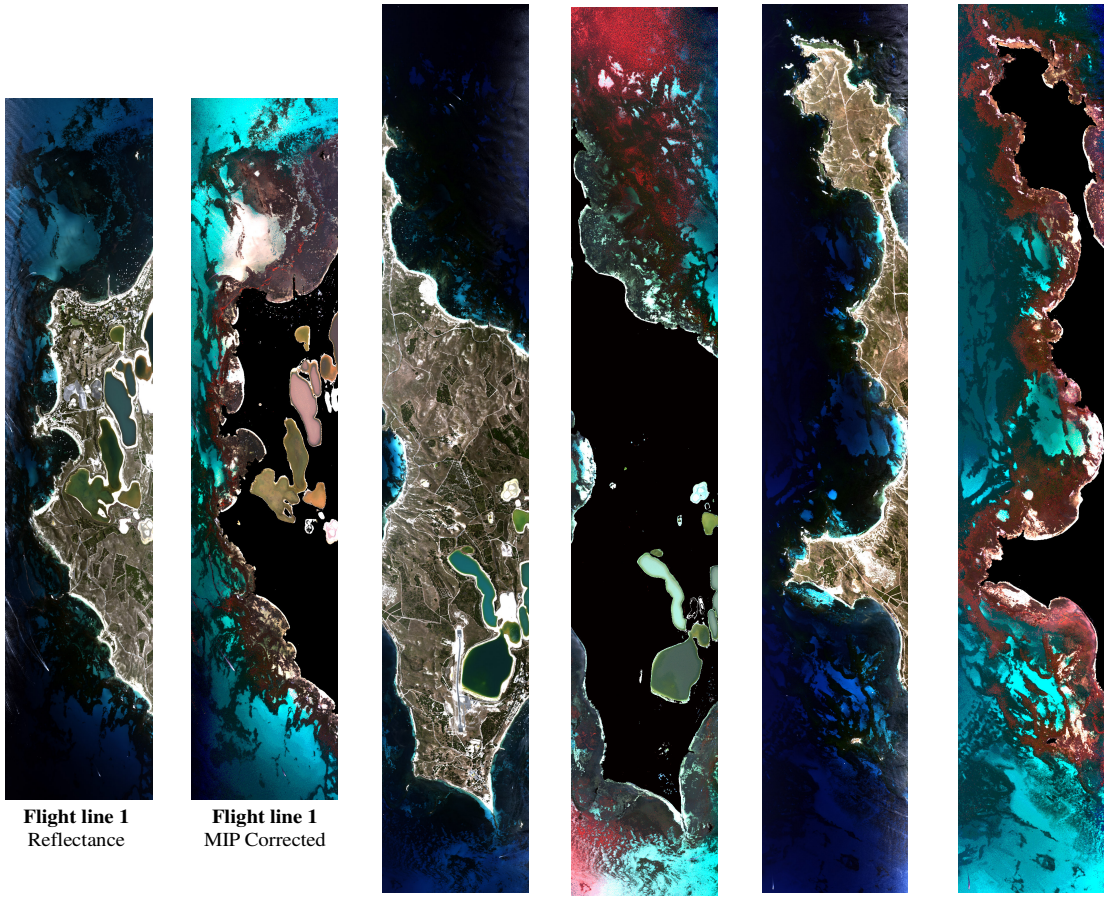

Figure 5-4: Three flight lines of HyMap hyperspectral data for Rottnest Island collected on the 26th April 2004, showing the raw reflectance and the MIP corrected reflectance for each flight line.

5.3.2 Image classification for benthic habitat maps and validation

A total of 727 ground validation points were collected around the Rottnest Island using the bathyscope method (Figure 5-5). These data were collected in depths ranging of 0.4 – 14.1 m, the maximum depth generally limited by the water clarity at the time of collection. Validation data were collected for most habitat components likely to be found at Rottnest Island (Figure 5-6). The spread of samples across most habitat categories was even with the exception of seagrass, which was biased towards *Posidonia*, due to its dominance at Rottnest Island. There is a declining number of total validation points from Level 1 to Level 4 (i.e. n = 727 at Level 1 down to 639 at Level 4) as assigning classes to some validation points become unfeasible beyond a certain level.

Level 1 classification was carried out for all the HyMap data in regions < 15 m depth. The bare sediment data were assessed to determine what percentage of bare sediment per pixel actually represented bare substrate in the field. The ideal threshold for percentage of bare sediment per pixel value was determined to be 40% with an accuracy of 95.0%. Using this threshold resulted in 966 hectares (33.8%) being classified as bare substrate and 1 888 hectares (66.2%) as bio-substrate (Figure 5-7).

The largest areas of bare substrate were found in the north-eastern quadrant of the reserve (53%) (Figure 5-8). The north- and south-western quadrants were dominated by bio-substrate, making up 80% and 88%, respectively. All quadrants, except the north-east, had a greater proportion of bio-substrate compared to bare substrate. Using the 727 ground validation points, the overall accuracy of the classification at Level 1 was calculated to be 95.0% and the *kappa* coefficient was 0.88 (Table 5-2). The *tau*

coefficient was calculated to be 0.88, which means that 88% more pixels were classified correctly than would be expected by chance (Green *et al.* 2000).

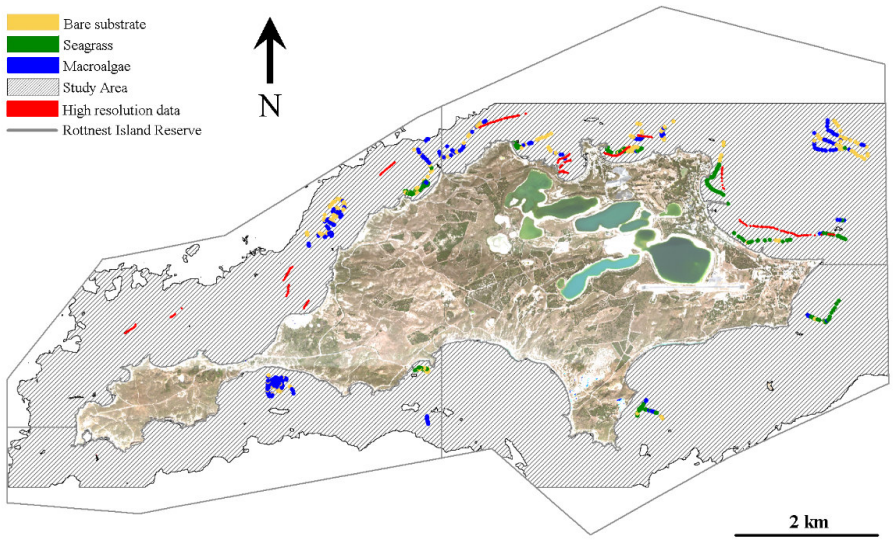

Figure 5-5: Spatial distribution of the 727 ground validation data points collected in Rottnest Island Reserve using the bathyscope method with colour coding representing their Level 2 classification and the high resolution data in red. The extent of the classified HyMap data is shown as the study area.

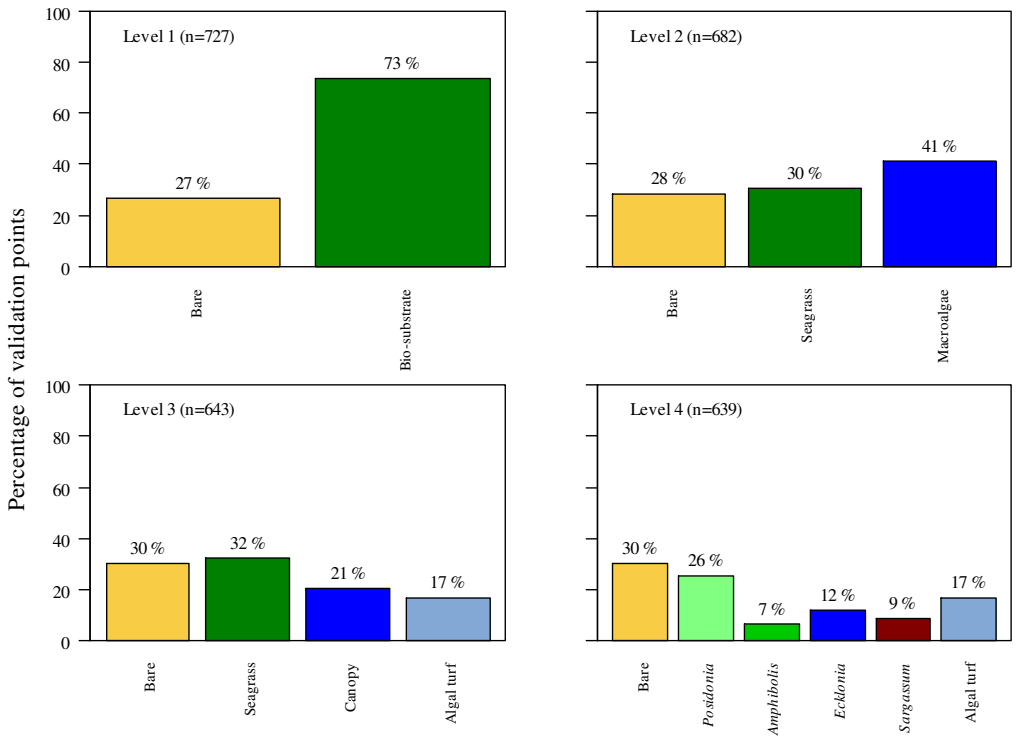

Figure 5-6: Representation of validation points within the habitat classification scheme classes at all levels of the classification scheme.

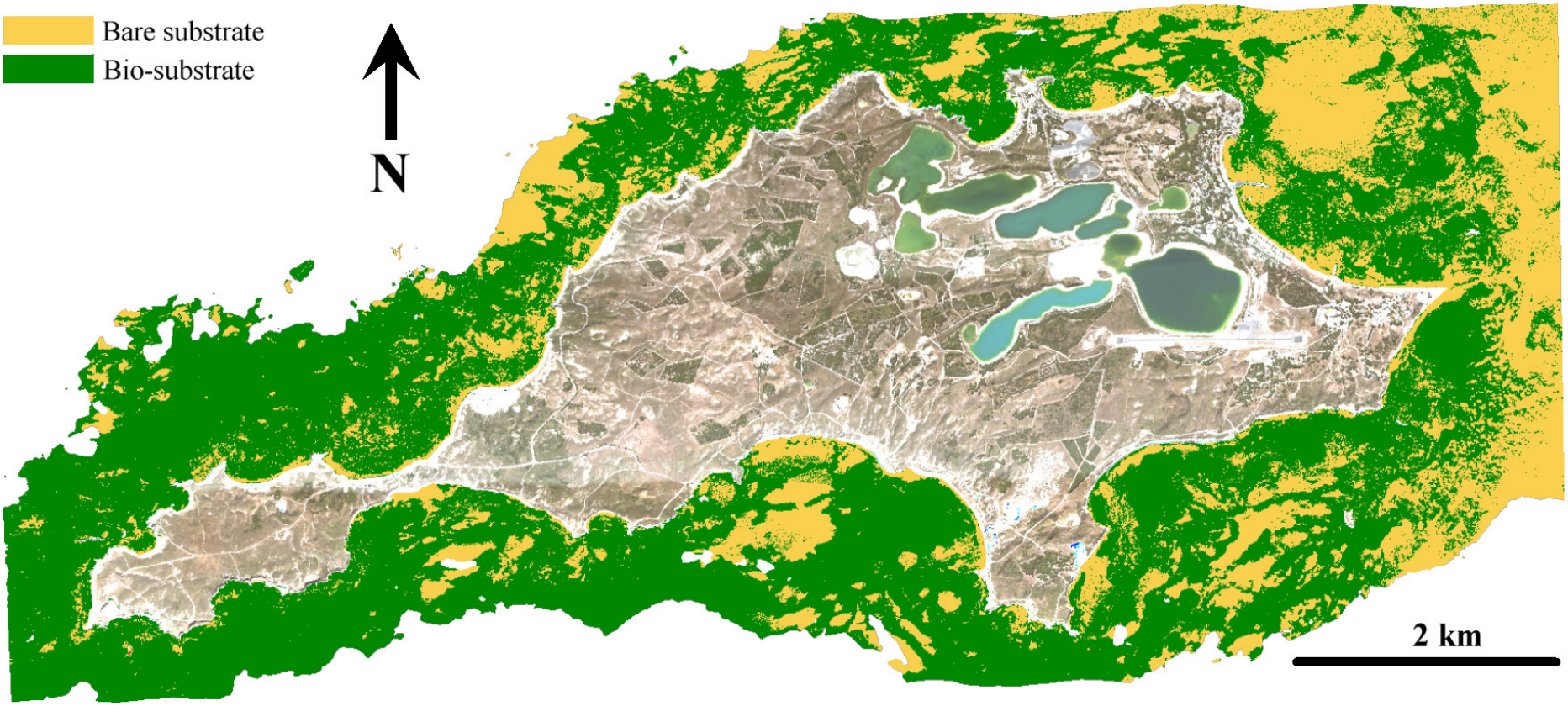

Figure 5-7: Level 1 benthic habitat map for Rottnest Island using the three HyMap flight lines and regions <15 m water depth.

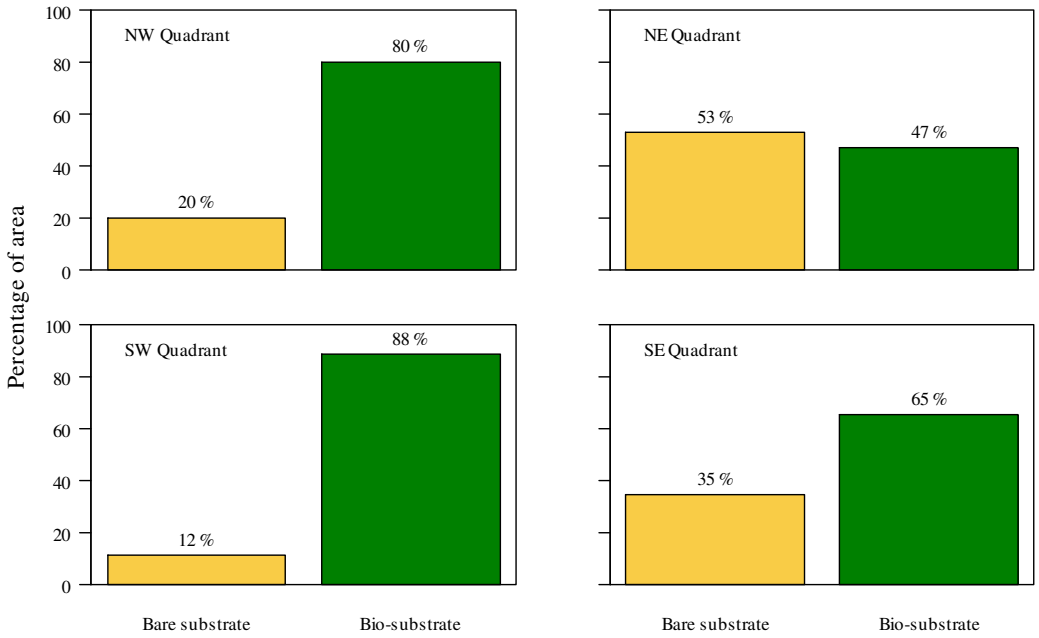

Figure 5-8: The breakdown of the benthic habitats for each quadrant of Rottnest Island at Level 1 of the habitat classification scheme.

Table 5-2: Error matrix for the accuracy assessment of the Level 1 benthic habitat classification at Rottnest Island.

	Reference class		
Mapped class	Bare substrate	Bio-substrate	User's accuracy
Bare substrate	183	26	87.6 %
Bio-substrate	10	508	98.1 %
Producer's accuracy	94.8 %	95.1 %	

The classification to Level 2 was carried out using 224 signatures from the spectral library, in three categories, macroalgae, seagrass and coral, and the spectral angle spectral metric. Initially, based on the optical classification, 40% of the bio-substrate was identified as being dominated by seagrass, 59% as dominated by macroalgae and the remaining 1% as dominated by coral. A second stage classification at Level 2 was carried out separately for each quadrant using the digital bathymetry model (DBM) and the relative exposure index values (see Chapter 3) (Table 5-3; Figure 5-9). These steps includes masking intertidal reef areas as those above mean sea level, seagrass areas redefined as macroalgae if their REI > 0.3 and redefining coral regions as macroalgae if

they were in water > 1m deep. After the second stage classification, 40% of the bio-substrate was identified as being dominated by seagrass, 59% as dominated by macroalgae and the remaining 1% as dominated by coral.

Table 5-3: Summary of the decision rules used for each quadrant in the second stage classification.

Decision rule	Data used	NW	NE	SE	SW
All substrates					
Height above mean sea level	DBM	☑	☑	☑	☑
Seagrass					
Relative exposure Index < REI_a	REI_{annual}	☑ REI_a=0.3	☒	☑ REI_a=0.7	☑ REI_a=0.3
Coral					
Depth > 1m	DBM	☑	☑	☑	☒

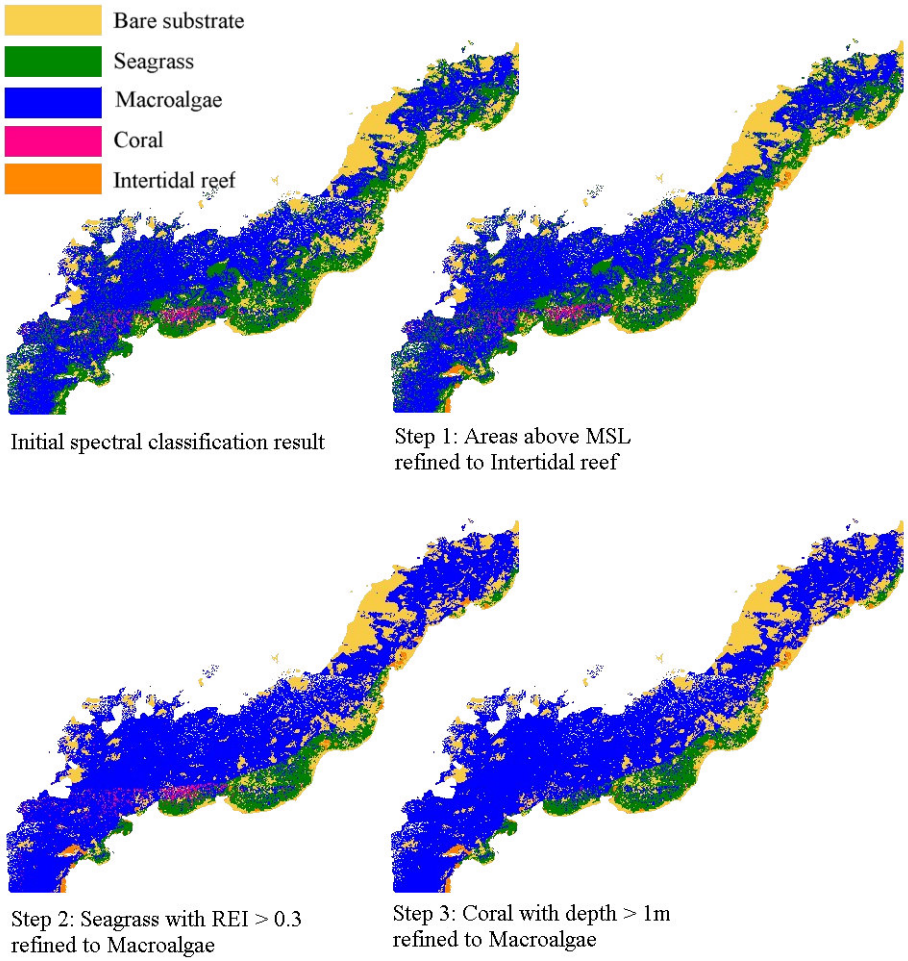

Figure 5-9: The post classification steps used to clean up the habitat classification at Level 2 for the north-west quadrant if the Rottnest Island Reserve.

After the second stage classification, 48 hectares of the bio-substrate were classified as intertidal reef, with the south-west quadrant having the largest area (19 ha) (Figure 5-10). The north-west quadrant had the largest proportion of macroalgae (69%) and only a small proportion of seagrass (9%) (Figure 5-11). The largest areas of seagrass occurred in the north-east quadrant, with 185 hectares and both western quadrants had very little seagrass coverage. A few small regions of coral were also identified, particularly at Parker Point where corals are known to occur. The probability maps, generated as part of the optical classification, that this classification was based on can be found in Appendix 2.

Using 682 validation points the overall accuracy was calculated as 93.3 %, and the greatest user's accuracy was for seagrass at 99.5 % (Table 5-4). The *kappa* coefficient was calculated at 0.90 and the *tau* coefficient indicated that 91% more pixels were classified correctly that would be by chance alone.

Table 5-4: Error matrix for the accuracy assessment of the Level 2 benthic habitat classification at Rottnest Island.

Mapped class	Reference class			
	Bare substrate	Seagrass	Macroalgae	User's accuracy
Bare substrate	183	18	13	85.5 %
Seagrass	1	184	0	99.5 %
Macroalgae	9	5	269	95.1 %
Producer's accuracy	94.8 %	88.9 %	95.4 %	

Although there were some inconsistencies apparent in the flight-line corrections, with a switch from pixels being classified as seagrass in flight-line two to macroalgae in flight line three in the south- east quadrant of the island, the second stage classification was able to correct for much of this (Figure 5-10).

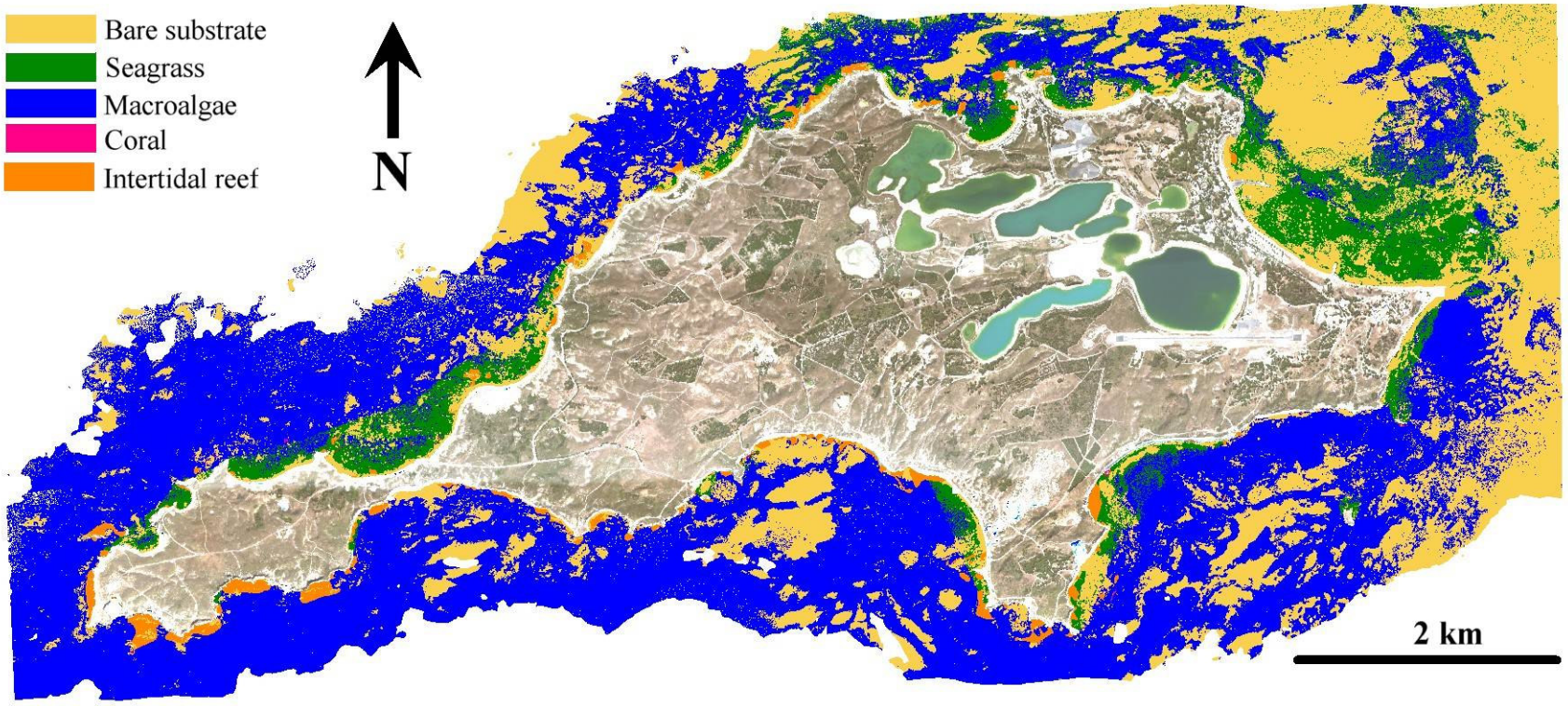

Figure 5-10: Level 2 benthic habitat map for Rottnest Island using three HyMap flight lines and limited to regions < 15m water depth

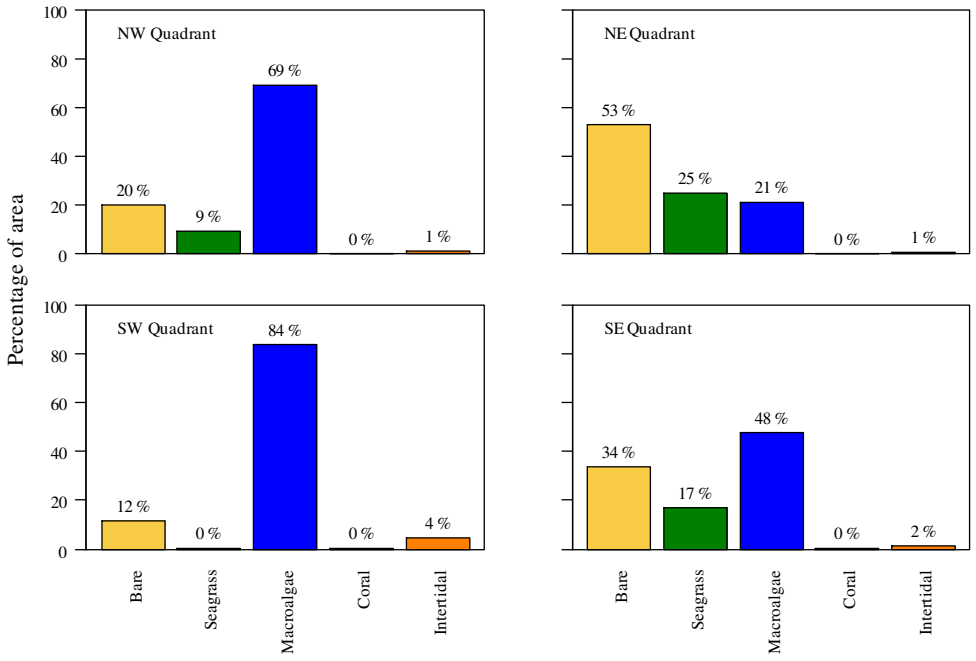

Figure 5-11: The breakdown of the benthic habitats for each quadrant of Rottnest Island, in water <15 m depth, at Level 2 of the habitat classification scheme.

Level 3 of the classification further separated macroalgae habitats into those dominated by canopy forming macroalgae and algal turf. A total of 148 signatures, using image bands 1 – 9 and the spectral angle spectral metric, were used to carry out the classification and resulted in 13.7 % (190 ha) of the macroalgae habitat being identified as canopy algae and 86.3% (1192 ha) identified as algal turf (Figure 5-12). Algal turf habitats were common in all four quadrants, with the greatest proportion in the south-west quadrant (76%) (Figure 5-13). The largest area of algal turf was found in the south-east quadrant (387 ha) and the largest area of canopy in the north-west quadrant.

Using 643 validation points the overall classification accuracy was calculated at 84.0 %, with a *kappa* coefficient of 0.78. The *tau* coefficient indicated that 80 % more pixels were classified correctly than would be expected by chance. The greatest producer's accuracy, excluding bare substrate, was found for the algal turf class (93.5 %) and the highest user's accuracy was for canopy algae (100%) (Table 5-5).

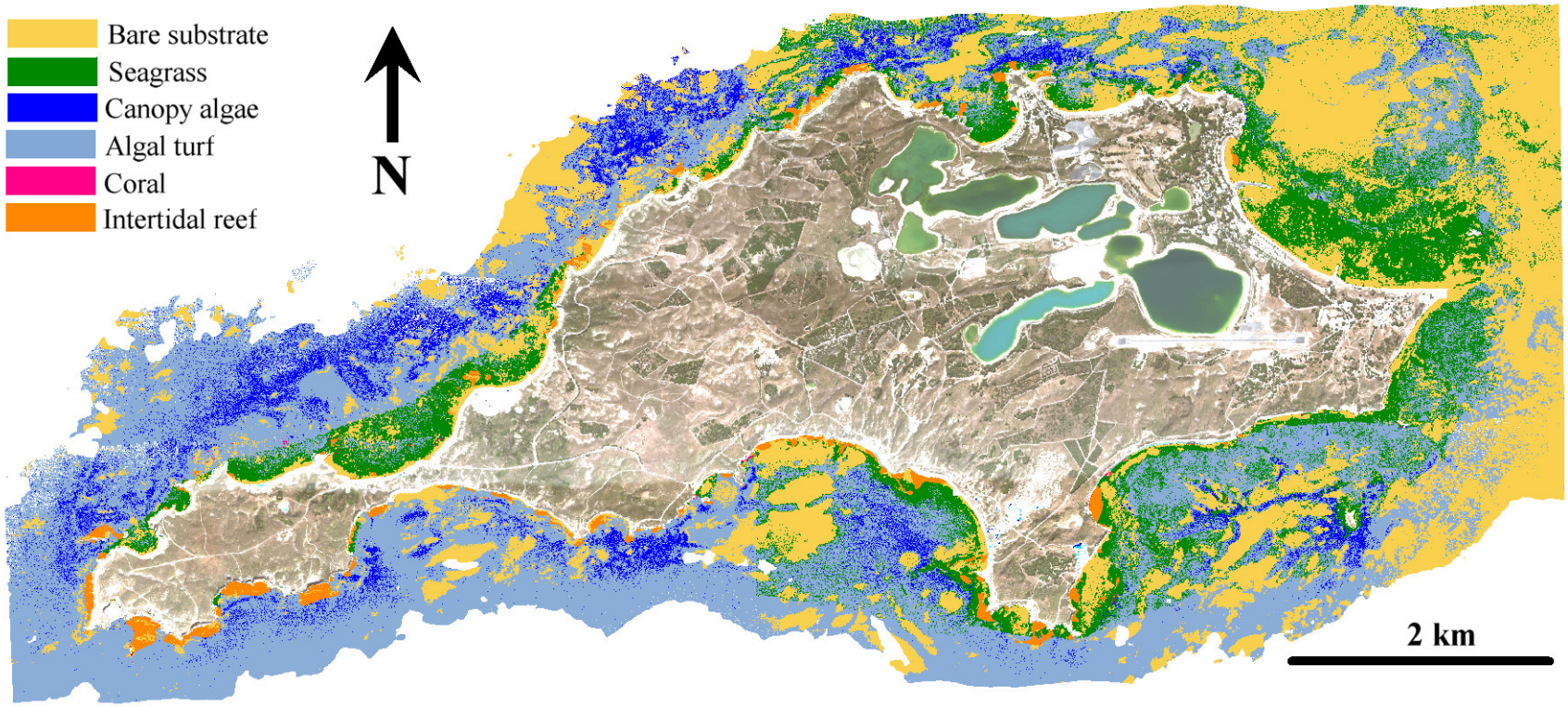

Figure 5-12: Level 3 benthic habitat map for Rottnest Island using three HyMap flight lines and limited to regions < 15m water depth.

At Level 4 of the classification scheme seagrass was identified as being dominated by either *Posidonia* or *Amphibolis* and canopy algae were identified as being dominated by either *Ecklonia* or *Sargassum* (Figure 5-14). *Scytothalia. doryocarpa* was not included as the separability analysis indicated it was very difficult to separate from either *Ecklonia* or *Sargassum*, and did not occur in large homogenous areas at Rottnest (M. Harvey, personal observation).

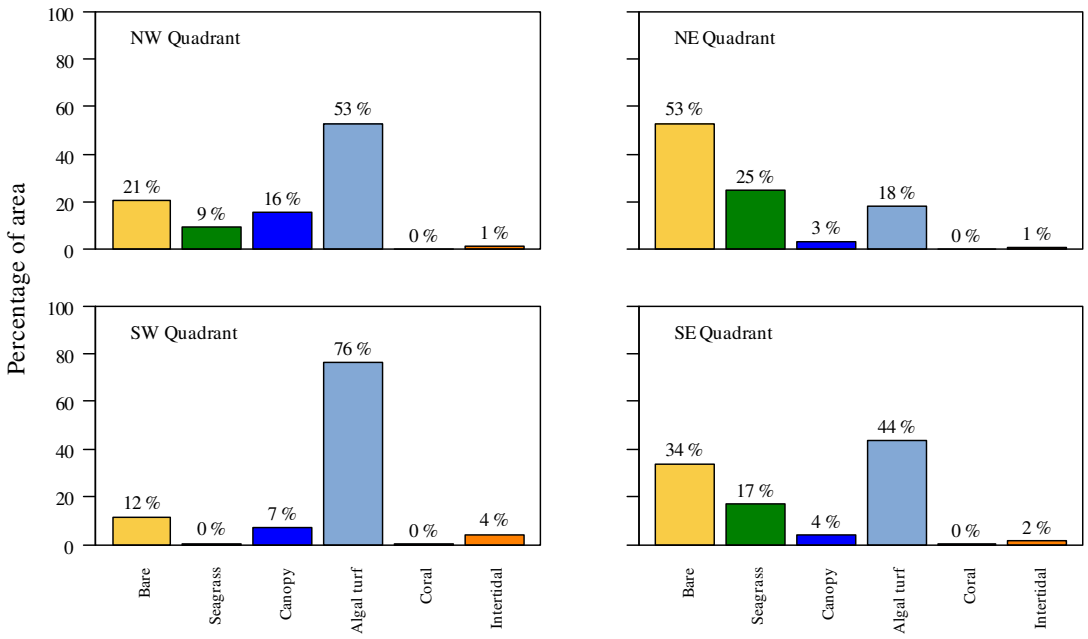

Figure 5-13: The breakdown of the benthic habitats for each quadrant of Rottnest Island at Level 3 of the habitat classification scheme.

Table 5-5: Error matrix for the accuracy assessment of the Level 3 benthic habitat classification at Rottnest Island.

	Reference Class				
Mapped class	Bare substrate	Seagrass	Canopy algae	Algal turf	User's accuracy
Bare substrate	181	21	21	7	78.7 %
Seagrass	2	185	6	0	95.9 %
Canopy algae	0	0	74	0	100.0 %
Turf algae	9	5	32	100	68.5 %
Producer's accuracy	94.3 %	87.7 %	55.6 %	93.5 %	

The classification algorithm determined that 15% of the seagrass identified at Level 2 was dominated by *Posidonia* and 34% was dominated by *Amphibolis*. The remainder of the seagrass was unable to be identified further due to a lack of spectral data in the image (i.e. too few image bands with useable data after water correction). In the three quadrants that seagrass was found to occur, a greater proportion of the pixels were identified as *Posidonia* than *Amphibolis* (Figure 5-15). *Ecklonia* was found to be the dominant in 33% (63 ha) of pixels classified as canopy algae and *Sargassum* in the remaining 127 hectares. The split of canopy algae into the two classes resulted in the classes being relatively evenly mixed spatially. In all four quadrants *Sargassum* was found to cover greater areas than *Ecklonia*, with the greatest proportion in the north-west quadrant (11%) (Figure 5-15).

The overall accuracy for Level 4 was calculated at 70.0%, with a *kappa* coefficient of 0.61. The *tau* coefficient indicated that 63% more pixels were classified correctly than would be expected by chance. The highest producer's accuracy was for *Amphibolis* (88.1%) and highest user's accuracy was for *Ecklonia* (100.0%) (Table 5-6). Both *Ecklonia* and *Sargassum* had low producer's accuracies (19.2% and 20%, respectively), being most commonly confused with the algal turf class.

Table 5-6: Error matrix for the accuracy assessment of the Level 4 benthic habitat classification at Rottnest Island.

	Reference Class						
Mapped class	Bare	*Posidonia*	*Amphibolis*	*Ecklonia*	*Sargassum*	Algal turf	User's accuracy
Bare	181	28	5	18	15	3	72.0 %
Posidonia	1	108	0	0	0	0	99.1 %
Amphibolis	1	5	37	2	4	0	75.5 %
Ecklonia	0	0	0	15	0	0	100.0%
Sargassum	0	0	0	1	11	0	91.8 %
Turf algae	9	23	0	42	25	73	42.4 %
Producer's accuracy	94.3 %	65.9 %	88.1 %	19.2 %	20.0 %	96.1 %	

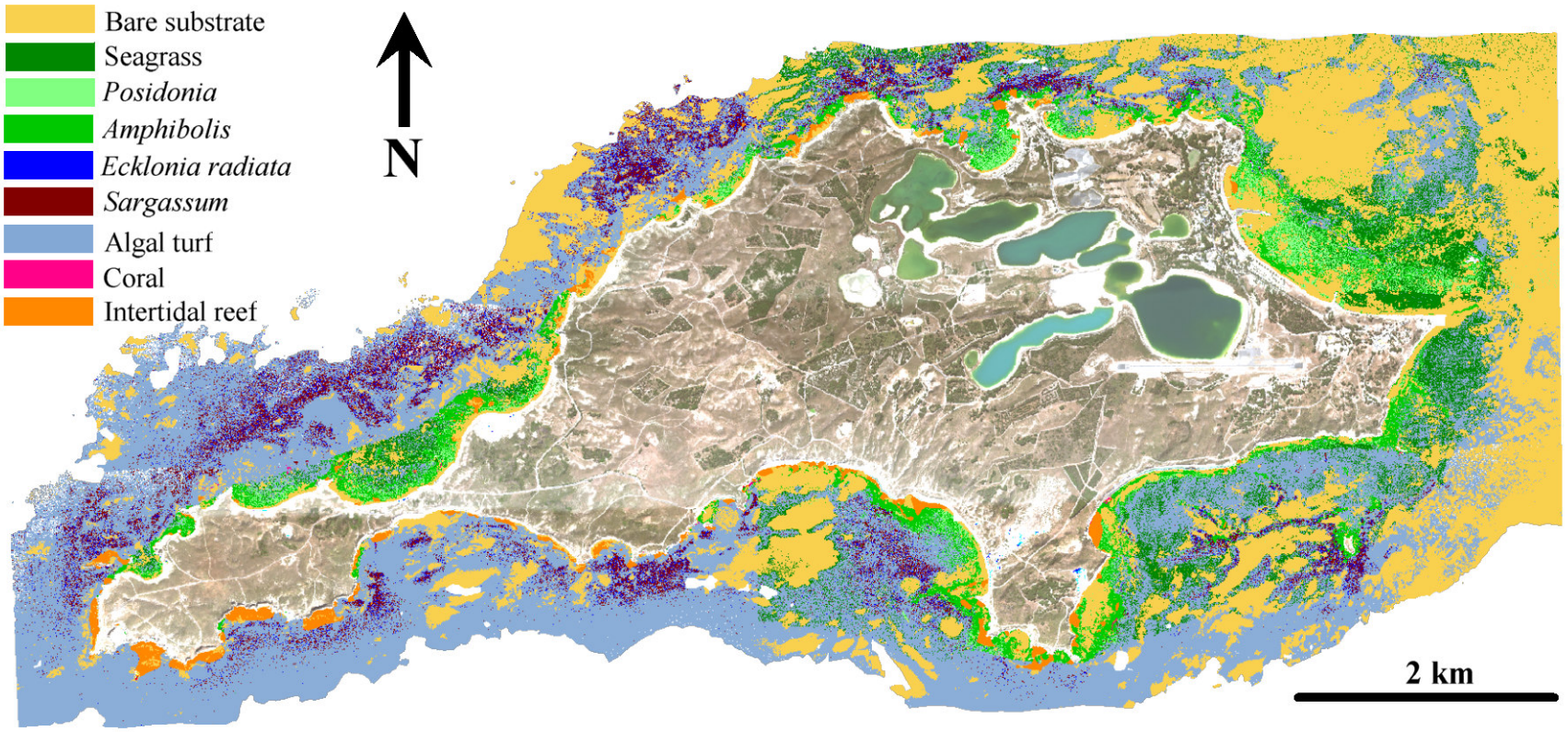

Figure 5-14: Level 4 benthic habitat map for Rottnest Island using three HyMap flight lines and limited to regions < 15m water depth.

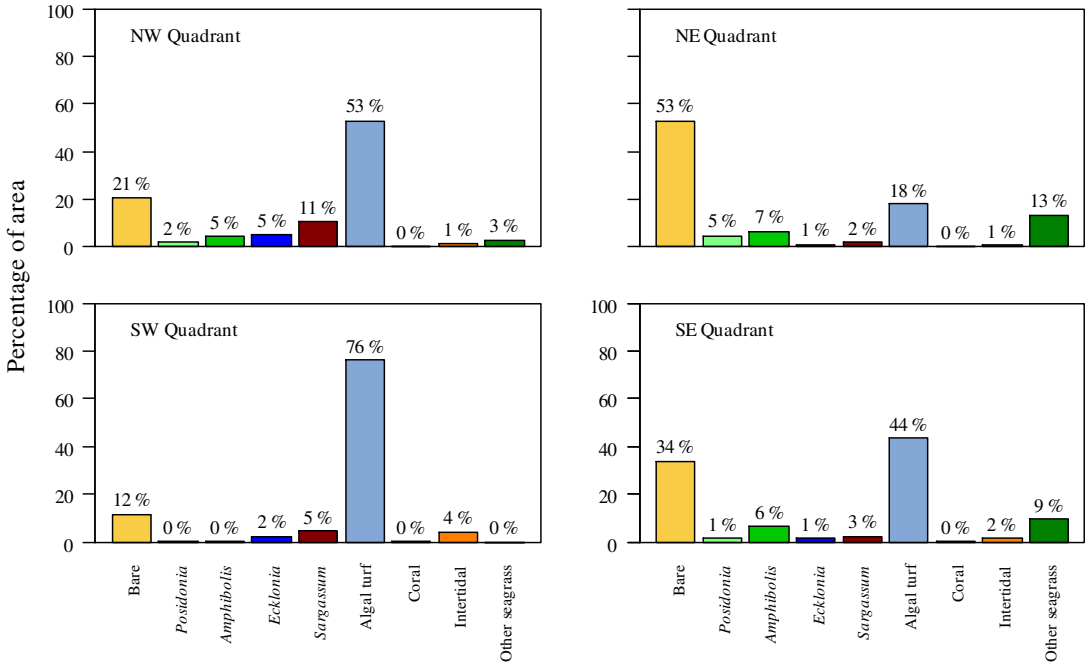

Figure 5-15: The breakdown of the benthic habitats for each quadrant of Rottnest Island at Level 4 of the habitat classification scheme.

A total of 154 high resolution samples were collected over two transects in Geordie Bay using the underwater drop camera system. These high resolution validation data showed the trend in the percentage contribution of the dominant habitats components and how the classification algorithm responded to these changes (Figure 5-16). For example, although bare substrate was present in many of the validation points, there were only a few pixels with sufficient coverage to be classified as bare substrate. Other examples are at Level 2, where seagrass was present, but only where it attains 100% was it classified as seagrass in the image. These data also highlighted some of the confusion between seagrass and macroalgae, particularly algal turf, in some pixels, most likely due to high epiphyte loads on the seagrass leaves.

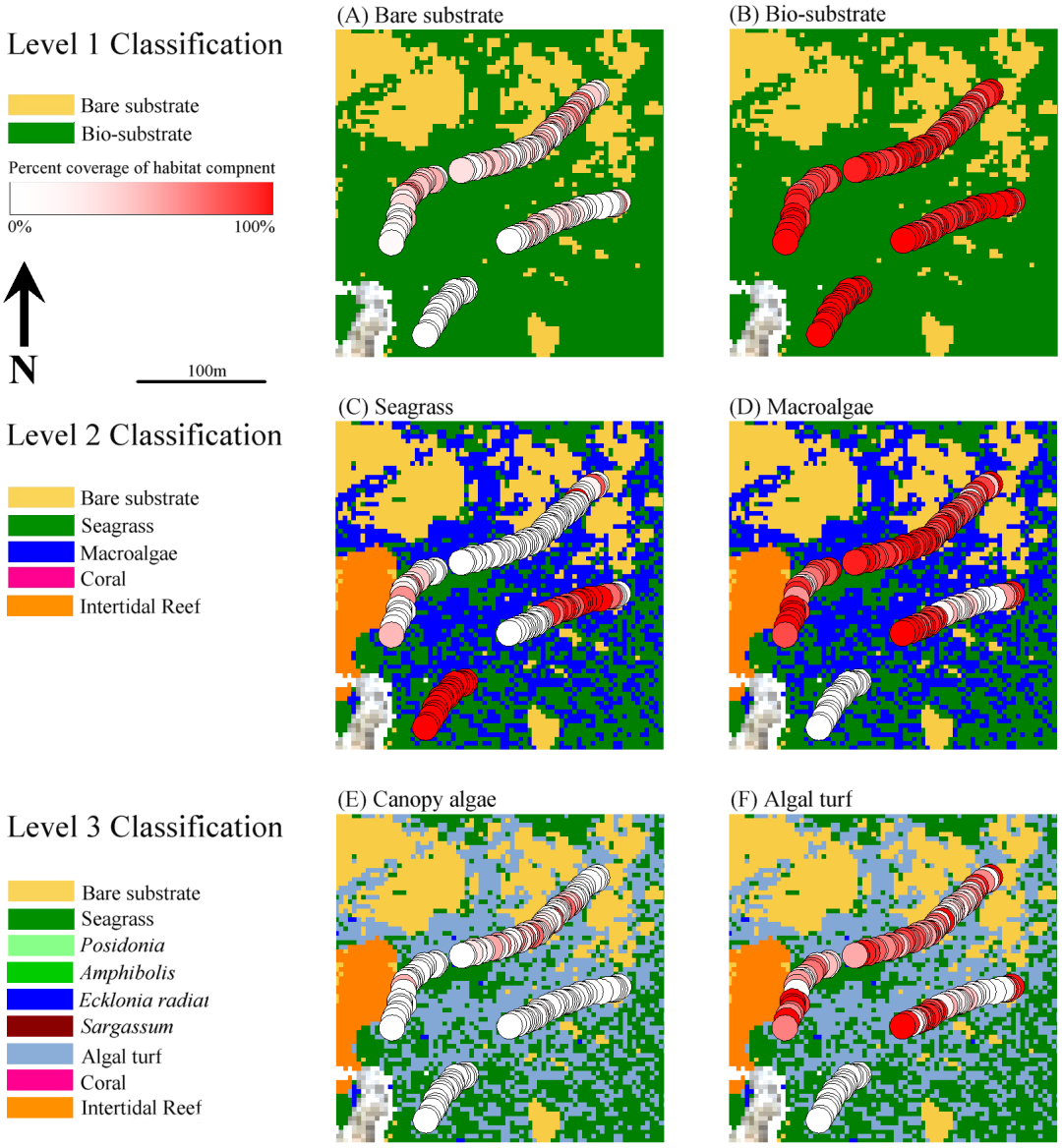

Figure 5-16: Examples of the percent coverage from the high resolution drop camera validation data for two transects (154 samples) collected in Geordie Bay. Bare substrate (A) and bio-substrate (B) overlayed on the Level 1 classification, seagrass (C) and macroalgae (D) overlayed on the Level 2 classification and canopy algae (E) and algal turf (F) overlayed on the Level 3 classification. The percent coverage ranges from zero to 100%

5.4 Discussion

This study is one of the first to map the spatial distribution of temperate marine benthic habitats using hyperspectral imagery in combination with an extensive spectral signature library of the dominant habitat components found in the region. The habitats were defined based on the presence of some habitat components to a genus level, such

as *Posidonia* and *Amphibolis*, which yielded accuracies exceeding 60%. Although the accuracy of the maps decreased as habitat components were identified to a higher level in the habitat classification scheme (i.e. from a general seagrass class to the genus *Posidonia*) the maps provided clear information about the spatial distribution and patch structure of the dominant marine benthic habitats. The results clearly show the differences in the benthic habitats around the island, from the bare substrate and seagrass dominated habitats on the north-east side of the island, to the more complex macroalgae dominated habitats at the more exposed western end. These patterns reflect the abiotic environmental variables, such as slope, benthic complexity and exposure, determined for Rottnest Island (Chapter 3), which made the use of the second stage classification possible.

A key requirement of this approach is the use of an appropriate water correction algorithm to correct the bottom reflectance signatures for the influence of the atmosphere and the overlying water column. The use of the Modular Inversion and Processing system (MIP) to carry out the water correction process has previously been shown to allow for accurate identification of the underlying substrates (Heege *et al.* 2004) and proved to be an appropriate and efficient means of processing the HyMap data prior to the classification of the benthic substrates at Rottnest Island. MIP requires minimal external inputs for the correction process and provides, as outputs, both an accurate spatial representation of the distribution of bare substrates and realistic bottom reflectance signatures. In addition, MIP also takes a realistic approach to determining if a corrected image band (i.e. data at a specific wavelength) contains useable data as a result of the correction process and outputs this information on a pixel by pixel basis, allowing for the classification algorithm to be trained to use only the available image

data. This has the benefit of allowing the classification algorithm to utilise the maximum available data for each pixel, and thus achieve the most accurate result possible.

Some issues were identified with the MIP corrections and benthic habitat classification at the boundaries of the individual flight lines, and in separating some habitat components within the image data. One of the most probable reasons for this relates to the generic signatures used as part of the MIP correction to remove the water column effects. Very general signatures, extracted from the image, were used to correct the HyMap data to test the robustness of the MIP algorithm in situations where very little *in situ* data existed. It is anticipated that with fine tuning of the MIP algorithms, using spectral signatures from the library, a more consistent and accurate result could be achieved as it should provide a clearer distinction between the key benthic habitats, particularly seagrass, canopy and turf algae. Testing of the classification algorithm using synthetic signatures indicated that in many cases it was likely that canopy algae would be misclassified as turf, a result reflected in the habitat maps. This can be attributed to both the error of classification, but also the way in which canopy and algal turf co-exist in the natural environment with algal turf generally found under canopy algae species. There was also an obvious misclassification of seagrass on very exposed sites on the west end of the island, which are more likely to be intertidal reefs or macroalgae dominated habitats which are often covered in green algae such as *Ulva* or. *Enteromorpha* species. These regions were corrected using a combination of contextual editing and a decision rule approach to separate out the intertidal platforms based on the depth. Although the actual sounding data used to create the digital bathymetry model (Chapter 3) were extremely sparse around most of the intertidal platforms, they still

provided sufficient detail to delineate the presence of the platforms in some regions. It should be noted here that these inadequacies in the bathymetry could potentially be overcome using MIP derived bathymetry. The relative exposure values generated in Chapter 3 were also used to assist with the correction of pixels misclassified as seagrass in the three most exposed quadrants of the island. This approach was a form of contextual editing as there were insufficient validation data in all quadrants to develop a statistical model of the most appropriate threshold values of the REI. There is also the potential to incorporate swell modelling into the exposure index and assess it on a seasonal or monthly basis to facilitate the development of a better model for the wave exposure experienced at each pixel in the data.

The benefit of the hierarchical approach taken in this study is the ability to utilise the most appropriate classification techniques to classify pixels into classes at each level of the classification scheme. This meant that specialised techniques could be developed to identify pixels at each level, based primarily on the results of spectral separation analysis of pure endmember spectra collected *in situ*. For example, the separation of pixels dominated by bio-substrate and those dominated by bare substrate was best achieved using the outputs generated by MIP as part of the water correction process. Masking these pixels from further analysis meant that the classification algorithm could focus on the remaining bio-substrate dominated pixels by only using signatures likely to be dominant in each pixel (e.g. seagrass) and, exclude those with a low probability of dominating the spectral signature of a pixel (e.g. sand). The hierarchical structure of the classification process had the added benefit of mimicking the natural patterns that exist in the benthic habitats at Rottnest Island, rather that assigning pixels to completely subjective classes that often occurs when using other classification methods, such as

unsupervised clustering techniques based solely on pixel similarity (Duda and Canty 2002).

The accuracy of 93% for the benthic habitat map at Level 2 (the differentiation between bare substrate, seagrass and macroalgae dominated habitats) compares favourably with those obtained in a study by Mumby and Edwards (2002) who achieved overall accuracies of 68% using the IKONOS satellite data collected at 4 m pixel resolution and 89% using CASI airborne multi-spectral data collected at a 1 m pixel resolution. These accuracies were for their coarse habitat maps that differentiated between coral, seagrass, macroalgae and sand, which relates to Level 2 in this study. Due to its limited distribution at Rottnest Island, coral was not included in the validation data. The producer's and user's accuracies for bare substrate of 94.82% and 88.83% respectively, compared favourably with those of Bertels *et al*. (2008) who achieved 93% and 81%, respectively, when classifying CASI hyperspectral data for a coral reef atoll in Indonesia. The accuracy result in this study indicated that the maps provide a good representation of the spatial distribution of the benthic habitats at Rottnest Island and also potential for improved results if the MIP corrections were further fine-tuned using *in situ* data.

The accuracy of the benthic habitat classifications were assessed in this study using a method that attempted to take into account the inherent spatial inaccuracy of the geo-location of both the image and the validation data collected in the field. This method is able to account for the spatial uncertainty when assessing the classification at the broad classes (i.e. Levels 1 and 2) in the classification scheme where the pixels tended to occur in patches. However, when attempting to assess the classification results at finer

class (e.g. Level 4), where the benthic habitat may vary from pixel to pixel, it becomes increasingly difficult to be certain that the point being assessed, is being matched to the correct location in the image. Every attempt was made to minimise the impact of this problem by taking into account the positional error of the validation data on a point by point basis, which enabled advantage to be taken of those data with greater accuracy and thus minimise the chances of errors in the accuracy assessment process. The high resolution validation data collected using the drop camera system could be used to overcome many of these issues if it were collected in such a way as to cover representative areas around Rottnest Island. Another issue that became apparent during the assessment of the classification results was the need, whenever possible, to collect validation data that spans as much of the image as possible, and in particular to ensure validation data are collected for each flight line. This is especially relevant in cases, such as this study, where new classification algorithms are being developed, as validation data is the only way to test the accuracy of the results with real image data.

In comparison to the existing habitat map for Rottnest Island produced as part of the Perth Coastal Waters Study (PCWS) (Ong *et al.* 1998) the new habitat maps at the various levels provide a marked increase in the resolution, both spatially and taxonomically, of the visual representation of the benthic habitats. Just using the Level 2 habitat map generated in this project, it is clear that although the broad-scale patterns in the habitat distribution are similar, there is significantly more detail recorded about the spatial structure of the habitats, (see Figure 2-2 and Figure 5-10). Although due to geo-location issues, direct comparison in not possible, the PCWS map had 26% bare substrate compared to 32% in the new habitat maps. In the PCWS map, seagrass and macroalgae covered 19% and 43%, respectively compared to 15% and 51% in the new

maps. The biggest difference was in intertidal reef which was 12% in the PCWS map and only 2% of the area in the current maps, most likely due to the decision rule used to define intertidal areas in the current map as being above the mean sea level as defined by the bathymetry. In contrast, the PCWS map defined intertidal area as areas close to mean sea level. Many of the other differences can be explained by the better spatial representation of the benthic habitats in the current habitat maps could also represent some real change in the distribution of the habitats.

This study is one the first to map the spatial distribution of marine benthic habitats using hyperspectral imagery in combination with an extensive spectral signature library of the dominant habitat components found in the region. This is a significant step towards being able to map marine benthic habits over large areas at a finer scale in terms of the habitats components which are able to be identified in the imagery. However, there is still considerable scope for continuing research into the integration of the hyperspectral image capture, processing, classification and accuracy assessment for the mapping of marine benthic habitats. Added to this there is need for research to be carried out into the interpretation and presentation of habitat maps in terms of their intended audiences. For example, an ecologist attempting to model the distribution of a particular species will require different spatial information than a manager or planner of a marine reserve.

6 Examples of management applications of the benthic habitat maps for Rottnest Island

6.1 Introduction

Marine benthic habitat maps are often produced using remote sensing techniques and use a pre-defined set of thematic classes to describe the spatial distribution of different habitat types. The usefulness of these maps to different marine conservation, planning and reporting applications depends on a range of factors including the spatial resolution, the thematic classes used and the overall accuracy of the map (Kirkman 1996). If these factors are taken into account, and the methods used to integrate these data with the different scenarios are appropriate, then habitat maps can provide answers to many planning and conservation questions at a range of scales (Cendrero 1989). The remote sensing approach to benthic habitat mapping is also one of the most cost-effective methods available when large geographic areas need to be covered or regular temporal data need to be collected (Mumby *et al.* 1999).

Marine benthic habitat maps have long been recognised as useful for marine conservation planning, especially with the increasing interest, and use of, systematic conservation planning (Margules and Pressey 2000, Meir *et al.* 2004, Stevens and Connolly 2004). A key factor in many marine conservation planning applications is to achieve representativeness with respect to the biodiversity present in the region being protected (Margules and Pressey 2000). As biodiversity can be difficult to quantify spatially in the marine environment, surrogates for biodiversity are often used and benthic habitats have been shown to be good surrogates for overall marine biodiversity (Ward *et al.* 1999, Rodrigues and Brooks 2007). To this end, accurate and up to date, benthic habitat maps can play a key role in the selection and location of marine

protected areas. An example of this is the re-zoning of the Great Barrier Reef in 2004, which was achieved using a systematic approach based on outputs of MARXAN, and resulted in a network of no-take areas that made up 33% of the overall area of the marine park (Fernandes *et al.* 2005).

The strong links between benthic habitats and associated assemblages of fish and invertebrates that have been established in both temperate and tropical waters provide a sound basis for the modelling of potential distribution of species based on their habitat preferences (Jenkins and Wheatley 1998, Friedlander 2001, O'Hara 2001, Curley *et al.* 2002, Harman *et al.* 2003). An example of this is the spatial modelling of the habitat suitability for a number of commercially important fish species in Port Phillip Bay, Victoria (Morris and Ball 2006). They used catch data from commercial fisheries and environmental variables including substrate type and depth to determine habitat suitability. Such modelling can be invaluable to fisheries managers when attempting to implement spatially oriented management actions, such as closures or when implementing marine protected areas designed to protect particular marine species. Mellin *et al.* (2007) determined that a strong relationship existed between the species richness and abundance of juvenile fishes on a reef in New Caledonia and environmental variables including depth, percentage cover of biotic and abiotic substrate, habitat heterogeneity and rugosity, mapped using remote sensing techniques. Beger and Possingham (2008) modelled the broad scale distribution of coral reef fishes at Kimbe Bay, Papa New Guinea using environmental data and concluded that such approaches may be able to assist with the design of marine reserves. Other studies have found relationships between habitats and fish assemblages in the southern Mexican Caribbean (Nunez-Lara and Arias-Gonzalez 1998) and Davies Reef, Australia (Arias-

Gonzalez *et al.* 2006). At a broader scale, Grober-Dunsmore *et al.* (2007, 2008) determined that landscape-scale metrics of habitat structure, such as habitat patch connectivity for coral reefs, could be used for surrogates for species diversity and abundance of coral reef fishes. These relationships can also provide invaluable data to other marine planning and management applications such as construction of ports or planning for remediation of potential pollution events.

Remotely-sensed habitat maps, and associated data, can often play a key role in the planning for marine infrastructure and operations, such as ports and harbours, in order to minimise potential marine impacts during construction and operation of the facility (Kirkman 1996). There are many issues associated with marine transport and infrastructure including, planning for and monitoring of dredging activities, pollution events and management of boat mooring activities, including their placement and maintenance. High resolution benthic habitat maps derived from hyperspectral imagery can provide data to assist with the planning for many of these activities and setting up suitable monitoring programs to asses their long-term impacts.

Pollution or contamination in the marine environment can take four main forms, namely physical (e.g. debris, suspended sediments), chemical (e.g. toxic compounds such as tributyltin and oil spills), biological (e.g. pathogens) and thermal (e.g. cooling water) (Clarke 1993). These contaminations can have significant effects on the overall health of the marine ecosystems. The role of remote sensing in the management of marine pollution can be summarised as detection, tracking and damage assessment following a pollution event (Clarke 1993). Habitat maps play a role in determining baseline conditions for the environment and monitoring the effects of pollution events. The

monitoring of the spatial extent and characteristics of sediment plumes from dredging can be routinely carried out using remote sensing techniques and related back to baseline habitat maps to assess the potential impacts. The effects of chemical pollutants such as oil spills, can be assessed in a similar manner once the extent of the spill is known, through remote sensing analysis of an existing spill or predictive spatial modelling of potential oil spills. The same is true for biological pollutants, such as sewage outfalls, or thermal pollution, such as hot water from power station cooling towers or desalinisation plants.

In any coastal port or marina that has a boat refuelling facility, such as the Rottnest Island fuel jetty in Thomson Bay, there is always the inherent risk of a hydrocarbon spill, typically in the form of either petrol or diesel. Although the majority of oil from most spills is either washed up on beaches or evaporates, there is a proportion that can affect the subtidal benthic habitats under certain environmental conditions (Lee and Page 1997). Oil can have long lasting effects on the environment, an example being the Exxon Valdez spill in 1989, where hydrocarbons remain present in intertidal beaches and continue to have a negative impact on the wildlife many years after the incident (Peterson *et al.* 2003). Given this, it would be useful to have information about the spatial extent that a potential oil spill may occupy under particular weather conditions and from this determine which benthic habitats may possibly be affected (Jordi *et al.* 2006). This information could assist marine planners and managers with the placement of refuelling facilities at the planning stage, especially in fragile marine environments, and for implementation of oil spill response plans.

The often negative impacts of anchoring and moorings on the marine environment has long been accepted. This issue is of particular concern at Rottnest Island where a study by Hastings *et al*. (1995) found that there was significant loss of seagrass due to mooring damage. Rottnest Island Authority has indicated its intent to investigate the feasibility of providing fixed moorings for commercial charter operators (Rottnest Island Authority 2003), which would require the placement of these moorings in an environmentally friendly manner. This would greatly benefit from some broad scale analysis of mooring placement using benthic habitats maps, such as those generated as part of this study.

Another major application for benthic habitat maps, from those that cover large geographic areas at a coarse resolution to those, such as this study, that cover a smaller geographic area at a much finer scale, is environmental reporting. The most recent State of the Environment report for Western Australia, released in 2007, found that, for the majority of the Western Australian coastline, no baseline on benthic habitats exists. Following from this was the recommendation to 'Establish a baseline of condition of the marine environment and develop a consistent monitoring network in the priority areas' (Environmental Protection Authority 2007). Remotely-sensed habitat maps provide ideal baseline data sets for shallow marine environments and allow for the development of monitoring strategies for future state of the environment reporting.

Four separate planning and management applications which utilise benthic habitat maps are demonstrated in this chapter. The first, a conservation planning example, acertains the changes in the extent of benthic habitats protected when the new expanded sanctuary zones were implemented in Rottnest Island Reserve in July 2007. The second

models the potential home range of *Panulirus cygnus* occupying reefs within Kingston Reef sanctuary zone at Rottnest Island. The density of lobsters on the reefs inside and outside Kingston Sanctuary zone was also modelled. The third runs a basic oil spill model, using NOAA's GNOME oil spill modelling environment (Beegle-Krause 2001), to track a small spill in Geordie Bay at Rottnest Island and assess which habitats may be affected. The final application aims to determine suitable sites for boat moorings at popular recreational dive sites within Rottnest Island Reserve, by spatially modelling site suitability for the environmentally sound placement of permanent moorings.

6.2 Methods

The series of case studies developed to demonstrate possible application of benthic habitat maps to conservation, planning and management within the RIR were limited to the spatial extent of the reserve, and within that, the extent of the benthic habitat maps based on the three flight lines of HyMap hyperspectral data (Figure 6-1).

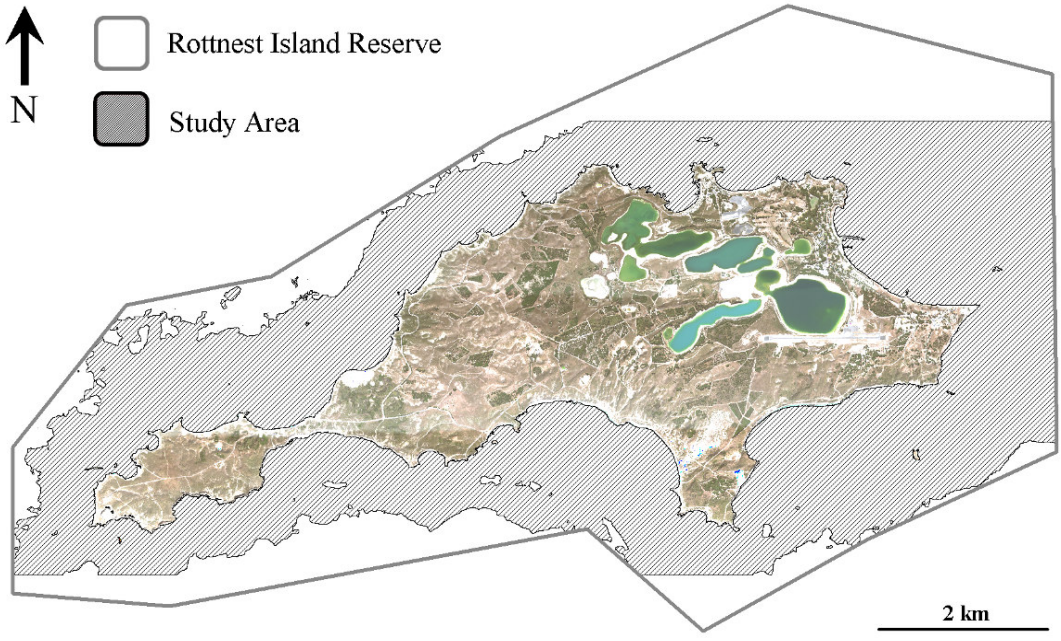

Figure 6-1: The study area for all the management application examples for Rottnest Island Reserve.

6.2.1 Ascertaining the extent of shallow benthic habitats protected by new sanctuary zones implemented in July 2007

The area of different benthic habitats protected within sanctuary zones in the Rottnest Island Reserve was determined for the sanctuary zones in place prior to 1st July 2007 and those implemented thereafter (Figure 6-2). The spatial extent of the benthic habitats was determined using Level 2 of the habitat classification scheme. The sanctuary zones at Kingston Reef and Parker Point were analysed in more detail as they were expanded as part of the new zoning plan. It should be noted that calculations of area made for these analyses were based on raster pixels at a resolution of 3.5m x 3.5m or in increments of 12.25m^2 and resulting estimates are often less accurate than those calculated using vector polygon data.

6.2.2 Modelling the potential home range and population size of the Western Rock Lobster, *Panulirus cygnus*, on reefs in the Rottnest Island Reserve

The potential home range for the Western Rock Lobster (*Panulirus cygnus*) occupying the three study reefs in the Kingston Reef sanctuary zone was determined by spatially modelling the nocturnal foraging distances of the lobsters as determined by Jernakoff *et al*. (1987). Using results of a study by Babcock *et al.* (2007) on the effects of the Kingston Reef sanctuary zone on the lobster population occupying reefs in and outside the sanctuary zones, the potential lobster population was also modelled for the same three reefs, and for a reef outside the sanctuary zone. The study was carried out on the north-eastern side of Rottnest Island, using three reefs located inside, and one reef outside, the Kingston Reef sanctuary zone (Figure 6-3). These reefs where chose due to their relatively simple structure and central location within the sanctuary zone.

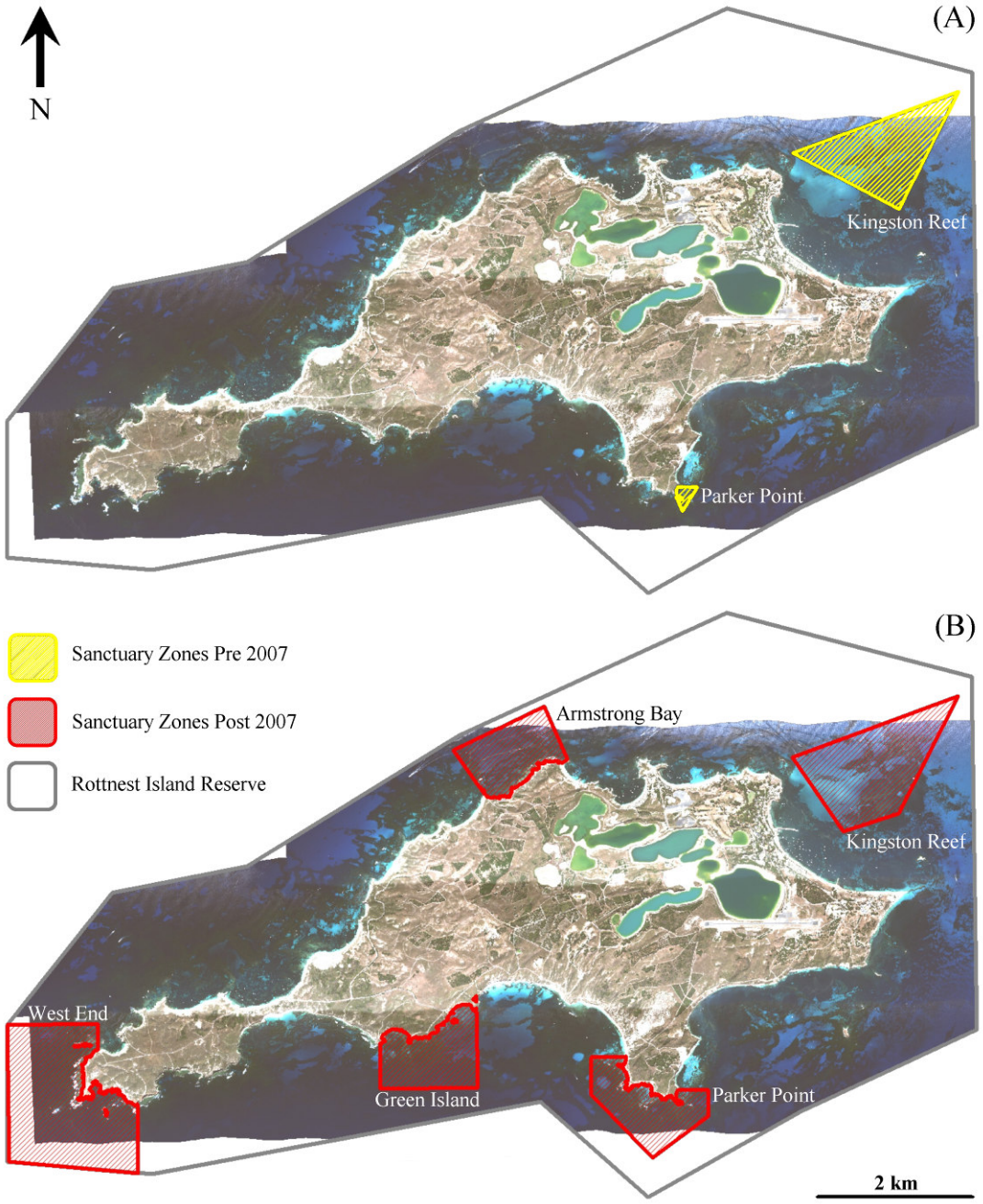

Figure 6-2: The sanctuary zones in Rottnest Island Reserve pre 2007 (a) and 2007 (b).

The study reefs were defined using the benthic complexity variable based on depth values (See Chapter 3). A threshold was applied to the benthic complexity data, which ranged from zero, for low complexity, to one, for maximum complexity, and which defined all pixels with values ≥ 0.8 as reefs.

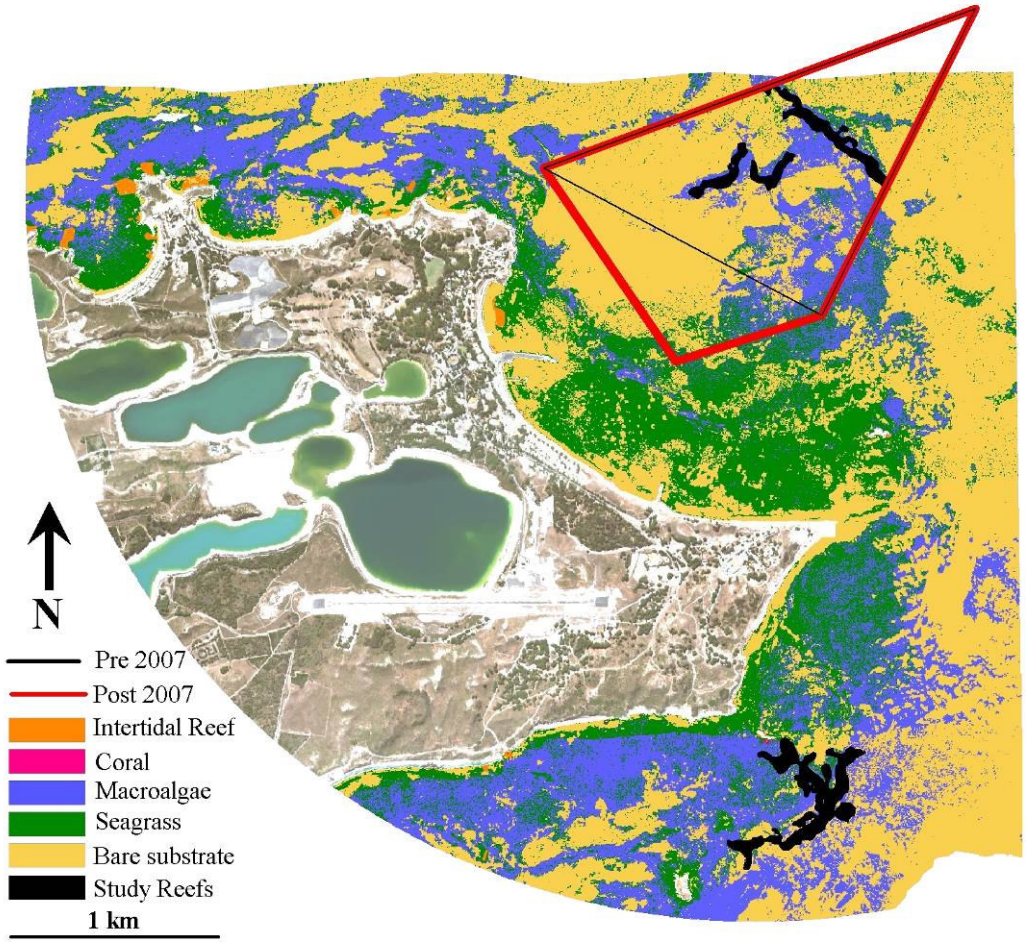

Figure 6-3: The study site for the Western Rock Lobster home range and population density models at Rottnest Island, with the Kingston Reef sanctuary zone pre and post July 2007.

The probability of lobsters foraging over certain distances from their home reef was determined by Jernakoff *et al*. (1987) who fitted their data of the total distance travelled by foraging lobsters to a Weibull distribution. For this study the assumption was made that for a lobster travelling a total distance, d_{total}, during a foraging trip, the maximum distance able to be travelled away from their home reef would be $d_{total}/2$. Based on this assumption a Weibull probability density function was generated using the maximum foraging distance divided by two as the upper limit of the distribution. The probability density function was defined as (modified from Jernakoff *et al.* 1987):

$$p(d) = qa2d^{a-1}\exp\left(-q2d^{a}\right)$$

where d refers to the distance travelled by a lobster from its home reef, a = 2.36 and q = exp(-13.93) (Figure 6-4). This function was applied spatially to the three study reefs within the Kingston Reef sanctuary zone to a maximum distance of 400 m (half the maximum distance recorded by Jernakoff et al. (1987)). The distribution of habitat types within the home range of the lobsters was determined and the potential impacts of the changes made in July 2007 to the Kingston Reef sanctuary zone on the lobster population were assessed.

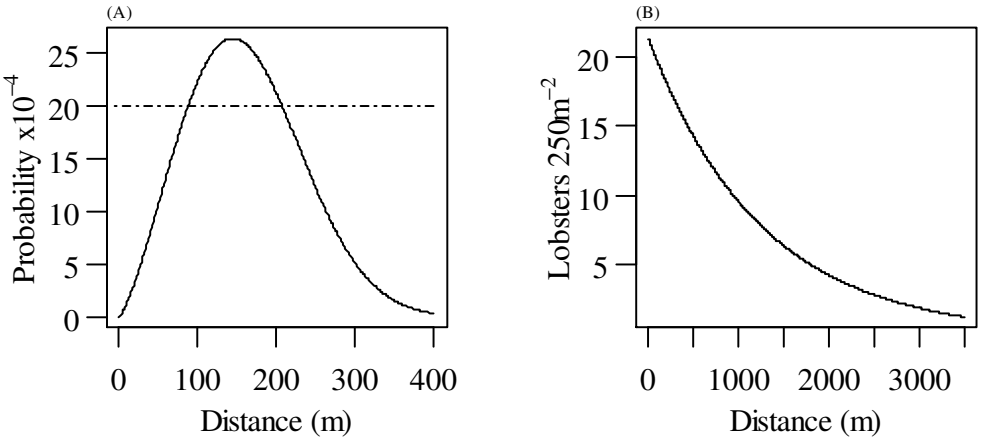

Figure 6-4: The probability distribution of maximum distances travelled by lobsters from their home reef (A) and the density of lobsters occupying a reef as a function of the distance from the centre of the Kingston Reef sanctuary zone (B).

The relationship between the densities of lobsters found on reefs as a function of the distance from the centre of the sanctuary zone was determined by Babcock *et al.* (2007). They determined that close to the centre of the sanctuary, the mean density was 22 lobsters per 250m^2, which declined to ~ 2 lobsters per 250m^2 at sites outside the reserve. From this, distances were estimated to allow for the fitting of a function to describe this relationship (Figure 6-4). The function derived to describe the lobster density ($L_{density}$) as a function of the distance from the centre of the sanctuary zone was:

$$L_{density} = 21.328 \exp(-0.0008 d).$$

The function was applied spatially using the distances measured from the centre of the Kingston Reef sanctuary zone and then converted to the number of lobster per pixel (i.e. 12.25m^2). The potential lobster populations of the reefs inside and outside the sanctuary were also calculated.

6.2.3 Modelling the shallow benthic habitats and beach environments potentially impacted from a floating pollutant spill

A basic GNOME oil spill model (Beegle-Krause 2001) was used to estimate the movement of an oil spill of 120 litres of non-weathering oil in Geordie Bay, Rottnest Island (31.99ºS, 115.55ºE). The model was run using a location file generated for Rottnest Island based solely on a coastline file where no data were included about the surface currents or tidal patterns. Wind data from 1 January 2006, recorded at five minute intervals at the Rottnest Island weather station, were used. The model was run for 30 min, tracking the movement of 1000 splots, which are points that represent the spilled oil in the environment, under two scenarios, namely, the forecast scenario, which included no uncertainty in the calculations, and the uncertainty scenario, which included an uncertainty factor in the model calculations. The benthic habitats potentially affected by the spill were assessed using both forecast scenario and uncertainty scenario results by constructing convex hull polygons for each splot point set and calculating the area of habitats potentially affected at Level 2 of the classification scheme. The length of affected shoreline was also predicted by assessing the distance over which the oil splots were beached under both the forecast and uncertainty model scenarios.

6.2.4 Modelling potential locations for boat moorings at popular dive sites within Rottnest Island Reserve

The mooring suitability model was based on five popular dive sites within the RIR which were converted to a point shapefile and reprojected to UTM Zone 50 South (WGS84) (Table 6-1). The model used four variables to define the optimal suitability of a location for a boat mooring, namely, the distance for the mooring from the dive site was 40 – 50 m, the mooring had to be located > 50 m from the shore on bare substrate at least 5 m from the edge of the bare patch and in water > 5 m depth. A function was developed to assign a suitability rating to each pixel in the study area. The ratings ranged from zero for unsuitable, to one for maximum suitability, for each of the four variables (Figure 6-5).

Table 6-1: Dive sites within Rottnest Island Reserve used for the dive site mooring suitability model. Coordinates are based on the WGS84 datum.

Dive site	Longitude	Latitude
Crystal Palace	115.5437 ° E	32.0267 ° S
Porpoise Caves	115.5434 ° E	32.0271 ° S
Swirl Reef	115.4671 ° E	32.0008 ° S
Lady Elizabeth Wreck	115.5479 ° E	32.0191 ° S
Macedon & Denton Wrecks	115.5555 ° E	31.9878 ° S

The final suitability for each pixel ($DV_{Suitability}$) was calculated using the following formula, which ranges from zero for an unsuitable site to one for maximum suitability:

$$DV_{Suitability} = \left(DV_{Site} + DV_{Shore} + DV_{Bare} + DV_{Depth}\right)/4$$

The suitability of a pixel based on its distance from the dive site was defined as:

$$DV_{Site} = \left[\left(\left(a \times D_{Site}{}^{2}\right) + \left(b \times D_{Site}\right) - c\right) \times \left(ABS\left(\left(Tanh\left(2 \times \left(D_{Site} - 50\right)/50\right) - 1\right)\right)\right)\right]/d$$

where DV_{Site} is the suitability of a pixel based on the distance from the dive site, D_{Site} is the distance from the dive site in metres represented spatially as a raster grid layer, a = -0.000107214, b = 0.031433275, c = 0.303636476 and d = 1.083591773. This function reached its maximum value of one at ~41 m and approached zero again at ~100 m (Figure 6-5). A spatial grid layer was created where each pixel measured the distance from the dive site to a maximum distance of 800 m.

The suitability of a pixel with respect to its distance from shore was defined by the function:

$$DV_{Shore} = \left(\left(-1\left(a \times e^{\left(-D_{Shore}/b\right)}\right)\right) + c\right)/c$$

where DV_{Shore} refers to the suitability of the pixel, D_{Shore} refers to the distance from shore in metres represented as a raster grid layer, a = 2.590708, b = 15.19684 and c = 2.57. The function ranged from zero to one (Figure 6-5).

The suitability of a pixel with respect to its position within a bare substrate patch was defined by the following function:

$$SV_{Bare} = -a + 2$$

where SV_{Bare} refers to the suitability of a pixel, and a refers to the mean value of a 5 x 5 pixel kernel filter for each pixel calculated based on the Level 1 benthic habitat map (the values will range 1 – 2). This function ranged from zero for minimum suitability of a pixel to one for maximum suitability (Figure 6-5).

The suitability of each pixel with respect to water depth (DV_{Depth}) was defined by the following function:

$$DV_{Depth} = \left(\left(\tanh\left(0.8 \times D_{Depth} - 3.5\right)\right) + 1\right) / 2$$

where D_{Depth} refers to the water depth for each pixel, obtained from the digital bathymetry model. The final values were then re-coded into two discrete classes, those being suitable sites ($0.75 < DV_{Suitability} < 0.85$) and optimal sites ($0.85 < DV_{Suitability} < 1.00$).

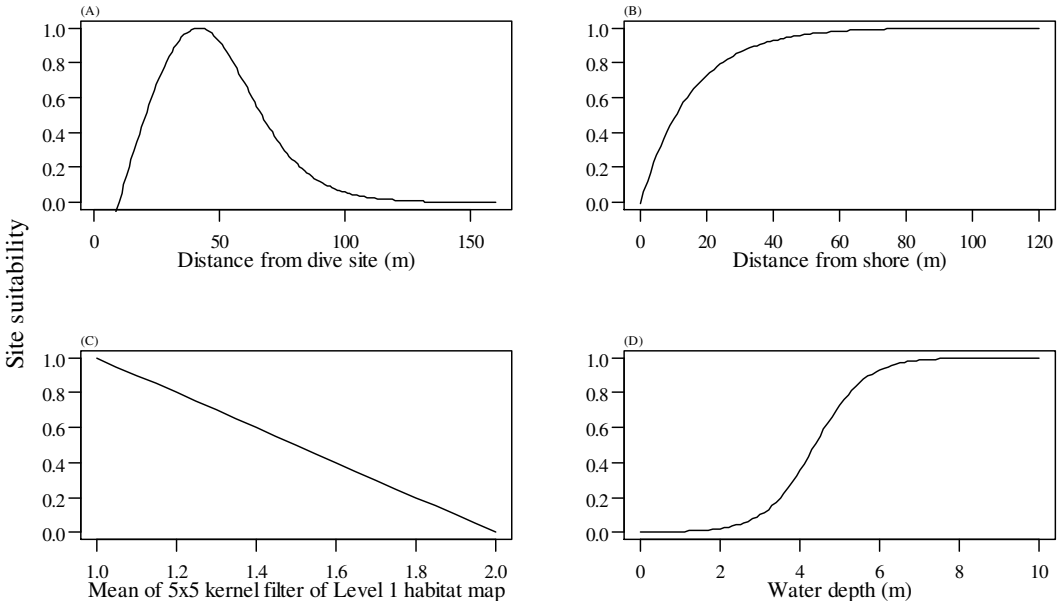

Figure 6-5: The functions used to define the suitability of each pixel for placing a boat mooring for a dive site. These functions define the suitability with respect to the distance from the dive site (A), the suitability with respect to the distance for the shore (B), the suitability with respect to its position within a bare patch (C) and its suitability based on the water depth (D).

6.3 Results

6.3.1 Ascertaining the extent of shallow benthic habitats protected by new sanctuary zones implemented in July 2007

The implementation of the new and extended sanctuary zones at Rottnest Island on 1 July 2007 resulted in the total area of benthic habitat protected within sanctuary zones increasing from 118 hectares to 610 hectares. Prior to the zone expansion in July 2007 the greatest proportion of the benthic habitats protected within the sanctuary zones was

bare substrate, making up 63% (75 ha) of the protected regions (Figure 6-6). However, after the zone expansion bio-substrate became the dominant habitat type protected, making up 60.3% (368 ha) of the total sanctuary area.

Although there was an increase in the area of all habitats protected at Level 2 of the classification scheme, the greatest increase was for macroalgae habitats which increased by 229 hectares and went from contributing 26% to overall sanctuary area, to 50% (Figure 6-6). The bare substrate habitat class which made up the majority of the habitats protected prior to July 2007 (63%) decreased to 25% after the implementation of the new sanctuary zones in July 2007.

The Kingston Reef sanctuary zone was increased in size during the implementation of the new sanctuary zones in July 2007 and increased in area by ~40 hectares (Figure 6-2). The area of seagrass habitat protected increased by 6 hectares and macroalgae by 5 hectares. The Parker Point sanctuary zone increased in size by ~85 hectares, with macroalgae being the habitat class with the greatest increase in area (43 ha), going from contributing 23% of the sanctuary zone to 56% (Figure 6-6). Although a coral colony of *Pocillopora* is known to exist within the Parker Point sanctuary zone, it was not identified in the hyperspectral data most likely due to the occurrence of macroalgae on and around many of the colonies, particularly at the time of year the HyMap imagery was flown (April, at the end of summer). This highlights the importance of such information (i.e. seasonal algal growth) that may need to be taken into account when collecting remotely sensed imagery for benthic habitat mapping projects.

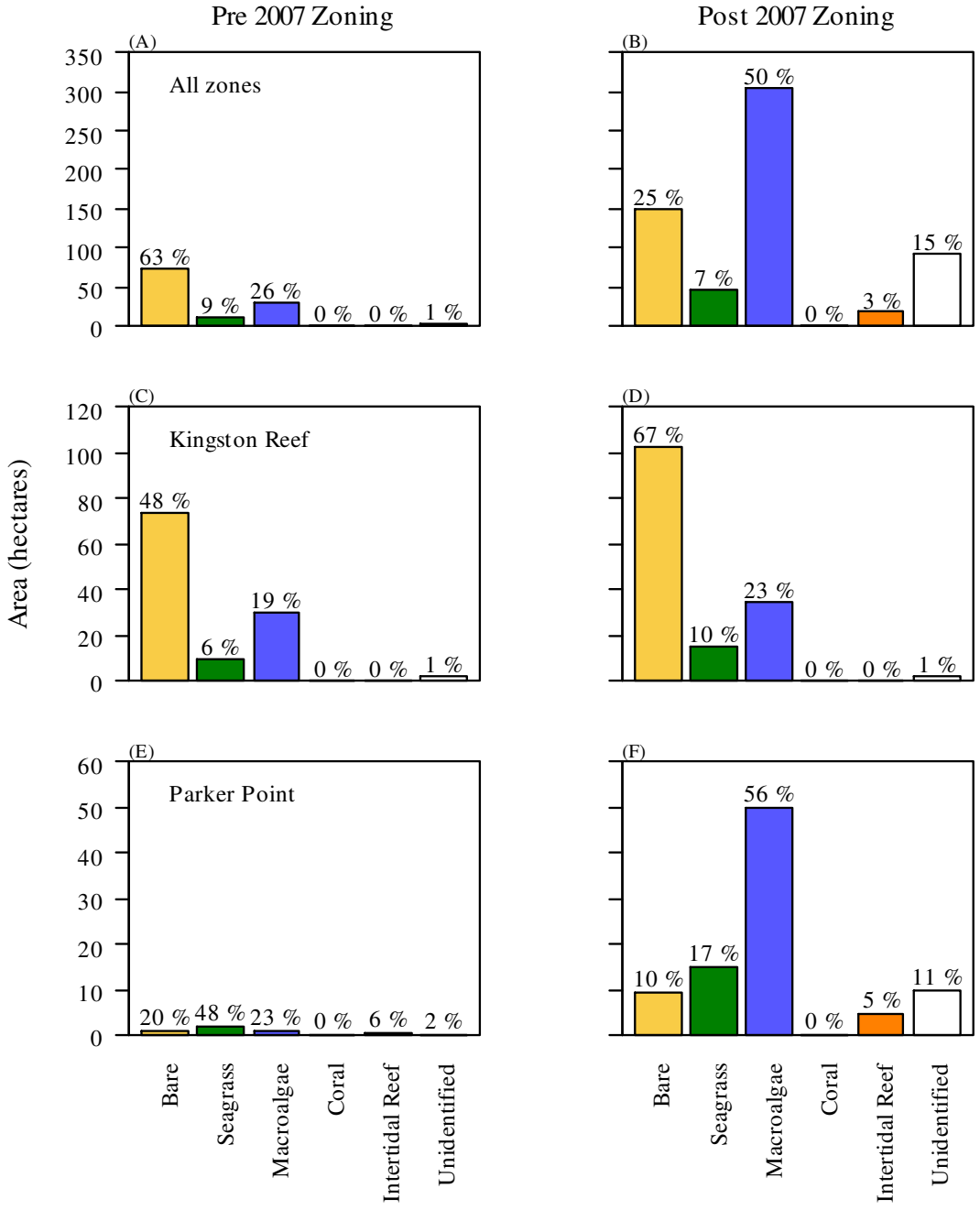

Figure 6-6: The area of different habitat types protected within all sanctuary zones within the Rottnest Island Reserve (A,B), Kingston Reef (C,D) and Parker Point (E,F) sanctuary zones prior to July 2007 and after the new zone implementation in July 2007. Values above bars are the percentage of the total area represented by each chart. Unidentified habitats are those areas that fall outside the HyMap imagery.

6.3.2 Modelling the potential home range and population size of the Western Rock Lobster, *Panulirus cygnus*, on reefs in the Rottnest Island Reserve

The distance from the three study reefs within Kingston Reef sanctuary zone was calculated for each pixel to a maximum distance of 400 m (Figure 6-7). The probability of lobsters foraging to each pixel was calculated and the zone of highest probability was then separated (Figure 6-7).

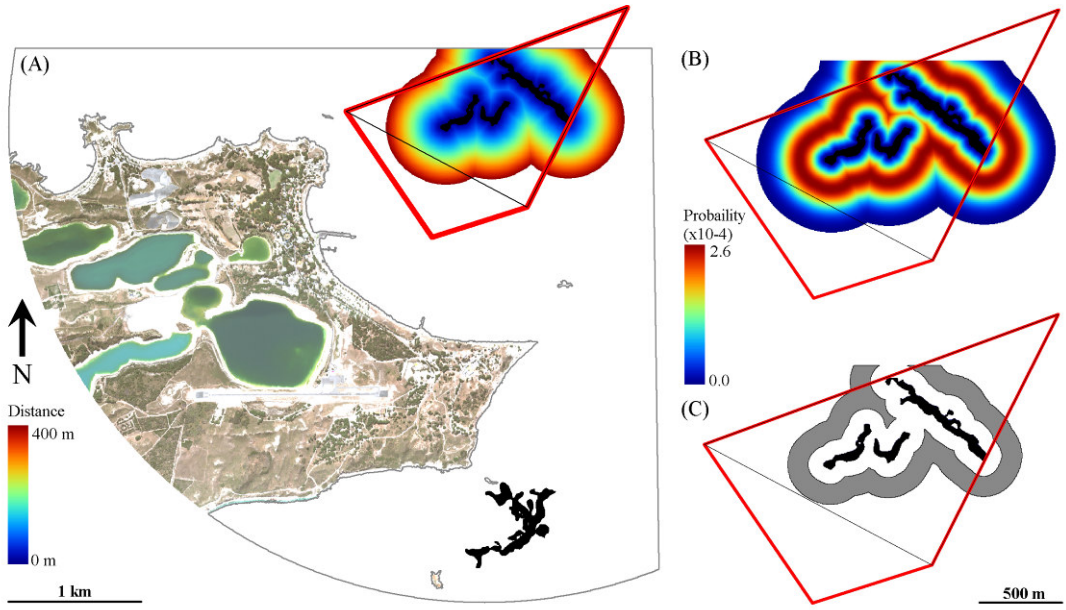

Figure 6-7: The distance from the reefs within Kingston Reef sanctuary zone (A), the probability of lobsters travelling to a location as a function of the distance from the reef (B) and the zone of highest probability were lobsters could travel to (C).

The habitat type with the greatest area within the Kingston Reef sanctuary zone located within the lobster home range in pre 2007 and post 2007 was bare substrate with 66.7 and 76.1 hectares, respectively (Figure 6-8). With the change to the boundaries of the Kingston Reef sanctuary zone in July 2007, there was very little change to the total area of seagrass and macroalgae within the home range of the lobsters occupying the study reefs (Figure 6-8).

The area of habitats within the region of maximum probability was not affected by the change to the boundaries of the sanctuary zone (Figure 6-7). In both pre 2007 and post 2007 the majority was again bare substrate (24.9 ha) and there were 4.5 and 1.9 hectares of macroalgae and seagrass, respectively (Figure 6-8).

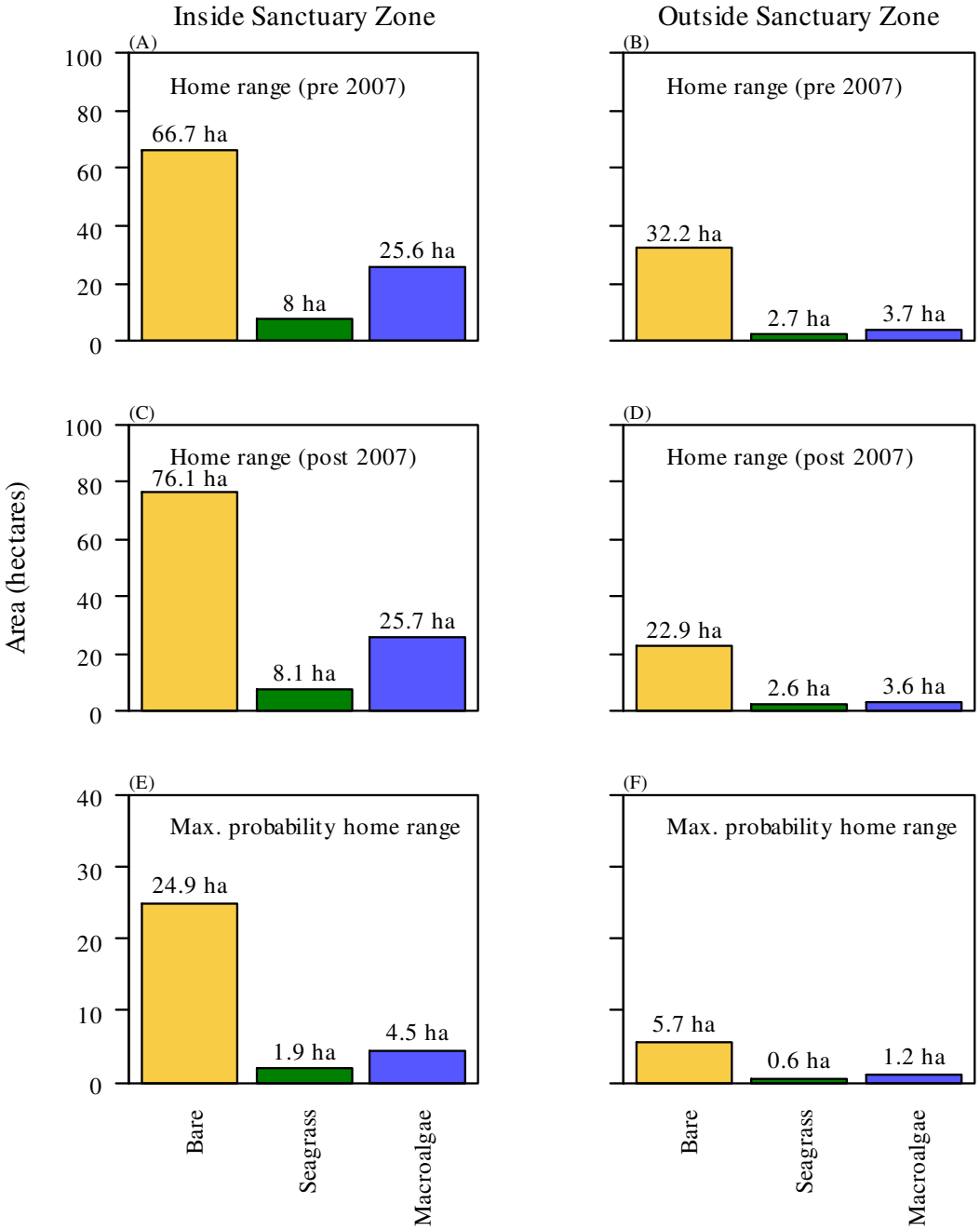

Figure 6-8: The area of the habitats defined at Level 2 for the home range inside and outside of the pre 2007 sanctuary zone (A, B), the post 2007 sanctuary zone (C, D) and the maximum probability range for both years (E, F) of the Western Rock Lobsters occupying the study reefs in the Kingston Reef sanctuary zone.

The distance from the centre of the Kingston Reef sanctuary zone was calculated for each pixel out to 3 500 m (Figure 6-9). The density of lobsters per pixel was calculated for each of the reefs inside and outside of the Kingston Reef sanctuary zone (Figure 6-10; Figure 6-11). The mean lobster density within the sanctuary zone was 0.79 lobsters per pixel and outside was 0.1 lobsters per pixel. There were two distinct groupings in the data for the sanctuary zone, one from the two smaller reefs closer to the centre of the sanctuary zone and the second from the reef closer to the sanctuary zone boundary (Figure 6-11). Using the lobster density data, the total potential population for the Kingston Reefs was estimated to be 4 348 lobsters and for the outside reef was 846 lobsters.

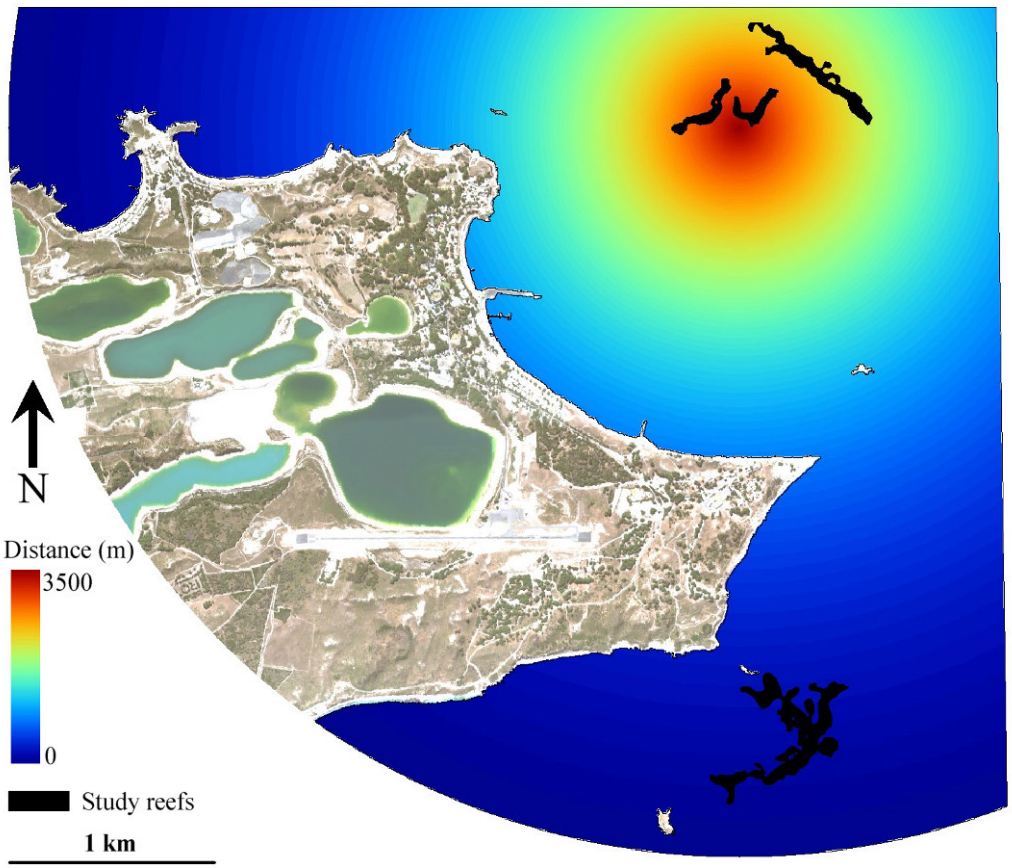

Figure 6-9: The distances from the centre of Kinston Reef sanctuary zone used to calculate lobster densities.

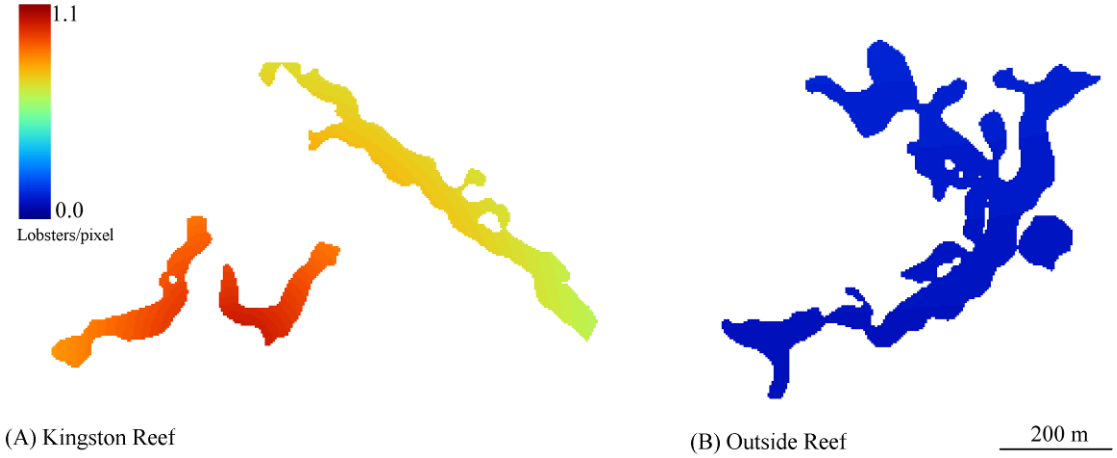

Figure 6-10: The estimated density of lobsters per pixel (12.25m^2) for the two study reefs in Rottnest Island Reserve.

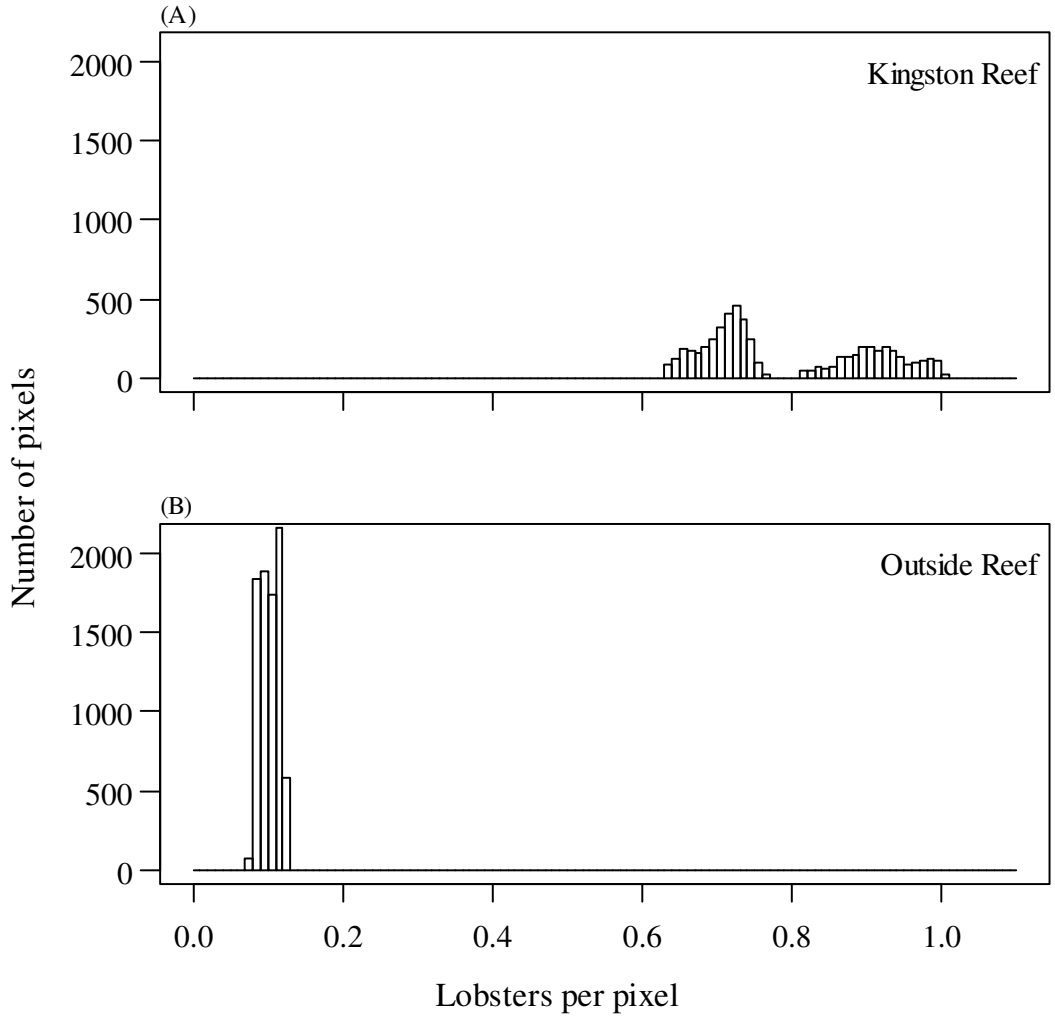

Figure 6-11: Distribution of the estimated density of lobsters per pixel for reefs inside (A) and outside (B) the Kingston Reef Sanctuary Zone.

6.3.3 Modelling the shallow benthic habitats and beach environments potentially impacted from a floating pollutant spill

The GNOME oil spill model indicated that, under the wind conditions specified in the model, and without any influence of surface current and tides, a total of 11.2 hectares and 20.7 hectares of benthic habitat could potentially be affected under the forecast and uncertainty model scenarios, respectively (Figure 6-12). Under the forecast scenario, 1.1 km of the shoreline could potentially be affected by beached oil, while under the uncertainty scenario a total of 2.6 km of shoreline could be affected (Figure 6-12).

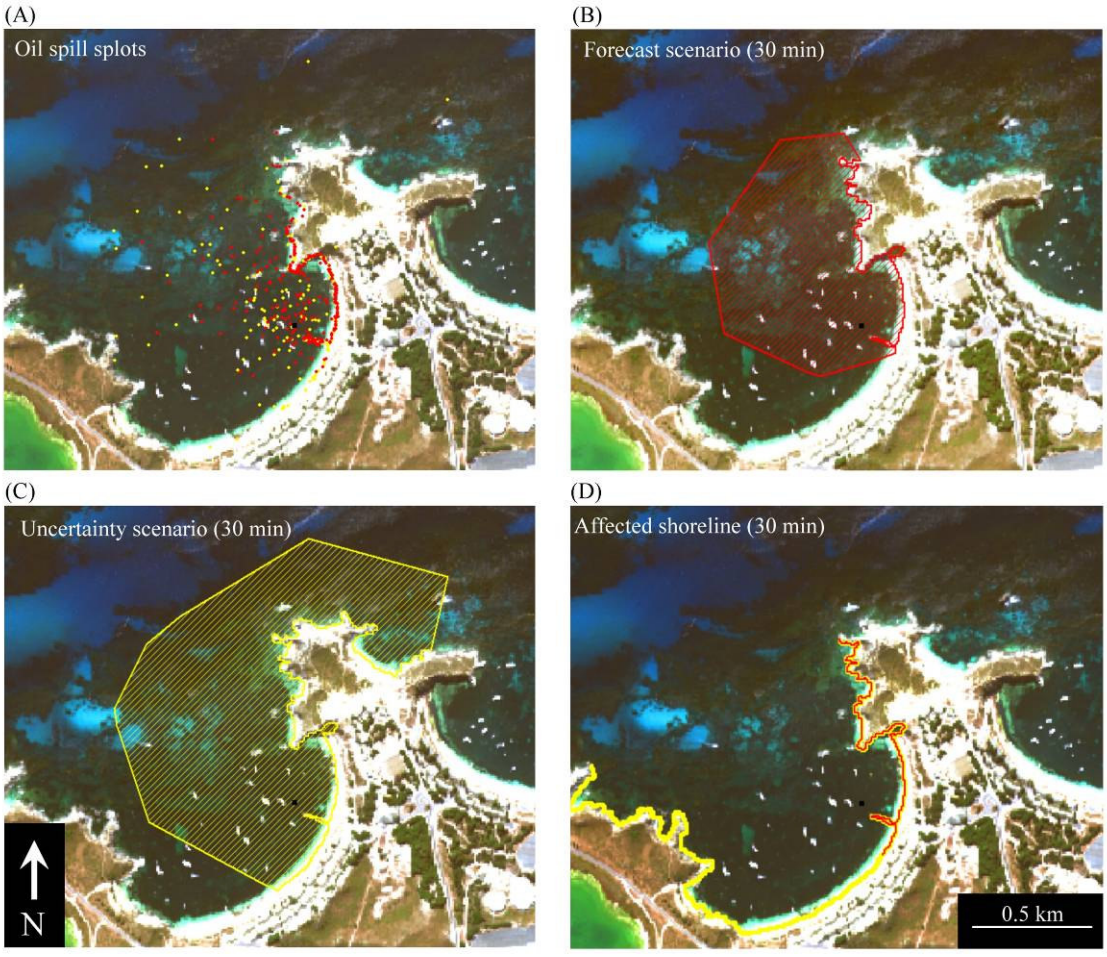

Figure 6-12: The results of the GNOME oil spill model after 30 minutes indicating the location of the oil splots (A), the potential area of benthic habitats affected under the forecast scenario (B), the potential benthic habitats affected under the uncertainty scenario (C) and the potentially affected shoreline under both scenarios (D). Red indicates the forecast scenario and yellow the uncertainty scenario.

The area of bio-substrate habitat potentially affected by the oil spill was significantly greater than bare substrate under both scenarios. Under the uncertainty scenario up to 17.7 hectares of bio-substrate could potentially be affected by the oil, with 8.7 hectares being seagrass habitat, 7.5 hectares macroalgae and the remaining 1.5 hectares being intertidal reefs (Figure 6-13). Under both scenarios, there was a large area of intertidal reefs affected, which is important to note as they are highly susceptible to oil spills (Lee and Page 1997).

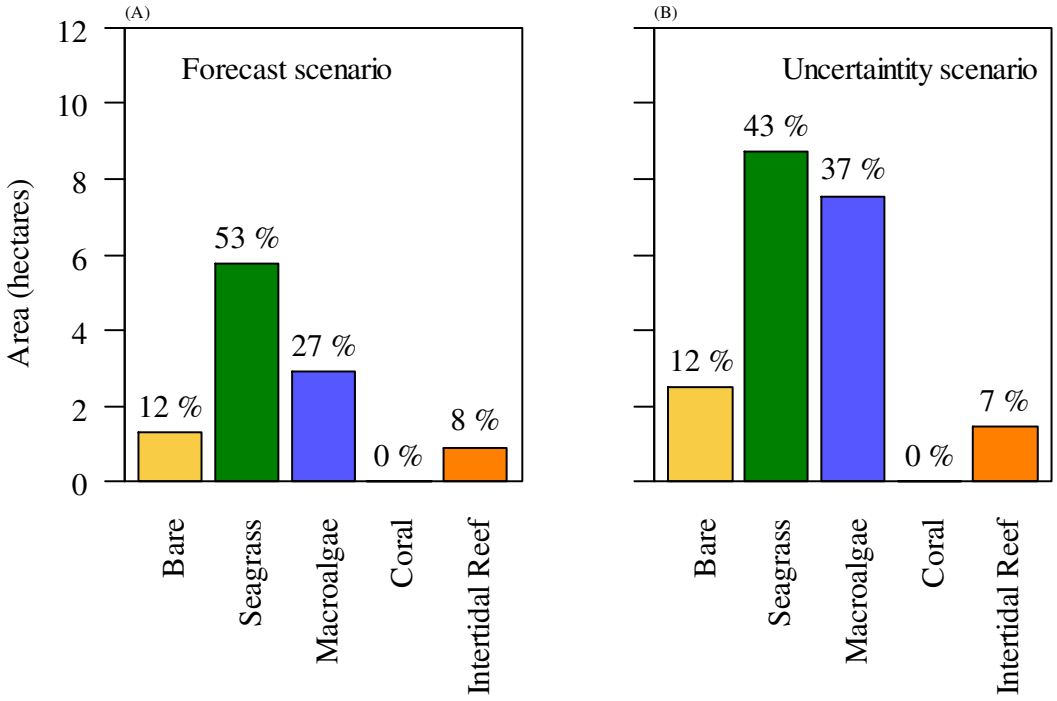

Figure 6-13: Potential area of benthic habitats affected by the Geordie Bay oil spill under both the forecast (A) and the uncertainty (B) scenarios. Values above bars represent the percentage of the total affected area under each scenario.

6.3.4 Modelling potential locations for boat moorings at popular dive sites within Rottnest Island Reserve

Suitable locations for the placement of environmentally sound boat moorings were able to be determined at all five dive sites (Figure 6-14; Table 6-2). No optimal locations were found at Swirl Reef, mostly due to the depth of the waters surrounding the dive

site restricting the model extent. A more in depth analysis of the results for the Macedon and Denton Wrecks site found that 3 062 m^2 provided optimal locations, with a further 4 875 m^2 providing suitable locations (Figure 6-14). Due to the close proximity of the Crystal Palace and Porpoise Caves dive sites, their results were combined and 4 177 m^2 were classed as optimal and 7 558 m^2 classed as suitable for the location of a mooring (Table 6-2).

Table 6-2: The area of optimal and suitable locations for the placement of boat moorings at dive sites within Rottnest Island Reserve.

Dive site	Optimal (m^2)	Suitable (m^2)	Total (m^2)
Crystal Palace Porpoise Caves	4177	7558	11 735
Swirl Reef	0	159	159
Lady Elizabeth Wreck	1617	2695	4312
Macedon & Denton Wrecks	3062	4875	7937

6.4 Discussion

All the example applications presented in this chapter have demonstrated the usefulness of the benthic habitat maps, and associated environmental variables, produced as part of this study, to a range of marine conservation, planning and reporting applications. The applications presented here are by no means an exhaustive list, but merely illustrate what is possible given suitable input data

The changes to the sanctuary zones within Rottnest Island Reserve, implemented in July 2007, resulted in a significant improvement in the amount of benthic habitats protected. There was almost a six-fold increase in the total area protected with the expansion of two existing sanctuary zones, Kingston Reef and Parker Point, and the creation of three

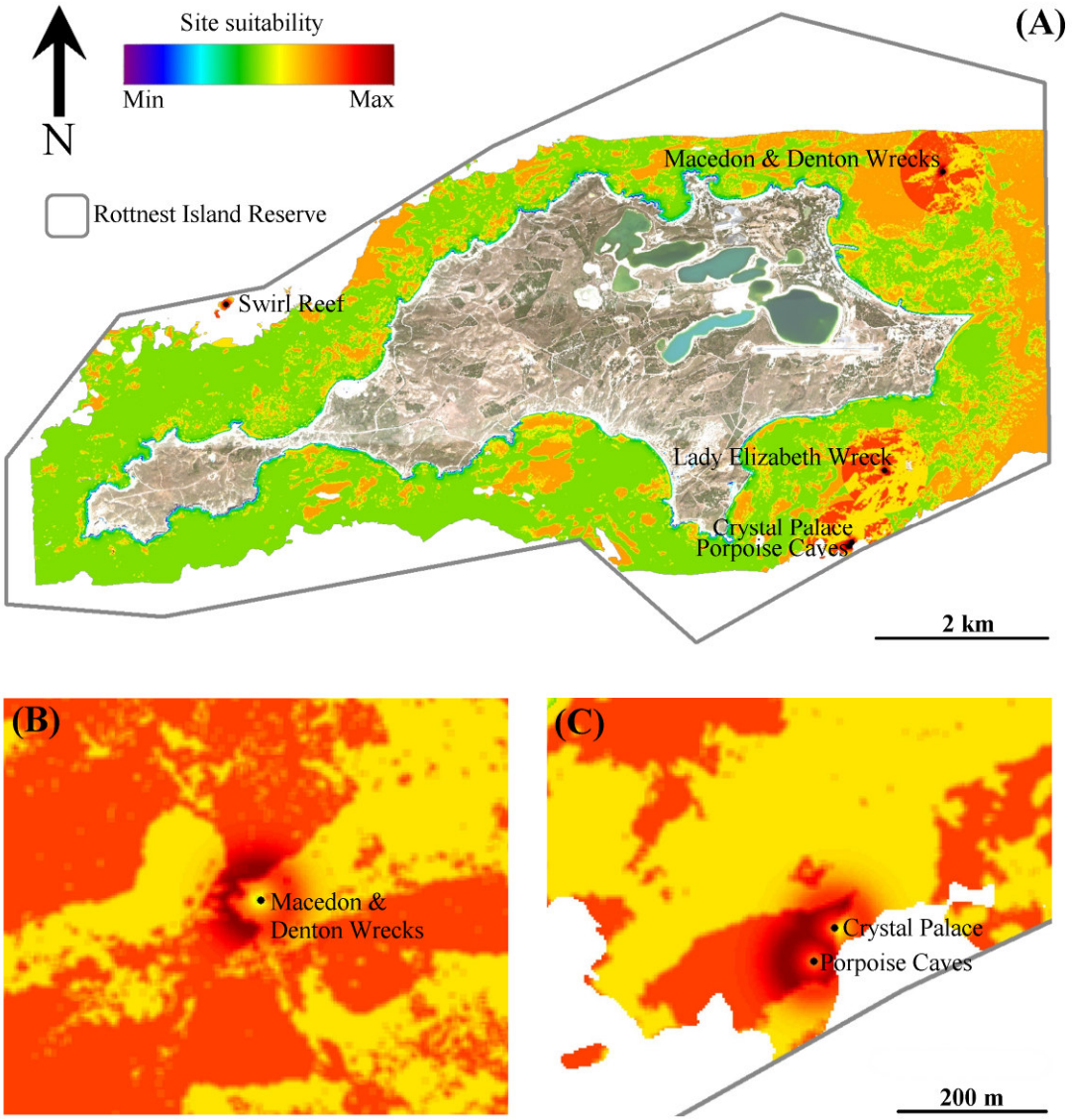

Figure 6-14: Results of suitability modelling for the location of boat moorings for five dive sites within Rottnest Island Reserve (A) and details for the Macedon and Denton Wrecks (B) and Crystal Palace and Porpoise Caves (C) dive sites. The site suitability scale refers to how suitable a pixel is for the placement of a permanent boat mooring based on a set of four predictor variables.

new sanctuary zones, Green Island, West End and Armstrong Bay (Rottnest Island Authority 2007). There were also changes in the proportion of habitat types protected by the sanctuary zones, with a shift from bare substrate being dominant pre 2007 to macroalgae habitats being dominant after 2007. These data could also be used as layers in systematic conservation planning approaches, such as MARXAN or C-Plan, used to

determine the boundaries of protected areas that meet ecological and social requirements of the planners (Leslie *et al.* 2003, Sarkar *et al.* 2006). For example, information about the spatial distribution of benthic habitats were needed as inputs for the marine reserve networks designed using MARXAN for the Great Barrier Reef and the Californian coastline (Fernandes *et al.* 2005, Klein *et al.* 2008).

The information contained in the benthic habitat maps, in combination with other environmental data, such as depth, benthic complexity or exposure, can be used to develop models to describe the habitat suitability for a range of fish and invertebrate species, their possible foraging behaviour and population structure (Morris and Ball 2006). As lobsters are known to rarely forage in a straight line (Jernakoff *et al.* 1987), the assumption made in the home range model, that the distance travelled by a lobster during a night foraging trip was in a straight line away from its den, is likely to result in an over estimate of the home range of the lobsters within the model. Nevertheless, the model indicated that the majority of the Western Rock Lobsters (*Panulirus cygnus*) that occupied the study reefs within Kingston Reef sanctuary zone would generally forage within the boundaries of the sanctuary zone and thus reduce the likelihood that they would be caught in lobster pots placed near sanctuary boundaries. Even with enticement of baited traps, Jernakoff and Phillips (1988) determined that the greatest straight line distance travelled by a lobster from its den to a trap was 120 m. This would then lead to the conclusion that the size of the Kingston Reef sanctuary is appropriate for the protection of the Western Rock Lobster, a finding supported by the work of Babcock *et al*. (2007) who determined that the density of lobsters above the legal size (76 mm) within the sanctuary was 50 times higher than that outside. More recent work by MacArther *et al*. (2008) found that 90% of lobster foraging activity occurred within

60m of the nearest high-relief reef, which further backs the conclusion that most lobsters within the Kingston reef sanctuary zone would be protected from fishing effort. Although this model required large assumptions about the data used to create it, the general patterns in the population structure described by Babcock *et al.* (2007) could be clearly visualised and the theoretical population size could be calculated based on the available habitat. Given a more comprehensive data set, a significantly more accurate model could be developed to model the potential changes in the population structure in the newly created sanctuary zones, by linking habitat suitability models with the population models. This could potentially provide a comprehensive data set on the spatial distribution of habitats and their associated fauna, which could feed back into a range of marine conservation or planning applications, such as determining the potential impacts of a pollution event, such as an oil spill, on their population.

The very basic oil spill model that was developed for Rottnest Island was used to demonstrate the potential impact on shallow benthic and shoreline habitats of a small pollution event. It needs to be re-iterated that the GNOME model used was only an example and had insufficient data inputs to generate reliable or even realistic results. Nevertheless, the outputs of a properly developed and calibrated model would be very similar and as such, the information gained would be obtained in an equivalent format. The results indicated that there would be a large area potentially affected, especially along the shoreline where the effects of an oil spill can be extremely detrimental to the environment and long lasting (Peterson *et al.* 2003). The Australian Marine Safety Authority has developed an oil spill response plan using the OILMAP oil spill model that provides comprehensive outputs that could be utilised to plan for potential spill at

Rottnest Island. This sort of analysis is well suited to examining other pollution such as the outputs from sewage outfalls or desalination plants, both issues at Rottnest Island.

The model used to determine the most environmentally sound locations for the placement of permanent boat moorings at popular dive sites within Rottnest Island Reserve is especially relevant to the Rottnest Island Authority, as their management plan indicates a decision to investigate the placement of moorings at some sites. The model, based on the criteria used to define the model, indicated the regions most suitable for moorings and could be used to guide more intense field surveys prior to the actual placement of the moorings. The suitability model could be significantly improved by integrating other data sources such as exposure models, to determine the sea conditions the mooring would be exposed to, and information from dive charter operators on their frequency of usage at particular sites. The habitat maps for Rottnest Island can also provide a baseline to facilitate the monitoring of impacts resulting from the mooring installation or usage of the area by divers (Garrabou *et al.* 1998, Rouphael and Inglis 2002).

As demonstrated by the example applications developed in this chapter, remotely sensed shallow water benthic habitat maps can provide an extremely useful data set for a range of marine conservation and planning scenarios. The habitat maps generated in this study provide a comprehensive 2004 baseline for future state of the environment reporting for Rottnest Island Reserve and the techniques developed to generate these maps can be applied to create maps in shallow coastal waters along much of the Western Australian coastline. This would contribute towards building a comprehensive

baseline data set for the shallow coastal environments of Western Australia as a basis for regional marine planning and future monitoring activities.

7 Conclusions

A systematic benthic habitat classification for a region is invaluable for generating useful habitat maps for many applications (Mumby and Harbourne 1999). This is especially relevant at the regional planning level by enabling the integration of all available data sets to assist in the development of habitat maps for entire regions. Added to this, using a habitat classification scheme that is ecologically meaningful is essential to the resulting maps being useful for applications such as guiding field sampling programs for biodiversity studies, marine park planning, pollution impact assessment, modelling the distributions of associated fauna and any other applications that link ecology to the habitat classes (Mumby and Harbourne 1999, Shears *et al.* 2004).

This project aimed to develop a systematic hierarchical classification scheme for the shallow water benthic habitats of Rottnest Island that was ecologically relevant and able to be mapped using hyperspectral remote sensing techniques. Secondly, a spectral library of *in situ* spectral signatures for the habitat components defined in the classification scheme was created, and spectral separability analysis was used to determine which benthic habitats could be realistically separated at each level using the HyMap image data. The hierarchical nature of the classification scheme has a number of benefits, the first being the ability to guide the classification of pixels to a higher level by limiting the analysis to the habitat components that are likely to occur, given the identification of the habitat class at a lower level (e.g. restricting the analysis of macroalgae pixels to being either canopy or algal turf). Secondly, the scheme is applicable to habitat classifications carried out using other forms of remotely-sensed data, such as acoustics, that can only differentiate between classes at a lower level (e.g.

bare substrate, bio-substrate), making it possible to integrate the resulting maps seamlessly to allow for mapping from deep subtidal environments through to the shoreline. This can then provide broad scale habitat maps relevant to regional marine planning and finer scale maps for areas of high conservation value to assist with marine park planning. The key to this approach is to integrate the ecological knowledge about the benthic habitats and the components that constitute them (biotic and abiotic), to determine the most appropriate habitat classification scheme to use when mapping the shallow water benthic habitats of a region.

Obtaining a comprehensive spectral library of the components that contribute to the benthic habitats found at Rottnest Island was an essential step in the process of classifying the image data. Its creation was guided by the hierarchical habitat classification scheme so that the set of spectral signatures could realistically represent the HyMap image data obtained at a pixel scale. This can also be a limitation of classification techniques based on a spectral library. The spectral library needs to be comprehensive and have signatures from all possible habitats that might occur in an image pixel to avoid incorrect pixel classification.

The novel method for spectral separability and hyperspectral image classification developed as part of this study has proved to be effective for mapping shallow water benthic habitats in the clear, temperate waters of Rottnest Island. The separation analysis highlighted the importance of working hierarchically and also of having sufficient spectral data in the library to test classification techniques using modelled spectral signatures that replicate what would occur in an image pixel. Having this quality of data can give the user the ability to test the performance of a classification

algorithm to identify different benthic habitats in a controlled environment and determine which approach is best for each particular split in the classification scheme. This approach was applied successfully in this project and resulted in different inputs and spectral distance metrics being found to be optimal for identifying pixels at each split in the hierarchical habitat classification scheme. Although the spectral separability analysis was carried out at HyMap spectral resolution, the same process could be applied to data at the spectral resolution of any available sensor, such as Quickbird or Landsat. However, it should be noted that one would expect the analysis to be less effective due to limitations in the spatial or spectral resolution of other sensors.

Applying the classification algorithm to the hyperspectral image data resulted in the identification of some dominant habitat components to species level (e.g., *Ecklonia radiata*) and others to genus (e.g. *Posidonia*) which is an improvement to the existing habitat maps created as part of the Perth coastal waters study (Ong *et al.* 1998). However, the general patterns in the spatial arrangement of benthic habitats were comparable at lower levels in the classification scheme.

It is important to note that the success of the classification algorithm is reliant on hyperspectral image data being subjected to a rigorous and systematic correction for the influence the atmosphere, the air/water interface and the overlying water column. This study used data corrected using the Modular Inversion Processing System (MIP) which provided the bottom reflectance data that could be utilised by the classification algorithm (Heege *et al.* 2004, Heege and Fischer 2004). The MIP approach to water correction was a perfect partner for the classification algorithm developed as it has a number of ancillary data outputs that indicate the quality and availability of the

corrected bottom reflectance data on a pixel by pixel basis for the image. This allows the image classification algorithm to utilise the most appropriate combination of image bands and spectral metrics when classifying each pixel. This approach provided the information required to obtain the most accurate maps from the image classification, but also provided guidance on how to best interpret these maps.

The strength of the classification approach taken in this project was the hierarchical manner in which it was implemented. This meant that issues with misclassification identified at Level 2 could be corrected, using contextual editing based on environmental variables developed around the digital bathymetry model, before classification was carried out to Levels 3 and 4. This resulted in a more accurate result that better represented the spatial distribution of the benthic habitats of Rottnest Island. Added to this, the results of the classification algorithm testing, using mixture analysis, were used to aid the interpretation of the final habitat maps. For example, testing the classification algorithm at Level 3, to separate macroalgae into the canopy algae or algal turf classes, indicated that canopy will often be misidentified as algal turf, which means that in the final map there may be some areas identified as turf that are actually canopy algae. These misclassifications are a result of a number of factors including the heterogeneous nature of macroalgae habitats at Rottnest Island and the limited ability of the algorithm to separate the classes, even when using pure *in situ* spectral signatures.

Another essential tool in providing the highest quality habitat maps is a rigorous and appropriate accuracy assessment. The accuracy assessment taken in this study was appropriate for the classification at the lower levels in the habitat classification scheme, when habitat classes tend to clump (occur in groups of homogenous groups of pixels),

but at the higher levels, when real changes in the benthic habitats class occur between individual pixels, it was less appropriate. The reason for this was the spatial inaccuracy in the data collection method and meant that these fine scale changes in the benthic habitats were not captured in the validation data or able to be assessed in relation to the image data. Added to this were the broad thematic classes applied to the bathyscope validation data where only the dominant habitat component was recorded, rather than percentage contribution of each component. This made it impossible to assess the fine scale trends observed in the field in the classified image. The finer scale accuracy assessment based on benthic habitat photographs (drop camera) provided a good alternative method which had a high level of spatial and thematic accuracy by virtue of the quantitative nature of the data collected. As was demonstrated, this approach allows for the trends observed in the field to be assessed in direct relation to the classified image as data was recorded about the percentage composition of each validation point for a similar area as recorded by a pixel. This sort of assessment is essential when attempting to classify benthic habitats to a level where real changes in the classification will occur at a pixel level.

The application of benthic habitat maps to marine planning, management and reporting applications has been well recognised. The development of techniques that increase our ability to classify remotely sensed data to a much finer scale will increase the number of applications that they can be used for. However this increase in thematic resolution has to be considered carefully to ensure that the results are still applicable at broader, regional scales. This is where it is of key importance to use a systematic habitat classification scheme that can be applied at all the required spatial and thematic scales.

This project took an integrated approach to utilise hyperspectral image data, in conjunction with ecological knowledge and information on the abiotic environment, to map shallow water benthic habitats in a temperate environment. This approach is necessary to provide results that are appropriate for a range of users, from ecologists to marine managers and planners.

8 References

Abal, E. G. and W. C. Dennison 1996. "Seagrass depth range and water quality in Southern Moreton Bay, Queensland, Australia." *Marine and Freshwater Research* 47: 763-771.

Albert, A. and C. D. Mobley 2003. "An analytical model for subsurface irradiance and remote sensing reflectance in deep and shallow case-2 waters." *Optics Express* 11: 2873-2890.

Amidor, I. 2002. "Scattered data interpolation methods for electronic imaging systems: a survey." *Journal of Electronic Imaging* 11: 157-176.

Anderfouet, S., M. Zubia and C. Payri 2004. "Mapping and biomass estimation of the invasive brown algae *Turbinaria ornata* (Turner) J. Agardh and *Sargassum mangarevense* (Grunow) Setchell on heterogeneous Tahitian coal reefs using 4-meter resolution IKONOS satellite data." *Coral Reefs* 23: 26-38.

Angel, A. and F. P. Ojeda 2001. "Structure and trophic organization of subtidal fish assesmblages on the northern Chilean coast: the effect of habitat complexity." *Marine Ecology Progress Series* 217: 81-91.

ANZECC 1998. Guidelines for establishing the national representative system of marine protected areas, Environment Australia. Canberra, Australia, 15 pp.

Arias-Gonzalez, J. E., T. J. Done, C. A. Page, A. J. Cheal, S. Kininmonth and J. R. Garza-Perez 2006. "Towards a reefscape ecology: relating biomass and trophic structure of fish assemblages to habitat at Davies Reef, Australia." *Marine Ecology Progress Series* 320: 29-41.

Armstrong, R. A. 1993. "Remote sensing of submerged vegetation canopies for biomass estimation." *International Journal of Remote Sensing* 14: 621-627.

Australian Government Department of the Environment Water Heritage and the Arts 2007. The south-west marine bioregional plan: bioregional profile, Australian Government Department of the Environment, Water, Heritage and the Arts. 199 pp.

Babcock, R. C., J. C. Phillips, M. Lourey and G. Clapin 2007. "Increased density, biomass and egg production in an unfished population of Western Rock Lobster (*Panulirus cygnus*) at Rottnest Island, Western Australia." *Marine and Freshwater Research* 58: 286-292.

Babin, M., A. Morel, V. Fournier-Sicre, F. Fell and D. Stramski 2003. "Light scattering properties of marine particles in coastal and open ocean waters as related to the particle mass concentration." *Limnology and Oceanography* 48: 843-859.

Banks, S. A. and G. A. Skilleter 2002. "Mapping intertidal habitats and an evaluation of their conservation status in Queensland, Australia." *Ocean and Coastal Management* 45: 485-509.

Bassett, S. D. and T. C. Edwards Jr. 2003. "Effect of different sampling schemes on the spatial placement of conservation reserves in Utah, USA." *Biological Conservation* 113: 141-151.

Becker, B. L., D. P. Lusch and J. Qi 2005. "Identifying optimal spectral bands from *in situ* measurments of Great Lakes coastal wetlands using second-derivative analysis." *Remote Sensing of Environment* 97: 238-248.

Beegle-Krause, C. J. 2001. General NOAA oil spill modeling environment (GNOME): a new spill trajectory model. *Proceedings of the 2001 International Oil Spill Conference*. pp 865-871.

Beeton, R. J. S., K. I. Buckley, G. J. Jones, D. Morgan, R. E. Reichelt and D. Trewin 2006. Australia State of the Environment 2006, Independent report to the Australian Government Minister for the Environment and Heritage, Department of Environment and Heritage. Canberra, 132 pp.

Beger, M. and H. P. Possingham 2008. "Environmental factors that influence the distribution of coral reef fishes: modelling occurrence data for broad-scale conservation and augment." *Marine Ecology Progress Series* 361: 1-13.

Behrens, T. M. 2005. DEMAT- DEM analysis tool. Institute for Soil Science and Soil Conservation, University Giessen, Germany. Avaliable online @ http://www.esri.com/

Bekkby, T., L. Erikstad, V. Bakkestuen and A. Bjorge 2002. "A landscape ecological approach to coastal zone applications." *Sarsia* 87: 396-408.

Benfield, S. L., H. M. Guzman, J. M. Mair and J. A. T. Young 2007. "Mapping the distribution of coral reefs and associated sublittoral habitats in Pacific Panama: a comparison of optical satellite sensors and classification methodologies." *International Journal of Remote Sensing* 28: 5047-5070.

Berry, P. F. and P. E. Playford 1992. "Territoriality in a subtropical kyphosid fish associated with macroalgae polygons on reef platforms at Rottnest Island, Western Australia." *Journal of the Royal Society of Western Australia* 75: 67-73.

Bertels, L., T. Vanderstraete, S. Van Coillie, E. Knaeps, S. Sterckx, R. Goossens and B. Deronde 2008. "Mapping of coral reefs using hyperspectral CASI data; a case study: Fordata, Tanimbar, Indonesia." *International Journal of Remote Sensing* 29: 2359-2391.

Bickers, A. N. 2003. Cost effective marine habitat mapping from small vessels using GIS, sidescan sonar and video. *Coastal GIS 2003: an integrated approach to Australian coastal issues. (Wollongong Papers on Maritime Policy No 14)*. C.

D. Woodroff and R. A. Furness. Wollongong, NSW, University of Wollongong 105-124 pp.

Black, R., K. Fisher, A. Hill and P. McShane 1979. "Physical and biological conditions on a steep intertidal gradient at Rottnest Island, Western Australia." *Australian Journal of Ecology* 4: 67-74.

Borowitzka, M. A., R. C. Lethbridge and L. Charlton 1990. "Species richness, spatial distribution and colonisation pattern of algal and invertebrate epiphytes on the seagrass *Amphibolis griffithii*." *Marine Ecology Progress Series* 64: 281-291.

Bricaud, A., A. Morel and L. Prieur 1981. "Absorption by dissolved organic matter of the sea (yellow substance) in the UV and visible domains." *Limnology and Oceanography* 26: 43-53.

Brockmann Consult 2008. BEAM-Visat. Avaliable online @ http://www.brockmann-consult.de/beam/index.html

Brooke, B. 2001. "The distribution of carbonate eolianite " *Earth-Science Reviews* 55: 135-164.

Brooke, B., J. Creasey and M. Sexton 2006. Geomorphology of the Perth coast and Rottnest Shelf - a regional analysis of palaeoshoreline features. *GIS for the coastal zone: a selection of papers from CoastGIS 2006* C. D. Woodroff, E. Bruce, M. Puotinen and R. A. Furness. Wollongong, New South Wales, University of Wollongong 331 - 342 pp.

Brown, C. J., K. M. Cooper, W. J. Meadows, D. S. Limpenny and H. L. Rees 2002. "Small-scale mapping of sea-bed assemblages in the eastern English Channel using sidescan sonar and remote sensing techniques." *Estuarine, Coastal and Shelf Science* 54: 263-278.

Burrough, P. A. and R. A. McDonnell 1998. *Principles of geographical information systems*, Oxford University Press. 194 pp.

Burrows, M. T., R. Harvey and L. Robb 2008. "Wave exposure indices from digital coastlines and the prediction of rocky shore community structure." *Marine Ecology Progress Series* 353: 1-12.

Call, K. A., J. T. Hardy and D. O. Wallin 2003. "Coral reef habitat discrimination using multivariate spectral analysis and satellite remote sensing." *International Journal of Remote Sensing* 24: 2627-2639.

Carruthers, T. J. B., W. C. Dennison, G. A. Kendrick, M. Waycott, D. I. Walker and M. L. Cambridge 2007. "Seagrasses of south-western Australia: A conceptual synthesis of the world's most diverse and extensive seagrass meadows." *Journal of Experimental Marine Biology and Ecology* 350: 21-45.

Cendrero, A. 1989. "Mapping and evaluation of coastal areas for planning." *Ocean and Shoreline Management* 12: 427-462.

Chang, C. 2000. "An information-theoretic approach to spectral viarability, similarity, and discrimination for hyperspectral image analysis." *IEEE Transactions on Information Theory* 46: 1927-1932.

Chang, C., S. S. Chiang, J. A. Smith and I. W. Ginsberg 2002. "Linear spectral random mixture analysis for hyperspectral imagery." *IEEE Transactions on Geoscience and Remote Sensing* 40: 375-392.

Clarke, C. D. 1993. "Satellite remote sensing of marine pollution." *International Journal of Remote Sensing* 14: 2985-3004.

Clarke, D. J. and I. G. Eliot 1983. "Mean sea-level and beach-width variation at Scarborough, Western Australia." *Marine Geology* 51: 251-267.

Clarke, K. R., P. J. Somerfield and M. G. Chapman 2006. "On resemblance measures for ecological studies, including taxonomic dissimilarities and a zero-adjusted Bray–Curtis coefficient for denuded assemblages." *Marine Ecology Progress Series* 330: 55-80.

Clarke, K. R. and R. M. Warwick 2001. *Change in marine communities: an approach to statistical analysis and interpretation*. Plymouth, Primer-E. 168 pp.

Coleman, M. A. 2002. "Small-scale spatial variability in intertidal and subtidal turfing algal assemblages and the temporal generality of these patterns." *Journal of Experimental Marine Biology and Ecology* 267: 53-74.

Commonwealth of Australia 1998. Australia's Oceans Policy, Volume 1, Environment Australia. Canberra, Australia, 1 49 pp.

Commonwealth of Australia 2006. A guide to the intergrated marine and coastal regionalisation of Australia Version 4.0, Department of the Environment and Heritage. Canberra, Australia, 15 pp.

Congalton, R. G. 1991. "A review of assessing the accuracy of classifications of remotely sensed data." *Remote Sensing of Environment* 37: 35-46.

Congalton, R. G. 2001. "Accuracy assesment and validation of remotely sensed and other spatial information." *International Journal of Wildland Fire* 10: 321-328.

Congalton, R. G. and K. G. Green 1999. *Assessing the accuracy of remotely sensed data: principles and practices*. Boca Raton, CRC\Lewis Press. 137 pp.

Connell, S. D. 2003. "The monopolization of understorey habitat by subtidal encrusting coralline algae: a test of the combined effects of canopy-mediated light and sedimentation." *Marine Biology* 142: 1065-1071.

Connell, S. D. 2007. Subtidal temperate rocky habitats: habitat heterogeneity at local to continental scales. *Marine Ecology*. S. D. Connell and B. M. Gillanders. Melbourne, Australia, Oxford University Press 378-401 pp.

Connolly, R. M. 1994. "A comparison of fish assemblages from seagrass and unvegetated areas of a southern Australian estuary " *Australian Journal of Marine and Freshwater Research* 45: 1033-1044.

Cressie, N. A. C. 1991. *Statistics for spatial data*. New York, John Wiley and Sons, Inc. 900 pp.

Cresswell, G. R. 1996. "The Leeuwin Current near Rottnest Island, Western Australia." *Journal of Marine and Freshwater Research* 47: 483-487.

Cresswell, G. R. and J. L. Peterson 1993. "The Leeuwin Current south of Western Australia." *Journal of Marine and Freshwater Research* 44: 285-303.

Cullinan, V. I., M. A. Simmons and J. M. Thomas 1997. "A Bayesian test of hierarchy theory: scaling up variability in plant cover from field to remotely sensed data." *Landscape Ecology* 12: 273-285.

Curley, B. G., M. J. Kingsford and B. M. Gillanders 2002. "Spatial and habitat-related patterns of temperate reef fish assemblages: implications for the design of marine protected areas." *Journal of Marine and Freshwater Research* 53: 1197-1210.

de Carvalho, O. A. and P. R. Meneses 2000. Spectral correlation mapper (SCM): an improvement on the spectral angle mapper (SAM). *Summaries of the 9th JPL Airborne Earth Science Workshop*, JPL Publication. 00-18 65-74 pp.

Dekker, A. G., V. E. Brando and J. M. Anstee 2005. "Retrospective seagrass change detection in a shallow coastal tidal Australian lake." *Remote Sensing of Environment* 97: 415-433.

Dekker, A. G., G. Bryne, V. E. Brando and J. M. Anstee 2003. Hyperspectral mapping of intertidal rock platform vegetation as a tool for adaptive management. *CSIRO Land and Water, Remote Sensing and Spatial Analysis, Technical Report 9/03*, CSIRO Land and Water. Canberra, 78 pp.

Department of Defence 2009. Australian national tide tables 2009, Australian Hydrographic Publication 11, Department of Defence. Australia, 372 pp.

Department of Environmental Protection 1996. Southern Metropolitan Coastal Waters Study (1991-1994) Final Report, Department of Environmental Protection. Perth, Western Australia, 288 pp.

Desmet, P. J. J. 1997. "Effects of interpolation errors on the analysis of DEMs." *Earth Surface Processes and Landforms* 22: 563-580.

Drake, N. A., S. Mackin and J. J. Settle 1999. "Mapping vegetation, soils and geology in semiarid shrublands using spectral matching and mixtures modeling of SWIR AVIRIS imagery." *Remote Sensing of Environment* 68: 12-25.

Du, Y., C. I. Chang, H. Ren, C. C. Chang, J. O. Jensen and F. D'Amico 2004. "New hyperspectral discrimination measure for spectral characteriztion." *Optical Engineering* 43: 1777-1786.

Du, Y., C. I. Chang, H. Ren, F. D'Amico and J. O. Jensen 2003. "A new hyperspectral discrimination measure for spectral similarity." *Algorithms and technologies for mutlispectral, hyperspectral and ultraspectral imagery IX. Proeceedings of SPIE* Vol. 5093: 430-439.

Duda, T. and M. Canty 2002. "Unsupervised classification of satellite imagery: choosing a good algorithm." *International Journal of Remote Sensing* 23: 2193-2212.

Dustan, P., E. Dobson and G. Nelson 2001. "Landsat Thematic Mapper: detection of shifts in community composition of coral reefs." *Conservation Biology* 15: 892-902.

Edgar, E. J. and C. Shaw 1993. Inter-relationships between sediments, seagrasses, benthic invertebrates and fishes in shallow marine habitats off south-western Australia. *The Marine Flora and Fauna of Rottnest Island, Western Australia*. F. Wells, D. I. Walker, H. Kirkman and R. Lethbridge. Perth, Western Australian Museum. 2 429-442 pp.

Edgar, G. J. and C. Shaw 1995. "The production and trophic ecology of shallow-water fish assemblages in southern Australia III. General relationships between sediments, seagrasses, invertebrates and fishes." *Journal of Experimental Marine Biology and Ecology* 194: 107-131.

Ekebom, J., P. Laihonen and T. Suominen 2003. "A GIS step-wise procedure for assessing physical exposure in fragmented archipelagos." *Estuarine, Coastal and Shelf Science* 57: 887-898.

England, P., J. C. Phillips, R. C. Babcock, G. Clapin, A. Sampey and N. Murphy 2006. Wave modelling and patterns in diversity in benthic communities. *Strategic Fund for the Marine Environment Final Report. Volume 2: the SFRME core projects*. J. K. Keesing, J. N. Heine, R. C. Babcock, P. D. Craig and J. A. Koslow 246-250 pp.

Environmental Protection Authority 2007. State of the environment report, Western Australia, Environmental Protection Authority. Perth, Westerm Australia, 340 pp.

ESRI 1999. ArcView GIS 3.2. ESRI. Avaliable online @ http://www.esri.com/

Faith, D. P., C. R. Margules, P. A. Walker, J. Stein and G. Natera 2001. "Practical application of biodiversity surrogates and percentage targets for conservation in Papua New Guinea." *Pacific Conservation Biology* 6: 289-303.

Faith, D. P. and P. A. Walker 1996. "Environmental diversity: on the best-possible use of surrogate data for assessing the relative biodiversity of sets of areas." *Biodiversity and Conservation* 5: 399-415.

Fernandes, L., J. Day, A. Lewis, S. Slegers, B. Kerrigan, D. Breen, D. Cameron, B. Jago, J. Hall, D. Lowe, J. Innes, J. Tanzer, V. Chadwick, L. Thompson, K. Gorman, M. Simmons, B. Barnett, K. Sampson, G. De' Ath, B. Mapstone, H. Marsh, H. P. Possingham, I. R. Ball, T. J. Ward, K. Dobbs, J. Aumend, D. Slater and K. Stapleton 2005. "Establishing representative no-take areas in the Great Barrier Reef: large-scale implementation of theory on marine protected areas." *Conservation Biology* 19: 1733-1744.

Ferrell, D. J. and J. D. Bell 1991. "Differences among assemblages of fish associated with *Zostera capricorni* and bare sand over a large spatial scale." *Marine Ecology Progress Series* 72: 15-24.

Fonseca, M. and S. S. Bell 1998. "Influence of physical setting on seagrass landscapes near Beaufort, North Carolina, USA." *Marine Ecology Progress Series* 171: 109-121.

Fonseca, M., P. E. Whitfield, N. M. Kelly and S. S. Bell 2002. "Modeling seagrass landscape patterns and associated ecological attributes." *Ecological Applications* 12: 218-237.

Fowler-Walker, M. J. and S. D. Connell 2002. "Opposing states of subtidal habitat across temperate Australia: consistency and predictability in kelp canopy-benthic associations." *Marine Ecology Progress Series* 240: 49-56.

Fox, N. J. and L. E. Beckley 2005. "Priority areas for conservation of Western Australian coastal fishes: a comparision of hotspot, biogeographical and complementarity approaches." *Biological Conservation* 125: 399-410.

Franke, R. 1982. "Scattered data interpolation: tests of some methods." *Mathematics of Computation* 38: 181-200.

Freitas, R., A. M. Rodrigues and V. Quintino 2003. "Benthic biotopes remote sensing using acoustics." *Journal of Experimental Marine Biology and Ecology* 285-286: 339-353.

Freitas, R., L. Sampaio, A. M. Rodrigues and V. Quintino 2005. "Sea-bottom classification across a shallow-water bar channel and near-shore shelf, using single-beam acoustics." *Estuarine, Coastal and Shelf Science* 65: 625-632.

Friedlander, A. 2001. "Essential fish habitat and the effective design of marine reserves: Application for marine ornamental fishes." *Aquarium Sciences and Conservation* 3: 135-150.

Friedlander, A., E. K. Brown, P. L. Jokiel, W. R. Smith and K. S. Rodgers 2003. "Effects of habitat, wave exposure, and marine protected area status on coral reef fish assemblages in the Hawaiian archipelago." *Coral Reefs* 22: 291-305.

Frost, N. J., M. T. Burrows, M. P. Johnson, M. E. Hanley and S. J. Hawkins 2005. "Measuring surface complexity in ecological studies." *Limnology and Oceanography. Methods* 3: 203-210.

Fyfe, S. K. 2003. "Spatial and temporal variation in spectral reflectance: Are seagrass species spectrally distinct." *Limnology and Oceanography* 48: 464-479.

Garcia-Charton, J. A. and A. Perez-Ruzafa 2001. "Spatial pattern and the habitat structure of a Mediterranean rocky reef fish local assemblage." *Marine Biology* 138: 917-934.

Garpe, K. C. and M. C. Ohman 2003. "Coral and fish distribution patterns in Mafia Island Marine Park, Tanzania: fish-habitat interactions." *Hydrobiologia* 498: 191-211.

Garrabou, J., E. Sala, A. Arcas and M. Zabala 1998. "The impact of diving on rocky sublittoral communities: a case study of a bryzoan population." *Conservation Biology* 12: 302-312.

Garrey, J., H. Maxwell and G. R. Cresswell 1981. "Dispersal of tropical marine fauna to the Great Australian Bight by the Leeuwin Current." *Australian Journal of Marine and Freshwater Research* 32: 493-500.

Garza-Perez, J. R., A. Lehmann and J. E. Arias-Gonzalez 2004. "Spatial prediction of coral reef habitats: integrating ecology with spatial modeling and remote sensing." *Marine Ecology Progress Series* 269: 141-152.

Gattuso, J. P., B. Gentili, C. M. Duarte, J. A. Kleypas, J. J. Middelburg and D. Antoine 2006. "Light availability in the coastal ocean: impact on the distribution of benthic photosynthetc organisms and their contribution to primary production." *Biogeosciences* 3: 489-513.

Gaylord, B. 2000. "Biological implications of surf-zone flow complexity." *Limnology and Oceanography* 45: 174-188.

Gentilli, J. 1972. *Australian climate patterns*. Adelaide, South Australia, Thomas Nelson Ltd. 285 pp.

Gersbach, G. H., C. B. Pattiaratchi, G. N. Ivey and G. R. Cresswell 1999. "Upwelling on the south-west coast of Australia - source of the Capes Current?" *Continental Shelf Research* 19: 363-400.

Godfrey, J. S., D. J. Vaudrey and S. D. Hahn 1986. "Observations of the shelf-edge current south of Australia, winter 1982." *Journal of Physical Oceanography* 16: 668-679.

Goldberg, N. A. 2007. "Colonization of subtidal macroalgae in a fucalean-dominated algal assemblage of southwestern Australia." *Hydrobiologia* 575: 423-432.

Goldberg, N. A. and G. A. Kendrick 2004. "Effects of island groups, depth, and exposure to ocean waves on subtidal macroalgal assemblages in the Recherche Archipelago, Western Australia." *Journal of Phycology* 40: 631-641.

Goodman, J. A., Z. P. Lee and S. L. Ustin 2008. "Influence of atmospheric and sea-surface corrections on retrieval of bottom depth and reflectance using a semi-analytical model: a case study in Kaneohe Bay, Hawaii." *Applied Optics* 47: F1 - F11.

Goodman, J. A. and S. L. Ustin 2007. "Classification of benthic composition in a coral reef environment using spectral unmixing." *Journal of Applied Remote Sensing* 1: 011501. doi:10.1117/1.2815907.

Goovaerts, P. 2000. "Geostatistical approaches for incorporating elevation into the spatial interpolation of rainfall." *Journal of Hydrology* 228: 113-129.

Gratwicke, B. and M. R. Speight 2005. "The relationship betwen fish species richness,abundance and habitat complexity in a range of shallow tropical marine habitats." *Journal of Fish Biology* 66: 650-667.

Gray, J. S. 1997. "Marine biodiversity: patterns, threats and conservation needs." *Biodiversity and Conservation* 6: 153-175.

Gray, J. S. 2001. "Marine biodiversity: the paradigms in patterns of species richness examined." *Scientia Marina* 65(Supp. 2): 41-56.

Green, E. P., P. J. Mumby, A. J. Edwards and C. D. Clarke 2000. *Remote sensing handbook for tropical coastal management*. Paris, United Nations Educational. 316 pp.

Grober-Dunsmore, R., T. K. Frazer, J. P. Beets, W. J. Lindberg, P. Zwick and N. A. Funicelli 2008. "Influence of landscape structure on reef fish assemblages." *Landscape Ecology* 23: 37-53.

Grober-Dunsmore, R., T. K. Frazer, W. J. Lindberg and J. Beets 2007. "Reef fish and habitat relationships in a Caribbean seascape: the importance of reef context." *Coral Reefs* 26: 201-216.

Guibas, L. and J. Stolfi 1985. "Primitives for the manipulation of general subdivisions and the computation of voronoi diagrams." *ACM Transactions on Graphics* 4: 74-123.

Halley, V. and E. Bruce 2007. "Thematic accuracy assessment of acoustic seabed data for shallow benthic habitat mapping." *International Journal of Environmental Studies* 64: 93-107.

Haltrin, V. I. 1999. "Chlorophyll-based model of seawater optical properties " *Applied Optics* 38: 6826-6832.

Hanson, C. E., C. B. Pattiaratchi and A. M. Waite 2005. "Seasonal production regimes off south-western Australia: influence of the Capes and Leeuwin Currents on phytoplankton dynamics." *Marine and Freshwater Research* 56: 1011-1026.

Hardy, R. L. 1990. "Theory and applications of the multiquadratic-biharmonic method." *Computers and Mathematical Applications* 19: 163-208.

Harman, N., E. S. Harvey and G. A. Kendrick 2003. "Differences in fish assemblages from different reef habitats at Hamelin Bay, south-western Australia." *Journal of Marine and Freshwater Research* 54: 177-184.

Harris, P. T., A. D. Heap, T. Whiteway and A. Post 2008. "Application of biophysical information to support Australia's representative marine protected area program." *Ocean and Coastal Management* 51: 701-711.

Hastings, K., P. Hesp and G. A. Kendrick 1995. "Seagrass loss associated with boat moorings at Rottnest Island, Western Australia." *Ocean and Coastal Management* 26: 225-246.

Hay, G. J., D. J. Marceau, P. Dube and A. Bouchard 2001. "A multiscale framework for landscape analysis: object-specific analysis and upscaling." *Landscape Ecology* 16: 471-490.

Hay, M. 1981. "The functional morphology of turf-forming seaweeds: persistence in stressful marine habitats." *Ecology* 62: 739-750.

Hayek, L. C. and M. A. Buzas 1997. *Surveying natural populations*. New York, Columbia University Press. 563 pp.

Heege, T., A. Bogner and N. Pinnel 2004. "Mapping of submerged aquatic vegetation with a physically based process chain." *Proceedings of SPIE International Society of Optical Engineering* 5233: 43-50.

Heege, T. and J. Fischer 2004. "Mapping of water constituents in Lake Constance using multispectral airborne scanner data and a physically based processing scheme." *Canadian Journal of Remote Sensing* 30: 77-86.

Hegge, B. J., I. Eliot and J. Hsu 1996. "Sheltered sandy beaches of southwestern Australia." *Journal of Coastal Research* 12(3): 748-760.

Hirzel, A. H., J. Hausser, D. Chessel and P. N. 2002. "Ecological-niche factor analysis: how to compute habitat-suitability maps without absence data?" *Ecology* 83: 2027-2036.

Hochberg, E. J. and M. J. Atkinson 2000. "Spectral discrimination of coral reef benthic communities." *Coral Reefs* 19: 164-171.

Hochberg, E. J. and M. J. Atkinson 2003. "Capabilities of remote sensors to classify coral, algae, and sand as pure and mixed spectra." *Remote Sensing of Environment* 85: 174-189.

Hochberg, E. J., M. J. Atkinson and S. Andrefouet 2003. "Spectral reflectance of coral reef bottom-types worldwide and implications for coral reef remote sensing." *Remote Sensing of Environment* 85: 159-173.

Hochberg, E. J., M. J. Atkinson, A. Apprill and S. Andrefouet 2004. "Spectral reflectance of coral." *Coral Reefs* 23: 84-95.

Hodgkin, E. P., L. Marsh and G. G. Smith 1959. "The littoral environment of Rottnest Island." *Journal of the Royal Society of Western Australia* 42: 85-88.

Holden, H. and E. LeDrew 1998. "Spectral discrimination of healthy and non-healthy corals based on cluster analysis, principal components analysis, and derivative spectroscopy." *Remote Sensing of Environment* 65: 217-224.

Holden, H. and E. LeDrew 1999. "Hyperspectral identification of coral reef features." *International Journal of Remote Sensing* 20: 2545-2563.

Holden, H. and E. LeDrew 2000. "Accuracy assesment of hyperspectral classification of coral reef features." *Geocarto International* 15: 5-11.

Holden, H. and E. LeDrew 2002. "Measuring and modelling water column effects on hyperspectral reflectance in a coral reef environment." *Remote Sensing of Environment* 81: 300-308.

Holland, J. H. 1992. *Adaptation in natural and artificial systems: an introductory analysis with applications to biology, control, and artificial intelligence*. Cambridge, Mass, MIT Press. 211 pp.

Holmes, K. W., K. P. Van Niel, G. A. Kendrick and B. Radford 2007. "Probabilistic large-area mapping of seagrass species distributions." *Aquatic Conservation: Marine and Freshwater Ecosystems* 17: 385-407.

Hope, P. K., W. Drosdowsky and N. Nicholls 2006. "Shifts in the synoptic systems influencing southwest Western Australia." *Climate Dynamics* 26: 751-764.

Howard, R. K. 1988. "Fish predators of the Western Rock Lobster (*Panulirus cygnus* George) in a nearshore nursery habitat." *Australian Journal of Marine and Freshwater Research* 39: 307-316.

Howard, R. K. 1989. "The structure of a nearshore fish community of Western Australia: diel patterns and the habitat role of limestone reefs." *Environmental Biology of Fishes* 24: 93-104.

Huber, W. 2002. Poly to points. Quantitative Decisions. Avaliable online @ www.quandec.com

Huisman, J. M. and D. I. Walker 1990. "A catalogue of the marine plants of Rottnest Island, Western Australia, with notes on their distribution and biogeography." *Kingia* 1: 349-459.

Hutchins, B. 1979. *The fishes of Rottnest Island*. Perth, Western Australia, Creative Research. 103 pp.

Hutchins, J. B. 1999. Mortality of *Pocillopora* coral at Rottnest Island, Western Australia. *Ninth International Marine Biological Workshop, The seagrass flora and fauna of Rottnest Island, Western Australia*, Rottnest Island, Western Australia, Western Australian Museum. pp 281-293.

Hutchinson, G. E. 1957. "Concluding remarks." *Cold Springs Harbour Symposium on Quanitative Biology* 22: 415-427.

Hyndes, G. A., A. J. Kendrick, L. D. MacArthur and E. Stewart 2003. "Differences in the species- and size-composition of fish assemblages in three distinct habitats with differing plant and meadow structure." *Marine Biology* 142: 1195-1206.

Hyndes, G. A., I. C. Potter and R. C. J. Lenanton 1996. "Habitat partitioning by whiting species (Sillaginidae) in coastal waters." *Environmental Biology of Fishes* 45: 21-40.

Irving, A. D. and S. D. Connell 2006. "Predicting understorey structure from the presence and composition of canopies: an assembly rule for marine algae." *Oecologia* 148: 491-502.

Irving, A. D., S. D. Connell and B. M. Gillanders 2004. "Local complexity in patterns of canopy-benthos associations produces regional patterns across temperate Australia." *Marine Biology* 144: 361-368.

ITT Visual Information Solutions 2007. ENVI (Version 4.3). ITT Visual Information Solutions. Avaliable online @ http://www.ittvis.com

James, N. P., L. B. Collins, Y. Bone and P. Hallock 1999. "Carbonates in a temperate realm: modern sediments on the southwest Australian shelf." *Journal of Sedimentary Research* 69: 1297-1321.

Jarvis, R. M. and R. Goodacre 2005. "Genetic algorithym optimization for pre-processing and variable selection of spectroscopic data." *Bioinformatics* 21: 860-868.

Jenkins, G. P. and M. J. Wheatley 1998. "The influence of habitat structure on nearshore fish assemblages in a southern Australian embayment: Comparison of shallow seagrass, reef-algal and unvegetated sand habitats, with emphasis on

their importance to recruitment." *Journal of Experimental Marine Biology and Ecology* 221: 147-172.

Jenness, J. S. 2003. Statistical distributions and summary data extension for ArcView 3.x. Jenness Enterprises. Avaliable online @ http://www.jennessent.com

Jenness, J. S. 2005a. Directional slope extension for ArcView 3.x. Jenness Enterprises. Avaliable online @ http://www.jennessent.com

Jenness, J. S. 2005b. Repeating shapes extension for ArcView 3.x. Jenness Enterprises. Avaliable online @ http://www.jennessent.com

Jenness, J. S. 2006. Grid tools extension for ArcView 3.x. Jenness Enterprises. Avaliable online @ http://www.jennessent.com

Jerlov, N. G. 1976. Optical classification of ocean water. *IN: Physical aspects of light in the sea*. Honolulu, University of Hawaii Press 45-49 pp.

Jernakoff, P. and J. Nielsen 1998. "Plant-animal associations in two species of seagrasses in Western Australia." *Aquatic Botany* 60: 359-376.

Jernakoff, P. and B. F. Phillips 1988. "Effect of a baited trap on the foraging movements of juvenile Western Rock Lobsters, *Panulirus cygnus* George." *Australian Journal of Marine and Freshwater Research* 39: 185-192.

Jernakoff, P., B. F. Phillips and R. A. Maller 1987. "A quantitative study of nocturnal foraging distances of Western Rock Lobster *Panulirus cygnus* George." *Journal of Experimental Marine Biology and Ecology* 113: 9-21.

Johansson, G. and P. Snoeijs 2002. "Macroalgal photsynthetic response to light in relation to thallus morphology and depth zonation." *Marine Ecology Progress Series* 244: 63-72.

Johnson, M. P., N. J. Frost, M. W. J. Mosley, M. F. Roberts and S. J. Hawkins 2003. "The area-independent effects of habitat complexity on biodiversity vary between regions." *Ecology Letters* 6: 126-132.

Jones, D. S. and G. J. Morgan 1993. An annotated checklist of Crustacea from Rottnest Island, Western Australia. *The Marine Flora and Fauna of Rottnest Island, Western Australia*. F. Wells, D. I. Walker, H. Kirkman and R. Lethbridge. Perth, Western Australian Museum. 1 135-162 pp.

Jordan, A. R., M. Lawler, V. Halley and N. Barrett 2005. "Seabed habitat mapping in the Kent Group of islands and its role in marine protected area planning." *Aquatic Conservation: Marine and Freshwater Ecosystems* 15: 51-70.

Jordi, A., M. I. Ferrer, G. Vizoso, A. Orfila, G. Basterretxea, B. Casas, A. Alvarez, D. Roig, B. Garau, M. Martinez, V. Fernandez, A. Fornes, M. Ruiz, J. J. Fornos, P. Balaguer, C. M. Duarte, I. Rodriguez, E. Alvarez, R. Onken, P. Orfila and J. Tinore 2006. "Scientific management of Mediterranean coastal zone: a hybrid

ocean forecasting system for oil spill and search and rescue operations." *Marine Pollution Bulletin* 53: 361-368.

Joyce, K. E., S. R. Phinn, C. M. Roelfsema, D. T. Neil and W. C. Dennison 2004. "Combining Land ETM+ and Reef Check classifications for mapping coral reefs: a critical assessment for the southern Great Barrier Reef, Australia." *Coral Reefs* 23: 21-25.

Karpouzli, E., T. J. Malthus and C. J. Place 2004. "Hyperspectral discrimination of coral reef benthic communities in the western Caribbean." *Coral Reefs* 23: 141-151.

Kearney, M. 2006. "Habitat, environment and niche: what are we modelling?" *OIKOS* 115: 186-191.

Keddy, P. A. 1982. "Quantifying within lake gradients of wave energy: Interrelationships of wave energy, substrate particle size and shoreline plants in Axle Lake, Ontario." *Aquatic Botany* 14: 41-58.

Kendall, M. A., K. R. Buja, J. D. Christensen, C. R. Kruer and M. E. Monaco 2004. "The seascape approach to coral ecosystem mapping: an integral component of understanding the habitat utilization patterns of reef fish." *Bulletin of Marine Science* 75: 225-237.

Kendall, M. S., O. P. Jensen, C. F. Alexander, D., G. McFall, R. Bohne and M. E. Monaco 2005. "Benthic mapping using sonar, video transects, and an innovative approach to accuracy assessment: a characterization of bottom features in the Georgia Bight." *Journal of Coastal Research* 21: 1154-1165.

Kendrick, G. A. 1993. *Sargassum* beds at Rottnest Island: Species composition and abundance. *The Marine Flora and Fauna of Rottnest Island, Western Australia*. F. Wells, D. I. Walker, H. Kirkman and R. Lethbridge. Perth, Western Australian Museum. 2 455-472 pp.

Kendrick, G. A., E. S. Harvey, T. Wernberg, N. Harman and N. A. Goldberg 2004. "The role of disturbance in maintaining diversity of benthic macroalgal assemblages in southwestern Australia." *The Japanese Journal of Phycology* 52 (Supplement): 5-9.

Kendrick, G. A., P. Lavery and J. C. Phillips 1999. "Influence of *Ecklonia radiata* kelp canopy on structure of macro-algal assemblages in Marmion Lagoon, Western Australia." *Hydrobiologia* 398/399: 275-283.

Kennelly, S. J. 1987. "Physical disturbance in an Australian kelp community. II. Effects on the understorey species due to differences in kelp cover." *Marine Ecology Progress Series* 40: 155-165.

Kennelly, S. J. 1989. "Effects of kelp canopies on understorey species due to shade and scour." *Marine Ecology Progress Series* 50: 215-224.

Keshava, N. 2004. "Distance metrics and band selection in hyperspectral processing with applications to material identification and spectral libraries." *IEEE Transactions on Geoscience and Remote Sensing* 42: 1552-1565.

Kirk, J. T. O. 1976. "Yellow substance (Gelbstoff) and its contribution to the attenuation of photosynthetically active radiation in some inland and coastal south-eastern Australian waters." *Australian Journal of Marine and Freshwater Research* 27: 61-71.

Kirk, J. T. O. 1994a. "Estimation of the absorption and scattering coefficients of natural waters by use of underwater irradiance measurements." *Applied Optics* 33: 3276-3278.

Kirk, J. T. O. 1994b. *Light & photosynthesis in aquatic ecosystems*. Great Britain, Cambridge University Press. 509 pp.

Kirkman, H. 1996. "Baseline and monitoring methods for seagrass meadows." *Journal of Environmental Management* 47: 191-201.

Kirkman, H. 1997. Seagrasses of Australia. *Australia:State of the environment technical paper series (Estuaries and the Sea)*, Department of the Environment Canberra, 36 pp.

Klein, C. J., C. Steinback, A. J. Scholz and H. P. Possingham 2008. "Effectiveness of marine reserve networks in representing biodiversity and minimising impact to fisherman: a comparison of two approaches used in California." *Conservation Letters* 1(44-51).

Klonowski, W. M., P. R. C. S. Fearns and M. R. Lynch 2007. "Retrieving key benthic cover types and bathymetry from hyperspectral imagery." *Journal of Applied Remote Sensing* 1: 011505.

Kostylev, V. E., B. J. Todd, G. B. J. Fader, R. C. Courtney, G. D. M. Cameron and R. A. Pickrill 2001. "Benthic habitat mapping on the Scotian Shelf based on multibeam bathymetry, surficial geology and seafloor photographs." *Marine Ecology Progress Series* 219: 212-137.

Kravchenko, A. N. 2003. "Influence of spatial structure on accuracy of interpolation methods." *Soil Science Society of America Journal* 67: 1564-1571.

Kruse, F. A., J. W. Boardman, A. B. Lefkoff, J. M. Young, K. S. Kierein-Young, T. D. Cocks, R. Jenssen and P. A. Cocks 2000. HyMap: An Australian hyperspectral sensor solving global problems - results from USA HyMap data acquisitions. *10th Australiasian Remote Sensing and Photogrammetry Conference*, Adelaide. pp

Kutser, T., A. G. Dekker and W. Skirving 2003. "Modelling spectral discrimination of Great Barrier Reef benthic communities by remote sensing instruments." *Limnology and Oceanography* 48: 497-510.

Landgrebe, D. 2003. *Signal theory methods in multispectral remote sensing*. New York, Wiley-Interscience. 508 pp.

Lauer, M. and S. Aswani 2008. "Integrating indigenous ecological knowledge and multi-spectral image classification for marine habitat mapping in Oceania." *Ocean and Coastal Management* 51: 495-504.

Lavery, P. S. and M. A. Vanderklift 2002. "A comparison of spatial and temporal patterns in epiphytic macroalgae assemblages of the seagrass *Amphibolis griffithii* and *Posidinia coriacea*." *Marine Ecology Progress Series* 236: 99-112.

Lee, R. F. and D. S. Page 1997. "Petroleum hydrocarbons and their effects in subtidal regions after major oil spills." *Marine Pollution Bulletin* 34: 928-940.

Lee, Z., K. L. Carder, C. D. Mobley, R. G. Steward and J. S. Patch 1998. "Hyperspectral remote sensing for shallow waters. I. A semianalytical model." *Applied Optics* 37: 6329-6338.

Lee, Z., K. L. Carder, C. D. Mobley, R. G. Steward and J. S. Patch 1999. "Hyperspectral remote sensing for shallow waters: 2. Deriving bottom depths and water properties by optimization." *Applied Optics* 38: 3831-3843.

Lehmann, A. 1998. "GIS modelling of submerged macrophyte distribution using generalized additive models." *Plant Ecology* 139: 113-124.

Lehmann, A., J. M. Overton and J. R. Leathwick 2002. "GRASP: generalized regression analysis and spatial prediction." *Ecological Modelling* 157: 189-207.

Lemm, A. J., B. J. Hegge and G. Masselink 1999. "Offshore wave climate, Perth (Western Australia), 1994-96." *Journal of Marine and Freshwater Research* 50: 95-102.

Leslie, H., M. Ruckelshaus, I. R. Ball, S. Andelman and H. P. Possingham 2003. "Using siting algorithms in the design of marine reserve networks." *Ecological Applications* 13(Supplement 1): 185-198.

Lesser, M. P. and C. D. Mobley 2007. "Bathymetry, water optical properties, and benthic classification of coral reefs using hyperspectral remote sensing imagery." *Coral Reefs* 26: 819-829.

Li, Z. 1988. "On the measure of digital terrain model accuracy." *Photogrammetric Record* 12: 873-877.

Li, Z., Q. Zhu and C. Gold 2005. *Digital terrain modeling: principles and methodology*. Boca Raton, Florida, USA, CRC Press. 318 pp.

Lillesand, T. M., R. W. Kiefer and J. W. Chipman 2004. *Remote sensing and image interpretation*. USA, John Wiley & Sons. 763 pp.

Louchard, E. M., R. P. Reid, F. C. Stephens, C. O. Davis, R. A. Leathers and T. V. Downes 2003. "Optical remote sensing of benthic habitats and bathymetry in coastal environments at Lee Stocking Island, Bahamas: A comparative spectral classification approach." *Limnology and Oceanography* 48: 511-521.

Louchard, E. M., R. P. Reid, F. C. Stephens, C. O. Davis, R. A. Leathers, T. V. Downes and R. Maffione 2002. "Derivative analysis of absorption features in hyperspectral remote sensing data of carbonate sediments." *Optics Express* 10: 1573-1584.

Lucey, P., M. Winter, E. Winter and D. Steutel 2001. "Efficient materials mapping for hyperspectral data." *Proceedings of SPIE International Society of Optical Engineering* 4381: 164-172.

Lucieer, V. 2007. Morphometric characterisation of rocky reefs using multibeam acoustic bathymetric data. *Geoscience and Remote Sensing Symposium, 2007. IGARSS 2007.* , Barcelona, Spain, IEEE International. pp 905-909.

Lundqvist, D., D. Jansen, T. Balstroem and C. Christiansen 2006. "A GIS-based method to determine maximum fetch applied to the North Sea - Baltic Sea transition." *Journal of Coastal Research* 22: 640-644.

Lyzenga, D. R. 1978. "Passive remote sensing techniques for mapping water depth and bottom features." *Applied Optics* 17: 379-383.

Lyzenga, D. R. 1981. "Remote sensing of bottom reflectance and water attenuation parameters in shallow water using aircraft and Landsat data." *International Journal of Remote Sensing* 2: 71-82.

Ma, Z. and R. L. Redmond 1995. "*Tau* coefficients for accuracy assesment of classification of remote sensing data." *Photogrammetric Engineering and Remote Sensing* 61: 435-439.

MacArthur, L. D., G. A. Hyndes, R. C. Babcock and M. A. Vanderklift 2008. "Nocturnally active western rock lobsters Panulirus cygnus forage close to shallow coastal reefs " *Aquatic Biology* 4: 201-210.

Madsen, J. D., P. A. Chambers, W. F. James, E. W. Koch and D. F. Westlake 2001. "The interaction between water movement, sediment dynamics and submerged macrophytes." *Hydrobiologia* 444: 71-84.

Margules, C. R. and R. L. Pressey 2000. "Systematic conservation planning." *Nature* 405: 243-253.

Margules, C. R., R. L. Pressey and P. H. Williams 2002. "Representing biodiversity: data procedures for identifying priority areas for conservation." *Journal of Bioscience* 27: 309-326.

Marsh, L. M. and D. L. Pawson 1993. Echinoderms of Rottnest Island. *The Marine Flora and Fauna of Rottnest Island, Western Australia*. F. Wells, D. I. Walker, H. Kirkman and R. Lethbridge. Perth, Western Australian Museum. 1 279-304 pp.

Masselink, G. and C. B. Pattiaratchi 2001. "Characteristics of the sea breeze system in Perth, Western Australia, and its effect on the nearshore wave climate." *Journal of Coastal Research* 17(1): 173-187.

McClanahan, T. R. 1994. "Kenyan coral reef lagoon fish: effects of fishing, substrate complexity, and sea urchins." *Coral Reefs* 13: 231-241.

McCormick, M. I. 1994. "Comparison of field methods for measuring surface topography and their associations with a tropical reef fish assemblage." *Marine Ecology Progress Series* 112: 87-96.

McCune, B. and J. B. Grace 2002. *Analysis of ecological communities*. USA, MjM Software Design. 300 pp.

Meir, E., S. Andelman and H. P. Possingham 2004. "Does conservation planning matter in a dynamic and uncertain world?" *Ecology Letters* 7: 615-622.

Mellin, C., S. Andrefouet and D. Ponton 2007. "Spatial predictability of juvenile fish species richness and abundance in a coral reef environment." *Coral Reefs* 26: 895-907.

Melville, A. J. and S. D. Connell 2001. "Experimental effects of kelp canopies on subtidal coralline algae." *Austral Ecology* 26: 102-108.

Milazzo, M., F. Badalamenti, G. Ceccherelli and R. Chemello 2004. "Boat anchoring on *Posidonia oceanica* beds in a marine protected area (Italy, western Mediterranean): effects of anchor types in different anchoring stages." *Journal of Experimental Marine Biology and Ecology* 299: 51-62.

Minghelli-Roman, A., J. R. M. Chisholm, M. Marchioretti and J. Jaubert 2002. "Discrimination of coral reflectance spectra in the Red Sea." *Coral Reefs* 21: 307-314.

Minnesota Department of Natural Resources 2007. DNR Garmin extension for ArcView 3.x. Minnesota Department of Natural Resources. Avaliable online @ http://www.dnr.state.mn.us/mis/gis/tools/arcview/extensions/extensions.html

Mishra, D., S. Narumalani, D. Rundquist and M. Lawson 2006. "Benthic habitat mapping in tropical marine environments using Quickbird multispectral data." *Photogrammetric Engineering and Remote Sensing* 72: 1037-1048.

Mishra, D., R., S. Narumalani, D. Rundquist and M. Lawson 2005a. "Characterizing the vertical diffuse attenuation coefficient for downwelling irradiance in coastal

waters: Implications for water penetration by high resolution satellite data." *ISPRS Journal of Photogrammetry and Remote Sensing* 60: 48-64.

Mishra, D., R., S. Narumalani, D. Rundquist and M. Lawson 2005b. "High-resolution ocean color remote sensing of benthic habitats: a case study at Roatan Island, Honduras." *IEEE Transactions on Geoscience and Remote Sensing* 43: 1592-1604.

Moghimi, S., G. Gayer, H. Gunther and M. Shafieefar 2005. "Application of third generation shallow water wave models in a tidal environment." *Ocean Dynamics* 55: 10-27.

Morgan, G. J. and F. E. Wells 1991. "Zoogeographic provinces of the Humboldt, Benguela and Leeuwin Current systems." *Journal of the Royal Society of Western Australia* 74: 59-69.

Morris, L. and D. Ball 2006. "Habitat suitability modelling of economically important fish species with commercial fisheries data." *ICES Journal of Marine Science* 63: 1590-1603.

Mumby, P. J., C. D. Clarke, E. P. Green and A. J. Edwards 1998a. "Benefits of water column correction and contextual editing for mapping coral reefs." *International Journal of Remote Sensing* 19: 203-210.

Mumby, P. J. and A. J. Edwards 2002. "Mapping marine environments with IKONOS imagery: enhanced spatial resolution can deliver greater thematic accuracy." *Remote Sensing of Environment* 82: 248-257.

Mumby, P. J., E. P. Green, C. D. Clarke and A. J. Edwards 1998b. "Digital analysis of multispectral airborne imagery of coral reefs." *Coral Reefs* 17(59-69).

Mumby, P. J., E. P. Green, A. J. Edwards and C. D. Clarke 1997. "Coral reef habitat mapping: how much detail can remote sensing provide?" *Marine Biology* 130: 193-202.

Mumby, P. J., E. P. Green, A. J. Edwards and C. D. Clarke 1999. "The cost-effectiveness of remote sensing for tropical coastal resources assessment and management." *Journal of Environmental Management* 55: 157-166.

Mumby, P. J. and A. R. Harbourne 1999. "Development of a systematic classification scheme of marine habitats to facilitate regional management and mapping of Caribbean coral reefs." *Biological Conservation* 88: 155-163.

Murphy, N., G. Clapin, R. C. Babcock, A. Sampey, J. C. Phillips and M. Kleczkowski 2006. Spatial trends in reef invertebrate communities. *Strategic Fund for the Marine Environment Final Report. Volume 2: the SFRME core projects*. J. K. Keesing, J. N. Heine, R. C. Babcock, P. D. Craig and J. A. Koslow 215-220 pp.

Murphy, R. J., A. J. Underwood, M. H. Pinkerton and P. Range 2005. "Field spectrometry: New methods to investigate epilithic micro-algae on rocky shores." *Journal of Experimental Marine Biology and Ecology* 325: 111-124.

Nanami, A., M. Nishihira, T. Suzuki and H. Yokochi 2005. "Species-specific habitat distribution of coral reef fish assemblages in relation to habitat characteristics in an Okinawan coral reef." *Environmental Biology of Fishes* 72: 55-65.

Naoum, S. and I. K. Tsanis 2004. "Ranking spatial interpolation techniques using a GIS-based DSS." *Global Nest Journal* 6: 1-20.

Naseer, A. and B. G. Hatcher 2004. "Inventory of the Maldives' coral reefs using morphometrics generated from Landsat ETM+ imagery." *Coral Reefs* 23: 161-168.

National Oceans Office 2004. South-east regional marine plan, implementing Australia's oceans policy in the south-east marine region, National Oceans Office. 110 pp.

Nunez-Lara, E. and E. Arias-Gonzalez 1998. "The relationship between reef fish community structure and environmental variables in the southern Mexican Caribbean." *Journal of Fish Biology* 53: 209-221.

O'Hara, T. D. 2001. "Consistency of faunal and floral assemblages within temperate subtidal rocky reef habitats." *Journal of Marine and Freshwater Research* 52: 853-863.

O'Hara, T. D. and G. C. B. Poore 2000. "Patterns of distribution for southern Australian marine echinoderms and decapods." *Journal of Biogeography* 27: 1321-1335.

Okin, G. S., D. A. Roberts, B. Murray and W. J. Okin 2001. "Practical limits on hyperspectral vegetation discrimination in arid and semiarid environments." *Remote Sensing of Environment* 77: 212-225.

Olenin, S. and J. P. Ducrotoy 2006. "The concept of biotope in marine ecology and coastal management." *Marine Pollution Bulletin* 53: 29-29.

Ong, C., P. Hick, J. Burt and A. Wyllie 1998. "Marine habitat mapping using data from the Geoscan airborne multi-spectral scanner." *Geocarto International* 13: 27-34.

Orth, R. J., K. L. Heck and J. van Montfrans 1984. "Faunal communities in seagrass beds: a review of the influence of plant structure and prey characteristics on predator-prey relationships." *Estuaries* 7: 339-350.

Palacios-Orueta, A. and S. L. Ustin 1998. "Remote sensing of soil properties in the Santa Monica mountains I. spectral analysis." *Remote Sensing of Environment* 65: 170-183.

Parry, D. M., M. A. Kendall, D. A. Pilgrim and M. B. Jones 2003. "Identification of patch structure within marine benthic landscapes using a remotely operated

vehicle." *Journal of Experimental Marine Biology and Ecology* 285-286: 497-511.

Pattiaratchi, C. B., B. J. Hegge, J. Gould and I. Eliot 1997. "Impact of sea-breeze activity on nearshore and foreshore processes in south-western Australia." *Continental Shelf Research* 17: 1539-1560.

Pearce, A. 1991. "Eastern boundary currents of the southern hemisphere." *Journal of the Royal Society of Western Australia* 74: 35-45.

Pearce, A. and C. B. Pattiaratchi 1999. "The Capes Current: a summer countercurrent flowing past Cape Leeuwin and Cape Naturaliste, Western Australia." *Continental Shelf Research* 19: 401-420.

Pearce, A., M. Rossbach, M. Tait and R. Brown 1999. Sea temperature variability of Western Australia 1990 to 1994. Fisheries Research Report No. 111, Fisheries Western Australia. Perth, Western Australia, 45 pp.

Peterson, C. H., S. D. Rice, J. W. Short, D. Esler, J. L. Bodkin, B. E. Ballachey and D. B. Irons 2003. "Long-term ecosystem response to the Exxon Valdez oil spill." *Science* 302: 2082-2086.

Phillips, J. C., R. C. Babcock, N. Murphy, G. Clapin, A. Sampey, M. Kleczkowski and M. Westera 2006. Spatial variation in reef algal community structure. *Strategic Fund for the Marine Environment Final Report. Volume 2: the SFRME core projects*. J. K. Keesing, J. N. Heine, R. C. Babcock, P. D. Craig and J. A. Koslow 166-183 pp.

Phillips, J. C., G. A. Kendrick and P. S. Lavery 1997. "A test of a functional group approach to detecting shifts in macroalgal communities along a disturbance gradient." *Marine Ecology Progress Series* 153: 125-138.

Playford, P. E. and R. E. J. Leech 1977. "Geology and hydrology of Rottnest Island." *Geological Survey of Western Australia* Report 6.

Pope, R. and E. Fry 1997. "Absorption spectrum (380 - 700 nm) of pure water. II Integrating cavity measurements." *Applied Optics* 36: 8710-8723.

Prince, J. 1995. "Limited effects of the sea urchin *Echinometra mathaei* (de Blainville) on the recruitment of benthic algae and macroinvertebrates into intertidal rock platforms at Rottnest Island, Western Australia." *Journal of Experimental Marine Biology and Ecology* 186: 237-258.

Purkis, S. J., J. A. Kenter, E. K. Oikonomou and I. S. Robinson 2002. "High-resolution ground verification, cluster analysis and optical model of reef substrate coverage on Landsat TM imagery (Red Sea, Egypt)." *International Journal of Remote Sensing* 23: 1677-1698.

Purkis, S. J. and R. Pasterkamp 2004. "Integrating *in situ* reef-top reflectance spectra with Landsat TM imagery to aid shallow-tropical benthic habitat mapping." *Coral Reefs* 23: 5-20.

Richardson, A. D., S. P. Duigan and G. P. Berlyn 2002. "An evaluation of noninvasive methods to estimate foliar chlorophyll content." *New Phytologist* 153: 185-194.

Ridgway, K. R. and S. A. Condie 2004. "The 5500-km-long boundary flow off western and southern Australia." *Journal of Geophysical Research* 109: C04017, doi:1029/2003JC001921.

Robila, S. A. 2005. "Using spectral distances for speedup in hyperspectral image processing." *International Journal of Remote Sensing* 26: 5629-5650.

Robila, S. A. and A. Gershman 2005. "Spectral matching accuracy in processing hyperspectral data." *IEEE Transactions on Geoscience and Remote Sensing* 1: 163-166.

Rodrigues, A. S. L. and T. M. Brooks 2007. "Shortcuts for biodiversity conservation planning: the effectiveness of surrogates." *Annual Review of Ecology, Evolution, and Systematics* 38: 713-737.

Rottnest Island Authority 2003. Rottnest Island Management Plan 2003-2008, Rottnest Island Management Authority. Perth, Western Australia, 128 pp.

Rottnest Island Authority 2007. Rottnest Island marine management strategy, Rottnest Island Authority. Perth, Western Australia, 25 pp.

Rouphael, A. B. and G. J. Inglis 2002. "Increased spatial and temporal variability in coral damage caused by recreational SCUBA diving." *Ecological Applications* 12: 427-440.

RSI 2004. *ENVI users guide (ENVI Version 4.1)*, Reseach Systems Incorporated. pp.

RSI 2005. ENVI 4.2. Reseach Systems Incorporated. Avaliable online @ http://ittvis.com

Rueda, C. A., J. A. Greenberg and S. L. Ustin 2005. StarSpan: A Tool for Fast Selective Pixel Extraction from Remotely Sensed Data. University of California at Davis. Avaliable online @ http://starspan.casil.ucdavis.edu

Ruuskanen, A., S. Back and T. Reitalu 1999. "A comparison of two cartographic exposure methods using *Fucus vesiculosus* as an indicator." *Marine Biology* 134: 139-145.

Sanderson, J. C. 1997. Subtidal macroalgae assemblages in temperate Australian coastal waters. Australia: State of the Environment Technical Paper Series (Estuaries and the Sea), Department of the Environment. Canberra, 129 pp.

Sanderson, P. G., I. Eliot, B. J. Hegge and S. Maxwell 2000. "Regional variation of coastal morphology in southwestern Australia: a synthesis." *Geomorphology* 34: 73-88.

Sarkar, S. and C. R. Margules 2002. "Operationalizing biodiversity for conservation planning." *Journal of Bioscience* 27: 299-308.

Sarkar, S., R. L. Pressey, D. P. Faith, C. R. Margules, T. Fuller, D. M. Stoms, A. Moffett, K. A. Wilson, K. J. Williams, P. H. Williams and S. Andelman 2006. "Biodiversity conservation planning tools: present status and challenges for the future." *Annual Review of Environmental Resources* 31: 123-159.

Savitzky, A. and M. J. E. Golay 1964. "Smoothing and differentiation of data by simplified least squares procedures." *Analytical Chemistry* 36: 1627-1639.

Scheibling, R. E. 1994. "Molluscan grazing and macroalgae zonation on a rocky intertidal platform at Perth, Western Australia " *Australian Journal of Ecology* 19: 141-149.

Schiel, D. R. 1988. "Algal interactions on shallow subtidal reefs in northern New Zealand: a review." *New Zealand Journal of Marine and Freshwater Research* 22: 481-489.

Schwarz, A.-M., C. Howard-Williams and J. Clayton 2000. "Analysis of relationships between maximum depth limits of aquatic plants and underwater light in 63 New Zealand lakes." *New Zealand Journal of Marine and Freshwater Research* 34: 157-174.

Schweizer, D., R. A. Armstrong and J. Posada 2005. "Remote sensing characterization of benthic habitats and submerged vegetation biomass in Los Roques Archipelago National Park, Venezuela." *International Journal of Remote Sensing* 26: 2657-2667.

Searle, D. J. and V. Semeniuk 1985. "The natural sectors of the Inner Rottnest Shelf coast adjoining the Swan Coastal Plain." *Journal of the Royal Society of Western Australia* 67: 116-136.

Shears, N. T., R. C. Babcock, C. A. J. Duffy and J. W. Walker 2004. "Validation of qualitative habitat descriptors commonly used to classify subtidal reef assemblages in north-eastern New Zealand." *New Zealand Journal of Marine and Freshwater Research* 38: 743-752.

Shepherd, K. D. and M. G. Walsh 2002. "Development of reflectance spectral libraries for characterization of soil properties." *Soil Science Society of America Journal* 66: 988-998.

Sibson, R. 1981. A brief description of natural neighbour interpolation. *Interpreting Multivariate Data*. V. Barnett. New York, John Wiley and Sons 21-36 pp.

Sims, D. A. and J. A. Gamon 2002. "Relationships between leaf pigment content and spectral reflectance across a wide range of species, leaf structures and development stages." *Remote Sensing of Environment* 81: 337-354.

Slaton, M. R., E. R. Hunt and W. K. Smith 2001. "Estimating near-infrared leaf reflectance from leaf structural characteristics." *American Journal of Botany* 88: 278-284.

Small, C. and J. W. T. Lu 2006. "Estimation and vicarious validation of urban vegetation abundance by spectral mixture analysis." *Remote Sensing of Environment* 100: 441-456.

Smallwood, C. B., L. E. Beckley and N. R. Sumner 2006. "Shore-based recreational angling in the Rottnest Island Reserve, Western Australia: spatial and temporal distribution of catch and fishing effort." *Pacific Conservation Biology* 12: 238-251.

Sotheran, I. S., R. L. Foster-Smith and J. Davies 1997. "Mapping of marine benthic habitats using image processing techniques within a raster-based geographic information system." *Estuarine, Coastal and Shelf Science* 44(Supplement A): 25-31.

Southwood, T. R. E. 1977. "Habitat, the templet for ecological strategies?" *Journal of Animal Ecology* 46: 337-365.

Steneck, R. S. and M. N. Dethier 1994. "A functional group approach to the structure of algal-dominated communities." *OIKOS* 69: 476-498.

Steneck, R. S., M. H. Graham, B. J. Bourque, D. Corbett, J. M. Erlandson, J. A. Estes and M. J. Tegner 2002. "Kelp forest ecosystems: biodiversity, stability, resilience and future." *Environmental Conservation* 29: 436-459.

Stevens, T. 2002. "Rigor and representativeness in marine protected area design." *Coastal Management* 30: 237-248.

Stevens, T. and R. M. Connolly 2004. "Testing the utility of abiotic surrogates for marine habitat mapping at scales relevant to management." *Biological Conservation* 119: 351-362.

Stevens, T. and R. M. Connolly 2005. "Local-scale mapping of benthic habitats to assess representation in marine protected areas." *Journal of Marine and Freshwater Research* 56: 111-123.

Story, M. and R. G. Congalton 1986. "Accuracy assesment: a user's perspective." *Photogrammetric Engineering and Remote Sensing* 52: 397-399.

Taniguchi, H. and M. Tokeshi 2004. "Effect of habitat complexity on benthic assemblages in a variable environment." *Freshwater Biology* 49: 1164-1178.

Tassan, S. 1996. "Modified Lyzenga's method for macroalgae detection in water with non-uniform composition." *International Journal of Remote Sensing* 17: 1601-1607.

Thorhaug, A., A. D. Richardson and G. P. Berlyn 2006. "Spectral reflectance of *Thalassia testudinum* (Hydrocharitaceae) segrass: low salinity affects." *American Journal of Botany* 93: 110-117.

Thorhaug, A., A. D. Richardson and G. P. Berlyn 2007. "Spectral reflectance of the seagrasses: *Thalassia testudinum*, *Halodule wrightii*, *Syringodium filiforme* and five marine algae." *International Journal of Remote Sensing* 28: 1487-1501.

Toohey, B., G. A. Kendrick, T. Wernberg, J. C. Phillips, S. Malkin and J. Prince 2004. "The effects of light and thallus scour from *Ecklonia radiata* canopy on an associated foliose algal assemblage: the importance of photoacclimation." *Marine Biology* 144: 1019-1027.

Toohey, B. D. 2007. "The relationship between physical variables on topographically simple and complex reefs and algal assemblage structure beneath an *Ecklonia radiata* canopy." *Estuarine, Coastal and Shelf Science* 71: 232-240.

Toohey, B. D., G. A. Kendrick and E. S. Harvey 2007. "Disturbance and reef topography maintain high local diversity in *Ecklonia radiata* kelp forests." *OIKOS* 116: 1618-1630.

Trautman, D. A. and M. A. Borowitzka 1999. "Distribution of the epiphytic organisms on *Posidonia australis* and *P. sinuosa*, two seagrasses with differing leaf morphology." *Marine Ecology Progress Series* 179: 215-229.

Underwood, A. J. and M. G. Chapman 1998. "Spatial analysis of intertidal assemblages on sheltered rocky shores." *Australian Journal of Ecology* 23: 138-157.

Underwood, A. J. and S. J. Kennelly 1990. "Ecology of marine algae on rocky shores and subtidal reefs in temperate Australia." *Hydrobiologia* 192: 3-20.

Underwood, A. J., M. J. Kingsford and N. L. Andrew 1991. "Patterns in shallow subtidal marine assemblages along the coast of New South Wales." *Australian Journal of Ecology* 6: 231-249.

United Nations 1993. "Convention on biological diversity." *United Nations - Treaty Series* 1760: 142-169.

Vanderklift, M. A. and G. A. Kendrick 2004. "Variation in abundance of herbivorous invertebrates in temperate subtidal rocky reef habitats." *Marine and Freshwater Research* 55: 93-103.

Vanderklift, M. A., T. J. Ward and J. C. Phillips 1998. "Use of assemblages derived from different taxonomic levels to select areas for conserving marine biodiversity." *Biological Conservation* 86: 307-315.

Vernon, J. E. N. and L. M. Marsh 1988. "Hermatypic corals of Western Australia." *Records of the Western Australian Museum* Supplement 29: 1-136.

Walker, B. K., B. Riegl and R. E. Dodge 2008. "Mapping coral reef habitats in southest Florida using a combined technique approach." *Journal of Coastal Research* 24: 1138-1150.

Ward, T. J., M. A. Vanderklift, A. O. Nicholls and R. A. Kenchington 1999. "Selecting marine reserves using habitats and species assemblages as surrogates for biological diversity." *Ecological Applications* 9: 691-698.

Wells, F. and D. I. Walker 1993. Introduction to the marine environment of Rottnest Island, Western Australia. *The Marine Flora and Fauna of Rottnest Island, Western Australia*. F. Wells, D. I. Walker, H. Kirkman and R. Lethbridge. Perth, Western Australian Museum. 1 1-10 pp.

Werdell, P. J. and C. S. Roesler 2003. "Remote assessment of benthic substrate composition in shallow waters using multispectral reflectance." *Limnology and Oceanography* 48: 557-567.

Wernberg, T., M. Coleman, A. Fairhead, S. Miller and M. Thomsen 2003a. "Morphology of *Ecklonia radiata* (Phaeophyta: Laminarales) along its geographic distribution in south-western Australia and Australasia." *Marine Biology* 143: 47-55.

Wernberg, T., G. A. Kendrick and J. C. Phillips 2003b. "Regional differences in kelp-associated assemblages on temperate limestone reefs in south-western Australia." *Diversity and Distributions* 9: 427-441.

Wernberg, T., G. A. Kendrick and B. D. Toohey 2005. "Modification of the physical environment by an *Ecklonia radiata* (Laminariales) canopy and implications for associated foliose algae." *Aquatic Ecology* 39: 419-430.

White, W. H., A. R. Harbourne, I. S. Sotheran, R. Walton and R. L. Forster-Smith 2003. "Using an acoustic ground discrimination system to map coral reef benthic classes." *International Journal of Remote Sensing* 24: 2641-2660.

Wildsmith, M., M. Harvey, F. J. Valesini, A. McDonald and A. Bivoltis 2008. Classifying shallow water benthic habitats in the Swan Marine Region. Final Report. Project 01-0608-HM, Centre for Fish and Fisheries Research, Murdoch University. Perth, Western Australia, 60 pp.

Wiley, E. O., K. M. McNyset, A. T. Peterson, C. R. Robins and A. M. Stewart 2003. "Niche modeling and geographic range predictions in the marine environment using a machine-learning algorithm." *Oceanography* 16: 120-127.

Womersley, H. B. S. and S. J. Edmonds 1952. "Marine coastal zonation in southern Australia in relation to a general scheme of classification." *The Journal of Ecology* 40: 84-90.

Wu, J. 1999. "Hierarchy and scaling: extrapolating information along a scaling ladder." *Canadian Journal of Remote Sensing* 25: 367-380.

Wu, J. and J. L. David 2002. "A spatially explicit hierarchical approach to modelling complex ecological systems: theory and applications." *Ecological Modelling* 153: 7-26.

Zar, J. H. 1999. *Biostatistical Analysis*. United States of America, Prentice Hall. 663 pp.

Zevenbergen, L. W. and C. R. Thorne 1987. "Qualitative analysis of land surface topography." *Earth Surface Processes and Landforms* 12: 47-56.

Zhang, J., B. Rivard and A. Sanchez-Azofeifa 2005. "Spectral unmixing of normalized reflectance data for the deconvolution of lichen and rock mixtures." *Remote Sensing of Environment* 95: 57-66.

Zhilin, L., Q. Zhu and C. Gold 2005. *Digital terrain modelling: principles and methodology*. USA, CRC Press. 318 pp.

Zurita, S. M. 2004. Marine protected area control site suitability analysis based on geomorphic interpretation of multibeam bathymetry data using GIS, Faculty of Earth Systems Science and Policy, California State University. Montery Bay, 33 pp.

Appendix 1: Spectral separation analysis results

Bare substrate/Bio-substrate

Table 0-1: Results of genetic algorithm optimisation for the best bands and spectral metric to separate the spectral signatures at Level 1 of the classification scheme (bare substrate/bio-substrate). The optimal result for each spectral metric is highlighted.

Spectral metric		Bands tested	Optimal bands	'R' statistic	p-value
SA –	Optimal	1 - 17	4, 17	0.683745	<0.001
	1	1 – 17	4, 17	0.683745	<0.001
	2	1 – 17	4, 10, 11	0.632195	<0.001
	3	1 – 17	4, 17	0.683745	<0.001
	4	1 – 17	4, 17	0.683745	<0.001
	5	1 – 17	4, 17	0.683745	<0.001
SCA –	Optimal	1 - 17	4, 15, 17	0.935240	<0.001
	1	1 – 17	4, 15, 17	0.935240	<0.001
	2	1 – 17	4, 15, 17	0.935240	<0.001
	3	1 – 17	4, 15, 17	0.935240	<0.001
	4	1 – 17	4, 15, 17	0.935240	<0.001
	5	1 – 17	4, 15, 17	0.935240	<0.001
SGA –	Optimal	1 - 17	1, 3	0.654422	<0.001
	1	1 – 17	1, 3	0.654422	<0.001
	2	1 – 17	1, 15	0.637712	<0.001
	3	1 – 17	1, 3	0.654422	<0.001
	4	1 – 17	1, 3	0.654422	<0.001
	5	1 – 17	1, 5, 6	0.623895	<0.001
SID –	Optimal	1 - 17	4, 17	0.497661	<0.001
	1	1 – 17	4, 10, 11	0.478181	<0.001
	2	1 – 17	4, 10, 11	0.478181	<0.001
	3	1 – 17	4, 17	0.497661	<0.001
	4	1 – 17	4, 10, 11	0.478181	<0.001
	5	1 – 17	4, 10, 11	0.478181	<0.001
SID(TAN) –	Optimal	1 - 17	16, 17	0.651613	<0.001
	1	1 – 17	16, 17	0.651613	<0.001
	2	1 – 17	4, 10, 11	0.530407	<0.001
	3	1 – 17	16, 17	0.651613	<0.001
	4	1 – 17	4, 10, 11	0.530407	<0.001
	5	1 – 17	4, 10, 11	0.530407	<0.001
SID(SIN) –	Optimal	1 - 17	4, 10, 11	0.528787	<0.001
	1	1 – 17	4, 10, 11	0.528787	<0.001
	2	1 – 17	4, 10, 11	0.528787	<0.001
	3	1 – 17	4, 10, 11	0.528787	<0.001
	4	1 – 17	4, 10, 11	0.528787	<0.001
	5	1 – 17	4, 10, 11	0.528787	<0.001

Table 0-2: Results of genetic algorithm optimisation for the best bands and spectral metric to separate the spectral signatures at Level 1 of the classification scheme (bare substrate vs bio-substrate). The optimal result for each spectral metric is highlighted.

Spectral metric		Bands tested	Optimal bands	'R' statistic	p-value
SA –	Optimal	1 - 9	4, 9	0.465046	<0.001
	1	1 - 9	4, 9	0.465046	<0.001
	2	1 - 9	4, 9	0.465046	<0.001
	3	1 - 9	4, 9	0.465046	<0.001
	4	1 - 9	4, 9	0.465046	<0.001
	5	1 - 9	4, 9	0.465046	<0.001
SCA –	Optimal	1 - 9	1, 2, 3, 9	0.805661	<0.001
	1	1 - 9	1, 2, 3, 9	0.805661	<0.001
	2	1 - 9	1, 2, 3, 9	0.805661	<0.001
	3	1 - 9	1, 2, 3, 9	0.805661	<0.001
	4	1 - 9	1, 2, 3, 9	0.805661	<0.001
	5	1 - 9	1, 2, 3, 9	0.805661	<0.001
SGA –	Optimal	1 - 9	1, 3	0.654422	<0.001
	1	1 - 9	1, 3	0.654422	<0.001
	2	1 - 9	1, 3	0.654422	<0.001
	3	1 - 9	1, 3	0.654422	<0.001
	4	1 - 9	1, 3	0.654422	<0.001
	5	1 - 9	1, 3	0.654422	<0.001
SID –	Optimal	1 - 9	4, 5	0.376518	<0.001
	1	1 - 9	4, 5	0.376518	<0.001
	2	1 - 9	4, 5	0.376518	<0.001
	3	1 - 9	4, 5	0.376518	<0.001
	4	1 - 9	4, 5	0.376518	<0.001
	5	1 - 9	4, 5	0.376518	<0.001
SID(TAN) –	Optimal	1 - 9	4, 9	0.385004	<0.001
	1	1 - 9	4, 9	0.385004	<0.001
	2	1 - 9	4, 9	0.385004	<0.001
	3	1 - 9	4, 9	0.385004	<0.001
	4	1 - 9	4, 9	0.385004	<0.001
	5	1 - 9	4, 9	0.385004	<0.001
SID(SIN) –	Optimal	1 - 9	4, 9	0.383069	<0.001
	1	1 - 9	4, 9	0.383069	<0.001
	2	1 - 9	4, 9	0.383069	<0.001
	3	1 - 9	4, 9	0.383069	<0.001
	4	1 - 9	4, 9	0.383069	<0.001
	5	1 - 9	4, 9	0.383069	<0.001

Macroalgae/Seagrass/Coral

Table 0-3: Results of the spectral separation analysis carried out using a genetic algorithm to determine the optimum band combination to separate between macroalgae, seagrass and coral dominated habitats for each spectral metric. Each test was carried out five times using 74 spectral signatures for the library and using HyMap bands 1 – 17. The optimal result for each spectral metric is highlighted.

Spectral metric		Bands tested	Optimal bands	'R' statistic	p-value
SA –	Optimal	1 - 17	4, 6, 10, 11	0.684107	<0.001
	1	1 – 17	4, 6, 10, 11	0.684107	<0.001
	2	1 – 17	4, 6, 10, 11	0.684107	<0.001
	3	1 – 17	4, 6, 10, 11	0.684107	<0.001
	4	1 – 17	4, 6, 10, 11	0.684107	<0.001
	5	1 – 17	4, 6, 10, 11	0.684107	<0.001
SCA –	Optimal	1 – 17	4, 6, 9	0.844120	<0.001
	1	1 – 17	4, 6, 9	0.844120	<0.001
	2	1 – 17	4, 6, 9	0.844120	<0.001
	3	1 – 17	4, 6, 9	0.844120	<0.001
	4	1 – 17	4, 6, 9	0.844120	<0.001
	5	1 – 17	4, 6, 9	0.844120	<0.001
SGA –	Optimal	1 – 17	1, 2	0.152039	0.001
	1	1 – 17	1, 2	0.152039	0.001
	2	1 – 17	1, 2	0.152039	0.001
	3	1 – 17	15, 16	0.062563	0.100
	4	1 – 17	1, 2	0.152039	0.001
	5	1 – 17	1, 2	0.152039	0.001
SID –	Optimal	1 – 17	4, 6, 10, 11	0.603431	<0.001
	1	1 – 17	4, 6, 10, 11	0.603431	<0.001
	2	1 – 17	4, 6, 10, 11	0.603431	<0.001
	3	1 – 17	4, 6, 10, 11	0.603431	<0.001
	4	1 – 17	4, 6, 10, 11	0.603431	<0.001
	5	1 – 17	4, 6, 10, 11	0.603431	<0.001
SID(TAN) –	Optimal	1 – 17	4, 6, 10, 11	0.634592	<0.001
	1	1 – 17	4, 6, 10, 11	0.634592	<0.001
	2	1 – 17	4, 6, 10, 11	0.634592	<0.001
	3	1 – 17	4, 6, 10, 11	0.634592	<0.001
	4	1 – 17	4, 6, 10, 11	0.634592	<0.001
	5	1 – 17	4, 6, 10, 11	0.634592	<0.001
SID(SIN) –	Optimal	1 – 17	4, 6, 10, 11	0.633844	<0.001
	1	1 – 17	4, 6, 10, 11	0.633844	<0.001
	2	1 – 17	4, 6, 10, 11	0.633844	<0.001
	3	1 – 17	4, 6, 10, 11	0.633844	<0.001
	4	1 – 17	4, 6, 10, 11	0.633844	<0.001
	5	1 – 17	4, 6, 10, 11	0.633844	<0.001

Table 0-4: Results of genetic algorithm optimisation for the best bands and spectral metric to separate the spectral signatures at Level 2 of the classification scheme

Spectral metric		Bands tested	Optimal bands	'R' statistic	p-value
SA –	Optimal	1 – 9	7, 9	0.647195	<0.001
	1	1 – 9	7, 9	0.647195	<0.001
	2	1 – 9	7, 9	0.647195	<0.001
	3	1 – 9	7, 9	0.647195	<0.001
	4	1 – 9	7, 9	0.647195	<0.001
	5	1 – 9	7, 9	0.647195	<0.001
SCA –	Optimal	1 – 9	4, 6, 9	0.844120	<0.001
	1	1 – 9	4, 6, 9	0.844120	<0.001
	2	1 – 9	4, 6, 9	0.844120	<0.001
	3	1 – 9	4, 6, 9	0.844120	<0.001
	4	1 – 9	4, 6, 9	0.844120	<0.001
	5	1 – 9	4, 6, 9	0.844120	<0.001
SGA –	Optimal	1 – 9	1, 2	0.152039	<0.001
	1	1 – 9	1, 2	0.152039	<0.001
	2	1 – 9	1, 2	0.152039	<0.001
	3	1 – 9	1, 2	0.152039	0.001
	4	1 – 9	1, 2	0.152039	<0.001
	5	1 – 9	1, 2	0.152039	<0.001
SID –	Optimal	1 – 9	7, 9	0.620409	<0.001
	1	1 – 9	7, 9	0.620409	<0.001
	2	1 – 9	7, 9	0.620409	<0.001
	3	1 – 9	7, 9	0.620409	<0.001
	4	1 – 9	7, 9	0.620409	<0.001
	5	1 – 9	7, 9	0.620409	<0.001
SID(TAN) –	Optimal	1 – 9	7, 9	0.629725	<0.001
	1	1 – 9	7, 9	0.629725	<0.001
	2	1 – 9	7, 9	0.629725	<0.001
	3	1 – 9	7, 9	0.629725	<0.001
	4	1 – 9	7, 9	0.629725	<0.001
	5	1 – 9	7, 9	0.629725	<0.001
SID(SIN) –	Optimal	1 – 9	7, 9	0.629528	<0.001
	1	1 – 9	7, 9	0.629528	<0.001
	2	1 – 9	7, 9	0.629528	<0.001
	3	1 – 9	7, 9	0.629528	<0.001
	4	1 – 9	7, 9	0.629528	<0.001
	5	1 – 9	7, 9	0.629528	<0.001

Canopy/Algal turf

Table 0-5: Results of the spectral separation analysis carried out using a genetic algorithm to determine the optimum band combination to separate between canopy and turf algae dominated habitats for each spectral metric. Each test was carried out five times using 42 spectral signatures for the library and using HyMap bands 1 – 17. The optimal result for each spectral metric is highlighted.

Spectral metric		Bands tested	Optimal bands	'R' statistic	p-value
SA –	Optimal	1 - 17	6, 8	0.785458	<0.001
	1	1 – 17	6, 8	0.785458	<0.001
	2	1 – 17	5 , 6, 8, 9	0.756628	<0.001
	3	1 – 17	5 , 9	0.753422	<0.001
	4	1 – 17	5 , 6, 8, 9	0.756628	<0.001
	5	1 – 17	6, 8	0.785458	<0.001
SCA –	Optimal	1 – 17	1, 6, 8	0.712286	<0.001
	1	1 – 17	1, 5, 6, 8, 9, 15	0.633274	<0.001
	2	1 – 17	1, 5, 6, 8, 9, 15	0.633274	<0.001
	3	1 – 17	1, 5, 6, 8, 9, 15	0.633274	<0.001
	4	1 – 17	1, 6, 8	0.712286	<0.001
	5	1 – 17	1, 6, 8	0.712286	<0.001
SGA –	Optimal	1 – 17	6, 14	0.138973	<0.001
	1	1 – 17	6, 14	0.138973	<0.001
	2	1 – 17	1, 4, 5, 6, 14	0.130316	<0.001
	3	1 – 17	6, 14	0.138973	<0.001
	4	1 – 17	6, 14	0.138973	<0.001
	5	1 – 17	6, 14	0.138973	<0.001
SID –	Optimal	1 – 17	6, 7, 8	0.782868	<0.001
	1	1 – 17	5, 6, 8, 9	0.744517	<0.001
	2	1 – 17	5, 6, 8, 9	0.744517	<0.001
	3	1 – 17	6, 8	0.773563	<0.001
	4	1 – 17	5, 6, 8, 9	0.744517	<0.001
	5	1 – 17	6, 7, 8	0.782868	<0.001
SID(TAN) –	Optimal	1 – 17	6, 7, 8	0.786376	<0.001
	1	1 – 17	5, 6, 8, 9	0.751705	<0.001
	2	1 – 17	5, 6, 8, 9	0.751705	<0.001
	3	1 – 17	5, 6, 8, 9	0.751705	<0.001
	4	1 – 17	6, 7, 8	0.786376	<0.001
	5	1 – 17	6, 7, 8	0.786376	<0.001
SID(SIN) –	Optimal	1 – 17	6, 7, 8	0.786343	<0.001
	1	1 – 17	6, 7, 8	0.786343	<0.001
	2	1 – 17	5, 6, 8, 9	0.751965	<0.001
	3	1 – 17	6, 7, 8	0.786343	<0.001
	4	1 – 17	5, 6, 8, 9	0.751965	<0.001
	5	1 – 17	5, 6, 8, 9	0.751965	<0.001

Table 0-6: Results of the spectral separation analysis carried out using a genetic algorithm to determine the optimum band combination to separate between canopy and turf algae dominated habitats for each spectral metric. Each test was carried out five times using 42 spectral signatures for the library and using HyMap bands 1 – 9. The optimal result for each spectral metric is highlighted.

Spectral metric		Bands tested	Optimal bands	'R' statistic	p-value
SA –	Optimal	1 – 9	6, 7, 8	0.792431	<0.001
	1	1 – 9	6, 7, 8	0.792431	<0.001
	2	1 – 9	6, 7, 8	0.792431	<0.001
	3	1 – 9	6, 7, 8	0.792431	<0.001
	4	1 – 9	6, 7, 8	0.792431	<0.001
	5	1 – 9	6, 7, 8	0.792431	<0.001
SCA –	Optimal	1 – 9	4,5,9	0.733485	<0.001
	1	1 – 9	4,5,9	0.733485	<0.001
	2	1 – 9	4,5,9	0.733485	<0.001
	3	1 – 9	4,5,9	0.733485	<0.001
	4	1 – 9	4, 7, 8	0.714110	<0.001
	5	1 – 9	4, 7, 8	0.714110	<0.001
SGA –	Optimal	1 – 9	1, 2	0.074004	<0.05
	1	1 – 9	1, 2	0.074004	<0.05
	2	1 – 9	1, 2	0.074004	<0.05
	3	1 – 9	1, 2	0.074004	<0.05
	4	1 – 9	1, 2	0.074004	<0.05
	5	1 – 9	1, 2	0.074004	<0.05
SID –	Optimal	1 – 9	6, 7, 8	0.782868	<0.001
	1	1 – 9	6, 7, 8	0.782868	<0.001
	2	1 – 9	6, 7, 8	0.782868	<0.001
	3	1 – 9	6, 7, 8	0.782868	<0.001
	4	1 – 9	6, 7, 8	0.782868	<0.001
	5	1 – 9	6, 7, 8	0.782868	<0.001
SID(TAN) –	Optimal	1 – 9	6, 7, 8	0.786376	<0.001
	1	1 – 9	6, 7, 8	0.786376	<0.001
	2	1 – 9	6, 7, 8	0.786376	<0.001
	3	1 – 9	6, 7, 8	0.786376	<0.001
	4	1 – 9	6, 7, 8	0.786376	<0.001
	5	1 – 9	6, 7, 8	0.786376	<0.001
SID(SIN) –	Optimal	1 – 9	6, 7, 8	0.786343	<0.001
	1	1 – 9	6, 7, 8	0.786343	<0.001
	2	1 – 9	6, 7, 8	0.786343	<0.001
	3	1 – 9	6, 7, 8	0.786343	<0.001
	4	1 – 9	6, 7, 8	0.786343	<0.001
	5	1 – 9	6, 7, 8	0.786343	<0.001

Posidonia/Amphibolis

Table 0-7: Results of the spectral separation analysis carried out using a genetic algorithm to determine the optimum band combination to separate between *Posidonia* and *Amphibolis* dominated habitats for each spectral metric. Each test was carried out five times using 24 spectral signatures for the library and using HyMap bands 1 – 17. The optimal result for each spectral metric is highlighted.

Spectral metric		Bands tested	Optimal bands	'R' statistic	p-value
SA –	Optimal	1 - 17	13, 15	0.472842	<0.001
	1	1 – 17	13, 15	0.472842	<0.001
	2	1 – 17	13, 15	0.472842	<0.001
	3	1 – 17	13, 15	0.472842	<0.001
	4	1 – 17	13, 15	0.472842	<0.001
	5	1 – 17	13, 15	0.472842	<0.001
SCA –	Optimal	1 – 17	1, 13, 15	0.444030	<0.001
	1	1 – 17	1, 13, 15	0.444030	<0.001
	2	1 – 17	1, 13, 15	0.444030	<0.001
	3	1 – 17	1, 13, 15	0.444030	<0.001
	4	1 – 17	1, 13, 15	0.444030	<0.001
	5	1 – 17	1, 13, 15	0.444030	<0.001
SGA –	Optimal	1 – 17	6, 9, 17	0.065987	0.059
	1	1 – 17	6, 7, 8, 14, 17	0.060939	0.101
	2	1 – 17	6, 7, 8, 14, 17	0.060939	0.101
	3	1 – 17	6, 7, 8, 14, 17	0.060939	0.102
	4	1 – 17	7, 14	0.064514	0.006
	5	1 – 17	6, 9, 17	0.065987	0.059
SID –	Optimal	1 – 17	13, 15	0.474525	<0.001
	1	1 – 17	13, 15	0.474525	<0.001
	2	1 – 17	13, 15	0.474525	<0.001
	3	1 – 17	13, 15	0.474525	<0.001
	4	1 – 17	13, 15	0.474525	<0.001
	5	1 – 17	13, 15	0.474525	<0.001
SID(TAN) –	Optimal	1 – 17	13, 15	0.473684	<0.001
	1	1 – 17	13, 15	0.473684	<0.001
	2	1 – 17	13, 15	0.473684	<0.001
	3	1 – 17	13, 15	0.473684	<0.001
	4	1 – 17	13, 15	0.473684	<0.001
	5	1 – 17	13, 15	0.473684	<0.001
SID(SIN) –	Optimal	1 – 17	13, 15	0.473684	<0.001
	1	1 – 17	13, 15	0.473684	<0.001
	2	1 – 17	13, 15	0.473684	<0.001
	3	1 – 17	13, 15	0.473684	<0.001
	4	1 – 17	13, 15	0.473684	<0.001
	5	1 – 17	13, 15	0.473684	<0.001

Table 0-8: Results of the spectral separation analysis carried out using a genetic algorithm to determine the optimum band combination to separate between *Posidonia* and *Amphibolis* dominated habitats for each spectral metric. Each test was carried out five times using 24 spectral signatures for the library and using HyMap bands 1 – 9. The optimal result for each spectral metric is highlighted.

Spectral metric		Bands tested	Optimal bands	'R' statistic	p-value
SA –	Optimal	1 – 9	1, 2	0.111520	<0.05
	1	1 – 9	1, 2, 3, 4	0.026973	0.229
	2	1 – 9	1, 2	0.111520	0.033
	3	1 – 9	1, 2	0.111520	0.035
	4	1 – 9	1, 2	0.111520	0.031
	5	1 – 9	1, 2	0.111520	0.032
SCA –	Optimal	1 – 9	1, 6	0.194910	0.001
	1	1 – 9	1, 6	0.194910	0.001
	2	1 – 9	1, 6	0.194910	0.002
	3	1 – 9	1, 6	0.194910	0.003
	4	1 – 9	1, 6	0.194910	0.002
	5	1 – 9	1, 6	0.194910	0.002
SGA –	Optimal	1 – 9	7, 8, 9	0.053263	0.110
	1	1 – 9	7, 8, 9	0.053263	0.116
	2	1 – 9	7, 8, 9	0.053263	0.111
	3	1 – 9	7, 8, 9	0.053263	0.113
	4	1 – 9	7, 8, 9	0.053263	0.115
	5	1 – 9	7, 8, 9	0.053263	0.110
SID –	Optimal	1 – 9	1, 2	0.111625	0.030
	1	1 – 9	1, 2	0.111625	0.034
	2	1 – 9	1, 2	0.111625	0.032
	3	1 – 9	1, 2	0.111625	0.031
	4	1 – 9	1, 2	0.111625	0.031
	5	1 – 9	1, 2	0.111625	0.030
SID(TAN) –	Optimal	1 – 9	1, 2	0.111836	0.031
	1	1 – 9	1, 2	0.111836	0.031
	2	1 – 9	1, 2	0.111836	0.035
	3	1 – 9	1, 2	0.111836	0.039
	4	1 – 9	1, 2	0.111836	0.035
	5	1 – 9	1, 2	0.111836	0.033
SID(SIN) –	Optimal	1 – 9	1, 2	0.111836	0.029
	1	1 – 9	1, 2	0.111836	0.032
	2	1 – 9	1, 2	0.111836	0.029
	3	1 – 9	1, 2	0.111836	0.033
	4	1 – 9	1, 2	0.111836	0.033
	5	1 – 9	1, 2	0.111836	0.033

Ecklonia/Sargassum/Scytothalia doryocarpa

Table 0-9: Results of the spectral separation analysis carried out using a genetic algorithm to determine the optimum band combination to separate between *Ecklonia, Sargassum* and *S. doryocarpa* dominated habitats for each spectral metric. Each test was carried out five times using 23 spectral signatures for the library and using HyMap bands 1 – 17. The optimal result for each spectral metric is highlighted.

Spectral metric		Bands tested	Optimal bands	'R' statistic	p-value
SA –	Optimal	1 - 17	6, 7	0.484790	<0.001
	1	1 – 17	6, 7	0.484790	<0.001
	2	1 – 17	4, 9, 11, 12	0.379830	<0.001
	3	1 – 17	5, 9, 11, 12	0.383119	<0.001
	4	1 – 17	4, 5, 9, 10, 13, 14	0.372979	<0.001
	5	1 – 17	5, 6, 7	0.441902	<0.001
SCA –	Optimal	1 – 17	9, 10, 11	0.408331	<0.001
	1	1 – 17	9, 11	0.384763	<0.05
	2	1 – 17	9, 10, 11	0.408331	<0.001
	3	1 – 17	7, 8, 11	0.351603	<0.05
	4	1 – 17	9, 11	0.384763	<0.05
	5	1 – 17	9, 10, 11	0.408331	<0.001
SGA –	Optimal	1 – 17	6, 7, 8, 9, 15	0.137024	<0.05
	1	1 – 17	6, 7, 8, 9, 15	0.137024	<0.05
	2	1 – 17	10, 12, 17	0.136476	<0.05
	3	1 – 17	6, 7, 8, 9, 15	0.137024	<0.05
	4	1 – 17	6, 7, 8, 9, 15	0.137024	<0.05
	5	1 – 17	6, 9, 10, 11, 17	0.125240	<0.05
SID –	Optimal	1 – 17	5, 6, 8	0.445053	<0.001
	1	1 – 17	5, 6, 8	0.445053	<0.001
	2	1 – 17	6, 7	0.488627	<0.001
	3	1 – 17	5, 6, 8	0.445053	<0.001
	4	1 – 17	5, 6, 8	0.445053	<0.001
	5	1 – 17	5, 6, 8	0.445053	<0.001
SID(TAN) –	Optimal	1 – 17	6, 7	0.487942	<0.001
	1	1 – 17	6, 7	0.487942	<0.001
	2	1 – 17	5, 6, 8	0.433817	<0.001
	3	1 – 17	5, 6, 7	0.443546	<0.001
	4	1 – 17	5, 6, 8	0.433817	<0.001
	5	1 – 17	5, 6, 7	0.443546	<0.001
SID(SIN) –	Optimal	1 – 17	6, 7	0.487942	<0.001
	1	1 – 17	5, 6, 7	0.443546	<0.001
	2	1 – 17	6, 7	0.487942	<0.001
	3	1 – 17	5, 6, 8	0.433817	<0.001
	4	1 – 17	4, 5, 8, 9, 13	0.383393	<0.001
	5	1 – 17	4, 5, 6 ,8	0.415182	<0.001

Table 0-10: Results of the spectral separation analysis carried out using a genetic algorithm to determine the optimum band combination to separate between *Ecklonia, Sargassum* and *S. doryocarpa* dominated habitats for each spectral metric. Each test was carried out five times using 23 spectral signatures for the library and using HyMap bands 1 – 9. The optimal result for each spectral metric is highlighted.

Spectral metric		Bands tested	Optimal bands	'R' statistic	p-value
SA –	Optimal	1 – 9	6, 7	0.484790	<0.001
	1	1 – 9	6, 7	0.484790	<0.001
	2	1 – 9	6, 7	0.484790	<0.001
	3	1 – 9	6, 7	0.484790	<0.001
	4	1 – 9	6, 7	0.484790	<0.001
	5	1 – 9	6, 7	0.484790	<0.001
SCA –	Optimal	1 – 9	3, 5	0.611263	<0.001
	1	1 – 9	3, 5	0.611263	<0.001
	2	1 – 9	3, 5	0.611263	<0.001
	3	1 – 9	7, 9	0.585092	<0.001
	4	1 – 9	3, 5	0.611263	<0.001
	5	1 – 9	3, 5	0.611263	<0.001
SGA –	Optimal	1 – 9	6, 7	0.123596	0.079
	1	1 – 9	6, 7	0.123596	0.080
	2	1 – 9	6, 7	0.123596	0.079
	3	1 – 9	6, 7	0.123596	0.078
	4	1 – 9	6, 7	0.123596	0.078
	5	1 – 9	6, 7	0.123596	0.081
SID –	Optimal	1 – 9	6, 7	0.488627	<0.001
	1	1 – 9	6, 7	0.488627	<0.001
	2	1 – 9	6, 7	0.488627	<0.001
	3	1 – 9	6, 7	0.488627	<0.001
	4	1 – 9	6, 7	0.488627	<0.001
	5	1 – 9	6, 7	0.488627	<0.001
SID(TAN) –	Optimal	1 – 9	6, 7	0.487942	<0.001
	1	1 – 9	6, 7	0.487942	<0.001
	2	1 – 9	6, 7	0.487942	<0.001
	3	1 – 9	6, 7	0.487942	<0.001
	4	1 – 9	6, 7	0.487942	<0.001
	5	1 – 9	6, 7	0.487942	<0.001
SID(SIN) –	Optimal	1 – 9	6, 7	0.487942	<0.001
	1	1 – 9	6, 7	0.487942	<0.001
	2	1 – 9	6, 7	0.487942	<0.001
	3	1 – 9	6, 7	0.487942	<0.001
	4	1 – 9	6, 7	0.487942	<0.001
	5	1 – 9	6, 7	0.487942	<0.001

Algal turf

Table 0-11: Results of the spectral separation analysis carried out using a genetic algorithm to determine the optimum band combination to separate between *Ecklonia*, *Sargassum* and *S. doryocarpa* dominated habitats for each spectral metric. Each test was carried out five times using 14 spectral signatures for the library and using HyMap bands 1 – 17. The optimal result for each spectral metric is highlighted.

Spectral metric		Bands tested	Optimal bands	'R' statistic	p-value
SA –	Optimal	1 - 17	8, 9, 10	0.671831	<0.001
	1	1 – 17	5, 6, 7, 13, 14, 16	0.607042	<0.05
	2	1 – 17	5, 8, 10	0.670423	<0.001
	3	1 – 17	8, 9, 10	0.671831	<0.001
	4	1 – 17	5, 7, 8, 9, 10, 11	0.656338	<0.001
	5	1 – 17	7, 8, 11, 13, 14, 16	0.602817	<0.05
SCA –	Optimal	1 – 17	3, 7, 9	0.870423	<0.001
	1	1 – 17	3, 7, 9	0.870423	<0.001
	2	1 – 17	3, 7, 9	0.870423	<0.001
	3	1 – 17	3, 7, 9	0.870423	<0.001
	4	1 – 17	3, 7, 9	0.870423	<0.001
	5	1 – 17	1, 3, 5, 7, 9	0.867606	<0.001
SGA –	Optimal	1 – 17	1, 6	0.304225	<0.05
	1	1 – 17	1, 9, 15	0.292958	<0.05
	2	1 – 17	1, 6	0.304225	<0.05
	3	1 – 17	1, 6	0.304225	<0.05
	4	1 – 17	1, 6	0.304225	<0.05
	5	1 – 17	2, 9, 15	0.301408	<0.05
SID –	Optimal	1 – 17	8, 10	0.629577	<0.05
	1	1 – 17	5, 8, 10, 11	0.628169	<0.001
	2	1 – 17	7, 14, 15, 16, 17	0.590141	<0.05
	3	1 – 17	8, 10	0.629577	<0.05
	4	1 – 17	7, 14, 15, 16, 17	0.590141	<0.05
	5	1 – 17	5,6, 7, 8, 10, 11, 14, 16	0.570423	<0.05
SID(TAN) –	Optimal	1 – 17	8, 9, 10	0.653521	<0.001
	1	1 – 17	5, 8, 10	0.645070	<0.05
	2	1 – 17	8, 9, 10	0.653521	<0.001
	3	1 – 17	6, 7, 14, 16	0.581690	<0.05
	4	1 – 17	8, 9, 10	0.653521	<0.001
	5	1 – 17	7, 14, 17	0.601408	<0.05
SID(SIN) –	Optimal	1 – 17	8, 9, 10	0.652113	<0.001
	1	1 – 17	8, 9, 10	0.652113	<0.001
	2	1 – 17	5, 7, 8, 9, 10, 11	0.632394	<0.05
	3	1 – 17	8, 10	0.640845	<0.001
	4	1 – 17	8, 9, 10	0.652113	<0.001
	5	1 – 17	5, 8, 10	0.645070	<0.001

Table 0-12: Results of the spectral separation analysis carried out using a genetic algorithm to determine the optimum band combination to separate between *Ecklonia, Sargassum* and *S. doryocarpa* dominated habitats for each spectral metric. Each test was carried out five times using 23 spectral signatures for the library and using HyMap bands 1 – 9. The optimal result for each spectral metric is highlighted.

Spectral metric		Bands tested	Optimal bands	'R' statistic	p-value
SA –	Optimal	1 – 9	5, 7	0.607042	<0.05
	1	1 – 9	5, 7	0.607042	<0.05
	2	1 – 9	5, 7	0.607042	<0.05
	3	1 – 9	5, 7	0.607042	<0.05
	4	1 – 9	5, 7	0.607042	<0.05
	5	1 – 9	5, 7	0.607042	<0.05
SCA –	Optimal	1 – 9	3, 7, 9	0.870423	<0.001
	1	1 – 9	3, 7, 9	0.870423	<0.001
	2	1 – 9	3, 7, 9	0.870423	<0.001
	3	1 – 9	3, 7, 9	0.870423	<0.001
	4	1 – 9	3, 7, 9	0.870423	<0.001
	5	1 – 9	3, 7, 9	0.870423	<0.001
SGA –	Optimal	1 – 9	1, 6	0.304225	<0.05
	1	1 – 9	1, 6	0.304225	<0.05
	2	1 – 9	1, 6	0.304225	<0.05
	3	1 – 9	1, 6	0.304225	<0.05
	4	1 – 9	1, 6	0.304225	<0.05
	5	1 – 9	1, 6	0.304225	<0.05
SID –	Optimal	1 – 9	5, 7	0.600000	<0.05
	1	1 – 9	5, 7	0.600000	<0.05
	2	1 – 9	5, 7	0.600000	<0.05
	3	1 – 9	5, 7	0.600000	<0.05
	4	1 – 9	5, 7	0.600000	<0.05
	5	1 – 9	5, 7	0.600000	<0.05
SID(TAN) –	Optimal	1 – 9	5, 7	0.601408	<0.05
	1	1 – 9	5, 7	0.601408	<0.05
	2	1 – 9	5, 7	0.601408	<0.05
	3	1 – 9	5, 7	0.601408	<0.05
	4	1 – 9	5, 7	0.601408	<0.05
	5	1 – 9	5, 7	0.601408	<0.05
SID(SIN) –	Optimal	1 – 9	5, 6, 7	0.601408	<0.001
	1	1 – 9	5, 7	0.601408	<0.05
	2	1 – 9	5, 7	0.601408	<0.05
	3	1 – 9	5, 6, 7	0.601408	<0.001
	4	1 – 9	5, 6, 7	0.601408	<0.05
	5	1 – 9	5, 6, 7	0.601408	<0.05

Appendix 2: Benthic habitat classification probability maps

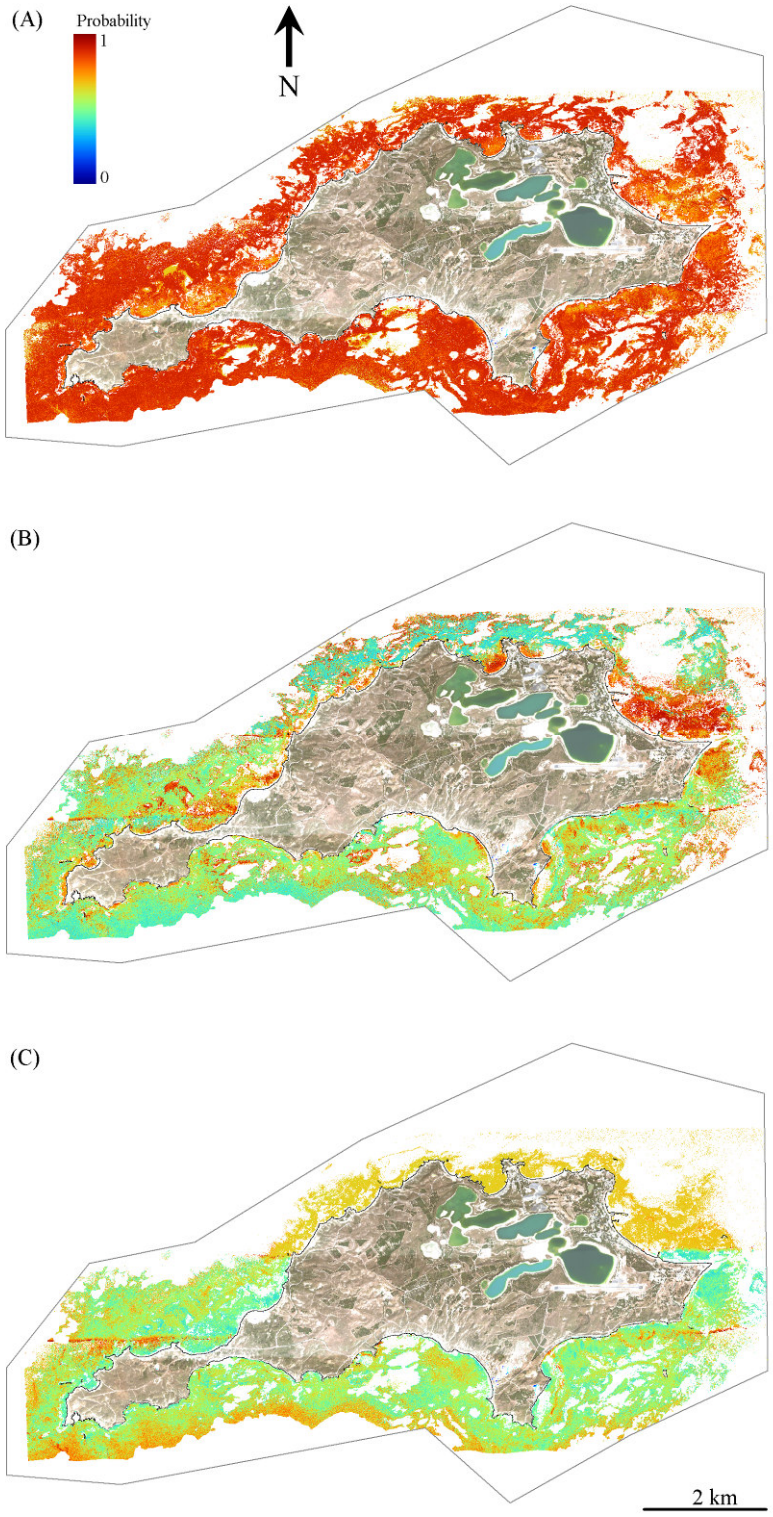

Figure 0-1: Probability maps for the separation of the bio-substrate class into macroalgae (A), seagrass (B) or coral (C).

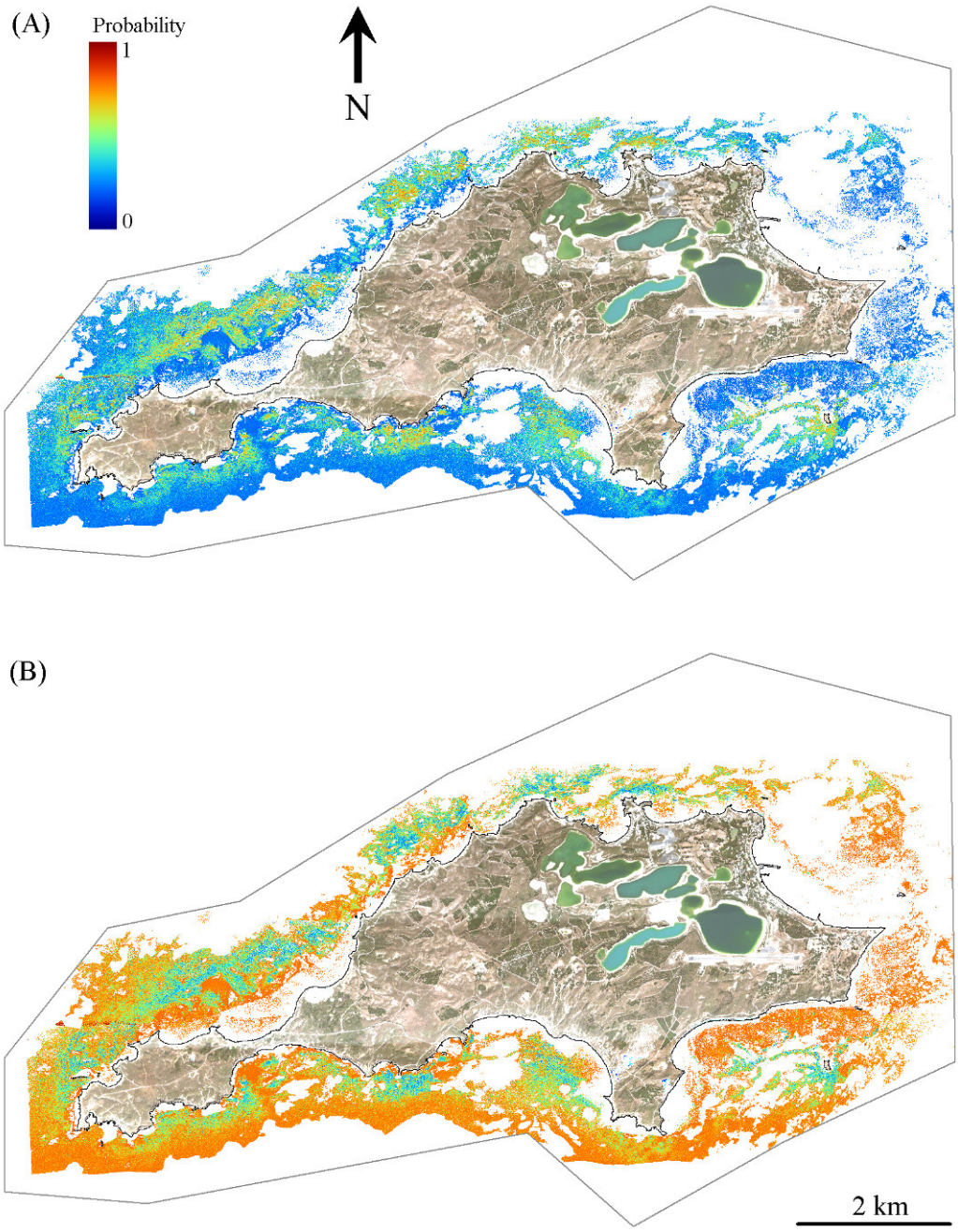

Figure 0-2: Probability maps for the separation of the macroalgae class into canopy algae (A) or algal turf (B).

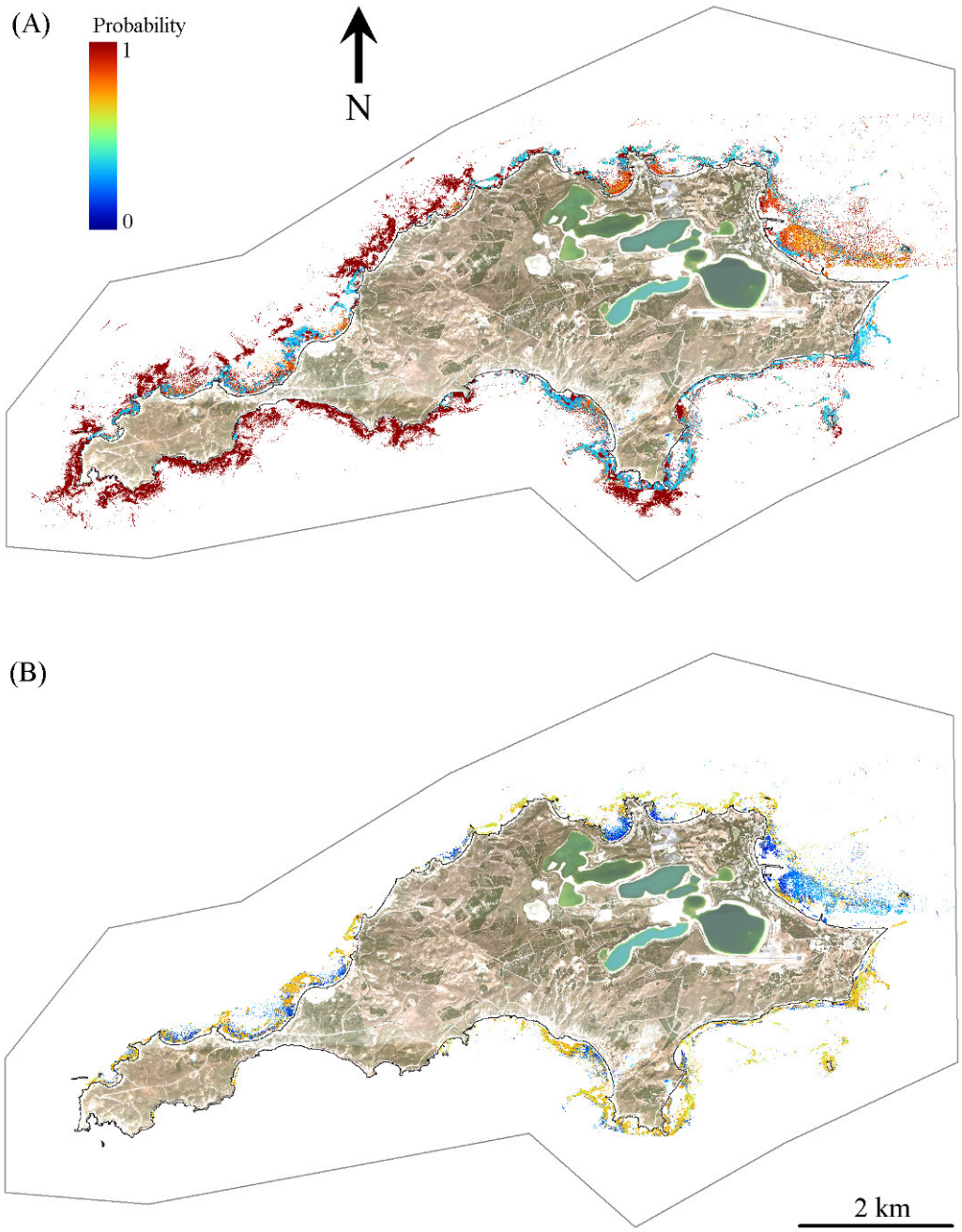

Figure 0-3: Probability maps for the separation of the seagrass class into *Posidonia* (A) or *Amphibolis* (B).

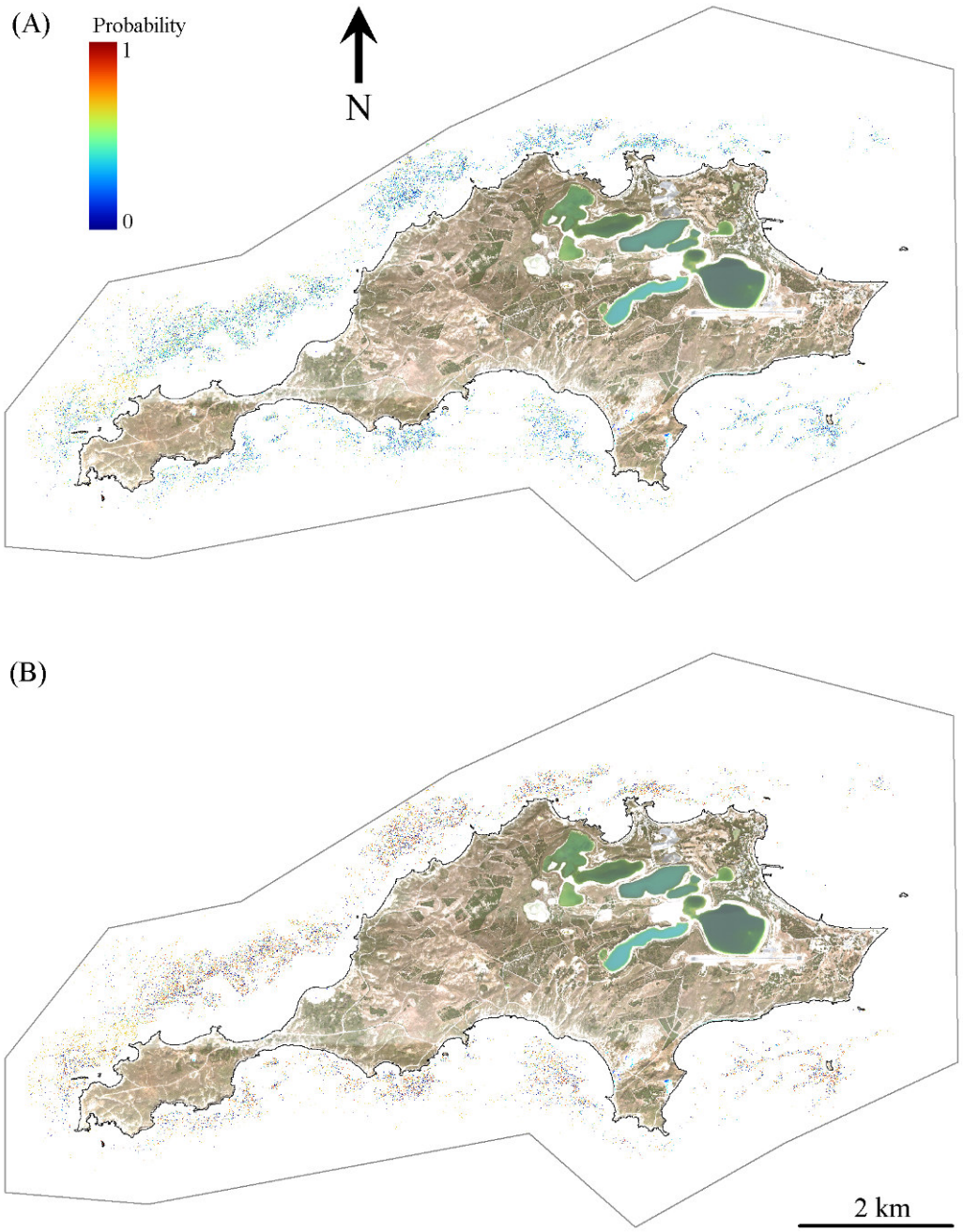

Figure 0-4: Probability maps for the separation of the canopy algae class into *Ecklonia radiata* (A) or *Sargassum* (B).